MARBLING FAT IN LIVESTOCK

EDITED BY: Xiao Li and Min Du
PUBLISHED IN: Frontiers in Veterinary Science, Frontiers in Genetics,
Frontiers in Molecular Biosciences and
Frontiers in Cell and Developmental Biology

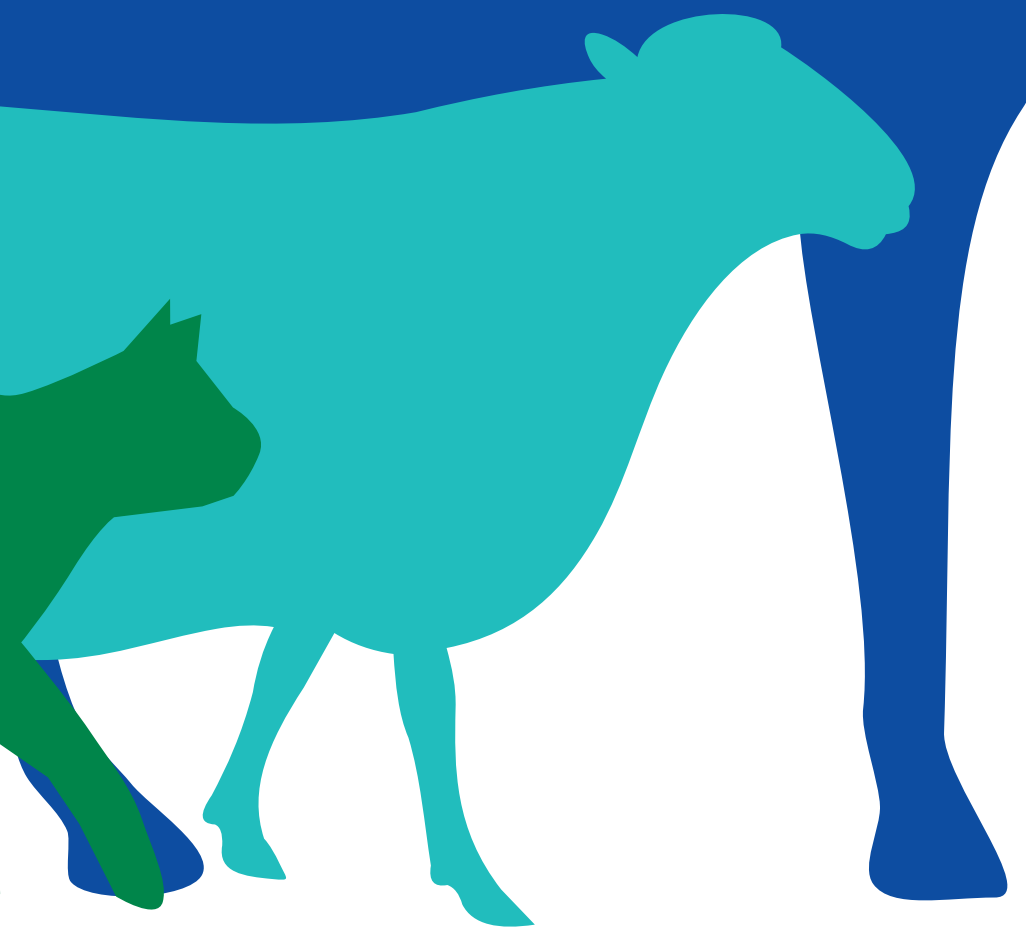

frontiers Research Topics

ISSN 1664-8714
ISBN 978-2-83250-613-4
DOI 10.3389/978-2-83250-613-4

About Frontiers

Frontiers is more than just an open-access publisher of scholarly articles: it is a pioneering approach to the world of academia, radically improving the way scholarly research is managed. The grand vision of Frontiers is a world where all people have an equal opportunity to seek, share and generate knowledge. Frontiers provides immediate and permanent online open access to all its publications, but this alone is not enough to realize our grand goals.

Frontiers Journal Series

The Frontiers Journal Series is a multi-tier and interdisciplinary set of open-access, online journals, promising a paradigm shift from the current review, selection and dissemination processes in academic publishing. All Frontiers journals are driven by researchers for researchers; therefore, they constitute a service to the scholarly community. At the same time, the Frontiers Journal Series operates on a revolutionary invention, the tiered publishing system, initially addressing specific communities of scholars, and gradually climbing up to broader public understanding, thus serving the interests of the lay society, too.

Dedication to Quality

Each Frontiers article is a landmark of the highest quality, thanks to genuinely collaborative interactions between authors and review editors, who include some of the world's best academicians. Research must be certified by peers before entering a stream of knowledge that may eventually reach the public - and shape society; therefore, Frontiers only applies the most rigorous and unbiased reviews.
Frontiers revolutionizes research publishing by freely delivering the most outstanding research, evaluated with no bias from both the academic and social point of view. By applying the most advanced information technologies, Frontiers is catapulting scholarly publishing into a new generation.

What are Frontiers Research Topics?

Frontiers Research Topics are very popular trademarks of the Frontiers Journals Series: they are collections of at least ten articles, all centered on a particular subject. With their unique mix of varied contributions from Original Research to Review Articles, Frontiers Research Topics unify the most influential researchers, the latest key findings and historical advances in a hot research area! Find out more on how to host your own Frontiers Research Topic or contribute to one as an author by contacting the Frontiers Editorial Office: frontiersin.org/about/contact

MARBLING FAT IN LIVESTOCK

Topic Editors:
Xiao Li, Northwest A&F University, China
Min Du, Washington State University, United States

Citation: Li, X., Du, M., eds. (2022). Marbling Fat in Livestock. Lausanne: Frontiers Media SA. doi: 10.3389/978-2-83250-613-4

Table of Contents

frontiers | Frontiers in Veterinary Science

TYPE Editorial
PUBLISHED 13 October 2022
DOI 10.3389/fvets.2022.1016428

OPEN ACCESS

EDITED AND REVIEWED BY
James Reecy,
Iowa State University, United States

*CORRESPONDENCE
Min Du
min.du@wsu.edu

SPECIALTY SECTION
This article was submitted to Livestock Genomics, a section of the journal Frontiers in Veterinary Science

RECEIVED 10 August 2022
ACCEPTED 13 September 2022
PUBLISHED 13 October 2022

CITATION
Du M and Li X (2022) Editorial: Marbling fat in livestock. *Front. Vet. Sci.* 9:1016428. doi: 10.3389/fvets.2022.1016428

Editorial: Marbling fat in livestock

Min Du[1]* and Xiao Li[2]

[1]Department of Animal Sciences, Washington State University, Pullman, WA, United States, [2]Key Laboratory of Animal Genetics, Breeding and Reproduction of Shaanxi Province, College of Animal Sciences and Technologies, Northwest A&F University, Yangling, China

KEYWORDS

marbling, livestock, intramuscular adipocytes, lipid metabolism, meat

Editorial on the Research Topic
Marbling fat in livestock

In animals used in food production, fat deposition is closely associated with production efficiency and meat quality. There are four major fat depots, including visceral, subcutaneous, intermuscular, and intramuscular fats, among which, only intramuscular fat (marbling fat) is critically important for the eating quality of meat. While most studies on intramuscular fat deposition concentrate on beef cattle traditionally, recent studies also emphasize its importance in determining the eating quality of pork, chicken, and other livestock species. Intramuscular fat development is due to both the formation of intramuscular adipocytes (hyperplasia) and their subsequent lipid accumulation (hypertrophy) (1). This special issue includes 12 articles on topics ranging from molecular mechanisms regulating intramuscular adipocyte formation and lipid accumulation. In addition, several species of livestock animals are covered.

Both intramuscular adipocyte hyperplasia and hypertrophy are affected by genetic, nutrition, and other environmental factors. In this issue, Sakowski et al. reviewed the genetic effects of European cattle breeds and their interaction with nutrition and other environmental factors. Due to their locations in the uterus, which restricts nutrient delivery to the fetuses, several piglets are born with much lower birth weights compared to their littermates. Zhao et al. showed that low and normal birth weight piglets differed in their ability to accumulate intramuscular fat, which was not affected by glutamate supplementation.

The RNA world is becoming increasingly complicated due to developments such as coding mRNAs and non-coding RNAs. After the transcription of pre-mRNAs, they are processed through splicing to form mature mRNAs. Alternative splicing produces different mRNAs which are translated into different protein isoforms. In addition, the introns that are spliced out often contain microRNAs (miRNAs) that are increasingly recognized for their regulatory roles in cell differentiation and animal development. In addition, non-coding RNAs are complex, including long non-coding RNAs (lncRNAs), piwi-interacting RNAs (piRNAs), small nucleolar RNAs (snoRNAs), miRNAs, and others (2). While most non-coding RNAs are linear, recent studies also identified circular RNAs (circRNAs), which have higher stability and can regulate animal development *via* sponging miRNAs or through other

mechanisms (3). Accumulating studies underscore the regulatory roles of non-coding RNAs in determining intramuscular fat development. In this issue, Li et al. profile the circular RNAs (circRNAs) in donkey muscle for their correlation with intramuscular fat deposition and found 127 differentially regulated circRNAs between low and high intramuscular fat groups, which target lipid metabolism. By comparing Wagyu and Chinese Red Steppe cattle, Yang et al. identified 115 differentially expressed and alternatively spliced genes, which affect lipid metabolism. Shu et al. found that several genes important for fatty acid metabolism have multiple alternative splicing, which was associated with intramuscular fat deposition in pigs. For miRNA, Xu et al. showed that miR-10a-5p affects intramuscular preadipocyte lipid accumulation by targeting Kruppel like factor 8 (KLF8) in goats.

Our understanding of the sources of intramuscular adipocytes remains limited. While most studies point to the fibro-adipogenic progenitor cells as the major source, the endothelial cells associated with blood vessels are an additional source (4). In addition, myogenic cells are a potential source of intramuscular adipocytes (5). Kim et al. showed that myoblasts are transdifferentiated into adipocytes in quails, which is promoted by the supplementation of retinoic acid. Following the formation of preadipocytes, these cells accumulate lipids to become mature adipocytes. Mao et al. showed that diacylglycerol acyltransferase 2 (DGAT2) stimulates lipid synthesis and thus adipocyte hypertrophy in pigeons. In addition, lipid accumulation differs among different fat depots. Through RNA-seq, Zhang et al. found that subcutaneous fat and visceral fat differ in the expression of genes regulating lipid metabolism. In addition, using RNA-seq, Bai et al. showed that long-chain acyl-CoA synthetase 1 (ACSL1) is correlated with unsaturated fatty acid synthesis in bovine adipocytes. Muscle fiber types and myosin heavy chain 3(MYH3) expression have been reported to affect marbling fat deposition. However, Huang et al. analyzed the variants in the MYH3 genes and found that there was no correlation between MYH3 variations and intramuscular fat content in several different pig breeds.

Finally, the marbling of beef carcasses is scored by inspecting the presence of intramuscular fat in the cross-section of *Ld* muscle. Depending on countries and geographical regions, the location of cross-cut is slightly different. In the US system, the marbling score is evaluated by ribbing between the 12^{th} to 13^{th} rib, while cuts at the fifth and tenth ribs are used in other countries. Liu et al. compared the marbling scores judged from the cut surface at the fifth and tenth ribs and, found that location did not affect the scores, showing ribbing location does not affect the marbling judgment.

In summary, articles in this issue cover several important aspects of intramuscular fat development and deposition, especially in RNA-seq and non-coding RNAs. While previous studies have focused on lipid metabolism and accumulation in mature adipocytes, new studies emphasize the importance of intramuscular fat formation, or the developmental sources of intramuscular adipocytes, in determining the degree of marbling fat deposition.

Author contributions

MD and XL wrote the manuscript and agreed on the submitted version. All authors contributed to the article and approved the submitted version.

Conflict of interest

The authors declare that the research was conducted in the absence of any commercial or financial relationships that could be construed as a potential conflict of interest.

Publisher's note

References

1. Du M, Huang Y, Das AK, Yang Q, Duarte MS, Dodson MV, et al. Meat science and muscle biology symposium: Manipulating mesenchymal progenitor cell differentiation to optimize performance and carcass value of beef cattle. *J Anim Sci.* (2013) 91:1419–27. doi: 10.2527/jas2012-5670

2. Dey BK, Mueller AC, Dutta A. Long non-coding RNAs as emerging regulators of differentiation, development, and disease. *Transcription.* (2014) 5:e944014. doi: 10.4161/21541272.2014.944014

3. Hansen TB, Jensen TI, Clausen BH, Bramsen JB, Finsen B, Damgaard CK, et al. Natural RNA circles function as efficient microRNA sponges. *Nature.* (2013) 495:384–8. doi: 10.1038/nature11993

4. Wang B, Fu X, Liang X, Deavila JM, Wang Z, Zhao L, et al. Retinoic acid induces white adipose tissue browning by increasing adipose vascularity and inducing beige adipogenesis of PDGFRalpha(+) adipose progenitors. *Cell Discov.* (2017) 3:17036. doi: 10.1038/celldisc.2017.36

5. Hu E, Tontonoz P, Spiegelman BM. Transdifferentiation of myoblasts by the adipogenic transcription factors PPAR gamma and C/EBP alpha. *Proc Natl Acad Sci USA.* (1995) 92:9856–60. doi: 10.1073/pnas.92.21.9856

frontiers in Genetics

ORIGINAL RESEARCH
published: 09 December 2020
doi: 10.3389/fgene.2020.587559

Identification of Candidate Circular RNAs Underlying Intramuscular Fat Content in the Donkey

*Bojiang Li[1], Chunyu Feng[1], Shiyu Zhu[1], Junpeng Zhang[1], David M. Irwin[2], Xiaoying Zhang[3], Zhe Wang[1] and Shuyi Zhang[1]**

[1] College of Animal Science and Veterinary Medicine, Shenyang Agricultural University, Shenyang, China, [2] Department of Laboratory Medicine and Pathobiology, University of Toronto, Toronto, ON, Canada, [3] Liaoning Province Engineering Center of Modern Agricultural Production Base, Shenyang, China

Intramuscular fat (IMF) content is a crucial indicator of meat quality. Circular RNAs (circRNAs) are a large class of endogenous RNAs that are involved in many physiological processes. However, the expression and function of circRNA in IMF in the donkey remains unresolved. Here we performed an expression profiling of circRNAs in the donkey longissimus dorsi muscle and identified 12,727 candidate circRNAs. Among these, 70% were derived from the exons of protein genes. Furthermore, a total of 127 differentially expressed (DE) circRNAs were identified in high (H) and low (L) IMF content groups, including 63 upregulated and 64 downregulated circRNAs. Gene Ontology (GO) and Kyoto Encyclopedia of Genes and Genomes (KEGG) pathway enrichment analysis of the host genes of the DE circRNAs showed that the host genes were enriched in lipid metabolism related GO terms (e.g., fatty acid beta-oxidation using acyl-CoA dehydrogenase and MLL3/4 complex), and signaling pathways (e.g., TGF-beta and lysine degradation signaling pathway). Further analyses indicated that 127 DE circRNAs were predicted to potentially interact with miRNAs, leading to the construction of circRNA-miRNA regulatory network. Multiple circRNAs can potentially function as sponges of miRNAs that regulate the differentiation of adipocytes. Our results provide valuable expression profile information for circRNA in the donkey and new insight into the regulatory mechanisms of circRNAs in the regulation of IMF content.

Keywords: circular RNA, expression profile, IMF, regulatory network, donkey

OPEN ACCESS

Edited by:
Xiao Li,
Northwest A&F University, China

Reviewed by:
Zhuanjian Li,
Henan Agricultural University, China
Renata Veroneze,
Universidade Federal de Viçosa, Brazil

****Correspondence:***
Shuyi Zhang
szhang@syau.edu.cn

Specialty section:
This article was submitted to Livestock Genomics, a section of the journal Frontiers in Genetics

Received: *26 July 2020*
Accepted: *18 November 2020*
Published: *09 December 2020*

Citation:
Li B, Feng C, Zhu S, Zhang J, Irwin DM, Zhang X, Wang Z and Zhang S (2020) Identification of Candidate Circular RNAs Underlying Intramuscular Fat Content in the Donkey. Front. Genet. 11:587559. doi: 10.3389/fgene.2020.587559

INTRODUCTION

The donkey (*Equus asinus*) is an important livestock animal in many countries including China and Italy (Polidori et al., 2015; Zhang X. et al., 2019), and plays a crucial role in human agricultural society by providing various products (meat, milk, and leather), acting as a draft force and transportation (Xia et al., 2019). Donkey meat was previously obtained from animals that were slaughtered at the end of their working lives, leading to poor quality meat with bad sensorial and nutritional characteristics (Lorenzo et al., 2014). In recent years, with the increasing mechanization of the world, donkey meat production from young males has improved the quality of the meat and attracted more customers for its consumption (Lorenzo et al., 2014). Therefore, donkey has increasingly become an important meat producing livestock. Donkey meat has recently been

recognized as a nutritious food for human consumption, as it contains high-quality protein, vitamins, and minerals (Polidori et al., 2015). For example, the protein content of donkey meat is 22.8%, and the potassium and phosphorus content are 343 and 212 mg per100 g, respectively (Polidori et al., 2008).

IMF, corresponds to the fat within muscles, and its amount is controlled by the number and size of intramuscular adipocytes (Li B. et al., 2018). A previous study indicated that the IMF content plays a key role in various quality traits of meat in many species (Hocquette et al., 2010). Increased levels of IMF content can positively influence sensory quality traits such as tenderness, juiciness, taste, and flavor (Bahelka et al., 2009). IMF content has a relatively high heritability in cattle (h^2 = 0.51) (Nogi et al., 2011) and pig (h^2 = 0.4–0.7) (Pena et al., 2016), which indicates that these animals can be selected for higher IMF content and bred to improve this trait in the next generation. However, there are currently no reports on the heritability of IMF in donkey. IMF content is complex quantitative trait, which is affected by multiple genetic components, environmental conditions, cellular signals and hormones (Cho et al., 2019). Therefore, identifying candidate genes and molecular markers could be useful in selection programs to improve IMF content in the donkey.

To date, groups that have studied donkey meat and carcass performance have focused on these traits (Polidori et al., 2008; De Palo et al., 2016), rather than the mechanisms that control them. Recently, many previous studies have shown that coding and non-coding RNAs (e.g., miRNA and lncRNA) regulate IMF formation in the pig, cattle and chicken (Li B. et al., 2018; Zhang et al., 2018, 2020; Zou et al., 2018). However, these mechanisms of coding or non-coding RNAs in the regulation of IMF deposition in the donkey is unknown. Circular RNAs (circRNAs) are a class of endogenous non-coding RNA that are processed from precursor mRNA (pre-mRNA) by back-splicing with a covalent linkage between the 3′ and 5′ ends (Dong et al., 2017). They are extensively distributed in mammalian cells and lack the typical 5′ caps and 3′ poly(A) tails of coding mRNA (Devaux et al., 2017). Recent studies have provided evidence that the expression levels of circRNAs are highly conserved among species (Legnini et al., 2017). Due to their non-linear structure, circRNAs have higher stability than linear RNAs and are involved in many different physiological processes (Rybak-Wolf et al., 2015; Sun et al., 2019). It has been shown that circRNAs play important roles in biological and physiological processes in livestock (Bahelka et al., 2009; Li H. et al., 2018; Cao et al., 2019). For example, 828 circRNAs were found to be significantly differently expressed between embryonic and adult bovine muscle tissues and that circLMO7 regulates myoblasts differentiation and survival through the sponging of miR-378a-3p (Wei et al., 2017). A recent study by Liu et al. (2018) demonstrated that a large number of circRNAs are significantly differently expressed during adipogenesis in subcutaneous fat in pigs (Liu et al., 2018). However, it is unknown whether circRNAs have any biological role during IMF formation in donkeys. Therefore, here we systematically investigated the expression profile of circRNAs in donkey longissimus dorsi muscles.

First, we performed expression profiling of circRNAs in the donkey longissimus dorsi muscles of donkey using RNA-seq. We then identified differentially expressed circRNAs between high (H) and low (L) IMF content. GO and KEGG analyses were conducted of the host genes of the differentially expressed circRNAs between H and L IMF content. Finally, we predicted that specific miRNAs were adsorbed by the differentially expressed circRNAs, allowing us to construct the circRNA-miRNA regulatory network in IMF.

MATERIALS AND METHODS

Ethics Statement

All animal procedures described in this study were conducted according to the animal husbandry guidelines of Shenyang Agricultural University. The studies in these animals were reviewed and approved by the Ethics Committee and Experimental Animal Committee of Shenyang Agriculture University.

Animals, Samples Collection, and Phenotypes Measurement

The animals used in this study were derived from 30 Liaoxi donkeys, and provided by Fuxin City Lv Xian Yuan Meat Food Co., Ltd. (Fuxin, China), which had been raised under standard conditions with *ad libitum* access to a mixture of cereal straw and grass hay, maize, bran, peas, minerals, vitamins, and water. At an age of about 15 months, all of the donkeys were slaughtered in the same abattoir (Fuxin, China). Longissimus dorsi muscle was collected and used for the measurement of IMF content and RNA extraction. Tissue samples for RNA extraction were immediately snap-frozen in liquid nitrogen, and then stored at −80 ℃ until use. IMF content of the longissimus dorsi muscle was measured using the Soxhlet extraction method as described previously (Li B. et al., 2018). Of the 30 samples tested, the three with the H IMF content and the three with the L IMF content were chosen for RNA extraction. The IMF content of the H and L groups were 6.34% (SEM = 0.47%) and 3.04% (SEM = 0.12%), respectively, which was significantly different ($P \leq 0.05$), however, the body weights of the animals in these two groups were not different.

RNA Isolation, Library Construction, and RNA Sequencing (RNA-Seq)

Total RNA was isolated from each sample using TRIzol (Invitrogen, Carlsbad, CA, United States) according to manufacturer's protocol. RNA concentration and purity were assessed using a NanoDrop 2000 spectrophotometer (Thermo Fisher Scientific, Waltham, MA, United States). The integrity of the RNA was assessed using an Agilent 2,100 Bioanalyzer (Agilent Technologies, Santa Clara, CA, United States). Ribosomal RNA (rRNA) was removed using a Ribo-Zero Magnetic Gold Kit (Epicenter, Madison, WI, United States). The linear-stranded RNA was removed by RNase R (Epicenter, Madison, WI, United States). Sequencing libraries were generated using NEBNext® Ultra™ Directional RNA Library Prep Kit for Illumina (NEB, Ipswich, United States) following manufacturer's recommendations. Sequencing of the libraries was performed on

an Illumina Novaseq 6,000 system with PE150 sequencing mode by Novogene Co., Ltd. (Beijing, China).

CircRNA Sequencing Analysis

Clean reads were obtained by removing those composed of adapters, contain ploy-N, and low-quality sequences (containing more than 50% low-quality bases) from the raw data. All of the downstream analyses were based on the clean high-quality data. Clean reads were then aligned with the donkey reference genome (ASM303372v1) using the Burrows-Wheeler Aligner (BWA)-MEM (Li and Durbin, 2009). CIRI2 (Gao et al., 2018) software was applied to obtain back-spliced junction reads for circRNA prediction. The expression levels of individual circRNA were calculated as RPM (reads per million mapped reads). DESeq2 (Love et al., 2014) was used to identify differentially expressed (DE) circRNAs between the H and L groups. We defined circRNAs that had a fold change ≥ 2 or < 0.5 with a Benjamini-Hochberg method corrected $p \leq 0.05$ between the two groups as significant differentially expressed circRNA.

GO and KEGG Pathway Enrichment Analysis

Gene Ontology (GO) enrichment analysis of the host genes of all differentially expressed circRNAs was performed by the clusterProfiler R package using default parameters (Yu et al., 2012). GO terms with a Benjamini-Hochberg method corrected $p < 0.05$ were considered significantly enriched. We used KOBAS software (Wu et al., 2006) with default parameters to test the statistical enrichment of all host genes of the differentially expressed circRNAs in KEGG pathways. Pathways with a Benjamini-Hochberg method corrected $p < 0.05$ were considered significantly enriched.

Prediction of CircRNA-miRNA Interactions

We used miRanda software (John et al., 2004) with "-sc 140 -en -10 -scale 4 -strict" to identify putative circRNA-miRNA interactions and Cytoscape software (Shannon et al., 2003) was used to construct the circRNA-miRNA networks.

Quantitative Reverse-Transcription PCR Analysis

Total RNA was extracted from longissimus dorsi muscle used in the RNA-seq using TRIzol (Invitrogen, Carlsbad, CA, United States), and then reverse-transcribed into complementary DNA (cDNA) using Primescript RT Master Kit (Takara, Dalian, China) according to the manufacturer's instructions. According to the method of selecting DE circRNA in other studies (Zhang G. et al., 2019; Tian et al., 2020), we randomly select 5 DE circRNAs from the up-regulated and down-regulated DE circRNAs using sample function in R software, respectively. Primers for the differentially expressed circRNAs were designed using primer5 (Singh et al., 1998). All the primers used are listed in **Supplementary Table S1**. Quantitative Reverse-Transcription PCR (qRT-PCR) was performed with AceQ qPCR SYBR Green Master Mix (Vazyme, Nanjing, China) in a reaction volume of 20 μL. The cycling parameters were as follows: 95°C for 5 min, followed by 40 amplification cycles, each at 95°C for 10 s, then 60°C for 30 s. All reactions were performed in triplicate for each sample. Relative expression levels of the differentially expressed circRNAs were calculated by the $2^{-\Delta\Delta Ct}$ method as reported previously (Wei et al., 2017; Cheng et al., 2019). The glyceraldehyde-3-phosphate dehydrogenase (GAPDH) gene was used as a reference to normalize the relative expression of the circRNAs.

Statistical Analyses

Statistical analyses were conducted using SPSS 20.0 (SPSS Inc., Chicago, IL, United States). Statistical significance of the difference between the two groups was calculated using a Student's *t*-test. A value of $p < 0.05$ was considered to represent a statistically significant difference.

RESULTS

Characterization of CircRNAs in Longissimus Dorsi Muscles

To identify the circRNAs expression profile in donkey longissimus dorsi muscles, we performed RNA-seq and mined the data for circRNAs. In total, 663,324,766 raw reads (327,437,586 for H and 335,887,180 for L group) were generated from the six sequencing libraries (**Supplementary Table S2**). After removing low-quality, poly-N containing, and adapter-containing reads from the raw reads, 318,388,574 and 326,916,290 clean reads were obtained, for the H and L groups, respectively (**Supplementary Table S2**). An average of 82.49% (range: 78.58–85.87%) of the reads were mapped to the donkey genome (ASM303372v1) (**Supplementary Table S3**). A total of 12,727 circRNAs that were supported by at least two junction reads were identified from longissimus dorsi muscle and spliced from 3,251 genes (**Supplementary Table S4**). Approximately 70% of the circRNAs from both groups were derived from the exons of protein genes, while some of them were from intronic or intergenic regions (**Figure 1A**). The lengths of most of the identified circRNAs were less than 1,000 nucleotides (nt) (**Figure 1B**). Among the circRNA-producing genes, most host genes preferred to generate a single circRNA instead of multiple circRNA (**Figure 1C**). The majority of the identified circRNA species that originate from protein-coding genes contain two or three exons (**Figure 1D**).

Identification of DE CircRNAs Between H and L IMF Muscles

To identify candidate circRNAs affecting IMF content in donkey longissimus dorsi muscle, we calculated the expression level of each identified circRNAs and tested for differential expression of circRNAs between the H and L IMF content groups. Our results indicate that the density distribution of circRNA expression was not significantly different between the H and L IMF content groups (**Figure 2A**), however, 127 DE circRNAs were identified, including 63 upregulated and 64 downregulated

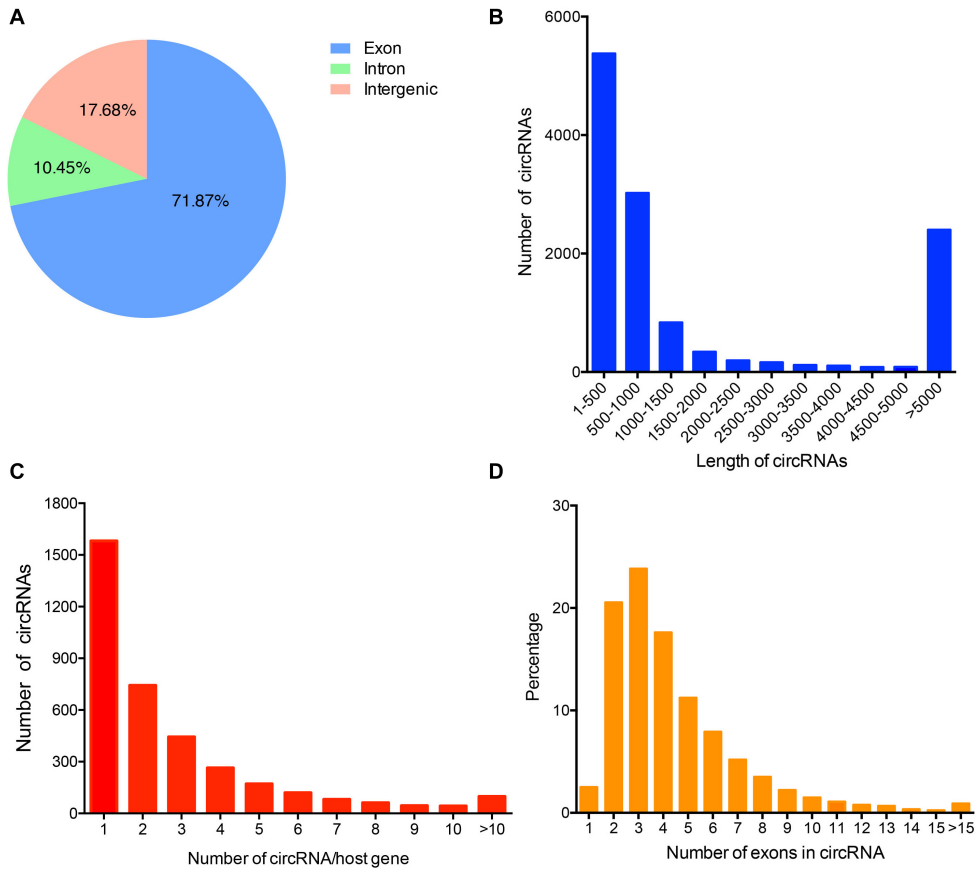

FIGURE 1 | Characteristics of the circRNAs identified in donkey muscle tissue. **(A)** Genomic origin of the identified circRNAs. **(B)** Length distribution of the identified circRNAs. **(C)** Distribution of the number of circRNA per gene. **(D)** The percentage of circRNAs was calculated based on the number of exons each circRNA in the exon-derived circRNAs.

circRNAs in the H IMF content group (**Figures 2B,C**). Detailed information on each DE circRNAs is provided in **Supplementary Table S5**. Among the candidates, novel_circ_0000323 was the most upregulated circRNA and novel_circ_0000319 was the most downregulated circRNA in the H IMF content group (**Supplementary Table S5**). **Figure 2D** shows a heatmap of the expression pattern of the DE circRNAs from the six samples, which indicates that the samples from the H IMF content group could be clearly distinguished from those from the L IMF content group.

Experimental Validation of the DE CircRNAs

To verify the reliability of the RNA-seq data, we use qRT-PCR to detect the expression levels of DE circRNAs. We tested the expression of randomly selected five upregulated circRNAs (novel_circ_0010172, novel_circ_0007969, novel_circ_0011073, novel_circ_0002126, and novel_circ_0010184) and downregulated circRNAs (novel_circ_0012311, novel_circ_0007411, novel_circ_0002621, novel_circ_0009905, and novel_circ_0002071). Divergent primers for each circRNA were designed to amplify the back-splice sequences (**Figure 3A**). PCR products of the divergent primers for each circRNA were confirmed by Sanger sequencing (**Figure 3B** and **Supplementary Figure S1**). Moreover, qRT-PCR results indicate that these circRNAs were significantly differentially expressed between H and L IMF groups ($p < 0.05$; **Figure 3C**), and the Pearson correlation coefficient of the log2(fold change) data between the qRT-PCR and RNA-Seq was 0.95 ($p < 0.05$; **Figure 3D**), suggesting that the DE circRNAs identified by RNA-Seq were reliable.

Enrichment Analysis of the Host Genes of DE CircRNAs

A previous study demonstrated that circRNA abundance is negatively correlated with their linear host gene mRNA and that there is a competition between pre-mRNA splicing and circRNA production (Ashwal-Fluss et al., 2014). To explore and analyze the potential biological function of these DE circRNAs, we performed GO and KEGG enrichment analysis of the host genes of the DE circRNAs. GO enrichment analysis indicated that 48, 37, and 36 GO terms were significantly enriched in biological process, cellular component, and molecular function, respectively (**Supplementary Table S6**). Among the most enriched GO terms,

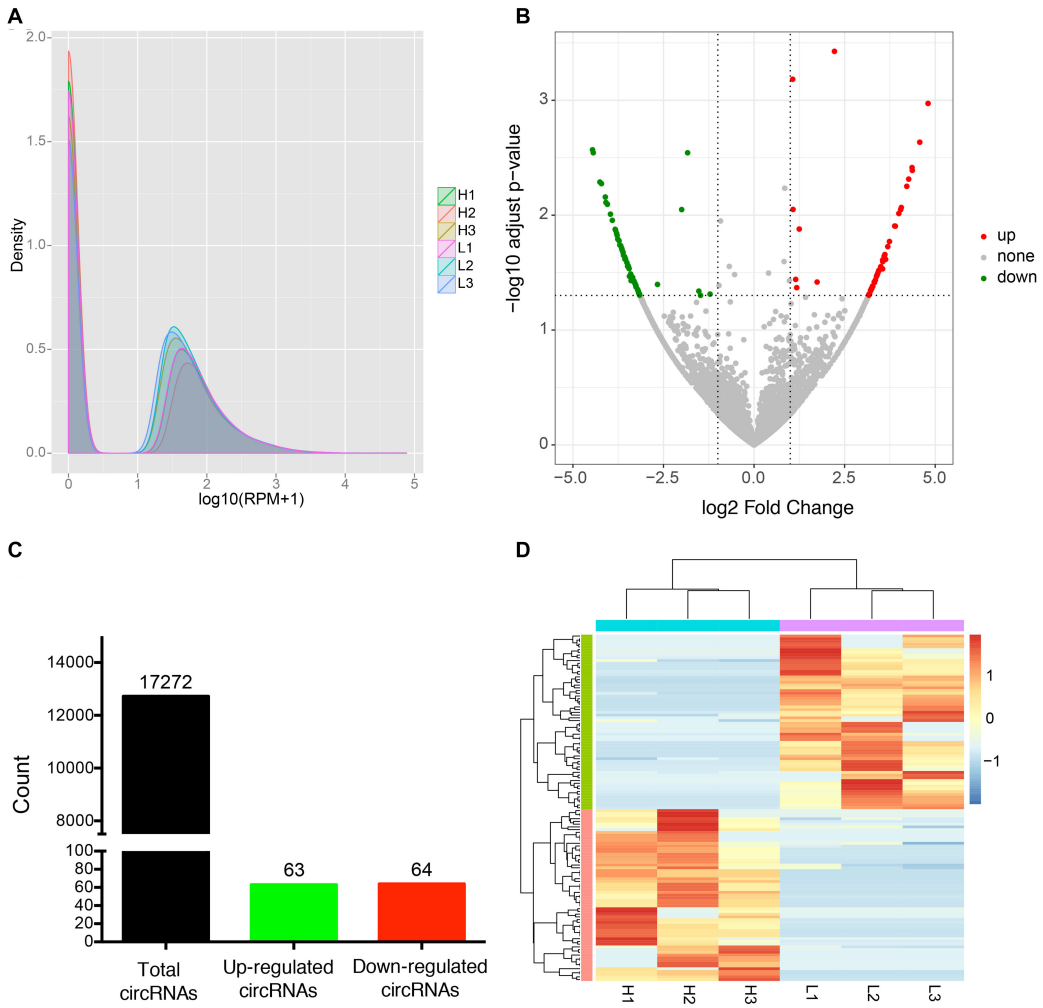

FIGURE 2 | Differential expression analysis of circRNAs between H and L IMF groups. **(A)** Density plot of the expression density distribution of circRNAs in each sample. **(B)** Volcano plot of all DE circRNAs between the H and L IMF groups. *X*-axis represents the value of log2 (H/L) and the *Y*-axis represents the value of –log10 (*p*-value). **(C)** Number of total, up-regulated and down-regulated circRNAs between the H and L IMF groups. **(D)** Clustered heatmap of the expression patterns of the DE circRNAs from three H and three L IMF samples.

some of them were associated with lipid metabolism (e.g., fatty acid beta-oxidation using acyl-CoA dehydrogenase and MLL3/4 complex) (**Figure 4A**). Moreover, the KEGG enrichment analysis indicated that the host genes of the DE circRNAs were significantly enriched in 12 pathways, including related to lipid metabolism (e.g., TGF-beta and lysine degradation signaling pathway) (**Figure 4B**).

Putative Functions of the DE CircRNAs as MiRNA Sponges

A previous study has shown that circRNA can act as miRNA sponges by acting as binding sites (Li X. et al., 2018). Some microRNAs (miRNAs) function as stimulators or inhibitors in adipocyte differentiation (Arner and Kulyte, 2015). To determine whether the DE cricRNA identified in this study can potentially function as miRNA sponges to regulate adipogenesis, we tested the ability of the DE circRNAs to bind to miRNAs. The circRNA-miRNA regulatory networks showed that 17,088 circRNA-miRNA interactions could be predicted based on 127 DE circRNAs and 690 miRNAs (**Supplementary Table S7**). Interestingly, we found that many of the upregulated circRNAs potentially function as sponges for many miRNA genes associated with adipogenesis such as miR-429, miR-224, miR-125a-5p, miR-223, miR-145, and miR-302a (**Figure 5A**). Additionally, many of the downregulated circRNAs also potentially bind miRNAs such as to miR-181a, miR-144, miR-199a-5p, and miR-127 (**Figure 5B**).

DISCUSSION

With the advancement of high-throughput sequencing technologies and bioinformatics, a large number of circRNAs have been identified in the human (Li S. et al., 2018), mouse

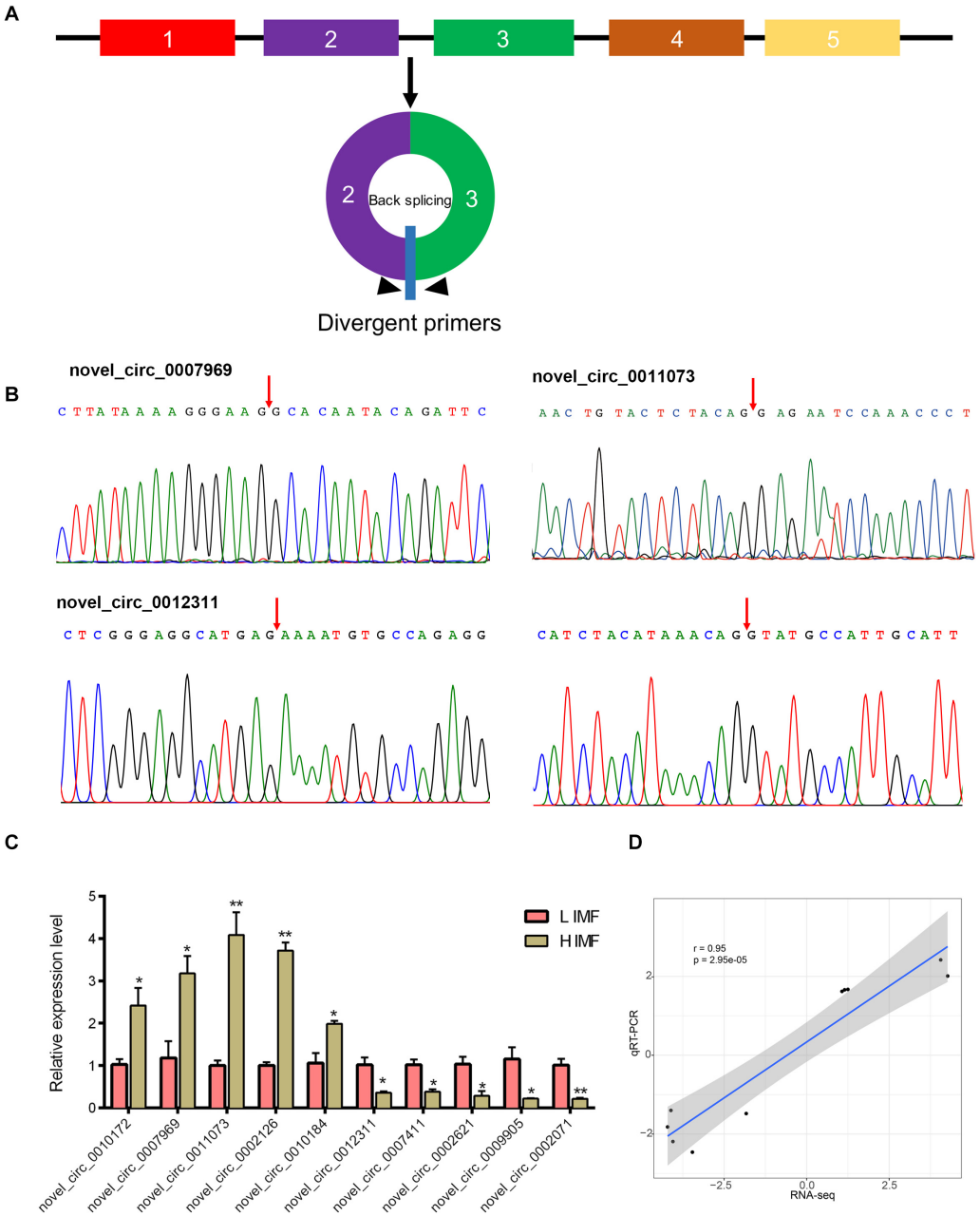

FIGURE 3 | Validation of DE circRNAs by qRT-PCR. **(A)** Schematic of the divergent primer design for circRNAs. **(B)** Representative PCR products sequenced to validate the backsplice sequence of the circRNAs. Arrow represents the backsplice junction. **(C)** Expression level of DE circRNAs in H and L IMF samples were determined by qRT-PCR. $^{*}p < 0.05$; $^{**}p < 0.01$, two-tailed *t*-test. **(D)** Pearson correlation coefficient of the log2(fold change) data between qRT-PCR and RNA-Seq.

(Legnini et al., 2017), chicken (Shen et al., 2019), pig (Hong et al., 2019; Li et al., 2020), cattle (Li H. et al., 2018), and sheep (Li X.Y. et al., 2019) genomes. Recently, the circRNA database CircAtlas[1] has integrated over one million circRNAs from 6 species (human, macaca, mouse, rat, pig, and chicken) (Wu et al., 2020). However, the expression profiles and biological characteristics of circRNAs in the donkey has not been examined.

Here we performed a comprehensive profile of circRNAs in the donkey using RNA-seq and identified 12,727 unique circRNAs in longissimus dorsi muscle samples. These results provide the foundation for establishing a donkey circRNA database and allowing future research on the potential role of circRNA in muscle development in the donkey. In this study, the major circRNAs were found to be derived from back-splicing of exons, which is consistent with previous studies in pig (Liang et al., 2017), chicken (Ouyang et al., 2017), and cattle

[1]http://circatlas.biols.ac.cn/

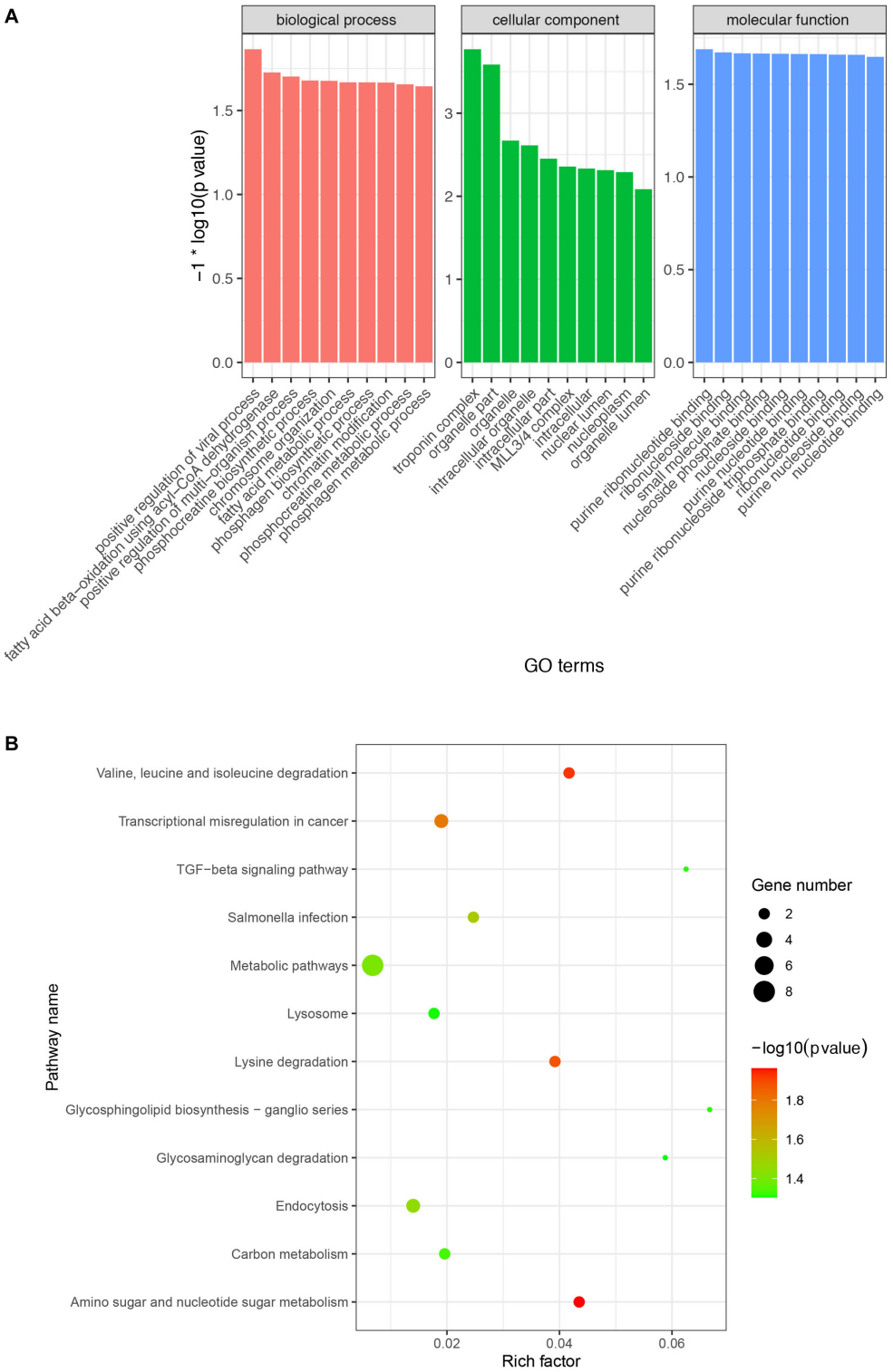

FIGURE 4 | Gene Ontology (GO) and KEGG enrichment analysis of host genes of the DE circRNAs. **(A)** Most enriched GO terms in biological process, cellular component, and molecular function. *X*-axis represents GO terms and the *Y*-axis represents the value of -log10 (*p*-value). **(B)** Significantly enriched signaling pathways of the host genes of the DE circRNAs. The *X*-axis represents rich factor and the *Y*-axis represents pathway. Size and color of the bubble represent the number of host genes enriched in the pathway and enrichment significance, respectively.

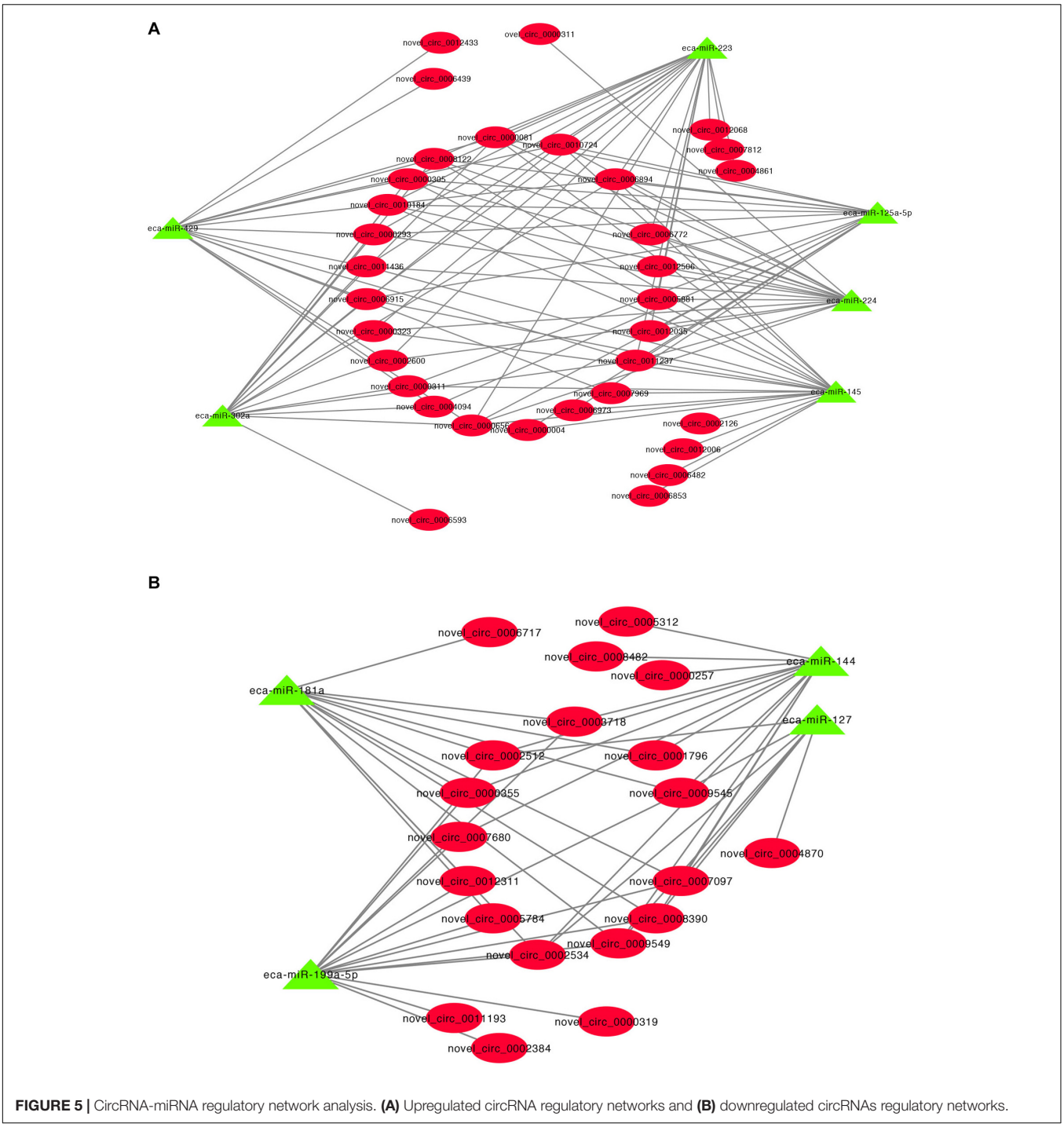

FIGURE 5 | CircRNA-miRNA regulatory network analysis. **(A)** Upregulated circRNA regulatory networks and **(B)** downregulated circRNAs regulatory networks.

(Wei et al., 2017) muscle. This result suggests that the circRNAs are highly similar in distribution pattern and evolutionarily conserved among different species. Moreover, our results show that the identified circRNAs contain multiple exons, with most containing two or three exons, which is similar to the circRNAs in many other species (Zhang et al., 2014; Wei et al., 2017), suggesting many host preferentially produce two or three circRNAs in donkey.

Previous studies have demonstrated that circRNAs are a large class of widespread and diverse endogenous RNAs in animals that play critical roles in many physiological and pathological processes, including fat (Jiang et al., 2020), muscle (Zhang P. et al., 2019), and cancer (Xie et al., 2020) development. For example, Jiang et al. (2020) characterized the expression profile of circRNA in fat tissue during developmental stages of the calf and adult cow and demonstrated that the circFUT10

regulates adipocyte cell proliferation and differentiation by sponging the miRNA let-7c (Jiang et al., 2020). Moreover, several studies have found that circRNAs are involved in muscle traits in the pig (Liang et al., 2017; Sun et al., 2017) and chicken (Chen et al., 2019). Recent studies have shown a potential role for circRNAs in IMF deposition in the yak based on the differentially expression of circRNAs between muscle and adipose tissue (Wang et al., 2020). In this study, we obtained the expression profiles of circRNA from muscle with differing IMF content, and identified 127 differentially expressed circRNAs between three H and L IMF samples. However, the expression level of these DE circRNAs in a large number of individuals are still needed to be confirmed. Furthermore, 10 DE circRNAs detected by qRT-PCR are significantly differentially expressed between H and L groups, indicating the DE circRNA results are reliable. These results suggest that these DE circRNAs play an important role in IMF deposition, and that circRNAs may affect livestock meat quality through the formation of IMF.

Since circRNAs are produced from precursor mRNA (pre-mRNA) by back-splicing, the production of circRNA can reduce the amount of linear transcripts by competing with linear splicing (Ashwal-Fluss et al., 2014; Liu et al., 2018). This suggests that circRNAs can act in an important role under physiological conditions to regulate the expression of their host genes. In this study, GO enrichment of host genes of DE circRNAs yielded some GO terms that are involved in lipid metabolism including MLL3/4 complex, fatty acid beta-oxidation using acyl-CoA dehydrogenase, fatty acid metabolic process, methyltransferase complex and histone deacetylase binding. Histone methyltransferases MLL3/4 play a crucial role in adipogenesis (Lee et al., 2020) and the deletion of MLL3 in mice results in significantly decreased amounts of white fat (Lee et al., 2008). For example, novel_circ_0009716, a down-regulated circRNA from the H IMF group, is derived from the histone mono-methyltransferase MLL4 (KMT2D), suggesting that it can regulate IMF formation through the MLL3/4 complex. Moreover, novel_circ_0007020 is derived from the MIER1 gene, which is enriched in the histone deacetylase binding GO term. A previous study indicated that MIER1 can bind to BAHD1 to form a hub for histone deacetylases and methyltransferases that are involved in energy metabolism (Lakisic et al., 2016). Therefore, novel_circ_0007020 might be involved in IMF formation by repressing the levels of its linear mRNA for MIER1. In addition, we found that host genes of the differently expressed circRNAs were significantly enriched in 12 pathways, including related to lipid metabolism (e.g., TGF-beta and lysine degradation signaling pathway). TGFβ and its downstream effector have been reported to play important roles in regulating glucose and energy homeostasis (Yadav et al., 2011). Previous study has shown that increased IMF deposition is due to lysine restriction in pig diets (Madeira et al., 2013). These evidences indicate that DE cricRNAs can regulate TGF-beta and lysine degradation signaling pathway by competing with host mRNA splicing, which ultimately affect IMF deposition. Together, all these results suggest that these differentially expressed circRNAs affect the physiological functions of their host genes leading to the regulation of IMF deposition.

It has been shown that circRNA can act as competing endogenous RNAs (ceRNAs) to sponge miRNAs and prevent them from binding and suppressing their target mRNAs (Chen, 2020). For example, circHIPK2 regulates astrocyte activation, via regulation of autophagy and endoplasmic reticulum (ER) stress, through targeting of MIR124-2HG and SIGMAR1 (Huang et al., 2017). We identified 17,088 circRNA-miRNA interactions in this study and these results suggest that DE circRNAs have a regulatory role in IMF deposition via the sequestration of miRNAs. MicroRNAs (miRNAs) are a class of small non-coding RNA that regulate target gene expression, and can stimulate or inhibit the differentiation of adipocytes in adipose tissue (Arner and Kulyte, 2015). Our current study revealed that many DE circRNAs may act as endogenous sponges of miRNAs including miR-429 (Peng et al., 2016), miR-224 (Zhang Y. et al., 2019), miR-125a-5p (Du et al., 2018), miR-223 (Li F. et al., 2019), miR-145 (Guo et al., 2012), miR-302a (Jeong et al., 2014), miR-181a (Zhang Z. et al., 2019), miR-144 (Shen et al., 2018), miR-199a-5p (Shi et al., 2014), and miR-127 (Gao et al., 2019) that are involved in the regulation of adipogenesis. miR-125a-5p is negatively involved with IMF content by targeting *KLF13* and *ELOVL6* (Du et al., 2018). We predicted that fifteen upregulated DE circRNA, such as novel_circ_0010184, can able to bind miR-125a-5p. Moreover, novel_circ_0010184 was upregulated in H IMF content compared to L IMF content using qRT-PCR in this study. Therefore, these results suggest that these circRNAs might be a sponge of miR-125a-5p and promote increases in IMF content. A downregulated DE circRNA, novel_circ_0012311, might function as sponge for miR-181a that facilitates porcine preadipocyte differentiation by targeting TGFBR1, indicating that novel_circ_0012311 might inhibit IMF preadipocyte differentiation through the miR-181a/TGFBR1 axis in donkey. Consequently, our results suggest that DE circRNAs have important roles in the regulation of IMF adipogenesis by acting as miRNA sponges to inhibit the miRNA targeting of genes.

CONCLUSION

We identified 12,727 circRNAs in the donkey longissimus dorsi muscle, thus, expanding our understanding of the complexity of the donkey transcriptome. The host genes were enriched in lipid metabolism related GO terms and signaling pathways, and DE circRNAs act as adipogenesis related miRNAs sponge, which provide insight into our understanding of the functions of circRNA in IMF content. Our results provide evidence that circRNAs have an important regulatory role in IMF content and this information might be useful for future research into circRNA and the regulation of IMF deposition.

DATA AVAILABILITY STATEMENT

The data used in our study have been deposited in NCBI SRA (accession codes PRJNA647167).

ETHICS STATEMENT

The animal study was reviewed and approved by the Ethics Committee and Experimental Animal Committee of Shenyang Agriculture University. Written informed consent was obtained from the owners for the participation of their animals in this study.

AUTHOR CONTRIBUTIONS

SZha conceived the study. BL, CF, SZhu, JZ, and XZ conducted the experiments. ZW analyzed the data. BL wrote the manuscript. DI revised the manuscript. All authors contributed to the article and approved the submitted version.

FUNDING

This work was supported by the grants from the Educational Department of Liaoning Province (Climbing Scholar), the Organization Department of Liaoning Provincial Committee of China (No. XLYC1907018), and the Shenyang Agricultural University Research Start-up Funding (No. 880418062).

SUPPLEMENTARY MATERIAL

The Supplementary Material for this article can be found online at: https://www.frontiersin.org/articles/10.3389/fgene.2020.587559/full#supplementary-material

REFERENCES

Arner, P., and Kulyte, A. (2015). MicroRNA regulatory networks in human adipose tissue and obesity. *Nat. Rev. Endocrinol.* 11, 276–288. doi: 10.1038/nrendo.2015.25

Ashwal-Fluss, R., Meyer, M., Pamudurti, N. R., Ivanov, A., Bartok, O., Hanan, M., et al. (2014). circRNA biogenesis competes with pre-mRNA splicing. *Mol. Cell.* 56, 55–66. doi: 10.1016/j.molcel.2014.08.019

Bahelka, I., Oravcova, M., Peskovicova, D., Tomka, J., Hanusova, E., Lahucky, R., et al. (2009). Comparison of accuracy of intramuscular fat prediction in live pigs using five different ultrasound intensity levels. *Animal* 3, 1205–1211. doi: 10.1017/S1751731109004480

Cao, Z. B., Gao, D., Xu, T. T., Zhang, L., Tong, X., Zhang, D. D., et al. (2019). Circular RNA profiling in the oocyte and cumulus cells reveals that circARMC4 is essential for porcine oocyte maturation. *Aging Us* 11, 8015–8034. doi: 10.18632/aging.102315

Chen, B., Yu, J., Guo, L., Byers, M. S., Wang, Z., Chen, X., et al. (2019). Circular RNA circHIPK3 promotes the proliferation and differentiation of chicken myoblast cells by sponging miR-30a-3p. *Cells* 8:177. doi: 10.3390/cells8020177

Chen, L. L. (2020). The expanding regulatory mechanisms and cellular functions of circular RNAs. *Nat. Rev. Mol. Cell. Biol.* 21, 475-490. doi: 10.1038/s41580-020-0243-y

Cheng, Z., Yu, C., Cui, S., Wang, H., Jin, H., Wang, C., et al. (2019). circTP63 functions as a ceRNA to promote lung squamous cell carcinoma progression by upregulating FOXM1. *Nat. Commun.* 10:3200. doi: 10.1038/s41467-019-11162-4

Cho, I. C., Park, H. B., Ahn, J. S., Han, S. H., Lee, J. B., Lim, H. T., et al. (2019). A functional regulatory variant of MYH3 influences muscle fiber-type composition and intramuscular fat content in pigs. *PLoS Genet.* 15:e1008279. doi: 10.1371/journal.pgen.1008279

De Palo, P., Maggiolino, A., Milella, P., Centoducati, N., Papaleo, A., and Tateo, A. (2016). Artificial suckling in Martina Franca donkey foals: effect on in vivo performances and carcass composition. *Trop. Anim. Health Prod.* 48, 167–173. doi: 10.1007/s11250-015-0940-2

Devaux, Y., Creemers, E. E., Boon, R. A., Werfel, S., Thum, T., Engelhardt, S., et al. (2017). Circular RNAs in heart failure. *Eur. J. Heart Fail.* 19, 701–709. doi: 10.1002/ejhf.801

Dong, Y. P., He, D., Peng, Z. Z., Peng, W., Shi, W. W., Wang, J., et al. (2017). Circular RNAs in cancer: an emerging key player. *J. Hematol. Oncol.* 10:2. doi: 10.1186/s13045-016-0370-2

Du, J., Xu, Y., Zhang, P., Zhao, X., Gan, M., Li, Q., et al. (2018). MicroRNA-125a-5p affects adipocytes proliferation, differentiation and fatty acid composition of porcine intramuscular fat. *Int. J. Mol. Sci.* 19:501. doi: 10.3390/ijms19020501

Gao, Y., Wang, Y., Chen, X., Peng, Y., Chen, F., He, Y., et al. (2019). MiR-127 attenuates adipogenesis by targeting MAPK4 and HOXC6 in porcine adipocytes. *J. Cell. Physiol.* 234, 21838–21850. doi: 10.1002/jcp.28660

Gao, Y., Zhang, J., and Zhao, F. (2018). Circular RNA identification based on multiple seed matching. *Brief. Bioinform.* 19, 803–810. doi: 10.1093/bib/bbx014

Guo, Y., Chen, Y., Zhang, Y., Zhang, Y., Chen, L., and Mo, D. (2012). Up-regulated miR-145 expression inhibits porcine preadipocytes differentiation by targeting IRS1. *Int. J. Biol. Sci.* 8, 1408–1417. doi: 10.7150/ijbs.4597

Hocquette, J. F., Gondret, F., Baeza, E., Medale, F., Jurie, C., and Pethick, D. W. (2010). Intramuscular fat content in meat-producing animals: development, genetic and nutritional control, and identification of putative markers. *Animal* 4, 303–319. doi: 10.1017/S1751731109991091

Hong, L., Gu, T., He, Y., Zhou, C., Hu, Q., Wang, X., et al. (2019). Genome-wide analysis of circular RNAs mediated ceRNA regulation in porcine embryonic muscle development. *Front. Cell. Dev. Biol.* 7:289. doi: 10.3389/fcell.2019.00289

Huang, R., Zhang, Y., Han, B., Bai, Y., Zhou, R., Gan, G., et al. (2017). Circular RNA HIPK2 regulates astrocyte activation via cooperation of autophagy and ER stress by targeting MIR124-2HG. *Autophagy* 13, 1722–1741. doi: 10.1080/15548627.2017.1356975

Jeong, B. C., Kang, I. H., and Koh, J. T. (2014). MicroRNA-302a inhibits adipogenesis by suppressing peroxisome proliferator-activated receptor gamma expression. *FEBS Lett.* 588, 3427–3434. doi: 10.1016/j.febslet.2014.07.035

Jiang, R., Li, H., Yang, J., Shen, X., Song, C., Yang, Z., et al. (2020). circRNA profiling reveals an abundant circFUT10 that promotes adipocyte proliferation and inhibits adipocyte differentiation via sponging let-7. *Mol. Ther. Nucleic Acids* 20, 491–501. doi: 10.1016/j.omtn.2020.03.011

John, B., Enright, A. J., Aravin, A., Tuschl, T., Sander, C., and Marks, D. S. (2004). Human MicroRNA targets. *PLoS Biol.* 2:e363. doi: 10.1371/journal.pbio.0020363

Lakisic, G., Lebreton, A., Pourpre, R., Wendling, O., Libertini, E., Radford, E. J., et al. (2016). Role of the BAHD1 chromatin-repressive complex in placental development and regulation of steroid metabolism. *PLoS Genet.* 12:e1005898. doi: 10.1371/journal.pgen.1005898

Lee, J., Saha, P. K., Yang, Q. H., Lee, S., Park, J. Y., Suh, Y., et al. (2008). Targeted inactivation of MLL3 histone H3-Lys-4 methyltransferase activity in the mouse reveals vital roles for MLL3 in adipogenesis. *Proc. Natl. Acad. Sci. U.S.A.* 105, 19229–19234. doi: 10.1073/pnas.0810100105

Lee, J. E., Cho, Y. W., Deng, C. X., and Ge, K. (2020). MLL3/MLL4-associated PAGR1 regulates adipogenesis by controlling induction of C/EBPbeta and C/EBPdelta. *Mol. Cell. Biol.* 40:e00209-20. doi: 10.1128/MCB.00209-20

Legnini, I., Di Timoteo, G., Rossi, F., Morlando, M., Briganti, F., Sthandier, O., et al. (2017). Circ-ZNF609 is a circular RNA that can be translated and functions in myogenesis. *Mol. Cell.* 66, 22–26. doi: 10.1016/j.molcel.2017.02.017

Li, B., Weng, Q., Dong, C., Zhang, Z., Li, R., Liu, J., et al. (2018). A key gene, PLIN1, can affect porcine intramuscular fat content based on transcriptome analysis. *Genes* 9:194. doi: 10.3390/genes9040194

Li, B., Yin, D., Li, P., Zhang, Z., Zhang, X., Li, H., et al. (2020). Profiling and functional analysis of circular RNAs in porcine fast and slow muscles. *Front. Cell. Dev. Biol.* 8:322. doi: 10.3389/fcell.2020.00322

Li, F., Li, D., Zhang, M., Sun, J., Li, W., Jiang, R., et al. (2019). miRNA-223 targets the GPAM gene and regulates the differentiation of intramuscular adipocytes. *Gene* 685, 106–113. doi: 10.1016/j.gene.2018.10.054

Li, H., and Durbin, R. (2009). Fast and accurate short read alignment with burrows-wheeler transform. *Bioinformatics* 25, 1754–1760. doi: 10.1093/bioinformatics/btp324

Li, H., Wei, X. F., Yang, J. M., Dong, D., Hao, D., Huang, Y. Z., et al. (2018). circFGFR4 Promotes Differentiation of Myoblasts via Binding miR-107 to Relieve Its Inhibition of Wnt3a. *Mol. Ther. Nucleic Acids* 11, 272–283. doi: 10.1016/j.omtn.2018.02.012

Li, S., Ma, Y., Tan, Y., Ma, X., Zhao, M., Chen, B., et al. (2018). Profiling and functional analysis of circular RNAs in acute promyelocytic leukemia and their dynamic regulation during all-trans retinoic acid treatment. *Cell Death Dis.* 9:651. doi: 10.1038/s41419-018-0699-2

Li, X. Y., Li, C. Y., Wei, J. C., Ni, W., Xu, Y. R., Yao, R., et al. (2019). Comprehensive expression profiling analysis of pituitary indicates that circRNA participates in the regulation of sheep estrus. *Genes* 10:90. doi: 10.3390/genes10020090

Li, X., Yang, L., and Chen, L. L. (2018). The biogenesis, functions, and challenges of circular RNAs. *Mol. Cell.* 71, 428–442. doi: 10.1016/j.molcel.2018.06.034

Liang, G., Yang, Y., Niu, G., Tang, Z., and Li, K. (2017). Genome-wide profiling of *Sus scrofa* circular RNAs across nine organs and three developmental stages. *DNA Res.* 24, 523–535. doi: 10.1093/dnares/dsx022

Liu, X., Liu, K. Q., Shan, B. S., Wei, S. J., Li, D. F., Han, H. Y., et al. (2018). A genome-wide landscape of mRNAs, lncRNAs, and circRNAs during subcutaneous adipogenesis in pigs. *J. Anim. Sci. Biotechnol.* 9:76. doi: 10.1186/s40104-018-0292-7

Lorenzo, J. M., Sarries, M. V., Tateo, A., Polidori, P., Franco, D., and Lanza, M. (2014). Carcass characteristics, meat quality and nutritional value of horsemeat: a review. *Meat Sci.* 96, 1478–1488. doi: 10.1016/j.meatsci.2013.12.006

Love, M. I., Huber, W., and Anders, S. (2014). Moderated estimation of fold change and dispersion for RNA-seq data with DESeq2. *Genome Biol.* 15:550. doi: 10.1186/s13059-014-0550-8

Madeira, M. S., Costa, P., Alfaia, C. M., Lopes, P. A., Bessa, R. J., Lemos, J. P., et al. (2013). The increased intramuscular fat promoted by dietary lysine restriction in lean but not in fatty pig genotypes improves pork sensory attributes. *J. Anim. Sci.* 91, 3177–3187. doi: 10.2527/jas.2012-5424

Nogi, T., Honda, T., Mukai, F., Okagaki, T., and Oyama, K. (2011). Heritabilities and genetic correlations of fatty acid compositions in longissimus muscle lipid with carcass traits in Japanese Black cattle. *J. Anim. Sci.* 89, 615–621. doi: 10.2527/jas.2009-2300

Ouyang, H., Chen, X., Wang, Z., Yu, J., Jia, X., Li, Z., et al. (2017). Circular RNAs are abundant and dynamically expressed during embryonic muscle development in chickens. *DNA Res.* 25, 71–86. doi: 10.1093/dnares/dsx039

Pena, R. N., Ros-Freixedes, R., Tor, M., and Estany, J. (2016). Genetic marker discovery in complex traits: a field example on fat content and composition in pigs. *Int. J. Mol. Sci.* 17:2100. doi: 10.3390/ijms17122100

Peng, Y., Chen, F. F., Ge, J., Zhu, J. Y., Shi, X. E., Li, X., et al. (2016). miR-429 inhibits differentiation and promotes proliferation in porcine preadipocytes. *Int. J. Mol. Sci.* 17:2047. doi: 10.3390/ijms17122047

Polidori, P., Pucciarelli, S., Ariani, A., Polzonetti, V., and Vincenzetti, S. (2015). A comparison of the carcass and meat quality of Martina Franca donkey foals aged 8 or 12 months. *Meat Sci.* 106, 6–10. doi: 10.1016/j.meatsci.2015.03.018

Polidori, P., Vincenzetti, S., Cavallucci, C., and Beghelli, D. (2008). Quality of donkey meat and carcass characteristics. *Meat Sci.* 80, 1222–1224. doi: 10.1016/j.meatsci.2008.05.027

Rybak-Wolf, A., Stottmeister, C., Glazar, P., Jens, M., Pino, N., Giusti, S., et al. (2015). Circular RNAs in the mammalian brain are highly abundant, conserved, and dynamically expressed. *Mol. Cell* 58, 870–885. doi: 10.1016/j.molcel.2015.03.027

Shannon, P., Markiel, A., Ozier, O., Baliga, N. S., Wang, J. T., Ramage, D., et al. (2003). Cytoscape: a software environment for integrated models of biomolecular interaction networks. *Genome Res.* 13, 2498–2504. doi: 10.1101/gr.1239303

Shen, L., Li, Q., Wang, J., Zhao, Y., Niu, L., Bai, L., et al. (2018). miR-144-3p Promotes Adipogenesis Through Releasing C/EBPalpha From Klf3 and CtBP2. *Front. Genet.* 9:677. doi: 10.3389/fgene.2018.00677

Shen, X., Liu, Z., Cao, X., He, H., Han, S., Chen, Y., et al. (2019). Circular RNA profiling identified an abundant circular RNA circTMTC1 that inhibits chicken skeletal muscle satellite cell differentiation by sponging miR-128-3p. *Int. J. Biol. Sci.* 15, 2265–2281. doi: 10.7150/ijbs.36412

Shi, X. E., Li, Y. F., Jia, L., Ji, H. L., Song, Z. Y., Cheng, J., et al. (2014). MicroRNA-199a-5p affects porcine preadipocyte proliferation and differentiation. *Int. J. Mol. Sci.* 15, 8526–8538. doi: 10.3390/ijms15058526

Singh, V. K., Mangalam, A. K., Dwivedi, S., and Naik, S. (1998). Primer premier: program for design of degenerate primers from a protein sequence. *Biotechniques* 24, 318–319. doi: 10.2144/98242pf02

Sun, J., Xie, M., Huang, Z., Li, H., Chen, T., Sun, R., et al. (2017). Integrated analysis of non-coding RNA and mRNA expression profiles of 2 pig breeds differing in muscle traits. *J. Anim. Sci.* 95, 1092–1103. doi: 10.2527/jas.2016.0867

Sun, L. F., Zhang, B., Chen, X. J., Wang, X. Y., Zhang, B. W., Ji, Y. Y., et al. (2019). Circular RNAs in human and vertebrate neural retinas. *RNA Biol.* 16, 821–829. doi: 10.1080/15476286.2019.1591034

Tian, J., Fu, Y., Li, Q., Xu, Y., Xi, X., Zheng, Y., et al. (2020). Differential expression and bioinformatics analysis of CircRNA in PDGF-BB-induced vascular smooth muscle cells. *Front. Genet.* 11:530. doi: 10.3389/fgene.2020.00530

Wang, H., Zhong, J., Zhang, C., Chai, Z., Cao, H., Wang, J., et al. (2020). The whole-transcriptome landscape of muscle and adipose tissues reveals the ceRNA regulation network related to intramuscular fat deposition in yak. *BMC Genomics* 21:347. doi: 10.1186/s12864-020-6757-z

Wei, X. F., Li, H., Yang, J. M., Hao, D., Dong, D., Huang, Y. Z., et al. (2017). Circular RNA profiling reveals an abundant circLMO7 that regulates myoblasts differentiation and survival by sponging miR-378a-3p. *Cell Death Dis.* 8:e3153. doi: 10.1038/cddis.2017.541

Wu, J., Mao, X., Cai, T., Luo, J., and Wei, L. (2006). KOBAS server: a web-based platform for automated annotation and pathway identification. *Nucleic Acids Res.* 34, W720–W724. doi: 10.1093/nar/gkl167

Wu, W., Ji, P., and Zhao, F. (2020). CircAtlas: an integrated resource of one million highly accurate circular RNAs from 1070 vertebrate transcriptomes. *Genome Biol.* 21:101. doi: 10.1186/s13059-020-02018-y

Xia, X., Yu, J., Zhao, X., Yao, Y., Zeng, L., Ahmed, Z., et al. (2019). Genetic diversity and maternal origin of Northeast African and South American donkey populations. *Anim. Genet.* 50, 266–270. doi: 10.1111/age.12774

Xie, M., Yu, T., Jing, X., Ma, L., Fan, Y., Yang, F., et al. (2020). Exosomal circSHKBP1 promotes gastric cancer progression via regulating the miR-582-3p/HUR/VEGF axis and suppressing HSP90 degradation. *Mol. Cancer* 19:112. doi: 10.1186/s12943-020-01208-3

Yadav, H., Quijano, C., Kamaraju, A. K., Gavrilova, O., Malek, R., Chen, W., et al. (2011). Protection from obesity and diabetes by blockade of TGF-beta/Smad3 signaling. *Cell. Metab.* 14, 67–79. doi: 10.1016/j.cmet.2011.04.013

Yu, G., Wang, L. G., Han, Y., and He, Q. Y. (2012). clusterProfiler: an R package for comparing biological themes among gene clusters. *OMICS* 16, 284–287. doi: 10.1089/omi.2011.0118

Zhang, G., Diao, S., Zhang, T., Chen, D., He, C., and Zhang, J. (2019). Identification and characterization of circular RNAs during the sea buckthorn fruit development. *RNA Biol.* 16, 354–361. doi: 10.1080/15476286.2019.1574162

Zhang, H. M., Xia, H. L., Jiang, H. R., Mao, Y. J., Qu, K. X., Huang, B. Z., et al. (2018). Longissimus dorsi muscle transcriptomic analysis of Yunling and Chinese simmental cattle differing in intramuscular fat content and fatty acid composition. *Genome* 61, 549–558. doi: 10.1139/gen-2017-0164

Zhang, M., Han, Y., Zhai, Y., Ma, X., An, X., Zhang, S., et al. (2020). Integrative analysis of circRNAs, miRNAs, and mRNAs profiles to reveal ceRNAs networks in chicken intramuscular and abdominal adipogenesis. *BMC Genomics* 21:594. doi: 10.1186/s12864-020-07000-3

Zhang, P., Chao, Z., Zhang, R., Ding, R., Wang, Y., Wu, W., et al. (2019). Circular RNA regulation of myogenesis. *Cells* 8:885. doi: 10.3390/cells8080885

Zhang, X. O., Wang, H. B., Zhang, Y., Lu, X., Chen, L. L., and Yang, L. (2014). Complementary sequence-mediated exon circularization. *Cell* 159, 134–147. doi: 10.1016/j.cell.2014.09.001

Zhang, X., Li, H., Yu, J., Zhou, X., Ji, C., Wu, S., et al. (2019). Label-free based comparative proteomic analysis of whey proteins between different milk yields of Dezhou donkey. *Biochem. Biophys. Res. Commun.* 508, 237–242. doi: 10.1016/j.bbrc.2018.11.130

Zhang, Y., Wang, Y., Wang, H., Ma, X., and Zan, L. (2019). MicroRNA-224 impairs adipogenic differentiation of bovine preadipocytes by targeting LPL. *Mol. Cell. Probes* 44, 29–36. doi: 10.1016/j.mcp.2019.01.005

Zhang, Z., Gao, Y., Xu, M. Q., Wang, C. J., Fu, X. H., Liu, J. B., et al. (2019). miR-181a regulate porcine preadipocyte differentiation by targeting TGFBR1. *Gene* 681, 45–51. doi: 10.1016/j.gene.2018.09.046

Zou, C., Li, L., Cheng, X., Li, C., Fu, Y., Fang, C., et al. (2018). Identification and functional analysis of long intergenic non-coding RNAs underlying intramuscular fat content in pigs. *Front. Genet.* 9:102. doi: 10.3389/fgene.2018.00102

Conflict of Interest: The authors declare that the research was conducted in the absence of any commercial or financial relationships that could be construed as a potential conflict of interest.

frontiers in Veterinary Science

ORIGINAL RESEARCH
published: 29 March 2021
doi: 10.3389/fvets.2021.611153

Are Marbling and the Prediction of Beef Eating Quality Affected by Different Grading Sites?

Jingjing Liu[1], *Grzegorz Pogorzelski*[2], *Alix Neveu*[3], *Isabelle Legrand*[4], *David Pethick*[5], *Marie-Pierre Ellies-Oury*[1,6] *and Jean-François Hocquette*[1]*

[1] *INRAE, Université Clermont Auvergne, VetAgro Sup, UMR1213, Recherches sur les Herbivores, Clermont-Ferrand, France,* [2] *Department of Technique and Food Development, Faculty of Human Nutrition and Consumer Sciences, Warsaw University of Life Sciences (WULS-SGGW), Warsaw, Poland,* [3] *École Nationale Supérieure Agronomique de Toulouse, Toulouse, France,* [4] *Institut de l'Elevage, Service Qualité des Carcasses et des Viandes, MRA-NA, Limoges, France,* [5] *School of Veterinary and Life Sciences, Murdoch University, Perth, WA, Australia,* [6] *Bordeaux Sciences Agro, Bordeaux, France*

For the European abattoirs, the preferred carcass grading site is at the fifth rib, and cutting at the tenth rib as in Australia could lead to a lower economic value of the carcass. Therefore, the objective of this study was to compare the grading scores of marbling and the meat and fat color on *Musculus longissimus thoracis et lumborum* (LTL) at the fifth and the tenth thoracic vertebrae. The consequences on the prediction of beef eating quality using the Meat Standards Australia (MSA) grading scheme were also evaluated for cull cows, which produce the majority of beef consumed in France. Carcasses from 208 French cattle, mainly Limousine cows, were graded according to the Australian Beef Carcase Chiller Assessment System (ABCAS) used for the implementation of the MSA system. The results indicate that there was no significant difference in the marbling score, between the fifth and the tenth ribs and hence in the MSA index and in the Global Quality [meat quality (MQ4)] scores calculated from marbling values from either the fifth rib or the tenth rib. However, the meat color at the tenth rib was significantly darker than that at the fifth rib ($p < 0.01$), and the fat color at the tenth rib was significantly yellower than that at the fifth rib ($p < 0.001$). The results of this study suggest that the grading of marbling can be conducted on *M.* LTL at the fifth thoracic vertebrae for routine use of the MSA system in France and, more generally, in Europe. However, further investigation and adjustment would be needed for other critical MSA scores (such as rib fat thickness) while respecting the European carcass quartering practices.

Keywords: marbling, meat color, fat color, grading site, beef carcass, Meat Standards Australia (MSA) grading scheme

OPEN ACCESS

Edited by:
Xiao Li,
Northwest a and F University, China

Reviewed by:
Marjeta Candek-Potokar,
Agricultural Institute of Slovenia, Slovenia
Xin Luo,
Shandong Agricultural University, China

***Correspondence:**
Jean-François Hocquette
jean-francois.hocquette@inrae.fr

Specialty section:
This article was submitted to Livestock Genomics, a section of the journal Frontiers in Veterinary Science

Received: *28 September 2020*
Accepted: *08 February 2021*
Published: *29 March 2021*

Citation:
Liu J, Pogorzelski G, Neveu A, Legrand I, Pethick D, Ellies-Oury M-P and Hocquette J-F (2021) Are Marbling and the Prediction of Beef Eating Quality Affected by Different Grading Sites? Front. Vet. Sci. 8:611153. doi: 10.3389/fvets.2021.611153

INTRODUCTION

A regular decline in beef consumption has become a big challenge for the European beef industry (1). France, the largest beef producer in Europe, has also experienced a decreasing trend in beef consumption (2). However, despite the declining consumption, FranceAgriMer (3) reported that the household interest in premium beef was growing. Ellies-Oury et al. (4) also demonstrated that an eating quality guarantee scheme would be of interest to French consumers.

To date, the most advanced beef grading scheme is probably the Meat Standards Australia (MSA) system, which has been known as the most well-established beef eating quality guarantee

system (1). The aim of the MSA grading system is to ensure that, when consumers purchase a cut of beef, it will have the eating quality promised by the MSA label when it is cooked according to the recommended method (5). The meat quality (MQ4) score was developed to rank the potential eating quality of individual muscle cuts, and the MSA index is used to assess the average eating quality across the whole beef carcass (6).

In France, where 61% of the beef consumption originates from cull cows (7), the "Label Rouge" quality sign has been used to ensure the eating quality of cuts for the consumer, especially for beef produced from the late-maturing breeds (such as Charolais or Limousine breeds). Recently within the framework of the French national food conference (8), the French meat sector represented by Interbev decided to increase the proportion of labeled beef using the "Label Rouge" and other quality signs. The purpose is to assist consumers to make purchase decisions with reliable label guidance (4), which is consistent with the aim of the MSA grading scheme. Indeed, the latter is a reliable description system of eating quality that could form a basis for retail pricing and generate product confidence for consumers (9).

Subsequently, several research efforts have been conducted in Europe to disseminate the MSA methodology as a reference (10–12) under the auspices of the United Nations Economic Commission for Europe (UNECE) (13). Being one of the critical steps in the MSA system, carcass grading parameters contribute to the basis of the beef palatability prediction model (14). Carcass grading is performed under the guidance of the Australian Beef Carcase Chiller Assessment System (ABCAS). According to ABCAS, marbling, meat color, and fat color can be assessed on *Musculus longissimus thoracis et lumborum* (LTL) at any ribbing site from the fifth to the thirteenth rib (15) for cattle routinely slaughtered in Australia, most of which are young steers and heifers. This type of research is still lacking with regard to old cows and/or mainly late-maturing breeds for any potential application of the MSA in the European countries, particularly France.

In general, the most common grading site used by abattoirs in Australia is from the tenth rib to the twelfth rib (16). In contrast, in the European system, quarter carcasses are sometimes sold to the market without further processing. Consequently, the quartering site in most cases is at the fifth thoracic vertebrae, and so the cutting at the tenth thoracic vertebrae would often negatively influence the economic value of the hindquarters.

Thus, the present study aimed to investigate any difference in LT marbling scores, which were collected according to the ABCAS procedure between the fifth and the tenth thoracic vertebrae along with the meat color and the fat color. The potential impact of the different grading sites on the prediction of beef eating quality (through MQ4 scores for each cut and the MSA index for the whole carcass) was also examined. To complete the previous research with young animals from early-maturing breeds (15), this study was mainly conducted with cull cows (which are the major source of beef in France and, thus, have a strong economic significance) from a famous and highly distributed late-maturing breed (the Limousine), producing beef that were already commercialized with the "Label Rouge" quality sign.

MATERIALS AND METHODS

Animals and Experimental Design

The data used in this study were from 208 carcasses (including 157 Limousine breeds) provided by a commercial slaughterhouse in Limoges, France. All carcasses were assessed 24 h after *post-mortem*. Carcasses were graded by using a single MSA-accredited grader for at least 20 min after the cutting to allow the meat to bloom. Assessments, primarily at the tenth rib site and the secondarily at the fifth rib site, were carried out by using the same grader, who is highly experienced with carcass grading according to ABCAS specifications. He is also an official grading trainer recognized by AUS-MEAT. The conditions of the carcass and the environment, including ribbing height and angle and grading practices, such as light angle, are consistent for all assessments conducted at the two rib sites. For the experiment, the AUS-MEAT marbling, MSA marbling, meat color, and fat color were assessed at the fifth and the tenth rib of the same half carcasses (16). The basic information of the current samples is presented in **Table 1**. European conformation and fat scores were both converted into a continuous 15-point scale as described in the previous study (17).

Data Collection

All assessments were conducted by following the specifications of the ABCAS and the AUS-MEAT Reference Standards, which include the ossification score at the carcass level, as well as the assessment of marbling, meat color, and fat color on *M.* LTL.

The AUS-MEAT marbling score reflects the number of marbling, ranging from 0 to 9 in increments of one. The MSA marbling score is used to provide a more precise marbling scale in comparison to the AUS-MEAT and is based on the United States Department of Agriculture system (18): it provides scores ranging from 100 to 1,190 in increments of 10. The MSA marbling score indicates not only the amount of marbling but also the size, fineness, and distribution of fat inclusions in muscles (19).

The fat and meat colors are scored according to the AUS-MEAT scale. Fat color is from 0 to 9. Meat color is from 1A, 1B, 1C, and then from 2 to 7 (which was converted into the following scale in this study: 1, 1.33, 1.66, 2 to 7).

Prediction of MQ4 Scores and the MSA Index

The MSA grading scheme allows the calculation or the prediction of a single palatability or MQ4 score that describes the complete eating experience of a consumer. It is defined as the combination of four sensory traits, namely tenderness, juiciness, flavor liking, and overall liking (20).

The MSA prediction model allows the prediction of MQ4 scores of individual muscles from the carcass for a range of aging time, hanging method, or cooking techniques using a multiple regression approach. The parameters used to predict MQ4 include, among others, animal sex, carcass weight, hanging technique, hump height, ossification score, marbling score, rib fat depth, ultimate pH, and days aged (20). In this study, MQ4 scores were predicted for three cuts [called CUB045 [*M. longissimus*

TABLE 1 | Number, mean, SD, minimum, and maximum values for the basic carcass traits.

	n	Mean	SD	Min	Max
Age (days)	204	3,458	1,835	228	7,422
Carcass weight (kg)	204	356.5	95.8	126.8	729.7
Ultimate pH	198	5.7	0.16	5.3	6.3
Ossification score	185	480	160.8	100	590
European conformation score[a]	204	8.7 (*R* =)	3.1	1	13
European fat score[b]	204	7.0 (3-)	1.00	3	9
Hump height (cm)	204	6.9	2.5	3.5	18

[a]*European conformation score converted from P (–/=/+), O (–/=/+), R (–/=/+), U (–/=/+), and E (–/=/+) to 1–15;* [b]*European fat score converted from 1 (–/=/+), 2 (–/=/+), 3 (–/=/+), 4 (–/=/+), and 5 (–/=/+) to 1–15.*

thoracis (LT)], STA045, and STP045 (*M.* LTL) in the MSA grading scheme] that represent different portions of *M.* LTL, where the marbling scores have been recorded. All carcasses were assumed to be Achilles hung (the most common method) and the cuts were assumed to be aged for 10 days and grilled. The prediction of MQ4 scores was made twice for each cut with the same inputs except for marbling scores, which were recorded either at the fifth rib or at the tenth rib, the predictions were made using the SP2009 version of the MSA model.

Then, the MSA index was predicted at the carcass level using the same inputs. The MSA index corresponds, by definition, to the sum of the predicted MQ4 scores of all MSA cuts, the weight of each was calculated as the percentage of the total weight of the MSA cuts in the carcass. To enable a standardized index reporting, inputs are standardized for the calculation of the MSA index: all carcasses are assumed to be Achilles hung (the most common method), and all cuts are assumed to be aged for 5 days and cooked according to the most common cooking method for each cut (6). In this study, the MSA index was predicted twice with the same inputs except for marbling scores, with values recorded either at the fifth rib or at the tenth rib; the predicted outputs are with respect to the aging times of 10 and 20 days, the cooking methods of grill and roast, and the hanging methods of tenderstretch and Achilles tendon.

Overall, the MQ4 scores and the MSA index for 164 carcasses were predicted in total due to some missing data. A precise description and visual support of the MSA methodology and the prediction of MQ4 (MQ4 scores and MSA Index) are indicated in the study of McGilchrist et al. (6), Polkinghorne et al. (14), and Bonny et al. (20).

Statistical Analysis

All statistical analyses were performed by using the R software (version 3.5.2). Significant differences between means of raw data, MQ4 scores, and the MSA index for the two grading sites were determined by using an ANOVA with "aov" function.

A Pearson's correlation analysis of raw data, MQ4 scores, and the MSA index were performed by using "stat_cor" and "pairs. panels" functions to determine correlation coefficients between the carcass characteristics at both the sites (fifth and tenth ribs).

Linear regression models for MQ4 scores using two sets of marbling scores from the fifth rib and the tenth rib were done by using "lm" (linear model) function.

Scatter plots were made by using "ggscatter" function with "add reg.line" and "stat_cor".

RESULTS

Grading Scores, Predicted MQ4 Scores, and MSA Index

Grading scores of the AUS-MEAT marbling, MSA marbling, meat color, and fat color which were assessed on the LT muscle at the fifth rib and the tenth rib are presented in **Table 2**. There were no significant differences between the values of AUS-MEAT and the MSA marbling scores at two different locations. In contrast to marbling, there were significant differences in the meat and the fat color between the fifth rib and the tenth rib. The meat color at the tenth rib was significantly darker than that at the fifth rib ($p < 0.01$). The fat color at the tenth rib was significantly yellower than that at the fifth rib ($p < 0.001$) (**Table 2**).

In addition to the marbling scores, no significant difference was observed between the fifth rib and the tenth rib for the predicted MQ4 scores of three muscle cuts, namely *M.* LT, *M.* LTL at the anterior striploin piece, and *M.* LTL at the posterior striploin piece (**Table 2**). Similarly, no significant difference was observed for the predicted MSA scores for other cuts (**Table 2**), as well as for the MSA index calculated from the MQ4 of the different cuts of the carcass (**Table 2**).

Correlations Between Carcass Characteristics and Grading Scores at the Two Grading Sites

Table 3 presents the correlations between the ossification score (which reflects animal maturity) and the ribeye assessment scores (AUS-MEAT marbling, MSA marbling, meat color, and fat color) either at the fifth rib or at the tenth rib.

Strong relationships for the marbling score were observed either for AUS-MEAT measurements and MSA measurements. Indeed, the correlation coefficients between the fifth rib and the tenth rib range from 0.74 to 0.91 ($p < 0.001$).

Furthermore, there was a moderate correlation for the meat color between the fifth rib and the tenth rib ($r = 0.43$, $p < 0.001$). A significant correlation for fat color between the fifth rib and the tenth rib was also observed ($r = 0.70$, $p < 0.001$). In addition, the ossification score had a significant and positive correlation

TABLE 2 | Number, mean, minimum, maximum scores, SEM of marbling, meat color, and fat color scores determined at the fifth and the tenth ribs.

	5th rib				10th rib					
	n	Mean	Min	Max	*n*	Mean	Min	Max	SEM	*P*-value
AUS MB[1]	208	0.7	0	5	207	0.7	0	4	0.06	0.95
MSA MB[2]	208	288	100	750	207	291	100	680	7.2	0.73
Meat color	208	2.5[b]	1B	6	208	2.9[a]	1B	7	0.07	0.003
Fat color	197	2.5[b]	0	6	196	3.5[a]	0	9	0.11	<0.001
MQ4 CUB045[3]	164	58	46	72	164	58	46	69	0.39	0.97
MQ4 STA045[4]	164	52	40	67	164	52	40	65	0.42	0.95
MQ4 STP045[5]	164	50	37	66	164	50	37	63	0.44	0.94
MQ4 OYS036[6]	164	64	57	73	164	64	57	72	0.27	0.94
MQ4 BLD096[7]	164	48	37	61	164	48	37	58	0.39	0.98
MQ4 RMP131[8]	164	46	36	58	164	46	36	57	0.39	0.92
MQ4 KNU066[9]	164	41	31	53	164	41	31	51	0.37	0.97
MQ4 OUT005[10]	164	38	28	49	164	38	28	49	0.39	0.95
MQ4 EYE075 [11]	164	37	25	54	164	37	25	51	0.47	0.99
MQ4 CHK074[12]	164	55	45	67	164	55	45	65	0.34	0.99
MSA index	164	52	43	64	164	52	42	62	0.38	0.92

[1]*AUSMB, AUS-MEAT Marbling score;* [2]*Meat Standards Australia (MSA) MB, MSA Marbling score;* [3]*Meat quality CUB045, MQ4 score of CUB045 (M. longissimus thoracis);* [4]*MQ4 STA045, MQ4 score of STA045 (M. longissimus thoracis et lumborum, anterior striploin piece);* [5]*MQ4 STP045, MQ4 score of STP045 (M. longissimus thoracis et lumborum, posterior striploin piece);* [6]*MQ4 OYS036, M. infraspinatus;* [7]*MQ4 BLD096, M. triceps brachii caput longum;* [8]*MQ4 RMP131, M. gluteus medius;* [9]*MQ4 KNU066, M. rectus femoris;* [10]*MQ4 OUT005, M. biceps femoris;* [11]*MQ4 EYE075, M. semitendinosus; and* [12]*MQ4 CHK074, M. semispinalis capitis; hang method: AT (Achilles tendon), aging time: 10 days, cooking method: grill.*

[a,b]*Within a row, means with different letters are significantly different ($p < 0.05$) between the fifth and the tenth ribs.*

TABLE 3 | Correlation coefficients (*r*) among the assessment scores at the fifth rib and the tenth rib.

	AUSMB[1] 10th	MSAMB[2] 5th	MSAMB 10th	MC[3] 5th	MC 10th	FC[4] 5th	FC 10th	OSS[5]
AUSMB 5th	0.77***	0.88***	0.74***	0.06	0.16*	−0.1	−0.2**	0.21
AUSMB 10th	1	0.75***	0.91***	0.09	0.13	−0.14	−0.2**	0.18
MSAMB 5th		1	0.79***	0.02	0.21***	−0.14	−0.19**	0.31*
MSAMB 10th			1	0.06	0.21***	−0.15*	−0.19**	0.18
MC 5th				1	0.43***	0.1	0.06	0.1
MC 10th					1	0.1	0.13	0.03
FC 5th						1	0.7***	0.39***
FC 10th							1	0.36***

[1]*AUSMB, AUS-MEAT Marbling;* [2]*MSAMB, MSA Marbling;* [3]*MC, Meat Color;* [4]*FC, Fat Color; and* [5]*OSS, Ossification.*

***, **, *indicate that correlation is significantly different at the 0.001 level ($p < 0.001$), 0.01 level ($p < 0.01$), and 0.05 level ($p < 0.05$).*

with fat color scores at both the fifth and the tenth ribs ($r = 0.39$, $r = 0.36$, $p < 0.001$). However, ossification was not significantly associated with meat color.

Relationships of the MSA Index and MQ4 Scores Predicted From Marbling Scores Between the Two Grading Sites

For further implementation of the MSA grading scheme based on the grading at the fifth rib, it is crucial to determine the strength of the relationships between the MQ4 scores predicted by using the marbling score at the fifth rib or at the tenth rib. The results of the correlation analyses between the MQ4 scores for 10 cuts with 4 output combinations of the cooking method with hanging method, and with aging time are presented in **Table 4**. In addition, very small differences in the MQ4 scores between the fifth rib and the tenth rib can be observed as shown in **Table 4**. Also, the results of correlation analyses for the MSA index and the MQ4 score mainly for the three LT muscles are shown in scatter plots (**Figure 1**). Correlation coefficients were very high (from 0.88 to 0.98) and almost similar among the different output groups. For OUT005, extremely strong correlations ($r = 0.98$, $p < 0.001$) between the MQ4 scores were observed for the four groups. For CUB045, STA045, and STP045, strong and similar correlations between the MQ4 scores were observed by using the marbling inputs from either the fifth rib or the tenth rib, and with different aging times or hanging methods, the similar distribution and strong correlation for the MSA index

TABLE 4 | Pearson correlations and average differences between the MQ4 scores predicted by the marbling score assessed at the fifth rib and the tenth rib.

Cut	Cooking method: Grill				Cooking method: Roast			
	Hang method: Achilles Tendon				Aging time: 10 days			
	Aging time				Hang method			
	10 days		20 days		Achilles Tendon		Tenderstretch	
	Coefficient	Average difference (SD)	Coefficient	Average difference (SD)	Coefficient	Average difference (SD)	Coefficient	Average difference (SD)
CUB045[1]	0.91***	0.03 (2.05)	0.91***	0.03 (2.05)	0.91***	0.03 (2.05)	0.91***	0.03 (2.05)
STA045[2]	0.89***	0.07 (2.44)	0.89***	0.07 (2.44)	0.90***	0.07 (2.44)	0.89***	0.07 (2.44)
STP045[3]	0.88***	0.07 (2.67)	0.88***	0.07 (2.67)	0.89***	0.07 (2.67)	0.89***	0.07 (2.67)
OYS036[4]	0.97***	0.04 (0.77)	0.97***	0.04 (0.77)	0.97***	0.04 (0.77)	0.97***	0.04 (0.77)
BLD096[5]	0.97***	0.04 (1.15)	0.97***	0.04 (1.15)	0.97***	0.04 (1.15)	0.97***	0.04 (1.15)
RMP131[6]	0.98***	0.02 (0.76)	0.99***	0.02 (0.76)	0.99***	0.02 (0.76)	0.98***	0.02 (0.76)
KNU066[7]	0.97***	0.02 (1.14)	0.97***	0.02 (1.14)	0.97***	0.02 (1.14)	0.97***	0.02 (1.14)
OUT005[8]	0.98***	0.01 (0.98)	0.98***	0.01 (0.98)	0.98***	0.01 (0.98)	0.98***	0.01 (0.98)
EYE075[9]	0.98***	0.02 (1.14)	0.98***	0.02 (1.14)	0.98***	0.02 (1.14)	0.98***	0.02 (1.14)
CHK074[10]	0.94***	0.03 (1.52)	0.94***	0.03 (1.52)	0.93***	0.03 (1.52)	0.93***	0.03 (1.52)

[1]*CUB045, M. longissimus thoracis;* [2]*STA045, M. longissimus thoracis et lumborum. anterior striploin piece;* [3]*STP045, M. longissimus thoracis et lumborum. posterior striploin piece;* [4]*OYS036, M. infraspinatus;* [5]*BLD096, M. triceps brachii caput longum;* [6]*RMP131, M. gluteus medius;* [7]*KNU066, M. rectus femoris;* [8]*OUT005, M. biceps femoris;* [9]*EYE075, M. semitendinosus; and* [10]*CHK074, M. semispinalis capitis.*

****p < 0.001.*

MQ4 scores are indicated on a scale from 0 to 100.

and the MQ4 scores between the two grading sites can also be seen in **Figure 1**. Similarly, significantly strong relationships were observed for the MQ4 scores between the two grading sites for all other cuts with different output combinations, and the distribution and correlation are assumed to be the same strong as the three LT muscles. In addition, whereas the correlations between the two sets of MSA marbling scores was 0.79 ($p < 0.001$), there was a very significant strong correlation between the MSA indexes predicted from the marbling score of the fifth rib and the tenth rib ($r = 0.97$, $p < 0.001$) (**Figure 1**).

Linear regression was used to determine the contribution of the marbling score either from the fifth rib or from the tenth rib to explain the variability in the predicted MQ4 score. As shown in **Table 5**, for one individual cut, the MQ4 scores for the two models regressed by using the marbling score at the two grading sites are almost similar. For STA045 and STP045, the coefficients of determination ($R^2 = 0.45$, $R^2 = 0.50$) are relatively higher in comparison to other cuts, which are understandable since the marbling assessment was carried out on the *M.* LT. By contrast, a much lower R^2-value can be found for the other cuts, such as RMP131 and EYE 075 ($R^2 = 0.02$).

DISCUSSION

Marbling Scores at the Fifth and the Tenth Ribs

The marbling score was developed to estimate the intramuscular fat in the ABCAS system to be used in the MSA grading scheme with the ultimate objective to ensure the eating quality at the consumer end (20). In 2018, within the framework of the French national food conference (8), the French meat sector represented by Interbev recommended introducing the marbling score into the French beef grading scheme. As a result, the marbling assessment has been gradually introduced in one of the French local meat plants for the premium beef brand called "Or Rouge" based on the late-maturing Limousine breed. In this study, no significant difference in the marbling score was observed between the fifth rib and the tenth rib sites. In addition, the marbling scores assessed at these two sites were quite equally distributed up to 400, and higher levels were also observed. The level of marbling in French cattle is typically much lower than that in Australia (21), but the marbling level of the current sample is not very low and the marbling level between the two studied sites is indeed similar. In addition, we observed a strong relationship between the AUS-MEAT marbling score and the MSA marbling score, which suggests a strong consistency of the marbling score between the AUS-MEAT measurement and the MSA measurement [$r = 0.88$ (between MSAMB and AUSMB at the fifth rib), $r = 0.91$ (between MSAMB and AUSMB at the tenth rib)], as well as between the fifth rib and the tenth rib [$r = 0.77$ (between the AUSMB scores at the fifth and tenth ribs), $r = 0.79$ (between the MSAMB scores at the fifth and tenth ribs)]. These findings are consistent with that of Kruk et al. (22), who reported a high association between the AUS-MEAT marbling score and the MSA marbling score ($r = 0.76$). Similar to our results, Cook et al. (23) also found that the marbling scores from the thirteenth thoracic vertebrae to the fifth lumbar vertebrae were similar. Taylor and Johnson (24)

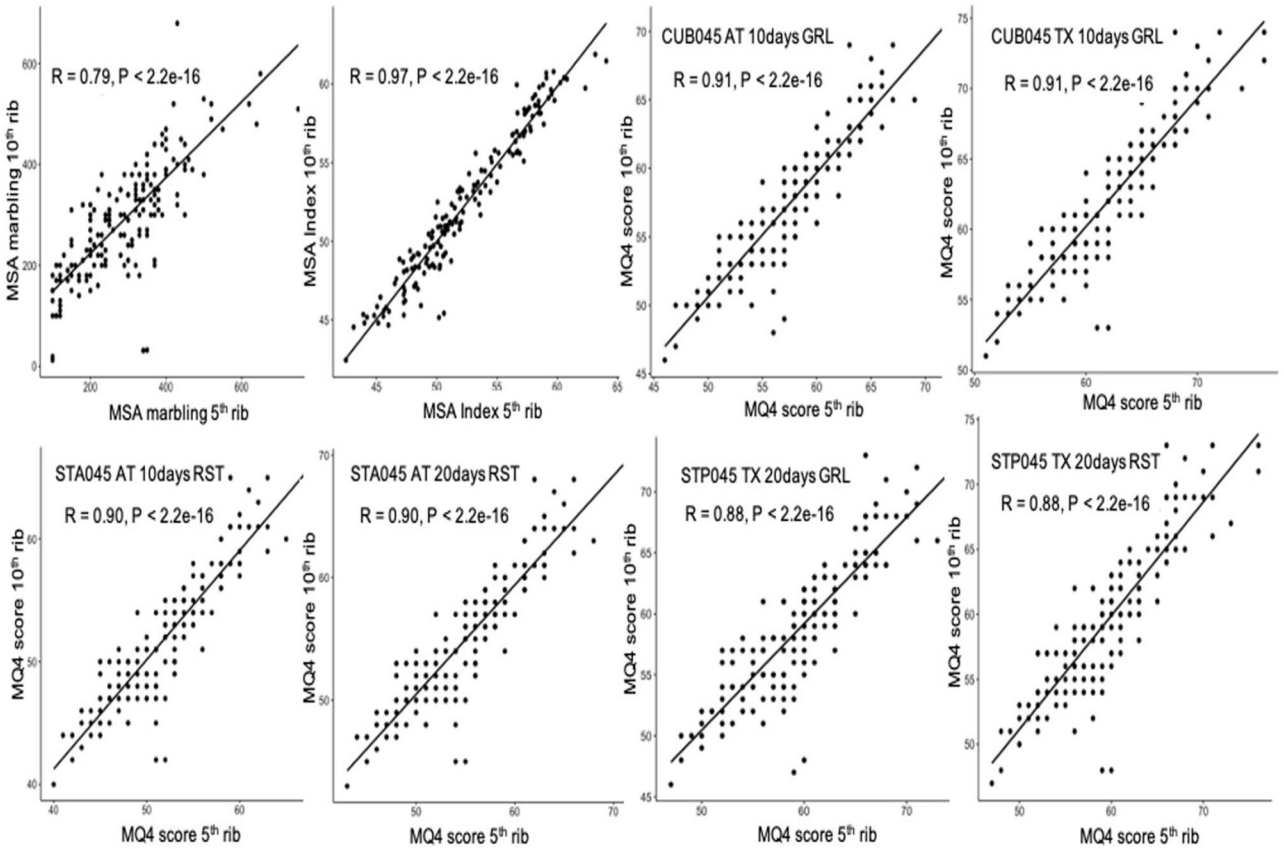

FIGURE 1 | Scatterplots of the Meat Standards Australia (MSA) index and meat quality (MQ4) scores with inputs of marbling scores from the fifth rib (x-axis) or the tenth rib (y-axis). CUB045, *M. longissimus thoracis*; STA045, *M. longissimus thoracis et lumborum*, anterior striploin piece; STP045, *M. longissimus thoracis et lumborum*, posterior striploin piece; AT, hang method—Achilles tendon; TX, hang method: tenderstretch; 10 days, 10 days aging; 20 days, 20 days aging; GRL, cooking method—grill; and RST, cooking method—roast.

TABLE 5 | Linear regression equations for indicating the MQ4 score using the marbling score assessment at the fifth rib and the tenth rib.

Cut	5^{th} rib	10^{th} rib
CUB045[1]	MQ4 score = 0.024***marbling+50.32 (R^2 = 0.37)	MQ4 score = 0.026***marbling+50.02 (R^2 = 0.37)
STA045[2]	MQ4 score = 0.028***marbling+43.08 (R^2 = 0.45)	MQ4 score = 0.031***marbling+42.51 (R^2 = 0.47)
STP045[3]	MQ4 score = 0.032***marbling+39.95 (R^2 = 0.50)	MQ4 score = 0.034***marbling+39.55 (R^2 = 0.51)
OYS036[4]	MQ4 score = 0.012***marbling+60.43 (R^2 = 0.19)	MQ4 score = 0.014***marbling+60.05 (R^2 = 0.22)
BLD096[5]	MQ4 score = 0.011***marbling+44.36 (R^2 = 0.07)	MQ4 score = 0.012***marbling+44.24 (R^2 = 0.07)
RMP131[6]	MQ4 score = 0.006***marbling+43.62 (R^2 = 0.02)	MQ4 score = 0.007***marbling+43.47 (R^2 = 0.03)
KUN066[7]	MQ4 score = 0.011***marbling+37.25 (R^2 = 0.08)	MQ4 score = 0.012***marbling+37.14 (R^2 = 0.09)
OUT005[8]	MQ4 score = 0.009***marbling+34.67 (R^2 = 0.05)	MQ4 score = 0.010***marbling+34.56 (R^2 = 0.06)
EYE075[9]	MQ4 score = 0.006***marbling+34.63 (R^2 = 0.02)	MQ4 score = 0.006***marbling+34.87 (R^2 = 0.01)
CHK074[10]	MQ4 score = 0.020***marbling+48.61 (R^2 = 0.30)	MQ4 score = 0.022***marbling+48.12 (R^2 = 0.34)

[1]*CUB045, M. longissimus thoracis;* [2]*STA045, M. longissimus thoracis et lumborum, anterior striploin piece;* [3]*STP045, M. longissimus thoracis et lumborum, posterior striploin piece;* [4]*OYS036, M. infraspinatus;* [5]*BLD096, M. triceps brachii caput longum;* [6]*RMP131, M. gluteus medius;* [7]*KNU066, M. rectus femoris;* [8]*OUT005, M. biceps femoris;* [9]*EYE075, M. semitendinosus; and* [10]*CHK074, M. semispinalis capitis.*

****p < 0.001.*

observed that the intramuscular fat content at the fifth rib was slightly higher than that at the tenth rib, whereas the marbling scores between the fifth rib and the tenth rib were almost the same. In addition, it was found that the marbling score of *M.* LT highly correlated with that of *M. longissimus lumborum* (LL) (r = 0.83) (25).

Our findings of marbling consistency between the different ribs were obtained by using the grader assessment. Indeed, when the graders score the carcasses, a small difference in marbling has been found across the different muscles and especially between STR045 and CUB045, in comparison with near infrared spectroscopy (NIR) measurements (25). Indeed, recent developments in the marbling assessment tend to use instrument-grading systems, which are likely to be more precise in comparison to human carcass graders. With this new type of technology, Acheson et al. (26) observed that the marbling score decreased from the thirteenth thoracic vertebrae to the fifth lumbar vertebrae. The contradictory results from the human graders may be due to the different marbling grading processes. In study by Acheson et al., a computer vision system, cold camera, and proprietary software were used to assess marbling, which seems to be a more objective and repeatable method in comparison to the assessment provided by the carcass grader. Nonetheless, Schulz and Sundrum (27) observed that the marbling scores at the tenth, eleventh, twelfth, and thirteenth ribs were strongly correlated ($r = 0.80–0.89$) by using a camera grading technology.

Marbling Is One of the Most Important Traits for Beef Eating Quality

Beef quality has a multifactorial determinism as shown by the various inputs in the MSA model (i.e., ossification and marbling scores, cut, aging time, hanging method, cooking method, and even use of hormone growth promoters). However, as most of these factors are fixed in this study (one aging time, one hanging method, and a limited range in the ossification score), variability in the marbling score becomes an important trait, which significantly contributes to beef eating quality.

In Europe, the main factors of carcass grading are the European conformation score and the fat score, which are compulsory (shown in **Table 1**) and therefore routinely used by the European beef industry. However, there is very poor and/or no relationship between the European classification scores and marbling, as well as with beef eating quality (28, 29). By contrast, marbling is not widely measured in Europe, particularly in France, except in some cases of "Label Rouge" animals (Label Rouge is officially a national label for food, non-food, and unprocessed agriculture products in France). In the slaughterhouse where this work was undertaken, the measurement of marbling was done for the beef premium brand of the Beauvallet Company "Or Rouge" based on the Limousine breed. Furthermore, high-marbled beef does not seem to be welcomed by the French consumers. Indeed, according to a beef consumption survey conducted in France (4), the low willingness to purchase beef for a quarter of the respondents is mainly due to their concerns of health risks caused by excess fat content, but marbling does contribute to eating quality. However, the willingness to purchase beef among French consumers decreased from 70% (before tasting) to 55% (after tasting) when beef samples were low-marbled the willingness to purchase beef among the same group of consumers increased from 30% (before tasting) to 80% (after tasting) when beef samples were high-marbled (30). This indicates that, even if a highly visible fatty meat seems unacceptable, the better eating quality of high-marbled beef could meet their eating expectations.

Most of the American and Australian consumers also prefer the visual appearance of low-marbled beef (31, 32). However, with efforts to increase the popularization of the relationships between intramuscular fat and eating quality, consumers started to change their mind and embrace fattier meat and even high-marbled beef (33). Consumers from Asian countries, particularly in Japan, are well-known to enjoy high-marbled beef, but Japanese consumers do also enjoy moderately marbled beef (34). Although the preferences of consumers for marbling levels differ across various countries, marbling is undoubtedly one of the multiple traits that highly contribute to beef eating quality (35), but its contribution to eating quality seems to vary according to the muscle as predicted by this study (**Table 5**).

Intramuscular fat deposition, and therefore marbling, depends on many factors such as nutrition, genetics, and, to a lower extent, animal maturity (36, 37). However, no correlation or a weak correlation (only with the MSA marbling score at the fifth rib) was found between the ossification score and the MSA marbling score (**Table 2**). This may be due to the carcasses graded in this study, which were from old animals (cows) of the Limousine breed and of similar age. This breed is a late maturing one and, more importantly, produces low-marbled beef (38). However, even the late-maturing cows develop more marbling than younger counterparts as they become older and physiologically mature. In fact, the marbling level is influenced by various factors such as expression and the presence of cellular factors (39). The processes determining the development of marbling of mature cows are poorly studied and require further investigation. The factors such as genetics, whole body fatness, energy intake previous to slaughter, and lifetime fat turnover associated with raising calves are potential subjects for future research.

Meat Color Characteristics at the Fifth Rib and the Tenth Rib

From a retail point of purchase, the meat color is one of the most critical traits for consumers to purchase beef (40). Various factors, such as diet, pH, and muscle type, and characteristics affect the meat color (41). The meat color depends on the ultimate pH that gradually increases from lumbar to thoracis, the pH at the fourth rib (LT) being higher than at the eleventh rib (LL) (42). Accordingly, LT should be darker than at the *lumborum* vertebrae (43). Contrary to this assumption and the previous observations in Australia with other animal types (15), the present study showed that the muscle at the tenth rib (LL) was significantly darker than the muscle at the fifth rib, suggesting the involvement of other factors.

The meat color also partly depends in part on the muscle fiber type (44). Indeed, oxygen diffusion is related to the muscle fiber type and results in more or less oxymyoglobin (45). The proportions of type I and type II A fibers in LT are higher than those in LL, the proportion of type II B fiber in LL is higher than that in LT (46). However, oxidative fibers (I and IIA) are known

to have a decreased rate in the extent of postmortem pH decline and lightness and inherently have an increase in redness due to a higher myoglobin concentration, thus resulting in darker meat when compared to glycolytic muscles (type II B) (47). In this way, the LT muscle is expected to be darker than the LL muscle. The current finding indicates that the meat color of LT at the tenth rib was darker than that at the fifth rib. Even though the tenth rib is close to the *lumborum* vertebrae, the muscle on the fifth rib and the tenth rib is still the LL muscle. The fiber type is therefore unlikely to be a reason for the observed color difference.

Practically, the meat color is not used in the current MSA grading system, but with it being used as a threshold in the old MSA system, the meat color should be three or less than three, and the carcass with a meat color more than four had to be rejected by the system. The proportion of the meat color higher than four at the fifth rib and the tenth rib is calculated in this study, and is 18% and 29%, respectively. In this way, the meat color assessment conducted at the tenth rib would have increased the possibility of being rejected in the older MSA system for some of the carcasses.

Fat Color Characteristics at the Fifth Rib and the Tenth Rib

The fat color is of practical importance for the beef industry since purchase willingness of the consumer is affected by the color, the white fat color being more desirable than the yellow fat color in many countries (48, 49). In the European market, too much yellow fat on the carcass is considered unacceptable (50). The fat color depends on age, gender, genotype, and nutrition. The yellowness is mainly explained by carotenes accumulating in fat tissue (48).

Whereas, Meat Livestock Australia indicates that carcasses may be ribbed at any site between the fifth rib and the thirteenth rib for grading (15), in the current study, the fat color score (3.5) at the tenth rib was significantly higher (and therefore yellower) than that at the fifth rib (2.5). Acheson et al. (26) reported that animals deposit intramuscular fat from the anterior to the posterior along the vertebrae. It is, therefore, possible to speculate that the significant difference in fat color between the fifth rib and tenth rib may also be due to a different accumulation rate of carotenoids between the posterior and anterior intermuscular fat. With an increase in maturity, more carotenoids could be concentrated at the tenth rib than that at the fifth rib. The significantly positive correlation observed between the fat color and the ossification score may also support the above hypothesis. This result supports the evidence that adipose tissues become more yellow as animal maturity increases (51). Moreover, Moon et al. (52) indicated that high-marbled beef tended to have a lower yellowness fat color due to the dilution of pigments in more fat, which is in line with a significantly negative correlation between fat color and marbling (**Table 3**).

MQ4 Scores and the MSA Index at the Fifth Rib and the Tenth Rib

The MSA beef eating quality score (MQ4) is a combination score of tenderness, juiciness, flavor liking, and overall liking for the individual cuts with a defined hanging method, aging time, and the cooking method (14). Marbling, as one of the input parameters, is used to predict the eating quality score (MQ4) of the individual cuts in the MSA cut-based model (20). The MSA index is a global score of the average eating quality and the potential merit of a whole beef carcass, which is calculated from the predictive eating quality scores of 39 MSA cuts. To further confirm the feasibility that the marbling assessment could be conducted at the fifth rib and not influence the eating quality prediction of individual cuts and the whole carcass, correlation analyses were performed with ten cuts to evaluate the relationships between the MQ4 scores at the fifth rib and the tenth rib. The results in the correlation analyses and scatter plots evidenced high and significant correlation coefficients and a similar distribution of the scores, demonstrating that the marbling assessment at either the fifth rib or the tenth rib has an extremely low impact on the prediction of the MQ4 scores for each cut. In addition, similar and strong correlations between the MQ4 scores predicted from the marbling scores recorded at the two ribs were observed for different hanging methods, aging times, and cooking methods. Moreover, the two MQ4 score models regressed by using the marbling score for one specific cut were found highly similar between the two marbling assessment sites (**Table 5**). Furthermore, we observed the same mean value of the MSA index (52) with no statistical difference ($p = 0.92$, **Table 2**) and significantly strong correlations between the MSA indexes predicted from the marbling scores from the fifth rib and the tenth rib ($r = 0.97$, $p < 0.001$, data not shown). All of these results indicate that the marbling assessment at the fifth rib or the tenth rib has no or very little impact on the prediction of the MQ4 score and the MSA index for different production and process combinations.

Another interesting finding is that the correlation coefficients between the MQ4 scores of the two grading sites was extremely high for some cuts, such as OUT005, i.e., higher than STA045 and STP045, while the regression model of OUT005 has a very low explanatory power (R^2-value) when using the marbling score to explain the variability of the MQ4 score. This is in-line with the fact that the marbling score measured on *M.* LTL might have less impact on the prediction of the MQ4 scores for other cuts due to a low or moderate correlation of the marbling scores between different cuts (25). In summary, without considering the influence of other MSA predictive parameters on the prediction of the MSA index and the MQ4 scores, it is feasible to assess the marbling at the fifth rib to routinely predict the MSA index and the MQ4 scores for French cattle.

CONCLUSION

This study has shown that there is no difference in the marbling scores determined by using the accredited trained graders according to the ABCAS protocol, between the fifth rib and the tenth rib, as well as in the predicted MSA index and the MQ4 scores from these two sets of values. This confirms that the marbling score could be determined at the fifth rib by using the accredited trained graders, i.e., where carcasses are

generally quartered in Europe. In contrast, meat color and fat color, not taken into the MSA model to predict eating quality of beef, are significantly different between the two grading sites. Given that Limousine cows are an important source of beef in France and that a little detailed work regarding the marbling distribution has been undertaken using cull cows, the current study is considered to be relevant to provide practical recommendations to the European (and especially the French) beef industry. Thus, this work supports potential implications in favor of the MSA implementation for the late maturing and low-marbled cattle breeds, such as Limousine, and also for potential MSA implementation in French beef plants. However, further work is needed to completely study the implementation of the ABCAS carcass grading system with respect to other critical carcass factors according to the MSA methodology while following the European carcass quartering practices.

DATA AVAILABILITY STATEMENT

The raw data supporting the conclusions of this article will be made available by the authors, without undue reservation.

ETHICS STATEMENT

Ethical review and approval was not required for the animal study because Data from cows was used from a commercial slaughterhouse at Limoges, France according to normal rules.

AUTHOR CONTRIBUTIONS

JL performed a statistical analysis and wrote the manuscript. GP and AN provided the data. IL and M-PE-O made a high contribution to the structure of the paper. DP provided prediction of the MQ4 score. J-FH conceived the study. All authors contributed to the article and approved the submitted version.

FUNDING

This research was included within the EcoMeat3G project funded by FEDER (convention no. AV0019409) and the Auvergne-Rhône Alpes Region and within the EcoRegMeat3G project funded by the French Agency of Research through the Institut Carnot France Futur Elevage. JL's scholarship was sponsored by the Chinese Scholarship Council (CSC).

REFERENCES

1. Hocquette JF, Ellies-Oury MP, Lherm M, Pineau C, Deblitz C, Farmer L. Current situation and future prospects for beef production in Europe—a review. Asian-australas. *J Anim Sci.* (2018) 31:1017. doi: 10.5713/ajas.18.0196
2. Sans P, Legrand I. Tendance d'évolution des caractéristiques des marchés. In: Ellies-Oury MP, Hocquette JF, editors. *La Chaîne de La Viande Bovine. Production, transformation, valorisation et consommation*. Paris: Editions Lavoisier (2018). p. 125–42.
3. FranceAgriMer. *Consommation des produits carnés en 2014, 4*, Montreuil. (2015). p. 15.
4. Ellies-Oury MP, Lee A, Jacob H, Hocquette JF. Meat consumption–what French consumers feel about the quality of beef? Ital. *J Anim Sci.* (2019) 18:646–56. doi: 10.1080/1828051X.2018.1551072
5. Meat and Livestock Australia (2010). Available online at: https://www.mla.com.au/globalassets/mla-corporate/generic/about-mla/annual-report-2009_10.pdf (accessed October 30, 2010).
6. McGilchrist P, Polkinghorne RJ, Ball AJ, Thompson J. The meat standards Australia index indicates beef carcass quality. *Animal.* (2019) 13:1750–7. doi: 10.1017/S1751731118003713
7. Institut de l'Elevage. *Les chiffres clés du GEB. Bovins 2020. Productions lait et viande*. (2020). Available online at: http://idele.fr/no_cache/recherche/publication/idelesolr/recommends/chiffres-cles-bovins-2020.html (accessed September 23, 2020).
8. Etats Généraux de l'Alimentation EGA (2018). Available online at: https://agriculture.gouv.fr/alimagri-les-etats-generaux-de-lalimentation (accessed October 2, 2018).
9. Meat and Livestock Australia (2011). Available online at: https://www.mla.com.au/globalassets/mla-corporate/generic/about-mla/anual-report-2010-11-final.pdf (accessed October 30, 2011).
10. Legrand I, Hocquette JF, Polkinghorne RJ, Pethick DW. Prediction of beef. eating quality in France using the Meat Standards Australia system. *Animal.* (2013) 7:524–9. doi: 10.1017/S1751731112001553
11. Chong FS, Farmer LJ, Hagan TDJ, Speers JS, Sanderson DW, Devlin DJ, et al. Regional, socioeconomic and behavioural-impacts on consumer acceptability of beef in Northern Ireland, Republic of Ireland and Great Britain. *Meat Sci.* (2019) 154:86–95. doi: 10.1016/j.meatsci.2019.04.009
12. Pogorzelski G, Wozniak K, Polkinghorne RJ, Wierzbicka A, Półtorak A. Polish consumer categorisation of grilled beef at 6mm and 25mm thickness into quality grades, based on Meat Standards Australia methodology. *Meat Sci.* (2020) 161:1–7. doi: 10.1016/j.meatsci.2019.107953
13. Hocquette JF, Ellies-Oury MP, Legrand I, Pethick D, Gardner G, Wierzbicki J, et al. Research in beef tenderness and palatability in the era of big data. *Meat Muscle Biol.* (2020) 4:1–13. doi: 10.22175/mmb.9488
14. Polkinghorne R, Thompson JM, Watson R, Gee A, Porter M. Evolution of the Meat Standards Australia (MSA) beef grading system. *Austral J Exp Agric.* (2008) 48:1351–9. doi: 10.1071/EA07177
15. AUS-MEAT. *Australian Beef Carcase Evaluation Chiller Assessment. Version 9, 16/07/2018*. Murarri, QLD: AUS-MEAT Limited (2018).
16. Meat Standards Australia beef information kit – MLA Australia livestock (2010). Available online at: https://www.mla.com.au/globalassets/mla-corporate/marketing-beef-and-lamb/msa_tt_beefinfokit_jul13_lr.pdf
17. Hickey JM, Keane MG, Kenny DA, Cromie AR, Veerkamp RF. Genetic. parameters for EUROP carcass traits within different groups of cattle in Ireland. *J Anim Sci.* (2007) 85:314–21. doi: 10.2527/jas.2006-263
18. United States Department of Agriculture. *Standards for Grades of Slaughter Cattle and Standards for Grades of Carcass Beef. Agricultural Marketing Services, USDWashington A DC, Government Printing Office*. (2017). Available online at: https://www.ams.usda.gov/sites/default/files/media/CarcassBeefStandard.pdf (accessed December 18, 2017).
19. Ferguson DM. Objective on-line assessment of marbling: a brief review. *Aust J Exp Agric.* (2004) 44:681–5. doi: 10.1071/EA02161
20. Bonny SP, O'Reilly RA, Pethick DW, Gardner GE, Hocquette JF, Pannier L. Update of Meat Standards Australia and the cuts based grading scheme for beef and sheep meat. *J Integr Agric.* (2018) 17:1641–54. doi: 10.1016/S2095-3119(18)61924-0
21. Hocquette JF, Legrand I, Jurie C, Pethick DW, Micol D. Perception in France of the Australian system for the prediction of beef quality (Meat Standards Australia) with perspectives for the European beef sector. *Anim Product Sci.* (2011) 51:30–6. doi: 10.1071/AN10045
22. Kruk ZA, Pitchford WS, Siebert BD, Deland MPB, Bottema CDK. Factors affecting estimation of marbling in cattle and the relationship between marbling scores and intramuscular fat. *Anim Product Austral.* (2002) 24:129–32. Available online at: https://www.researchgate.net/publication/

265575133_Factors_affecting_estimation_of_marbling_in_cattle_and_the_relationship_between_marbling_score_and_intramuscular_fat
23. Cook CF, Bray RW, Weckel KG. Variations in the quantity and distribution of lipid in the bovine longissimus dorsi. *J Anim Sci.* (1964) 23:329–31. doi: 10.2527/jas1964.232329x
24. Taylor DG, Johnson ER. Visual marbling score and chemical fat content of. *M. Longissimus* in beef carcasses. *Proc Austr Soc Anim Product.* (1992) 19:71–3.
25. Konarska M, Kuchida K, Tarr G, Polkinghorne RJ. Relationships between. marbling measures across principal muscles. *Meat Sci.* (2017) 123:67–78. doi: 10.1016/j.meatsci.2016.09.005
26. Acheson RJ, Woerner DR, Walenciak CE, Colle MJ, Bass PD. Distribution of marbling throughout the *M. longissimus* thoracis et Lumborum of beef carcasses using an instrument-grading system. *Meat Muscle Biol.* (2018) 2:303–8. doi: 10.22175/mmb2018.04.0005
27. Schulz L, Sundrum A. Assessing marbling scores of beef at the 10th rib vs. 12th rib of longissimus thoracis in the slaughter line using camera grading technology in Germany. *Meat Sci.* (2019) 152:116–20. doi: 10.1016/j.meatsci.2019.02.021
28. Bonny SPF, Pethick DW, Legrand I, Wierzbicki J, Allen P, Farmer LJ, et al. European conformation and fat scores have no relationship with eating quality. *Animal.* (2016) 10:996–1006. doi: 10.1017/S1751731115002839
29. Liu J, Chriki S, Ellies-Oury MP, Legrand I, Pogorzelski G, Wierzbicki J, et al. European conformation and fat scores of bovine carcasses are not good indicators of marbling. *Meat Sci.* (2020) 170:108233. doi: 10.1016/j.meatsci.2020.108233
30. Normand J. *Institut de L'Elevage, Lyon. "En France, quelles pistes pour enrayer. la baisse de consommation de viande bovine ?" PowerPoint*. (2017). http://idele.fr/fileadmin/medias/Documents/Perception_du_persille_et_du_conditionnement_sous_vide_-_Colloque_Interbev_2018-02-02.pdf (accessed February 2, 2017).
31. Egan AF, Ferguson DM, Thompson JM. Consumer sensory requirements for beef and their implications for the Australian beef industry. *Aust J Exp Agric.* (2001) 41:855–9. doi: 10.1071/EA00065
32. Killinger KM, Calkins CR, Umberger WJ, Feuz DM, Eskridge KM. Consumer visual preference and value for beef steaks differing in marbling level and color. *J Anim Sci.* (2004) 82:3288–93. doi: 10.2527/2004.82113288x
33. Frank D, Joo ST, Warner R. Consumer acceptability of intramuscular fat. *Korean J Food Sci Anim Resour.* (2016) 36:699–708. doi: 10.5851/kosfa.2016.36.6.699
34. Sasaki K, Ooi M, Nagura N, Motoyama M, Narita T, Oe M, et al. Classification and characterization of Japanese consumers' beef preferences by external preference mapping. *J Sci Food Agric.* (2017) 97:3453–62. doi: 10.1002/jsfa.8204
35. Motoyama M, Sasaki K, Watanabe A. Wagyu and the factors contributing. to its beef quality: a Japanese industry overview. *Meat Sci.* (2016) 120:10–8. doi: 10.1016/j.meatsci.2016.04.026
36. Pethick DW, Harper GS, Hocquette JF, Wang Y. Marbling biology–what do we know about getting fat into muscle. In: *Proceedings of Australian Beef–the Leader*. Armidale, NSW. (2006). p. 103–10.
37. Pflanzer SB, de FelícioPE. Moisture and fat content, marbling level and color of boneless rib cut from Nellore steers varying in maturity and fatness. *Meat Sci.* (2011) 87:7–11. doi: 10.1016/j.meatsci.2010.08.009
38. Malau-Aduli AEO, Edriss MA, Siebert BD, Bottema CDK, Pitchford WS. Breed differences and genetic parameters for melting point, marbling score and fatty acid composition of lot-fed cattle. *J Anim Physiol Anim Nutr.* (2000) 83:95–105. doi: 10.1046/j.1439-0396.2000.00254.x
39. Kern SA, Pritchard RH, Blair AD, Scramlin SM, Underwood KR. The influence of growth stage on carcass composition and factors associated with marbling development in beef cattle. *J Anim Sci.* (2014) 92:5275–84. doi: 10.2527/jas.2014-7891
40. Smith GC, Belk KE, Sofos JN, Tatum JD,Williams SN. Economic implications of improved color stability in beef. In: Decker E, Faustman C, Lopez-Bote CJ, editors. *Antioxidants in Muscle Foods: Nutritional Strategies to Improve Quality*. New York, NY: Wiley (2000). p. 397–426.
41. Mancini RA, Hunt M. Current research in meat color. *Meat Sci.* (2005) 71:100–21. doi: 10.1016/j.meatsci.2005.03.003
42. Janz JAM, Aalhus JL, Dugan MER, Price MA. A mapping method for the description of Warner–Bratzler shear force gradients in beef Longissimus thoracis et lumborum and Semitendinosus. *Meat Sci.* (2006) 72:79–90. doi: 10.1016/j.meatsci.2005.06.009
43. Hughes JM, Kearney G, Warner RD. Improving beef meat colour scores at carcass grading. *Anim Product Sci.* (2014) 54:422–9. doi: 10.1071/AN13454
44. Ozawa S, Mitsuhashi T, Mitsumoto M, Matsumoto S, Itoh N, Itagaki K, et al. The characteristics of muscle fiber types of longissimus thoracis muscle and their influences on the quantity and quality of meat from Japanese Black steers. *Meat Sci.* (2000) 54:65–70. doi: 10.1016/S0309-1740(99)00072-8
45. McKenna DR, Mies PD, Baird BE, Pfeiffer KD, Ellebracht JW, Savell JW. Biochemical and physical factors affecting discoloration characteristics of 19 bovine muscles. *Meat Sci.* (2005) 70:665–82. doi: 10.1016/j.meatsci.2005.02.016
46. Totland GK, Kryvi H. Distribution patterns of muscle fibre types in major muscles of the bull (Bos taurus). *Anat Embryol.* (1991) 184:441–50. doi: 10.1007/BF01236050
47. Wicks J, Beline M, Gomez JFM, Luzardo S, Silva SL, Gerrard D. Muscle energy metabolism, growth, and meat quality in beef cattle. *Agriculture.* (2019) 9:195. doi: 10.3390/agriculture9090195
48. Dunne PG, Monahan FJ, O'Mara FP, Moloney AP. Colour of bovine subcutaneous adipose tissue: a review of contributory factors, associations with carcass and meat quality and its potential utility in authentication of dietary history. *Meat Sci.* (2009) 81:28–45. doi: 10.1016/j.meatsci.2008.06.013
49. Ardeshiri A, Rose JM. How Australian consumers value intrinsic and extrinsic. attributes of beef products. *Food Qual Preference.* (2018) 65:146–63. doi: 10.1016/j.foodqual.2017.10.018
50. Dunne PG, O'Mara FP, Monahan FJ, Moloney AP. Changes in colour characteristics pigmentation of subcutaneous adipose tissue *M. longissimus* thoracisof heifers fed grass, grass silage or concentrate-based diets. *Meat Sci.* (2006) 74:231–41. doi: 10.1016/j.meatsci.2006.02.003
51. Inoue K, Shoji N, Honda T, Oyama K. Genetic relationships between meat. quality traits and fatty acid composition in Japanese black cattle. *Anim Sci J.* (2017) 88:11–8. doi: 10.1111/asj.12613
52. Moon SS, Yang HS, Park GB, Joo ST. The relationship of physiological. maturity and marbling judged according to Korean grading system to meat quality traits of Hanwoo beef females. *Meat Sci.* (2006) 74:516–21. doi: 10.1016/j.meatsci.2006.04.027

Conflict of Interest: The authors declare that the research was conducted in the absence of any commercial or financial relationships that could be construed as a potential conflict of interest.

frontiers in Veterinary Science

ORIGINAL RESEARCH
published: 29 April 2021
doi: 10.3389/fvets.2021.634577

Comparative Genome-Wide Alternative Splicing Analysis of Longissimus Dorsi Muscles Between Japanese Black (Wagyu) and Chinese Red Steppes Cattle

Xibi Fang[1†], Lixin Xia[1†], Haibin Yu[2], Wei He[1], Zitong Bai[1], Lihong Qin[3], Ping Jiang[2], Yumin Zhao[3], Zhihui Zhao[1,2] and Runjun Yang[1*]*

[1] College of Animal Science, Jilin University, Changchun, China, [2] College of Coastal Agricultural Sciences, Guangdong Ocean University, Zhanjiang, China, [3] Branch of Animal Husbandry, Jilin Academy of Agricultural Sciences, Changchun, China

OPEN ACCESS

Edited by:
Xiao Li,
Northwest A and F University, China

Reviewed by:
Xianyong Lan,
Northwest A & F University, China
Marcio Duarte,
Universidade Federal de Viçosa, Brazil

***Correspondence:**
Zhihui Zhao
zhzhao@jlu.edu.cn
Runjun Yang
yrj@jlu.edu.cn

[†] These authors have contributed equally to this work

Specialty section:
This article was submitted to Livestock Genomics, a section of the journal Frontiers in Veterinary Science

Received: 28 November 2020
Accepted: 10 March 2021
Published: 29 April 2021

Citation:
Fang X, Xia L, Yu H, He W, Bai Z, Qin L, Jiang P, Zhao Y, Zhao Z and Yang R (2021) Comparative Genome-Wide Alternative Splicing Analysis of Longissimus Dorsi Muscles Between Japanese Black (Wagyu) and Chinese Red Steppes Cattle. Front. Vet. Sci. 8:634577. doi: 10.3389/fvets.2021.634577

Alternative splicing is a ubiquitous regulatory mechanism in gene expression that allows a single gene generating multiple messenger RNAs (mRNAs). Significant differences in fat deposition ability and meat quality traits have been reported between Japanese black cattle (Wagyu) and Chinese Red Steppes, which presented a unique model for analyzing the effects of transcriptional level on marbling fat in livestock. In previous studies, the differentially expressed genes (DGEs) in *longissimus dorsi muscle* (*LDM*) samples between Wagyu and other breeds of beef cattle have been reported. In this study, we further investigated the differences in alternative splicing in *LDM* between Wagyu and Chinese Red Steppes cattle. We identified several alternative splicing types including cassette exon, mutually exclusive exons, alternative 5′ splice site, alternative 3′ splice site, alternative start exon, and intron retention. In total, 115 differentially expressed alternatively spliced genes were obtained, of which 17 genes were enriched in the metabolic pathway. Among the 17 genes, 5 genes, including *MCAT, CPT1B, HADHB, SIRT2*, and *DGAT1*, appeared to be the novel spliced candidates that affect the lipid metabolism in cattle. Additionally, another 17 genes were enriched in the Gene Ontology (GO) terms related to muscle development, such as *NR4A1*, *UQCC2*, *YBX3/CSDA*, *ITGA7*, etc. Overall, altered splicing and expression levels of these novel candidates between Japanese black cattle and Chinese Red Steppes revealed by RNA-seq suggest their potential involvement in the muscle development and fat deposition of beef cattle.

Keywords: cattle, meat traits, fat deposition, muscle development, RNA-seq

INTRODUCTION

Alternative splicing or alternative RNA splicing is a method to create different proteins from the same strand of DNA in mammalian cell. The structure and function of protein depend on the sequence of amino acids, which is dictated by the matured messenger RNA (mRNA). Current high-throughput sequencing technology suggests that alternative splicing is more widespread than initially thought, and alternative splicing is likely to be involved in various across tissue types and

developmental stages as well as among individuals and populations (1). Hence, alternative splicing is an important and ubiquitous regulatory mechanism to increase the informational diversity and functional capacity of a single gene during posttranscriptional processing, and it also provide a crucial bridge between the genome and the proteome.

The currently accumulated data have highlighted importance of alternative splicing in normal physiology and pathology in human, including cancer, immune and infectious diseases, and metabolic conditions (2). With the development of requirements and technology, many studies used different methods to resolve the alternative splicing on a genome-wide scale (3, 4) including microarray (5), expressed sequence tag (EST) (6), and sequencing. Pan et al. (7) analyzed alternative splicing complexity in human tissues showing transcripts from ∼95% of multiexon genes undergo alternative splicing by combining mRNA-Seq with expressed sequence tag (EST)-complementary DNA (cDNA) sequence data. The data of 15 diverse human tissue and cell line transcriptomes indicated that 92–94% of human genes undergo alternative splicing, and most alternative splicing and alternative cleavage events vary between tissues (8). These results also demonstrate the universality and utility of alternative splicing in mammal, and to further understand the alternative splicing will be a crucial effective method in the study of formation of human disease or perfect economic traits in livestock.

In previous studies, a larger number of transcriptomes were performed to analyze the genetics and to improve the production traits in livestock; the differentially expressed genes (DGEs) in *longissimus dorsi muscle* (*LDM*) samples among various breeds of beef cattle have been reported (9–12). However, the alternative splicing data on a genome-wide scale was rarely analyzed and studied in depth. In the present study, we analyzed the differences in expression levels and components of alternative splicing in *LMD* of Wagyu and Chinese Red Steppes cattle by RNA-seq, and the candidate functional alternative splicing types of genes related to meat traits were provided. The study allowed better genomic characterization of the cattle in terms of transcripts variability and analyzed the potential effect of alternative splicing of genes on muscle development and lipometabolism. It may provide a theoretical basis for the identification of functional transcripts and a potential genetic regulatory elements for the study of genetic mechanism of meat quality traits in beef cattle.

MATERIALS AND METHODS

Ethics Statement

Animal care and experiments were performed according to the guidelines established by the care and use of laboratory animals of the Jilin University Animal Care and Use Committee (Approval ID: 20140310).

Abbreviations: MCAT, malonyl-CoA-acyl carrier protein transacylase; CPT1B, carnitine palmitoyltransferase 1B; HADHB, hydroxyacyl-CoA dehydrogenase trifunctional multi enzyme complex subunit β; SIRT2, sirtuin 2; DGAT1, diacylglycerol O-acyltransferase 1; NR4A1, nuclear receptor subfamily 4 group A member 1; UQCC2, ubiquinol-cytochrome c reductase complex assembly factor 2; YBX3/CSDA, Y-box binding protein 3; ITGA7, integrin subunit alpha 7.

Animal and Samples

The three Japanese black cattle (28 months old) were randomly chosen from 20 males born from cows that were artificially inseminated with semen stocks from the same bull. The three Chinese Red Steppes cattle (28 months old) were similarly chosen from 20 males with a common father. Three Japanese black cattle and three Chinese Red Steppes cattle were provided by the National Research Center for Animal Transgenic Biotechnology, Inner Mongolia University (Hohhot, China) and the Branch of Animal Science, Jilin Academy of Agricultural Sciences (Gongzhuling, China), respectively. The two farms housing the two groups of cattle were located at similar altitudes with similar natural weather conditions. The cattle in both groups were raised under similar normal conditions on a diet of corn and hay with access to feed and water *ad libitum*.

The marble scores of the 12–13 rib eye meat of these two breeds were accessed according to the classification of beef marbling grade standard. The marble scores of the three Wagyu cattle are 7, 7, and 6, which belong to the Grade 4 meat quality level (good grade). In the other group, the marble scores of the three Chinese Red Steppes cattle were 2, 2, and 2, respectively, which belonged to the Grade 2 meat quality level (below average grade). The tissue samples were transported in dry ice and stored in liquid nitrogen in the laboratory.

RNA Extraction and Quality Analysis

Total RNA was isolated from *LDM* using Trizol reagent (Invitrogen, USA), treated with DNase I (NEB, Beijing, China), extracted with phenol-chloroform, and precipitated with ethanol. The quality and quantity of total RNA were determined using an Agilent 2100 Bioanalyzer (Agilent technologies, Palo Alto, CA). The mRNA was purified from total RNA using poly-T oligo-attached magnetic beads. From each sample, 1.5 μg of mRNA was used to construct six cDNA libraries for sequencing. The mRNA was treated with a Thermomixer (Eppendorf AG, Hamburg, Germany) to generate fragments with an average size of 200 bp (200 ± 25 bp) for the paired-end libraries. The fragmented mRNA was then used as templates for synthesizing the first-strand cDNA. The double-stranded cDNAs were purified and ligated to adaptors for Illumina paired-end sequencing. Library concentration was quantified by quantitative PCR (qPCR) and a Qubit® 2.0 Flurometer (Life Technologies, CA, USA), and the insert size was checked on an Agilent 2100 Bioanalyzer. The cDNA libraries were sequenced using the Illumina HiSeq2000 platform by the Beijing Genomics Institute, and 100 nt paired-end reads were generated. The raw data have been submitted to the Gene Expression Omnibus (GEO).

Analysis of Alternative Splicing and Prediction of Novel Transcripts of Genes

Clean high-quality reads were obtained from the raw reads by removing the adaptor sequences and low-quality reads. An RNA-Seq TopHat (v2.0.6) splicing junction mapper was used for RNA-Seq alignment (13). We used our own localized reads to calculate the number of reads for each gene and the read per kilobase and read per million (RPKM) values. Other statistical results were

also analyzed, such as gene range and depth and read distribution around start and stop codons.

The reads were mapped to the reference genome (*Bos taurus* UMD_3.1.1) using the ultra-fast, short-read mapping program Bowtie (http://www.bowtie-bio.sourceforge.net) (13). The mapped reads were assembled using MAQ (14) to identify possible splicing junctions, the unmapped reads are split into smaller segments to allow alignment to the reference genome, and splice junctions were defined by the seed expansion procedure. All junction reads must be at least 6 nt that exactly match each of the two adjacent areas of the potential junction sites, and all junction sites with N3 non-redundant reads in both group were filtered. Alternative splicing detector software based on junction reads (http://www.novelbio.com/asd/ASD.html) (15, 16), which recognizes and detects differential alternative splicing exons between two groups of RNA-Seq data, was used. We then counted the number of junction reads that matched either the inclusion or exclusion isoforms of both samples and calculated the *p*-value based on the junction read count between the samples using Fisher's exact test. Alternate exon read coverage for the corresponding gene was also calculated on the sample, and a second *p*-value based on the alternative exon read coverage for gene read coverage between samples was calculated using Fisher's exact test. The adjusted *p*-values were obtained by combining the two *p*-values using a weighted arithmetic expression to assess the statistical significance of alternative splicing between samples. Differentially expressed alternatively spliced genes between Japanese black cattle and Chinese Red Steppes were considered as differentially expressed according to adjusted $p < 0.05$.

Gene Ontology and Kyoto Encyclopedia of Genes and Genomics Enrichment Analysis

Differentially expressed alternatively spliced genes were implemented by the Gene Ontology (GO) seq R package (17). GO was used to determine and compare the functions of the differentially expressed alternatively spliced genes as biological process, molecular function, and cellular component, with corrected $p < 0.05$ considered significantly enriched. Association of the genes with pathways was computed with the Kyoto Encyclopedia of Genes and Genomics (KEGG) (18–20). The pathway with a corrected $p < 0.05$ was considered as significantly enriched.

Identification of Types and Quantification of Transcripts

One microgram total RNA was used to synthesize cDNA with the Transcriptor first-strand cDNA synthesis kit (Roche, USA) according to the manufacturer's recommendations. The primers were designed using Primer Premier 6.0 software (Premier BioSoft, Palo Alto, CA, USA) (**Supplementary Tables 1**, **2**). The types of transcripts were identified by PCR in a 25.0 μl reaction volume including 12.5 μl of 2× Taq PCR Master Mix (Vazyme, Nanjing, China), 0.5 μl of upstream and downstream primers (10 μM), 1.0 μl of cDNA, and 10.5 μl of ultrapure water. The PCR conditions were as follows: 95°C for 5 min; followed by 30 cycles of 95°C for 30 s, 57°C for 30 s, and 72°C for 1 min; and finally, 10 min extension at 72°C. The PCR products (8.0 μl) were run on 2% agarose gels.

Quantification of expression levels of differentially expressed alternatively spliced genes was detected by real-time PCR. Real-time PCR was performed using PCRmax Eco 48 (PCRmax, Staffordshire, UK). The real-time PCR system was as follows: 5 μl FastStart Universal SYBR Green Master (ROX) (Roche), 1 μl cDNA, 0.2 μl primer-F (10 μM), 0.2 μl primer-R (10 μM), and 3.6 μl RNase-free water. Reactions were incubated at 95°C for 10 min, followed by 40 cycles of 95°C for 10 s and 60°C for 30 s. β-Actin were used as reference genes, and relative expression levels were calculated using the $2^{-\Delta Ct}$. The data represent mean ± SEM from at least three independent experiments. Statistical analysis was performed by Student's *t* test at a significant level of $p < 0.05$.

RESULTS

RNA-seq and Transcriptome Analysis of Chinese Red Steppes and Japanese Black Cattle in *LDM*

A total of 268,490,636 reads were obtained from six samples in *LDM*. After filtering out low-quality data, 244,238,430 clean reads were mapped to *Bos taurus* (UMD_3.1.1). High-quality maps of the two breeds were obtained, and the unique mapping rates ranged from 87.3 to 88.3%. The details of the sequencing data quality of mRNA are shown in **Table 1**. The distribution of the reads on the chromosomes is shown in **Figure 1A**, and gene structure analysis was performed for each sample (**Figure 1B**). The sequence data were submitted to the GEO with the accession number of GSE161967.

Forms and Expression of Alternative Splicing

A total of eight alternative splicing forms were obtained through data mapping analysis, including cassette exon (Cassette), cassette multiple exon (Cassette multi), alternative 5′ splice site (A5SS), alternative 3′ splice site (A3SS), alternative start exon (AltStart), alternative end exon (AltEnd), intron retention (IR), and mutually exclusive exons (**Figure 2A**). In the genome-wide analysis, 12,241 alternatively spliced events corresponding to 5,295 genes were identified. Cassette was the most abundant alternatively spliced types, followed by A3SS, A5SS, AltStart, MXE, AltEnd, Cassette multi, and IR.

A total of 155 differentially expressed alternatively spliced events between two breeds were screened according to adjusted $p < 0.05$. The differentially expressed alternatively spliced events refer to 59 Cassette, 7 Cassette multi, 11 A3SS, 19 A5SS, 12 AltEnd, 37 AltStart, 5 IR, and 5 MXE (**Figure 2B**). One hundred forty-four genes corresponding to differentially expressed alternative splicing were found between Chinese Red Steppes and Japanese black cattle including *TPM2*, *STRIP2*, *CPT1B*, *SYNPO2L*, *SIRT2*, etc. The top 15 differentially expressed alternatively spliced genes are listed in **Table 2**.

TABLE 1 | Details of sequencing data by RNA-seq.

Samples	Total reads	Clean reads	UniqueMapped	ReadsFilter%	UniqueMappedRat%
RC4	44,709,588	40,838,760	36,079,522	91.34	88.3
RC5	44,176,132	40,116,014	35,296,746	90.81	88.0
RC6	44,182,490	39,604,308	34,923,036	89.64	88.2
WC616	44,422,250	40,611,916	35,477,651	91.42	87.3
WC719	46,072,046	41,931,354	36,696,481	91.01	87.5
WC921	44,928,130	41,136,078	36,315,824	91.56	88.3

WC616, WC719, WC921: longissimus dorsi muscle samples of Japanese black cattle (Wagyu); RC4, RC5, RC6: longissimus dorsi muscle samples of Chinese Red Steppes.

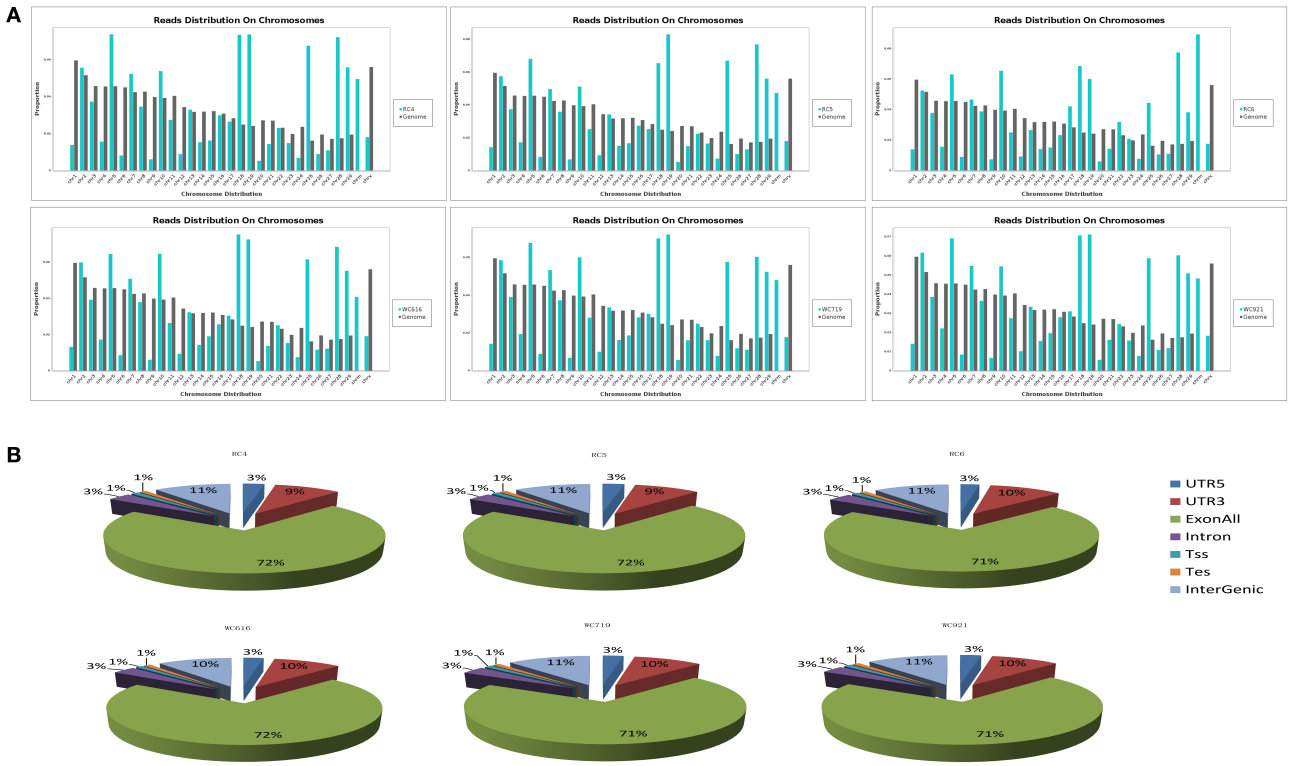

FIGURE 1 | The average distribution coverage at chromosomes of mapped reads. **(A)** The average distribution coverage at different chromosomes of the genome about mapped reads. **(B)** Functional genomic elements distribution of messenger RNA (mRNA) reads in different groups.

GO and KEGG Enrichment of Differentially Expressed Alternatively Spliced Genes

Functional enrichments on differentially expressed alternatively spliced genes by GO analysis found that 814, 532, and 232 GO terms were enriched in biological processes, molecular functions, and cellular components, respectively. A total of 216 biological processes, 115 molecular functions, and 54 cellular components were significantly enriched ($p < 0.05$). The most significantly enriched in biological processes included muscle filament sliding (GO: 0030049), muscle contraction (GO: 0006936), and cellular metabolic process (GO: 0044237). Muscle tendon junction (GO: 0005927), mitochondrion (GO: 0005739), and mitochondrial fatty acid beta-oxidation multienzyme complex (GO: 0016507) were among the most significantly enriched in cellular components. The most significantly enriched in molecular functions terms included poly(A) RNA binding (GO: 0044822), structural constituent of muscle (GO: 0008307), translation repressor activity, and nucleic acid binding (GO: 0000900). The top 15 GO terms in biological processes, molecular functions, and cellular components were listed by ascending order of corrected *p*-value, respectively (**Figure 3A**).

Functional enrichments on 59 differentially expressed alternatively spliced genes by KEGG analysis found that 138 pathways were enriched with 17 pathways significantly enriched ($p < 0.05$). These included metabolic pathway (PATH: 01100), vascular endothelial growth factor (VEGF) signaling pathway (PATH: 04370), mitogen-activated protein kinase (MAPK) signaling pathway (PATH: 04010), and apoptosis (PATH: 00730).

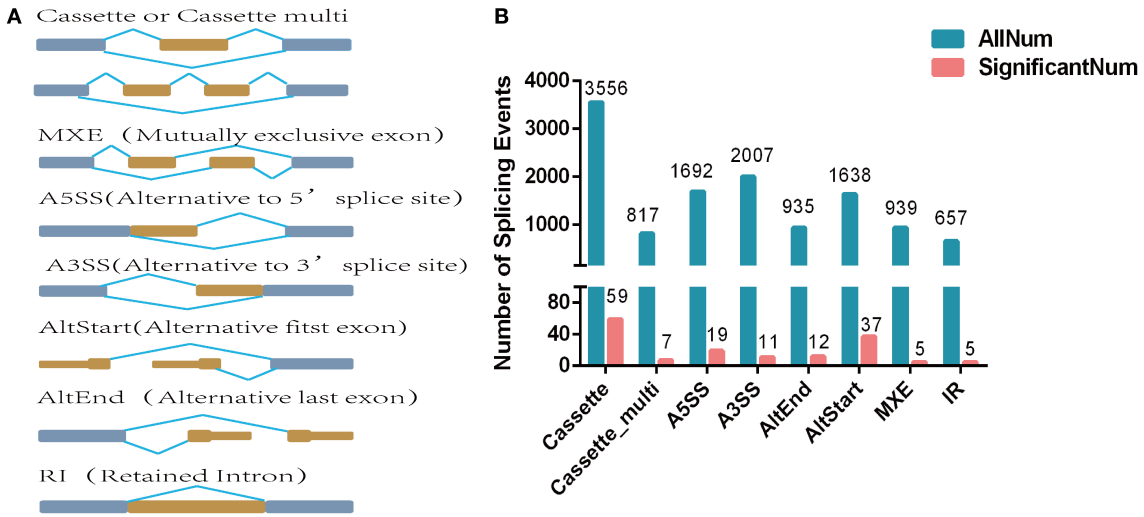

FIGURE 2 | Differentially expressed alternatively spliced genes analysis. **(A)** Alternative splicing types. **(B)** Number of alternative splicing types. The blue blocks represent exons, and the yellow blocks represent introns.

TABLE 2 | Top 15 differentially expressed alternatively spliced genes between Japanese Black cattle and Chinese Red Steppes.

AccID	Location	WCExp	RCExp	Adjusted_*p*-value	FDR	SplicingType
TPM2	chr8:60271071-60271204	226999::101410	225046::98571	0	0	MXE
STRIP2	chr4:94155770-94155850	20::194	31::80	3.41E-08	2.09E-04	AltEnd
CPT1B	chr5:120103992-120104146	12::972	66::533	1.03E-07	4.19E-04	A5SS
SYNPO2L	chr28:29800955-29801849	158::930	44::778	2.46E-07	7.53E-04	Cassette
SIRT2	chr18:48879590-48879636	103::673	232::496	4.06E-07	9.95E-04	Cassette
ENSBTAG00000023039	chr28:31054477-31054529	534::678	688::708	1.02E-06	0.002084	Cassette
BOLA	chr23:28502996-28503043	13::752	309::552	1.42E-04	0.247944	Cassette
BCL2L1	chr13:61771313-61771393	43::264	107::199	1.86E-04	0.283899	AltStart
KBTBD12	chr22:60298315-60298395	167::908	116::780	2.34E-04	0.318568	AltStart
MLF1	chr1:109764134-109764196	447::744	595::736	3.03E-04	0.37118	Cassette
NDRG2	chr10:26137053-26137094	5861::5809	2570::3758	4.71E-04	0.523886	Cassette
NSUN2	chr20:66752104-66752177	165::177	305::178	5.47E-04	0.557585	IR
PKIG	chr13:73715532-73715612	289::185	252::147	7.78E-04	0.732468	AltStart
TNNT1	chr18:62726592-62726626	39418::33204	44061::32517	0.001065696	0.931799	Cassette
RBM24	chr23:39842778-39842890	102::427	104::325	0.001341344	1	Cassette

The top 15 pathways are listed in **Figure 3B** by the ascending order of *p*-value.

Identification of Alternative Splicing Types and Verification of Expression Levels of Transcripts

To further test the accuracy of our sequencing and prediction data, *integrin subunit alpha 7 (ITGA7)* and *Y-box binding protein 3 (YBX3/CSDA)* were validated by PCR and real-time PCR. *CSDA* was predicted and identified two transcripts and the long transcript with a cassette of exon (**Figures 4A,B**). The expression levels of the transcript with a cassette of exon is higher in Japanese black cattle, and the long transcript expression levels were significantly lower than short in two breeds ($p < 0.05$) (**Figure 4C**). *ITGA7* was also identified as having two transcripts, and the type of alternative splicing is cassette (**Figures 4D,E**); moreover, the expression levels of genes were higher in Japanese black cattle, and the long transcript with a cassette of exon was lower than in Chinese Red Steppes (**Figure 4F**). The results indicated that the alternative splicing prediction based on RNA-seq data was reliable.

DISCUSSION

In the present study, 12,241 alternatively spliced events corresponding to 5,295 genes indicate the ubiquity of alternatively spliced genes in the bovine genome, and cassette is the most abundant alternatively spliced types like other species of

FIGURE 3 | Gene Ontology (GO) and Kyoto Encyclopedia of Genes and Genomes (KEGG) enrichment. **(A)** GO enrichment of differentially expressed genes. **(B)** KEGG enrichment of differentially expressed genes. BP, biological processes; MF, molecular functions; CC, cellular components.

livestock; this distribution pattern is also similar to that of other animals reported previously (7, 21, 22). Comprehensively, these results suggest that animals might possess similar alternative splicing forms.

Numerous alternative splicing events occur during cell differentiation and tissue maturation, suggesting that alternative splicing supports proper development. Although the mechanisms and outcomes of alternative splicing of individual transcripts are relatively well-understood in dairy and beef cattle, such as *angiopoietin like 6 (ANGPTL6)* (23), *transmembrane protein 95 (TMEM95)* (24), and *calpain 3 (CAPN3)* (25), the scopes and exact functions of this regulatory mechanism still remain to be investigated on novel transcripts and alternative splicing networks.

According to the KEGG enrichment, a total of 59 alternatively spliced genes were enriched in 138 pathways, of which 17 genes including *phosphatidylinositol 4-kinase beta (PI4KB)*, *diacylglycerol O-acyltransferase 1 (DGAT1)*, *uridine-cytidine kinase 1 like 1 (UCKL1)*, *NADH: ubiquinone oxidoreductase subunit C2 (NDUFC2)*, and *D-aspartate oxidase (DDO)* were enriched in metabolism pathways. The functional characterization of these genes is well-known in previous accumulated data. Therefore, we speculate that these genes also could mediate the formation of meat quality traits through the regulation of the related pathways by expression of different transcripts.

Although the differentially expressed alternative splicing in the same tissue of the same development stage should have totally similar alternative splicing, 155 differentially expressed alternatively spliced events between Japanese black cattle and Chinese Red Steppes were screened in the present study, which indicated that the corresponding genes or splicing events may be caused by the breed effect of fat deposition and muscle development capacity. Thus, understanding the function of the multiple transcripts and the effect of expression levels of each transcript such as *DGAT1*, *CPT1B*, *MCAT*, and *hydroxyacyl-CoA dehydrogenase trifunctional multi enzyme complex subunit beta (HADHB)* will be a key to study the formation of perfect quality meat traits in cattle.

The DNA sequence of *CPT1B* contains 8,755 bases, and it contains 19 exons and 18 introns reported in GenBank. *CPT1B* is reported as a key rate-limiting enzyme in the β-oxidation of fatty acids as well as playing an important role in regulating the decomposition and energy supply of fat (26, 27). Our previous study also found the single-nucleotide polymorphisms (SNPs) in the gene associated with meat quality. Moreover, the data of this study showed *CPT1B* has an alternative 5′ splice site at exon 7, and the novel transcript was a high expression in Japanese

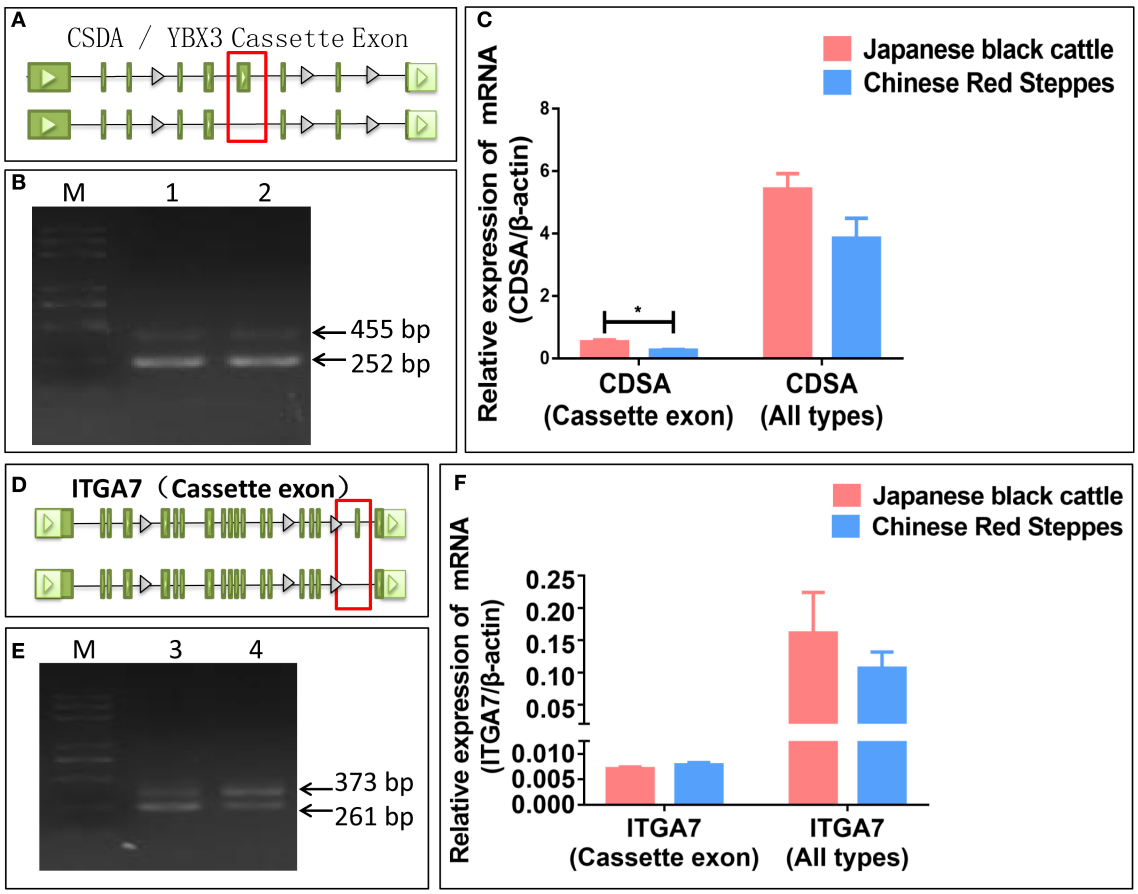

FIGURE 4 | Verification of splicing type and expression level. **(A)** The alternative splicing pattern of CDSA. **(B)** PCR validation of CDSA (Cassette). **(C)** The relative expression levels of CDSA. **(D)** The alternative splicing pattern of ITGA7. **(E)** PCR validation of ITGA7 (Cassette). **(F)** The relative expression levels of ITGA7. (1) CDSA PCR product of *LDM* in Japanese black cattle, (2) CDSA PCR product of LDM in Chinese Red Steppes, (3) ITGA7 PCR product of *LDM* in Japanese black cattle, and (4) ITGA7 PCR product of LDM in Chinese red steppes (M) trans 2K Plus DNA Marker. Green blocks represent exons.

black cattle. Therefore, the result indicated that the expression of different transcripts of *CPT1B* between the two breeds may be related to the capability in fat deposition, while there is few report on alternative splicing of this gene; thus, the specific functions and mechanisms of the two transcripts need further verification.

DGAT1 mediates triacylglycerol biosynthesis at the last committed step. It is widely known as the functional gene of milk fat and fatty acids contents (28–30), and also a gene could affect the fatty acids composition and fat content in the muscle and fat of beef cattle (31, 32). Alternative splicing of the *DGAT1* gene plays an important role in peanut triglyceride metabolism (33). Moreover, two alternative splicing types with different functions in triglyceride metabolism of *DGAT1* gene have been found in the diatom *Phaeodactylum tricornutum* (34). In the present study, two transcripts of *DGAT1* gene were also found in *LDM*; however, the structure and roles of alternative splicing are rarely reported in other studies in livestock; therefore, the functions of two alternative splicing types need further verification.

Although the present study found that many genes have novel transcripts with different expression levels, the specific genetic functions and regulation mechanisms of translated proteins by these mRNAs of the same gene on bovine muscle development, fat deposition, and meat quality traits still require further study.

CONCLUSIONS

In this study, we disclosed features of genome-wide alternative splicing in two breeds with significant differences in fat deposition ability and meat quality traits through comprehensive transcriptome analysis by RNA-seq. The results suggest that 5,295 genes correspond to alternative splicing in bovine genome. Moreover, we found that cassette is the most abundant alternatively spliced types like other species. The analysis of functional categories demonstrates that differentially expressed alternatively spliced genes, including *MCAT*, *CPT1B*, *HADHB*, *SIRT2*, and *DGAT1*, have been reported to have regulatory effects on meat quality traits in previous studies. The results indicated that different types of alternative splicing and regulatory networks constructed by them in this study might partially contribute to the significant variance in meat quality traits between Japanese black and Chinese Red Steppes cattle. Therefore, the study provided a new direction for revealing

the regulatory mechanism of gene regulatory elements on fat deposition and muscle development, which is the effects of different alternative splicing of candidate functional genes on marbling trait of beef cattle.

DATA AVAILABILITY STATEMENT

The datasets presented in this study can be found in online repositories. The names of the repository/repositories and accession number(s) can be found at: https://www.ncbi.nlm.nih.gov/genbank/, GSE161967.

ETHICS STATEMENT

The animal study was reviewed and approved by laboratory animals of the Jilin University Animal Care and Use Committee (Approval ID: 20140310).

AUTHOR CONTRIBUTIONS

ZZ and RY designed the study. LQ and PJ collected the samples. XF and HY collected the data. XF, LX, ZB, and WH conducted the bioinformatics analyses and wrote the manuscript. WH and YZ revised the manuscript. All authors read and approved the final manuscript.

FUNDING

This work was supported by the National Natural Science Foundation of China (31802034, 31972993, and 31772562) and the Jilin Scientific and Technological Development Program (20180101275JC).

ACKNOWLEDGMENTS

We are grateful to the Branch of Animal Science, Jilin Academy of Agricultural Sciences and National Research Center for Animal Transgenic Bio-technology, Inner Mongolia University for animal sampling. The authors thank Novel Bioinformatics Co., Ltd for the technical help in data analysis.

SUPPLEMENTARY MATERIAL

The Supplementary Material for this article can be found online at: https://www.frontiersin.org/articles/10.3389/fvets.2021.634577/full#supplementary-material

REFERENCES

1. Greenberg DS, Soreq H. Alternative Splicing. *Brenners Encyclopedia of Genetics.* 2nd ed. Amsterdam: Elsevier Inc. (2013). p. 97–8. doi: 10.1016/B978-0-12-374984-0.00043-7
2. Kim HK, Pham MHC, Ko KS, Rhee BD, Han J. Alternative splicing isoforms in health and disease. *Pflugers Arch.* (2018) 470:995–1016. doi: 10.1007/s00424-018-2136-x
3. Mironov AA, Fickett JW, Gelfand MS. Frequent alternative splicing of human genes. *Genome Res.* (1999) 9:1288–93. doi: 10.1101/gr.9.12.1288
4. Modrek B, Lee C. A genomic view of alternative splicing. *Nat Genet.* (2002) 30:13–9. doi: 10.1038/ng0102-13
5. Kwan T, Benovoy D, Dias C, Gurd S, Provencher C, Beaulieu P, et al. Genome-wide analysis of transcript isoform variation in humans. *Nat Genet.* (2008) 40:225–31. doi: 10.1038/ng.2007.57
6. Kim H, Klein R, Majewski J, Ott J. Estimating rates of alternative splicing in mammals and invertebrates. *Nat Genet.* (2004) 36:916–17. doi: 10.1038/ng0904-916
7. Pan Q, Shai O, Lee LJ, Frey BJ, Blencowe BJ. Deep surveying of alternative splicing complexity in the human transcriptome by high-throughput sequencing. *Nat Genet.* (2008) 40:1413–5. doi: 10.1038/ng.259
8. Wang ET, Sandberg R, Luo S, Khrebtukova I, Zhang L, Mayr C, et al. Alternative isoform regulation in human tissue transcriptomes. *Nature.* (2008) 456:470–6. doi: 10.1038/nature07509
9. He H, Liu X. Characterization of transcriptional complexity during longissimus muscle development in bovines using high-throughput sequencing. *PLoS ONE.* (2013) 8:e64356. doi: 10.1371/journal.pone.0064356
10. Lee HJ, Park HS, Kim W, Yoon D, Seo S. Comparison of metabolic network between muscle and intramuscular adipose tissues in hanwoo beef cattle using a systems biology approach. *Int J Genomics.* (2014) 2014:679437. doi: 10.1155/2014/679437
11. Keel BN, Zarek CM, Keele JW, Kuehn LA, Snelling WM, Oliver WT, et al. RNA-Seq Meta-analysis identifies genes in skeletal muscle associated with gain and intake across a multi-season study of crossbred beef steers. *BMC Genomics.* (2018) 19:430. doi: 10.1186/s12864-018-4769-8
12. Bazile J, Jaffrezic F, Dehais P, Reichstadt M, Klopp C, Laloe D, et al. Molecular signatures of muscle growth and composition deciphered by the meta-analysis of age-related public transcriptomics data. *Physiol Genomics.* (2020) 52:322–32. doi: 10.1152/physiolgenomics.00020.2020
13. Langmead B, Trapnell C, Pop M, Salzberg SL. Ultrafast and memory-efficient alignment of short DNA sequences to the human genome. *Genome Biol.* (2009) 10:R25. doi: 10.1186/gb-2009-10-3-r25
14. Li H, Ruan J, Durbin R. Mapping short DNA sequencing reads and calling variants using mapping quality scores. *Genome Res.* (2008) 18:1851–8. doi: 10.1101/gr.078212.108
15. Zhou X, Wu W, Li H, Cheng Y, Wei N, Zong J, et al. Transcriptome analysis of alternative splicing events regulated by SRSF10 reveals position-dependent splicing modulation. *Nucleic Acids Res.* (2014) 42:4019–30. doi: 10.1093/nar/gkt1387
16. Pavlyukov MS, Yu H, Bastola S, Minata M, Shender VO, Lee Y, et al. Apoptotic cell-derived extracellular vesicles promote malignancy of glioblastoma via intercellular transfer of splicing factors. *Cancer Cell.* (2018) 34:119–35. e110. doi: 10.1016/j.ccell.2018.05.012
17. Young MD, Wakefield MJ, Smyth GK, Oshlack A. Gene ontology analysis for RNA-seq: accounting for selection bias. *Genome Biol.* (2010) 11:R14. doi: 10.1186/gb-2010-11-2-r14
18. Ogata H, Goto S, Sato K, Fujibuchi W, Bono H, Kanehisa M. KEGG: kyoto encyclopedia of genes and genomes. *Nucleic Acids Res.* (1999) 27:29–34. doi: 10.1093/nar/27.1.29
19. Mao XZ, Cai T, Olyarchuk JG, Wei LP. Automated genome annotation and pathway identification using the KEGG Orthology (KO) as a controlled vocabulary. *Bioinformatics.* (2005) 21:3787–93. doi: 10.1093/bioinformatics/bti430
20. Kanehisa M, Sato Y, Morishima K. BlastKOALA and GhostKOALA: KEGG Tools for Functional Characterization of Genome and Metagenome Sequences. *J Mol Biol.* (2016) 428:726–31. doi: 10.1016/j.jmb.2015.11.006
21. Brooks AN, Yang L, Duff MO, Hansen KD, Park JW, Dudoit S, et al. Conservation of an RNA regulatory map between Drosophila and mammals. *Genome Res.* (2011) 21:193–202. doi: 10.1101/gr.108662.110
22. Ramani AK, Calarco JA, Pan Q, Mavandadi S, Wang Y, Nelson AC, et al. Genome-wide analysis of alternative splicing in Caenorhabditis elegans. *Genome Res.* (2011) 21:342–8. doi: 10.1101/gr.114645.110

23. Wu JY, Li AM, Cai HF, Zhang CG, Lei CZ, Lan XY, et al. Intron retention as an alternative splice variant of the cattle ANGPTL6 gene. *Gene.* (2019) 709:17–24. doi: 10.1016/j.gene.2019.05.031
24. Zhang SH, Cai HF, Yang Q, Shi T, Pan CY, Lei CZ, et al. Identification of novel alternative splicing transcript and expression analysis of bovine TMEM95 gene. *Gene.* (2016) 575:531–6. doi: 10.1016/j.gene.2015.09.026
25. Liu SY, Jiang H, Yuan B, Gao Y, Dai LS, Zhang JB. Characterization of a novel CAPN3 transcript generated by alternative splicing in cattle. *Genet Mol Res.* (2015) 14:457–63. doi: 10.4238/2015.January.23.20
26. Mcgarry JD, Sen A, Esser V, Woeltje KF, Weis B, Foster DW. New insights into the mitochondrial carnitine palmitoyltransferase enzyme system. *Biochimie.* (1991) 73:77–84. doi: 10.1016/0300-9084(91)90078-F
27. Mcgarry JD, Brown NF. The mitochondrial carnitine palmitoyltransferase system. From concept to molecular analysis. *Eur J Biochem.* (1997) 244:1–14. doi: 10.1111/j.1432-1033.1997.00001.x
28. Sorensen BM, Kazala EC, Murdoch GK, Keating AF, Cruz-Hernandez C, Wegner J, et al. Effect of CLA and other C18 unsaturated fatty acids on DGAT in bovine milk fat biosynthetic systems. *Lipids.* (2008) 43:903–12. doi: 10.1007/s11745-008-3216-z
29. Tabaran A, Balteanu VA, Gal E, Pusta D, Mihaiu R, Dan SD, et al. Influence of DGAT1 K232A Polymorphism on milk fat percentage and fatty acid profiles in romanian holstein cattle. *Anim Biotechnol.* (2015) 26:105–11. doi: 10.1080/10495398.2014.933740
30. Liu JJ, Wang ZQ, Li J, Li H, Yang LG. Genome-wide identification of diacylglycerol acyltransferases (DGAT) family genes influencing milk production in buffalo. *BMC Genet.* (2020) 21:26. doi: 10.1186/s12863-020-0832-y
31. Lozeman FJ, Middleton CK, Deng JT, Kazala EC, Verhaege C, Mir PS, et al. Characterization of microsomal diacylglycerol acyltransferase activity from bovine adipose and muscle tissue. *Comp Biochem Physiol B Biochem Mol Biol.* (2001) 130:105–15. doi: 10.1016/S1096-4959(01)00413-4
32. Kazala EC, Lozeman FJ, Mir PS, Aalhus JL, Schmutz SM, Weselake RJ. Fatty acid composition of muscle fat and enzymes of storage lipid synthesis in whole muscle from beef cattle. *Lipids.* (2006) 41:1049–57. doi: 10.1007/s11745-006-5055-0
33. Zheng L, Shockey J, Guo F, Shi LM, Li XG, Shan L, et al. Discovery of a new mechanism for regulation of plant triacylglycerol metabolism: the peanut diacylglycerol acyltransferase-1 gene family transcriptome is highly enriched in alternative splicing variants. *J Plant Physiol.* (2017) 219:62–70. doi: 10.1016/j.jplph.2017.09.009
34. Guiheneuf F, Leu S, Zarka A, Khozin-Goldberg I, Khalilov I, Boussiba S. Cloning and molecular characterization of a novel acyl-CoA:diacylglycerol acyltransferase 1-like gene (PtDGAT1) from the diatom Phaeodactylum tricornutum. *Febs J.* (2011) 278:3651–66. doi: 10.1111/j.1742-4658.2011.08284.x

Conflict of Interest: The authors declare that the research was conducted in the absence of any commercial or financial relationships that could be construed as a potential conflict of interest.

frontiers in Veterinary Science

ORIGINAL RESEARCH
published: 02 June 2021
doi: 10.3389/fvets.2021.672852

Evidence Against the Causal Relationship Between a Putative Cis-Regulatory Variant of *MYH3* and Intramuscular Fat Content in Pigs

Cong Huang†, Liepeng Zhong†, Xiaoxiao Zou, Yizhong Huang, Liping Cai and Junwu Ma**

State Key Laboratory for Swine Genetics, Breeding, and Production Technology, Jiangxi Agricultural University, Nanchang, China

OPEN ACCESS

Edited by:
James Reecy,
Iowa State University, United States

Reviewed by:
Gary Rohrer,
U.S. Meat Animal Research Center, Agricultural Research Service, United States Department of Agriculture (USDA), United States
Christopher K. Tuggle,
Iowa State University, United States

***Correspondence:**
Liping Cai
1052555361@qq.com
Junwu Ma
ma_junwu@hotmail.com

†These authors have contributed equally to this work and share first authorship

Specialty section:
This article was submitted to Livestock Genomics, a section of the journal Frontiers in Veterinary Science

Received: *26 February 2021*
Accepted: *29 April 2021*
Published: *02 June 2021*

Citation:
Huang C, Zhong L, Zou X, Huang Y, Cai L and Ma J (2021) Evidence Against the Causal Relationship Between a Putative Cis-Regulatory Variant of MYH3 and Intramuscular Fat Content in Pigs. Front. Vet. Sci. 8:672852. doi: 10.3389/fvets.2021.672852

Improving meat quality has become the main goal of modern pig breeding. Intramuscular fat content (IMF) is an important trait influencing meat quality of livestock, but the molecular mechanism behind this trait is still unclear. Recently, Cho et al. reported the discovery of the first causal mutation affecting IMF and red flesh color (a*) in pigs, namely *XM_013981330.2:g.−1805_−1810del*, a 6-bp deletion variant in the porcine *MYH3* promoter region. The objective of this study was to reassess the causality of this mutation for its potential commercial application. By Sanger sequencing, we firstly identified several new variants (including a 4-bp deletion) at or near the 6-bp deletion site, which formed four haplotypes in multiple breeds. Unexpectedly, the 6-bp deletion allele, previously determined as the *MYH3 Q* allele because of its significantly positive effect on IMF and a*, was found not only in Chinese indigenous breeds, but also in four western commercial breeds with relatively lower IMF levels, including Duroc, Large White, Landrace and Pietrain. More surprisingly, we found that the *MYH3 Q* allele and the haplotypes harboring it had no significant effects on IMF, marbling and color score in three large-scale divergent pig populations: the heterogeneous F6 and F7 pigs and commercial crossbred Duroc × (Landrace × Yorkshire) pigs. Transient transfection analysis in porcine satellite cells showed that the 6-bp deletion variants had a negligible effect on transcription of reporter gene, but could attenuate the MRF (myogenesis regulatory factors)-induced increase in luciferase activity of the *MYH3* promoter vector. The *MYH3* protein level in muscle did not differ significantly among the haplotype groups. Therefore, our results cannot support the causal relationship between the 6-bp deletion in *MYH3* and IMF trait, suggesting that the causal mutation for the IMF QTL on SSC12 needs to be further identified.

Keywords: *MYH3*, 6-bp deletion variant, causal mutation, meat quality traits, intramuscular fat content

INTRODUCTION

Intramuscular fat (IMF) content plays an important role in determining the eating quality of pork, such as tenderness, juiciness and flavor. Therefore, the pork with high IMF content and good eating quality is generally favored by consumers (1, 2). There are considerable variations in IMF contents among different pig breeds, especially between western commercial

pig breeds and Chinese native pig breeds (3–5), which suggests that heredity is a major determinant of IMF. In fact, a large number of quantitative trait loci (QTL) or candidate genes for IMF have been identified by linkage and genome-wide association (GWA) studies. However, despite the progress achieved in this field in recent years, molecular mechanisms behind IMF trait remains elusive, as few causative genes or causative mutations affecting IMF content of pork have been determined (6–10).

Recently, a study conducted by Cho et al. presented evidences that a 6-bp deletion (*XM_013981330.2:g.−1805_−1810del*) in the promoter region of *MYH3* is the first causal mutation that was identified for IMF and red flesh color (a*) in domestic pigs (11). They firstly identified a 488.1-kb critical region on porcine chromosome 12 (SSC12) that affects both IMF and a* by a joint linkage-linkage disequilibrium analysis in two independent F2 crosses between Korean native pigs (KNPs) and Western commercial breeds (Landrace and Duroc). In this critical region, only the *MYH3* gene, encoding myosin heavy chain 3, was found to be preferentially overexpressed in the skeletal muscle of KNPs than in that of Western commercial breeds. They further validated *MYH3* as a quantitative trait gene (QTG) using transgenic mice, and then discovered the *XM_013981330.2:g.−1805_−1810del* variant in the 5′-flanking region of *MYH3*, which deletion (*Q*) allele carriers exhibited significantly higher values of IMF and a* than wild-type (*q*) allele carriers. They demonstrated that this 6-bp deletion variant could abrogate the binding of the regulatory myogenic regulatory factors (MRFs, i.e., *MYOD*, *MYOD*, *MYF5* and *MRF4*) and act as a significantly weaker repressor, resulting in increased expression of *MYH3* in the skeletal muscle. In addition, they found that the *MYH3 Q* allele occurred exclusively in Asian domestic breeds (such as Chinese Neijiang, Chinese Putian, Chinese Xiang, and KNP) and Asian wild boars, but was almost absent in European and African wild boars, as well as European commercial pig breeds (including Large White, Landrace and Duroc, etc.), which indicates that this allele is of Asian origin.

In general, the effects of a causal mutation can be replicated in different populations. Unfortunately, we herein present genetic and functional evidence against the causal relationship of the *XM_013981330.2:g.−1805_−1810del* with meat quality traits. We found that the *MYH3 Q* allele was present not only in Chinese native breeds but also in four western commercial breeds including Duroc, Large White, Landrace and Pietrain. The effects of the 6-bp deletion variant and a novel 4-bp deletion variant at the same locus identified by us on the meat quality traits including IMF, marbling and color score were not significant in either heterogenous stock F6 pig population or a commercial hybrid Duroc × Landrace × Yorkshire (DLY) pig populations. And these two deletion variants were also not significantly associated with a* in both the heterogeneous F7 pigs and the DLY pigs. The protein expression level of *MYH3* in porcine longissimus muscle did not differ significantly among animals with different genotypes or haplotype combinations at the target *MYH3* locus. The findings thus demonstrate that the *MYH3 XM_013981330.2:g.−1805_−1810del* is unlikely to be causal mutation for the meat quality traits.

MATERIALS AND METHODS

Animals and Phenotypes

A total of 1391 pigs, including 751 F6 pigs and 587 F7 pigs from a heterogenous stock and 546 Duroc × (Yorkshire × Landrace) (DYL) pigs were used in this study. The pig heterogenous stock was established from 8 founder divergent pig breeds including 4 Chinese indigenous breeds (Erhualian, Laiwu, Bamaxing, and Tibetan) and 4 Western commercial breeds (Duroc, Large White, Landrace, and Pietrain), which has been described in greater detail elsewhere (12). The DYL pigs were all raised on a farm of the Jiangxi Guohong Group Co. Ltd. in Jiujiang city (Jiangxi Province), and they were randomly selected from the offspring of about 20 adult Duroc boars and hundreds of L × Y sows on the farm. All heterogenous animals were slaughtered at the age of 240 ± 3 days, and the DYL pigs were slaughtered at 180 ± 3 days. The total number of slaughter batches of F6, F7 and DYL were 23, 19, and 17, respectively. About 30–36 pigs were slaughtered in each batch. Meat quality measurement was conducted as reported previously (13). Briefly, the *longissimus dorsi* (LD) were collected from the left side of each carcass between the 11th-rib and the first lumbar vertebra for measurement of meat quality traits. Meat redness (a*) was measured by CM-2600d/2500d Minolta Chroma meter. Meat color scores (ranging from 1 to 6, with 1 = pale and 6 = dark), marbling scores (ranging from 1 to 10 with 1 = devoid and 10 = overly abundant) were subjectively evaluated according to National Pork Producer Council (NPPC) guidelines (14) and the IMF content was determined by using the Soxhlet method (15). Except for the IMF of the F7 pigs, all phenotypic data of the three populations have been collected.

Genotyping and Sequencing of the *MYH3* Locus

Genomic DNA was isolated from the ear tissue of each pig using a standard phenol/chloroform method and dissolved in Tris-EDTA buffer. The DNA quality and concentration were determined using a Nanodrop-1000 spectrophotometer (Thermo Fisher, USA). DNA samples from 94 F7 pigs were genotyped for the 6-bp deletion variant, *XM_013981330.2:g.−1805_−1810del*, in the promoter of *MYH3* using the PCR-RFLP method developed previously (11). A fragment with the expected size of 457bp covering the *XM_013981330.2:g.−1805_−1810del* mutation was amplified by PCR (primers: forward 5′ – GTG GGC AAA GGG ATG AAG - 3′; reverse 5′ – GGA ATA AGA ATG GGC AAA CG - 3′). And the amplicons were digested with the restriction endonuclease, *Hpy*CH4IV. Sanger sequencing of the PCR products from these F7 animals were conducted to determine the sequence variations located at and near the 6-bp deletion, and a set of haplotypes were subsequently constructed with the adjacent variations we identified. In addition, the Sanger sequencing method was also applied to determine the distribution of haplotypes in 51 pigs from 8 founder breeds of the heterozygous stock and in 546 DYL pigs. For all the F6 and F7 individuals, their haplotypes in the target area could be inferred from the next-generation sequencing (NGS) data (**Supplementary Table 1**), which were generated using the Illumina Xten platform (Illumina Inc. San Diego, CA). We

performed whole-genome NGS for each founder animals (F0) with an average coverage depth ∼30×. The genome of each F6 and F7 animal was sequenced to 7.8-fold average coverage. The methods for read mapping and genotype calling in our NGS data was described previously (12).

Dual-Luciferase Assay and Western Blotting Analysis

Pig muscle satellite cells (MZ-3319, mingzhoubio) were cultured in DMEM (Hyclone) containing 10% FBS (Gibco) and 1% penicillin-streptomycin reagent (Solarbio). Cells were grown at 37°C in humidified air containing 5% CO_2 (Thermo) until transfection. Then 20 μl lipo2000 were dissolved in 980 μl Opti-mem serum-free medium followed by mixture and setting for 5 min at room temperature. All *MYH3* luciferase reporter constructs were generated by subcloning 4 different haplotype sequences of about 90 bp centered by *XM_013981330.2:g.−1805_−1810del* in front of the luciferase gene in the pGL3 basic vector. The MZ-3319 cells were seeded by adding 1 ml cell suspension containing 5×10^5 cells/ml to each well of 6-well culture plate and then placed in a cell incubator at 37°C in humidified air containing 5% CO_2 until cells grow to 70–80% degrees of fusion. The mixture of 5 μl synthetic sequences and 245 μl Opti-mem of five synthetic sequences were added to the 200 μl mixtures of 4 μl lipo2000 and 196 μl Opti-mem serum-free medium. All transfection solutions static at room temperature for 20 min. Before transfection, the cells were rinsed once with sterile PBS and then 2 ml serum-free medium was added to each well of the cell plates. All transfection solutions were added slowly to the serum-free medium of each cell and then put the plates in cell incubator for 6 h at 37°C. After removing serum-free medium, complete medium was added to culture the cells. Cells were collected to carry out the subsequent experiments after 48 h transfection. Transfected cells were rinsed in PBS and then lysed in 1 × passive lysis buffer. Luciferase assays were performed using a Dual-Luciferase Reporter Assay System (Promega) to measure Renilla (internal control) and firefly (reporter construct) luciferase values. MRF genes, including *MYF5*, *MYOD*, *MYOG*, and *MRF4*, were co-transfected with an *MYH3* promoter and an internal control vector into MZ-3319 cells. After 48 h, the effects of four MRF gene on *MYH3* promoter activity were assayed using the Dual-Luciferase Reporter Assay System.

Western blot analysis was used for measuring the protein expression of the *MYH3* gene in *longissimus dorsi* muscle of 18 F7 pigs with different genotypes of the *MYH3* locus. In brief, total protein was isolated from cells using RIPA buffer (R0020; Solarbio) containing a PMSF protein inhibitor (100 mM; 1.5 ml). Protein concentrations were quantified by a BCA Protein Assay Kit (PICPI23223, Thermo Fisher Scientific, Inc., USA) after muscle tissue was totally lysed followed by centrifugation for 15 min at 4°C, 12,000 g. Proteins were separated by SDS-PAGE after the mixture of protein and SDS-PAGE loading buffer was kept in boiling water for 10 min (Leica HI1210, Leica Biosystems). Then the protein was semi-dry transferred onto immobilon-NC transfer membranes (HATF00010, Millipore Corporation), blocked in 5% fat-free milk for 1 h at room temperature and then incubated with primary antibodies (ab124205, Abcam plc.) in 5% milk overnight at 4°C. After being washed three times by TBST, the membrane was then incubated with secondary antibody for 1 h at 37°C. The bands of target proteins were visualized through an ECL imaging system (Tanon 5200, Shanghai).

Statistical Analysis

Association analyses between the *MYH3* polymorphisms (including *XM_013981330.2:g.−1805_−1810del*) and target traits in each population were conducted by using a general linear model (GLM) in R software (version 3.6.2). The linear model is shown below:

$$Y_{ijk} = \mu + S_i + B_j + G_k + W_{ijk} + e_{ijk} \quad (1)$$

where, Y_{ijk} is the phenotypic value of each trait, μ is overall mean for each trait, S_i is the effect of gender, B_j is the effect of slaughter batch, G_k is the effect of the *MYH3* genotypes or haplotype combinations, W_{ijk} is the covariate of slaughter weight, and e_{ijk} is the random error.

The least square mean ± standard error for each haplotype combination was obtained using the *lsmeans()* function in the lsmeans R package. Tukey pair-wise comparisons were subsequently conducted to get difference between groups by using the *cld()* function in the multcomp *R* package. The *P*-value < 0.05 was considered as significant.

RESULTS

Discovery of New Variants and Haplotypes in the Promoter of *MYH3*

Considering that the heterogenous F7 pigs had genetic polymorphisms of eight breeds, we conducted fragment analysis on 94 F7 pigs to uncover mutations around the 6-bp deletion, *XM_013981330.2:g.−1805_−1810del*, in the promoter of *MYH3* by PCR-based Sanger sequencing and PCR-RFLP methods. Sanger sequencing showed four haplotypes and seven haplotype combinations in those pigs (**Table 1** and **Supplementary Figure 1**). Two of the haplotypes (*H1* and *H2*) are previously known and the other two (*H3* and *H4*) are new. The haplotypes consisted of a single nucleotide insertion site (insert T or C), a SNP site (G > A) just 1-nt upstream of the 6-bp deletion and a deletion site (6-bp or 4-bp deletions). However, we noted that the PCR-RFLP with *Hpy*CH4IV endonuclease can only distinguish the mutate type *H2* from the other three haplotypes, while the two novel haplotypes *H3* and *H4*, albeit harboring the 6-bp deletion (the *MYH3 Q* allele) and the 4-bp deletion, respectively, were wrongly judged as corresponding to the *q* allele as the wild-type haplotype *H1* (**Table 1**). Although the *H2* and *H3* differ by only one SNP allele, the DNA strand with *H3* cannot be cleaved by *Hpy*CH4IV enzyme. Therefore, the PCR-RFLP method with *Hpy*CH4IV is not suitable for genotyping of the *MYH3 XM_013981330.2:g.−1805_−1810del* in pig populations with multiple haplotypes.

The Distribution of the Four Haplotypes in Eight Breeds

To detect the origin and distribution of the four haplotypes in eight founder breeds of the heterogenous stock pig population, we performed PCR and Sanger sequencing on genomic DNA from the F0 pigs in the population. **Table 2** shows that the *H1* haplotype was present in all the breeds. Surprisingly, the previously recognized *H2* haplotype harboring the *MYH3 Q* allele was found not only in the three Chinese native breeds (Tibetan, Erhualian and Laiwu) except Bamaxiang, but also in the four western commercial pig breeds, including Duroc, Large White, Pietrain and Landrace (**Table 2**). The new haplotype *H3*, also harboring the *MYH3 Q* allele, was detected exclusively in Bamaxiang, while another new haplotype *H4* distributed in Chinese Laiwu breed and the four commercial pig breeds. So the data demonstrates that all the 8 breeds had carriers of the *MYH3 XM_013981330.2:g.−1805_−1810del* variant which was considered to be responsible for the observed SSC12 QTL effect on IMF and a*.

The Effect of the Haplotypes on Meat Quality Traits in Three Pig Populations

Next, we sought to evaluate the effect of the four haplotypes on 4 meat quality traits including a*, color score, marbling score and IMF, in 751 F6 and 587 F7 pigs whose haplotypes were obtained from their next-generation sequencing (NGS) data. Based on the Sanger sequencing results of 94 F7 samples, the NGS-derived haplotypes were confirmed to be correct. Seven haplotype combinations were identified in both the F6 and F7 pigs. In each of the two populations, the number of animals with the 11, 12 haplotype combinations exceeded 133, while the number of samples with the 22 haplotype combination (having two copies of the 6-bp deletion) was only 29 and 13 in F6 and F7, respectively (**Table 3**). The result of association analysis in F6 pigs showed that the haplotypes was significantly ($P < 0.05$) associated with a* and IMF, but not color score and marbling (**Table 3**). Particularly, the difference in a* among the 7 haplotype combinations was highly significant ($P = 3.06E-07$), and the average of a* values were significantly lower in the pigs with the 11 and 13 haplotype combinations than those with 12 and 14 haplotype combinations. The means of IMF for the 11, 12, 13, and 14 haplotype combinations did not differ from each other. The difference in the IMF trait was only found between the 23 and 24 haplotype combinations in the F6 pigs. In contrast, the haplotypes was not significantly associated with a* in the F7. Although the 12 and 14 haplotype combinations from the F7 differed significantly ($P < 0.05$) in color score and Marbling, there was no significant difference in the two traits between the 11, 12, and 22 haplotype combinations in this population. The results suggest that neither

TABLE 1 | Identification of haplotypes containing the *MYH3* 6-bp deletion variant in heterogenous F7 pigs by Sanger sequencing.

Haplotype ID	Class	Haplotype sequences	Allele of the 6-bp deletion determined by PCR-RFLP
H1	Known	TG-GGGGAACAACA**GCAGTCC**TCCTGCT	*q*
H2	Known	TG**T**GGGGAACACAC**G------**TCCTGCT	*Q*
H3	New	TG**T**GGGGAACACAC**A------**TCCTGCT	*q*
H4	New	TG**C**GGGGAACACAC**AAG------**TCCTGCT	*q*

PCR-RFLP, PCR amplification and subsequent HpyCH4IV digest.
Different nucleotide repeats in the haplotypes are boxed.

TABLE 2 | The haplotype combinations found in 8 founder breeds of the heterogeneous stock population.

Breeds	Haplotype combinations						
	N	**11**	**12**	**13**	**14**	**22**	**33**
Chinese Bamaxiang	5			2			3
Chinese Tibetan	7	4	2			1	
Chinese Erhualian	6		5			1	
Chinese Laiwu	6		2		2	2	
Duroc	8	3	2		3		
Large White	6	3	2		1		
Pietrain	6	5	1				
Landrace	7	4	2		1		

N: The total number of animals in each pig breed.

TABLE 3 | Comparison of four meat quality traits among the haplotype combinations in the heterogenous F6, F7, and DYL pig populations (least square mean ± standard error).

Traits	Haplotype combinations							*P*-value
	11	**12**	**13**	**14**	**22**	**23**	**24**	
F6 ($N = 751$)								
N	272	224	114	58	29	34	20	
a*	0.99 ± 0.08^{a}	1.54 ± 0.09^{c}	1.08 ± 0.12^{ab}	1.74 ± 0.16^{c}	1.73 ± 0.23^{bc}	1.60 ± 0.21^{abc}	1.70 ± 0.28^{abc}	3.06E-07
Color score	2.74 ± 0.04^{a}	2.83 ± 0.05^{a}	2.73 ± 0.06^{a}	2.73 ± 0.09^{a}	2.91 ± 0.13^{a}	2.79 ± 0.11^{a}	2.59 ± 0.15^{a}	0.495
Marbling	2.64 ± 0.06^{a}	2.80 ± 0.07^{a}	2.85 ± 0.10^{a}	2.57 ± 0.14^{a}	3.10 ± 0.19^{a}	2.88 ± 0.17^{a}	2.38 ± 0.23^{a}	0.053
IMF (%)	2.08 ± 0.04^{ab}	2.17 ± 0.05^{ab}	2.08 ± 0.07^{ab}	1.98 ± 0.1^{ab}	2.21 ± 0.13^{ab}	2.37 ± 0.12^{b}	1.68 ± 0.16^{a}	0.011
F7 ($N = 587$)								
N	227	133	70	91	13	26	27	
a*	1.07 ± 0.11^{a}	1.49 ± 0.15^{a}	0.86 ± 0.20^{a}	1.07 ± 0.17^{a}	1.53 ± 0.45^{a}	1.20 ± 0.32^{a}	0.99 ± 0.32^{a}	0.146
Color score	3.09 ± 0.04^{ab}	3.19 ± 0.06^{b}	2.91 ± 0.08^{ab}	2.86 ± 0.07^{a}	2.88 ± 0.18^{ab}	3.07 ± 0.13^{ab}	3.18 ± 0.13^{ab}	0.003
Marbling	3.22 ± 0.06^{ab}	3.37 ± 0.09^{b}	3.04 ± 0.11^{ab}	2.93 ± 0.10^{a}	2.92 ± 0.26^{ab}	3.24 ± 0.18^{ab}	3.33 ± 0.18^{ab}	0.015
DYL ($N = 546$)								
N	434	73	5	33	NA	1	NA	
a*	1.20 ± 0.06^{a}	1.12 ± 0.11^{a}	1.24 ± 0.41^{a}	1.25 ± 0.17^{a}	NA	0.76	NA	0.660
Color score	3.02 ± 0.03^{a}	3.05 ± 0.06^{a}	2.89 ± 0.23^{a}	3.06 ± 0.09^{a}	NA	3	NA	0.868
Marbling	2.72 ± 0.04^{a}	2.69 ± 0.07^{a}	2.53 ± 0.27^{a}	2.75 ± 0.11^{a}	NA	2	NA	0.661
IMF (%)	1.82 ± 0.03^{a}	1.80 ± 0.07^{a}	1.70 ± 0.25^{a}	1.94 ± 0.10^{a}	NA	0.73	NA	0.389

Means with the same superscript letter (a-c) in a row are not significantly ($P < 0.05$) different.
IMF, intramuscular fat.
DYL, Duroc × (Landrace × Yorkshire) commercial hybrid pig.

haplotypes nor variants in the haplotype combinations including the *XM_013981330.2:g.−1805_−1810del* could significantly and positively influence both a* and IMF (or marbling).

Given that the four haplotypes were also found in Duroc, Landrace and Large White (or Yorkshire), we then examined whether the four haplotypes were associated with the meat quality traits in their hybrid DLY. In 546 DLY pigs, 5 haplotypes combinations including 11, 12, 13, 14, and 23 were detected through Sanger sequencing. The most predominant haplotype combination was 11, followed by 12 and 14, whose frequencies were 74.5, 13.4, and 6.0%, respectively (**Table 3**). However, we demonstrated that there was no significant difference in the analyzed 4 meat quality traits (a*, color score, marbling, and IMF) among those haplotype combinations (**Table 3**). Thus, the results of the analysis in the two populations strongly question that *XM_013981330.2:g.−1805_−1810del* is a causal mutation of the meat quality traits.

Functional Implication of the Haplotypes on *in vitro* and *in vivo* Gene Expression

The above-mentioned results motivated us to investigate whether the four haplotypes at 5′-flanking region of *MYH3* affect gene expression. To this end, we compared the four haplotype (*H1*, *H2*, *H3,* and *H4*) promoter driven luciferase activities through transient transfection assays in porcine satellite cells. The cells were co-transfected with reporter constructs containing one of the four haplotypes and an empty expression vector (as a control), each of the four MRFs (*MYH5*, *MYOD*, *MYOG,* and *MRF4*) expression vectors or all the four MRFs expression vectors. No significant differences were observed in luciferase activities among the four haplotypes in control cells transfected with empty expression vector (**Figure 1A**). Notably, the wild-type haplotype *H1* promoter construct exhibited a nearly 2–3-folds increase ($P < 0.05$) in luciferase activities after expression of either one or all of the MRFs. In contrast, these MRFs did not always enhance gene expression in the three mutant haplotypes constructs, and the extent to which they altered luciferase activities was significantly reduced (**Figure 1A**). The results suggest that the wild-type haplotype may be serve as an enhancer activated by the MRFs, but the mutations on it could impair the activation of transcription factor and the function of the element.

To further assess the effect of the four haplotypes on *MYH3* gene expression, we performed western blotting analysis on the protein extracted from the *longissimus dorsi* muscle of 18 F7 pigs with five different haplotype combinations (11, 12, 13, 14, and 22; 3 samples per haplotype combination). We did not observe significant difference in the *MYH3* protein levels between any pair of the haplotype combinations (**Figure 1B**), suggesting that the mutations detected in the *MYH3* promoter had negligible effect on *MYH3* expression in adult muscle.

DISCUSSION

Identification of major genes affecting meat quality traits will help to improve meat quality efficiently and yield significant

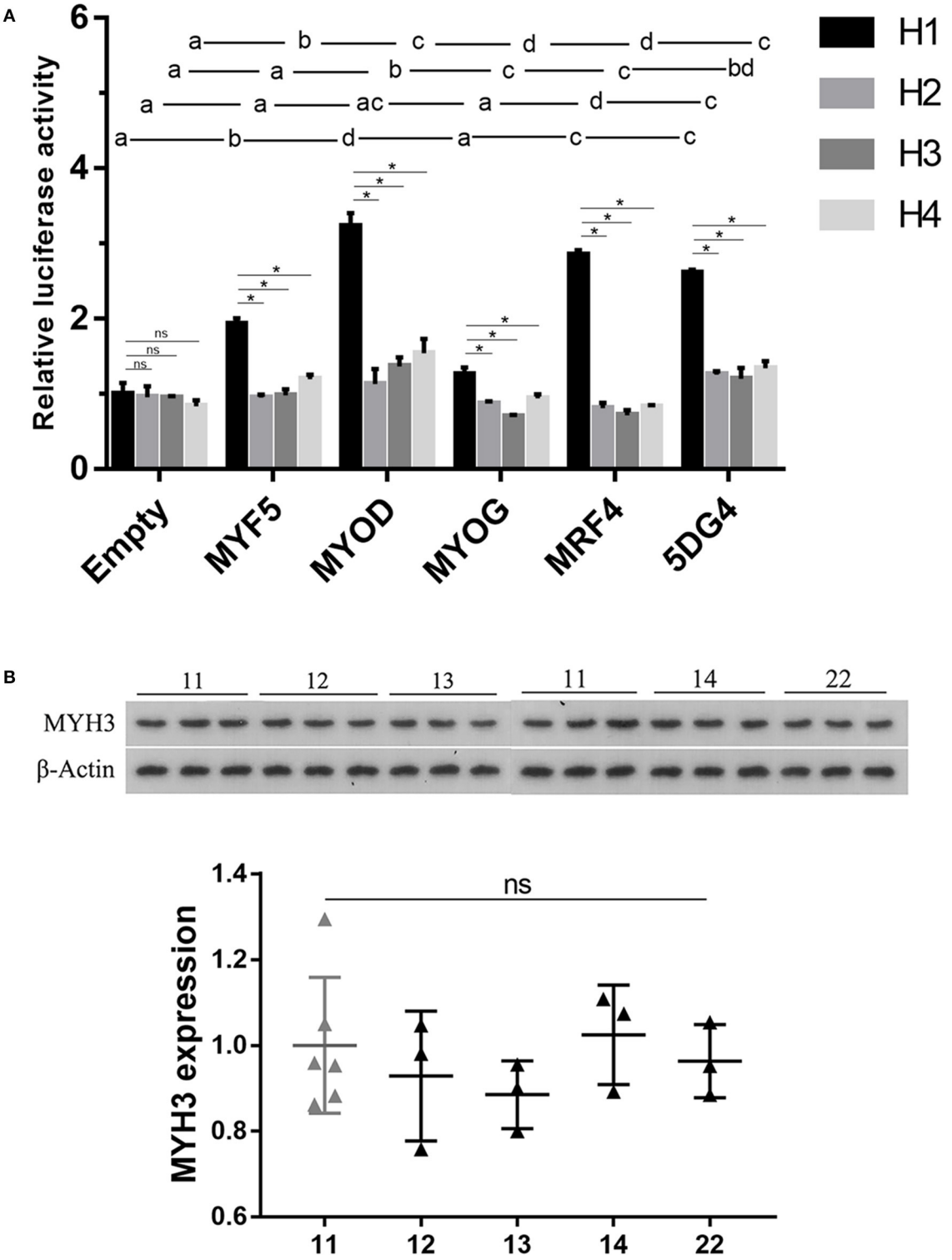

FIGURE 1 | Analysis of the effect of the identified four haplotypes on gene expression analyses of (upper) and western blotting assays of 18 LD muscle samples (lower). **(A)** Transient co-transfection assays of porcine muscle satellite cells. The various haplotype-luciferase reporter constructs were co-transfected with either one of the four MRF constructs or the four MRFs (5DG4). The luciferase activity did not differ significantly between groups with the same letter. Data histograms and error bars represent the mean ± standard error of triplicate independent samples. ns: $P > 0.05$, $^*P < 0.05$. **(B)** Western blot analysis of *MYH3* protein levels in muscle from animals with different haplotype combinations. The gene expression level was normalized from the gray value calculated by ImageJ. Data are presented as mean ± SD. ns: $P > 0.05$, $^*P < 0.05$.

economic benefits. This is clearly reflected in the breeding application of several causal genes and their causal mutations, such as *RYR1* R615C, *PRKAG3* R200Q, and *IGF2* intron3-g.3072G>A (16–18). The causalities between these genes and several meat quality traits have been endorsed by multiple studies. So far, only one study has shown that the 6-bp deletion, *XM_013981330.2:g.−1805_−1810del*, in the promoter of *MYH3* is very likely the first identified causal mutation underlying IMF. Its researchers also demonstrated that the significant effects of this mutation on IMF and a* were replicated in two independent cohorts: a Landrace × KNP F_2 intercross and a Duroc × KNP F_2 intercross. However, due to that the so-called *MYH3 Q* allele (i.e., 6-bp deletion allele) favorably associated with the meat quality traits in the two F2 populations originated only from the KNP pigs and not from other founder breeds, the length of linkage disequilibrium block surrounding the mutation would be too long (>700 kb) to make it difficult to determine whether the 6-bp deletion variant is the causal mutation itself or a marker closely linked to the causal mutation. Therefore, examining the segregation of the 6-bp deletion and its effect on meat quality in pigs with other genetic backgrounds may help verify whether or not it is a causal mutation. In this study, we first determined that *XM_013981330.2:g.−1805_−1810del* was segregating in the heterogeneous F6 and F7 pig populations derived from the intercross between 8 divergent founder breeds. But surprisingly, we further found that this mutation occurred in all the 8 founder breeds, including 4 Chinese indigenous breeds (Bamaxiang, Laiwu, Erhualian, and Tibetan) and 4 western commercial breeds (Duroc, Landrace, Large White and Pietrain). The result is not in agreement with the findings of Cho et al. (11) who did not find the *MYH3 Q* allele in Western commercial breeds. Therefore, their inference that the *MYH3 Q* allele is of Asian origin and likely predates domestication needs to be re-examined.

We further showed that the *MYH3 Q* allele had no significant impact on IMF, marbling and color score in the F6 or F7 populations, which is contrary to the result of the previous study (11). It is worth mentioning that the genome-wide association (GWA) study in the F6 pigs have identified a QTL for both IMF (*P*-value = 1.31E-22) and a* (*P*-value = 1.64E-26) located close to the *MYH3* gene on SSC12 (data not shown). Therefore, the 6-bp deletion variant could not be the cause of the IMF QTL on SSC12 detected in the F6 population. In addition, the *MYH3 Q* allele was also present in 78 (14.2%) out of the 546 DLY pigs tested, while our previous GWAS study showed that there was no QTL for IMF or a* adjacent to the *MYH3* gene in this DLY population (13). Obviously, the effects of the *MYH3 Q* allele on the 4 meat quality traits were also negligible in the DLY pigs. Thus, we replicated the results in both the F6 and DLY populations with and without the SSC12 QTL, respectively, strongly suggesting that the *XM_013981330.2:g.−1805_−1810del* is not the causal mutation for the meat quality traits.

It was noted that the haplotypes H2, H3, and H4 contains the same $(AC)_3$ nucleotide repeats, whereas the H1 has $(AAC)_2$ $(CAG)_2$ $(TCC)_2$ (there is a C that needs to be used for both the first 2 trinucleotide repeats) (**Table 1**). Since microsatellite segments may help open DNA structure and even cause disease (19), we evaluated whether this kind of variation was more likely to affect the meat quality traits. The association analysis showed that the nucleotide repeats had negligible effect on the four meat quality traits (**Supplementary Table 2**).

The transient transfection analysis of the porcine fibroblast cells performed by Cho et al. showed that the *MYH3 q* variant acts as a repressor element, whereas the *MYH3 Q* variant functions as a significantly weaker repressor, leading to increased transcription of *MYH3* in skeletal muscle of KNPs or *Q* allele carriers. However, we did not confirm that the 6-bp deletion variant can cause a significant change in the *MYH3* protein level in porcine skeletal muscle and the transcriptional activities of the luciferase reporter constructs containing the *MYH3 Q* and *q* haplotypes. Interestingly, we found that the *MYH3 q* variant site may be triggered to become an enhancer by overexpression of one of the MRFs in porcine muscle satellite cells, but the *MYH3 Q* variant significantly weakened the stimulatory effect of the MRFs. Some studies showed that Western lean-type pig breeds (such as Landrace, Large White, Yorkshire) had a significantly higher expression level of *MYH3* than Chinese indigenous fat-type pig breeds (such as Tongcheng, Mashen, Laiwu) (20–22). While, the expression level of *MYH3* gene was higher in Chinese Lantang pigs than in Landrace at the fetal stage (23). The regulatory mechanism of the variation in the expression of *MYH3* in muscle throughout swine lifespan remains to be elucidated.

CONCLUSIONS

Our results show that the *XM_013981330.2:g.−1805_−1810del* in the promoter of porcine *MYH3* did not significantly affect the meat quality traits in both Chinese × European crossbred pigs and Western commercial DLY crossbred pigs, which is not consistent with the assertion that this variant is the causal mutation underlying the meat-quality related QTL on SSC12. The *MYH3* gene is still one of the important candidate genes for the QTL. The molecular mechanism of the SSC12 QTL needs further study.

DATA AVAILABILITY STATEMENT

The data generated for the study are deposited in the (National Center for Biotechnology Information GenBank, https://www.ncbi.nlm.nih.gov/genbank/) repository, accession number (MW769011–MW769701).

ETHICS STATEMENT

The animal study was reviewed and approved by The Ethics Committee of Jiangxi Agricultural University.

AUTHOR CONTRIBUTIONS

CH and LZ contributed to the experiments, data analysis, and original draft writing. XZ conducted cell culture and experiments. LC and JM played leading roles in article revision, supervision, funding acquisition while YH assisted collecting the samples required for data analysis and experiments. All authors read and approved the submitted version.

FUNDING

This research was supported by the National Natural Science Foundation of China (31790413 and 31872339) and the National Key Research and Development Program of China (No. 2018YFD0500401).

ACKNOWLEDGMENTS

We are very grateful to Professor Lusheng Huang (the director of our laboratory) for his support and help in the revision of the paper and the use of the research materials. We would also like to thank Dr. Xinwei Xiong and Dr. Shaoming Fang for their contribution to the collection of some of the IMF data used in for this study.

SUPPLEMENTARY MATERIAL

The Supplementary Material for this article can be found online at: https://www.frontiersin.org/articles/10.3389/fvets.2021.672852/full#supplementary-material

Supplementary Figure 1 | Discovery of four haplotypes and 8 haplotype combinations at the *MYH3 XM_013981330.2:g.−1805_−1810del* promoter region by Sanger sequencing.

Supplementary Table 1 | The corresponding relationship between four haplotypes identified by Sanger sequencing and the alleles of the 5 variants detected by the next-generation sequencing (NGS).

Supplementary Table 2 | Comparison of four meat quality traits between genotypes of nucleotide repeats in the heterogenous F6, F7, and DYL pig populations.

REFERENCES

1. Brewer M. Consumer attitudes towards color and marbling of fresh pork. *Pork Qual.* (1998) 1:1–8.
2. Brewer M, Zhu L, McKeith F. Marbling effects on quality characteristics of pork loin chops: consumer purchase intent, visual and sensory characteristics. *Meat Sci.* (2001) 59:153–63. doi: 10.1016/s0309-1740(01)00065-1
3. Wu T, Zhang Z, Yuan Z, Lo L, Chen J, Wang Y, et al. Distinctive genes determine different intramuscular fat and muscle fiber ratios of the longissimus dorsi muscles in jinhua and landrace pigs. *PLoS ONE.* (2013) 8:e53181. doi: 10.1371/journal.pone.0053181
4. Chen W, Fang G, Wang S, Wang H, Zeng Y. Longissimus lumborum muscle transcriptome analysis of Laiwu and Yorkshire pigs differing in intramuscular fat content. *Genes Genomics.* (2017) 39:759–66. doi: 10.1007/s13258-017-0540-9
5. Cai C, Li M, Zhang Y, Meng S, Yang Y, Gao P, et al. Comparative transcriptome analyses of longissimus thoracis between pig breeds differing in muscle characteristics. *Front Genet.* (2020) 11:526309. doi: 10.3389/fgene.2020.526309
6. Won S, Jung J, Park E, Kim H. Identification of genes related to intramuscular fat content of pigs using genome-wide association study. *Asian Aust J Anim Sci.* (2018) 31:157–62. doi: 10.5713/ajas.17.0218
7. Ros-Freixedes R, Gol S, Pena R, Tor M, Ibáñez-Escriche N, Dekkers J, et al. Genome-wide association study singles out SCD and LEPR as the two main loci influencing intramuscular fat content and fatty acid composition in duroc pigs. *PLoS ONE.* (2016) 11:e0152496. doi: 10.1371/journal.pone.0152496
8. Davoli R, Luise D, Mingazzini V, Zambonelli P, Braglia S, Serra A, et al. Genome-wide study on intramuscular fat in Italian Large White pig breed using the PorcineSNP60 BeadChip. *J Anim Breed Genet.* (2016) 133:277–82. doi: 10.1111/jbg.12189
9. Ding R, Yang M, Quan J, Li S, Zhuang Z, Zhou S, et al. Single-locus and multi-locus genome-wide association studies for intramuscular fat in duroc pigs. *Front Genet.* (2019) 10:619. doi: 10.3389/fgene.2019.00619
10. Crespo-Piazuelo D, Criado-Mesas L, Revilla M, Castello A, Noguera J, Fernandez A, et al. Identification of strong candidate genes for backfat and intramuscular fatty acid composition in three crosses based on the Iberian pig. *Sci Rep.* (2020) 10:13962. doi: 10.1038/s41598-020-70894-2
11. Cho I, Park H, Ahn J, Han S, Lee J, Lim H, et al. A functional regulatory variant of MYH3 influences muscle fiber-type composition and intramuscular fat content in pigs. *PLoS Genet.* (2019) 15:e1008279. doi: 10.1371/journal.pgen.1008279
12. Ji J, Zhou L, Huang Y, Zheng M, Liu X, Zhang Y, et al. A whole-genome sequence based association study on pork eating quality traits and cooking loss in a specially designed heterogeneous F6 pig population. *Meat Sci.* (2018) 146:160–7. doi: 10.1016/j.meatsci.2018.08.013
13. Liu X, Xiong X, Yang J, Zhou L, Yang B, Ai H, et al. Genome-wide association analyses for meat quality traits in Chinese Erhualian pigs and a Western Duroc × (Landrace × Yorkshire) commercial population. *Genet Sel Evol.* (2015) 47:44. doi: 10.1186/s12711-015-0120-x
14. Berg E. *Pork Composition and Quality Assessment Procedures*. 1st ed. Des Moiners: National Pork Producer Council (NPPC) (2006).
15. Laack R, Stevens S, Stalder K. The influence of ultimate pH and intramuscular fat content on pork tenderness and tenderization. *J Anim Sci.* (2001) 79:392–7. doi: 10.2527/2001.792392x
16. Fujii J, Otsu K, Zorzato F, Leon S, Khanna V, Janice E, et al. Identification of a mutation in porcine ryanodine receptor associated with malignant hyperthermia. *Science.* (1991) 253:448–51. doi: 10.1126/science.1862346
17. Milan D, Jeon J, Looft C, Amarger V, Robic A, Thelander M, et al. A mutation in PRKAG3 associated with excess glycogen content in pig skeletal muscle. *Science.* (2000) 288:1248–51. doi: 10.1126/science.288.5469.1248
18. Laere A, Nguyen M, Braunschweig M, Nezer C, Collette C, Moreau L, et al. A regulatory mutation in IGF2 causes a major QTL effect on muscle growth in the pig. *Nature.* (2003) 425:832–6. doi: 10.1038/nature02064
19. Yamada S, Gendron T, Niccoli T, Genuth N, Grosely R, Shi Y, et al. RPS25 is required for efficient RAN translation of C9orf72 and other neurodegenerative disease-associated nucleotide repeats. *Nat Neurosci.* (2019) 22:1383–8. doi: 10.1038/s41593-019-0455-7
20. Hou X, Yang Y, Zhu S, Hua C, Zhou R, Mu Y, et al. Comparison of skeletal muscle miRNA and mRNA profiles among three pig breeds. *Mol Genet Genomics.* (2016) 291:559–73. doi: 10.1007/s00438-015-1126-3
21. Gao P, Cheng Z, Li M, Zhang N, Le B, Zhang W, et al. Selection of candidate genes affecting meat quality and preliminary exploration of related molecular

mechanisms in the Mashen pig. *Asian Aust J Anim Sci*. (2019) 32:1084–94. doi: 10.5713/ajas.18.0718

22. Damon M, Wyszynska-Koko J, Vincent A, Hérault F, Lebret B. Comparison of muscle transcriptome between pigs with divergent meat quality phenotypes identifies genes related to muscle metabolism and structure. *PLoS ONE*. (2012) 7:e33763. doi: 10.1371/journal.pone.0033763
23. Zhao X, Mo D, Li A, Gong W, Xiao S, Zhang Y, et al. Comparative analyses by sequencing of transcriptomes during skeletal muscle development between pig breeds differing in muscle growth rate and fatness. *PLoS ONE*. (2011) 6:e19774. doi: 10.1371/journal.pone.0019774

Conflict of Interest: The authors declare that the research was conducted in the absence of any commercial or financial relationships that could be construed as a potential conflict of interest.

frontiers in Veterinary Science

ORIGINAL RESEARCH
published: 21 June 2021
doi: 10.3389/fvets.2021.633898

Distinct Roles of Perilipins in the Intramuscular Deposition of Lipids in Glutamine-Supplemented, Low-, and Normal-Birth-Weight Piglets

Yaolu Zhao[1], Elke Albrecht[1], Zeyang Li[2], Johannes Schregel[2], Quentin L. Sciascia[2], Cornelia C. Metges[2] and Steffen Maak[1]*

[1] Institute of Muscle Biology and Growth, Leibniz Institute for Farm Animal Biology (FBN), Dummerstorf, Germany, [2] Institute of Nutritional Physiology "Oskar Kellner", Leibniz Institute for Farm Animal Biology (FBN), Dummerstorf, Germany

Piglets with low birth weight (LBW) usually have reduced muscle mass and increased lipid deposition compared with their normal-birth-weight (NBW) littermates. Supplementation of piglets with amino acids during the first days of life may improve muscle growth and simultaneously alter the intramuscular lipid deposition. The aim of the current study was to investigate the influence of glutamine (Gln) supplementation during the early suckling period on lipid deposition in the longissimus muscle (MLD) and the role of different perilipin (PLIN) family members in this process. Four groups were generated consisting of 72 male LBW piglets and 72 NBW littermates. Piglets were supplemented with either 1 g Gln/kg body weight or an isonitrogenous amount of alanine (Ala) between days post natum (dpn) 1 and 12. Twelve piglets per group were slaughtered at 5, 12, and 26 dpn, and muscle tissue was collected. Perilipins were localized by immunohistochemistry in muscle sections. The mRNA and protein abundances of PLIN family members and related lipases were quantified by quantitative RT-PCR (qPCR) and western blots, respectively. While PLIN1 was localized around lipid droplets in mature and developing adipocytes, PLIN2 was localized at intramyocellular lipid droplets, PLIN3 and 4 at cell membranes of muscle fibers and adipocytes, and PLIN5 in the cytoplasm of undefined cells. The western blot results indicated higher protein abundances of PLIN2, 3, 4, and 5 in LBW piglets ($p < 0.05$) at 5 dpn compared with their NBW littermates independent of supplementation, while not directly reflecting the mRNA expression levels. The mRNA abundance of *PLIN2* was lower while *PLIN4* was higher in piglets at 26 dpn in comparison with piglets at 5 dpn ($p < 0.01$). Relative mRNA expression of *LPL* and *CGI-58* was lowest in piglets at 5 dpn ($p < 0.001$). However, *ATGL* mRNA was not influenced by birth weight or supplementation, but the Spearman correlation coefficient analysis revealed close correlations with *PLIN2*, 4, and 5 mRNA at 5 and 26 dpn ($r > 0.5$, $p < 0.001$). The results indicated the importance of birth weight and age for intramuscular lipid deposition and different roles of PLIN family members in this process, but no clear modulating effect of Gln supplementation.

Keywords: glutamine, low birth weight, lipid deposition, muscle gene expression, perilipins, pig

OPEN ACCESS

Edited by:
Xiao Li,
Northwest A and F University, China

Reviewed by:
Xin Wu,
Chinese Academy of Sciences (CAS), China
Marcio Duarte,
Universidade Federal de Viçosa, Brazil

***Correspondence:**
Elke Albrecht
elke.albrecht@fbn-dummerstorf.de

Specialty section:
This article was submitted to Livestock Genomics, a section of the journal Frontiers in Veterinary Science

Received: *26 November 2020*
Accepted: *10 May 2021*
Published: *21 June 2021*

Citation:
Zhao Y, Albrecht E, Li Z, Schregel J, Sciascia QL, Metges CC and Maak S (2021) Distinct Roles of Perilipins in the Intramuscular Deposition of Lipids in Glutamine-Supplemented, Low-, and Normal-Birth-Weight Piglets. Front. Vet. Sci. 8:633898. doi: 10.3389/fvets.2021.633898

INTRODUCTION

Low-birth-weight (LBW) piglets normally have a higher mortality rate and growth retardation of muscles compared with their normal-birth-weight (NBW) littermates, which in turn causes a delay in whole body growth (1). Furthermore, LBW piglets normally have greater fat deposition (2) and exhibit increased fatness at slaughter age (1). In the current project, we attempted to ameliorate the disadvantages of the LBW piglets with adapted nutrition, in particular with glutamine (Gln) supplementation, which was assumed insufficient in maternal milk especially for LBW piglets (3, 4). In our previous investigation (5), we observed fewer muscle fibers and more intramyocellular lipid droplets at 5 days post natum (dpn) in LBW piglets. Moreover, Gln supplementation was shown to increase intramuscular availability of free Gln in skeletal muscle in a short term and to influence muscle fiber size, but had no influence on further muscle morphology traits and a minor influence on the abundance of myosin heavy chain isoforms. The current study focused on the process of lipid deposition and redistribution between muscle fibers and developing adipocytes as part of the muscle development and how it was influenced by birth weight (BiW) and Gln supplementation.

Skeletal muscle development includes myogenesis, adipogenesis, as well as fibrogenesis (6). During the whole lifetime of pigs, lipogenesis interplays and competes with muscle growth (7, 8). However, the lipid content in skeletal muscle is not just a storage of nutritional energy; it is of great importance for meat quality (9). Appropriate intramuscular lipids in pork promote flavor, tenderness, and juiciness (10), and consequently, intramuscular lipid development has become increasingly importantly raised in pork production. Intramuscular fat in pig represents only a small part of total body fat (6). The lipids within skeletal muscle are either stored in intramuscular adipocytes or within muscle fibers as intramyocellular lipid droplets (5). These intramuscular lipid droplets, also named lipid or fat bodies, play a vital role in lipid homeostasis in skeletal muscle (11). They function in storing lipids and supplying energy (11–13), as well as providing lipids for membrane synthesis (14) and protecting the cells from lipotoxicity (15). Moreover, the intramuscular lipid droplets were found to be formed *de novo* (16), and their formation and physical functions are controlled by a series of proteins, such as synaptosomal-associated protein 23 (SNAP23) (17), caveolins (18), PAT family (19), and others. Among these proteins, PAT family proteins, named after perilipin, adipophilin, or adipose differentiation-related protein (ADRP), and the tail-interacting protein of 47 kDa (TIP47) (20) have drawn increasing attention in recent years. There are two new members in this family, S3–12 (21) and myocardial lipid droplet protein—MLDP (22), also known as OXPAT (23) or lipid storage droplet protein 5 (LSDP5) (24). These five proteins, also known as PLIN1–5 (25), participate in the process of lipid droplet formation, stabilization, and lipolysis in different cells (26). The encoding genes can serve as suitable biomarkers when studying lipid deposition and adipocyte development within skeletal muscle in piglets.

Our hypothesis was that differences in intramuscular lipid deposition between LBW and NBW piglets are modulated by Gln supplementation, and different PLIN family members are involved in this process. Therefore, the objective of the current study was to investigate the expression pattern of *PLINs* in LBW and NBW piglets during the first weeks after birth on mRNA and protein level and their modulation by Gln supplementation.

MATERIALS AND METHODS

Animals and Sampling

The study involved German Landrace male piglets with 72 LBW and 72 NBW littermates, nursed and supplemented with Gln or an isonitrogenous amount of alanine (Ala) as described in detail in our former publication (5). Twelve piglets per group were sacrificed at 5, 12, or 26 dpn. The four treatment groups were named LBW-GLN, LBW-ALA, NBW-GLN, and NBW-ALA. Experimental procedures and animal care were carried out strictly according to the European Convention for the Protection of Vertebrate Animals used for Experimental and Other Scientific Purposes (2010/63/EU) and were approved by the responsible State Office for Agriculture, Food Safety and Fishing Mecklenburg Western Pomerania, Germany (permission no. 7221.3-1-026/16). Tissue of *musculus longissimus dorsi* (MLD) and *musculus semitendinosus* (MST) was collected immediately after slaughter, snap frozen in liquid nitrogen, and subsequently stored at −80°C until analysis.

Muscle Histology

Muscle serial sections of MLD and MST were cut 10-μm thick using a cryostat microtome (CM3050 S, Leica, Bensheim, Germany). The muscle sections were stained with hematoxylin and eosin (H/E, hematoxylin: Dako, Glostrup, Denmark; eosin: Chroma Gesellschaft, Münster, Germany) or Oil Red O according to standard protocols. The H/E-stained images were used for measurement, and the Oil Red O-stained images were used to verify the selected adipocytes. Images were taken with an Olympus BX43 microscope (Olympus, Hamburg, Germany) equipped with a UC30 color camera and analyzed with Cell^D imaging software (OSIS, Münster, Germany). At least 200 intramuscular adipocytes in both muscles were measured for each piglet using the interactive measurement module of the Cell^D software. If <200 adipocytes could be found, as in many of 5 dpn piglets, all available adipocytes were measured.

RNA Isolation, cDNA Synthesis, and Quantitative RT-PCR

Muscle RNA was isolated from MLD pieces (70–90 mg) using the RNeasy Fibrous Tissue Mini Kit (Qiagen, Hilden, Germany), following the manufacturer's instructions, and stored at −80°C. All RNA concentrations were measured with a NanoDrop ND-1000 spectrophotometer (Peqlab, Erlangen, Germany), and RNA integrity was determined using the Experion Automated Electrophoresis System and the RNA StdSens analysis chip (Bio-Rad, Munich, Germany). Then, first-strand cDNA was synthesized in a 20-μl reaction volume from 150 ng RNA with an iScript cDNA Synthesis Kit (Bio-Rad). Primers of reference and target genes were designed with Primer 3 web version 4.1.0 (http://primer3.ut.ee/) or adapted

TABLE 1 | Primer sequences used for qPCR.

Gene	Accession number	Forward primer (5′)	Reverse primer (3′)	Product size, bp
YWHAZ	NM_001315726.1	ATGCAACCAACACATCCTATC	GCATTATTAGCGTGCTGTCTT	178
PPIA	NM_214353.1	CACAAACGGTTCCCAGTTTT	TGTCCACAGTCAGCAATGGT	171
PLIN1	NM_001038638.1	GGGGTGTTGAGAAGGTGGTA	GGTGTGTTGAGAGATGGTGC	155
PLIN2	NM_214200.2	ATTGCCAACACTTACGCCTG	CGGTCACTGCTTCTTTGGTC	208
PLIN3	NM_001031778.1	ATCAGAGCTACTTCGTGCGT	AGTTTCTCCTGACCCTCCAC	196
PLIN4	NC_010444.4	CTGAGCAGCTTCTTTGGGTC	GGCTCCAGAGATCACCTTGT	219
PLIN5	NM_001123135.1	CCCTTTCTTCAGCAGCCTTC	GAGCTCCTCCTCAGTCATGG	207
LPL	NM_214286.1	CAGAGCCAAAAGAAGCAGCA	GGATGTTTTCACTCTCGGCC	170
CGI-58	NM_001012407.1	TCCCCTTGTCCTCCTTCATG	GGTTGTGTCCCAGCAAGATC	233
ATGL	NM_001098605.1	AGCACCTTCATTCCCGTGTA	TGGATGTTGGTGGAGCTGTC	176

from published papers [tyrosine 3-monooxygenase/tryptophan 5-monooxygenase activation protein zeta, YWHAZ (27); peptidylprolyl isomerase A, PPIA (28)], as shown in **Table 1**. All primers were synthesized by a commercial company (Sigma-Aldrich, Darmstadt, Germany). The annealing temperature of all primers was 60°C. To test these primers, qualitative polymerase chain reaction (PCR) was performed, and the products were subjected to 3% agarose gel electrophoresis and sequenced as described by Liu et al. (29). The quantitative RT-PCR (qPCR) was performed in duplicate as described by Schering et al. (30) with FastStart Essential DNA Green Master using a LightCycler® 96 real-time qPCR system (Roche, Basel, Switzerland). The mRNA expression values of target genes were normalized to two stable reference genes: *YWHAZ* and *PPIA*. The quantitation cycle (Cq) value was analyzed by the LightCycler® 96 system software. Efficiencies of amplifications were calculated by standard curves, which were calculated from serial dilutions (1:1, 1:10, 1:50, 1:100, and 1:200) using the formula ($Efficiency = 10^{-\frac{1}{slope}}$) and were within 1.8–2.2. The mRNA abundances were calculated as normalized relative quantities (NRQ) (31).

Immunohistochemistry

Tissue sections of MLD (thickness 8 μm) were cut with a CM3050 S cryostat microtome (Leica, Bensheim, Germany) and stained with antibodies against PLIN1–5 that were purchased from Novus Biologicals (NB110-40760, NB110-40878, NB110-40765, NBP2-13776, and NB110-60509; Wiesbaden-Nordenstadt, Germany). Fixation of muscle sections was done for 15 min in 4% paraformaldehyde. After washing 3 × 5 min with phosphate-buffered saline (PBS), the slides were incubated with 10% normal goat serum (NGS) in PBS for 15 min to block non-specific binding of the secondary antibody. Primary antibody (dilution 1:200 for PLIN1 and 4 and 1:100 for PLIN2, 3, and 5) incubation was performed for 1 h. Then, the slides were rinsed briefly, washed 3 × 10 min with PBS and subsequently incubated in the dark with secondary antibody (Alexa Fluor 488 Goat-Anti-Rabbit IgG, 1:1,000; Life Technologies, Darmstadt, Germany) for 45 min. Slides were washed 3 × 10 min with PBS, and the nuclei were stained with Hoechst 33258 for 5 min. After being washed 2× with PBS and 1× with distilled water for 5 min each, the slides were covered with ProLong Antifade (Thermo Fisher Scientific, Schwerte, Germany). All incubations were performed at room temperature in a humidity chamber. Two types of negative controls were generated to detect non-specific antibody binding, either blocking the primary antibodies with respective blocking peptides or omitting the primary antibody. No non-specific secondary antibody binding was detected, but weak non-specific binding of the antibodies against PLIN1 and 5 was observed (**Supplementary Figure 1**). Fluorescence signals were observed with a Nikon Microphot SA fluorescence microscope (Nikon, Düsseldorf, Germany) and a CC-12 color camera and recorded with Cell^F image analysis software (OSIS, Münster, Germany).

Western Blotting

Protein was isolated from all 144 MLD samples as described in details by Liu et al. (29) using CelLytic MT lyses reagent (Sigma-Aldrich, Munich, Germany) and protease inhibitor. Protein mixed with loading buffer was denatured at 95°C for 5 min and then loaded on Criterion TGX 12% gels (Bio-Rad) together with a molecular weight marker (PageRuler, Thermo Scientific, Schwerte, Germany). After electrophoresis, proteins were transferred to a polyvinylidene difluoride (PVDF) membrane (Trans-Blot Turbo Transfer Pack, Bio-Rad) with a semi dry blotter (Trans-Blot, Bio-Rad). The Smart Protein Layers (SPL) Western Kit Red (PR913-R, NH DyeAGNOSTICS, Halle, Germany) was used to enable reliable protein quantification. Membranes were blocked with 5% non-fat dry milk or 10% ROTI Block (Carl Roth, Karlsruhe, Germany) in Tris-buffered saline (TBS) for 1 h at room temperature. All membranes were incubated with the primary antibodies, which were also used for immunohistochemistry (PLIN1 and 2 diluted at 1:15,000 and PLIN3, 4, and 5 diluted at 1:5,000) and a HRP-conjugated secondary antibody (Rabbit TrueBlot HRP, Rockland Immunochemicals, Limerick, PA, USA; diluted at 1:25,000). The antibody label was detected with highly sensitive chemiluminescence substrate (SuperSignal West Femto, Thermo Scientific). Chemiluminescence and fluorescence of calibrators and total protein were recorded with a ChemoCam HR-16 imager (INTAS, Göttingen, Germany) and quantified with LabImage 1D software (Kapelan Bio-Imaging, Leipzig, Germany). Target protein band volume was normalized to total protein abundance, and the SPL

method enabled comparability among blots. All 144 samples were measured at least twice on separate blots (see example full blots in **Supplementary Figure 2**). Negative controls were generated to discriminate specific and non-specific antibody binding. Separate blots were processed that were incubated with the antibodies alone or with the antibodies together

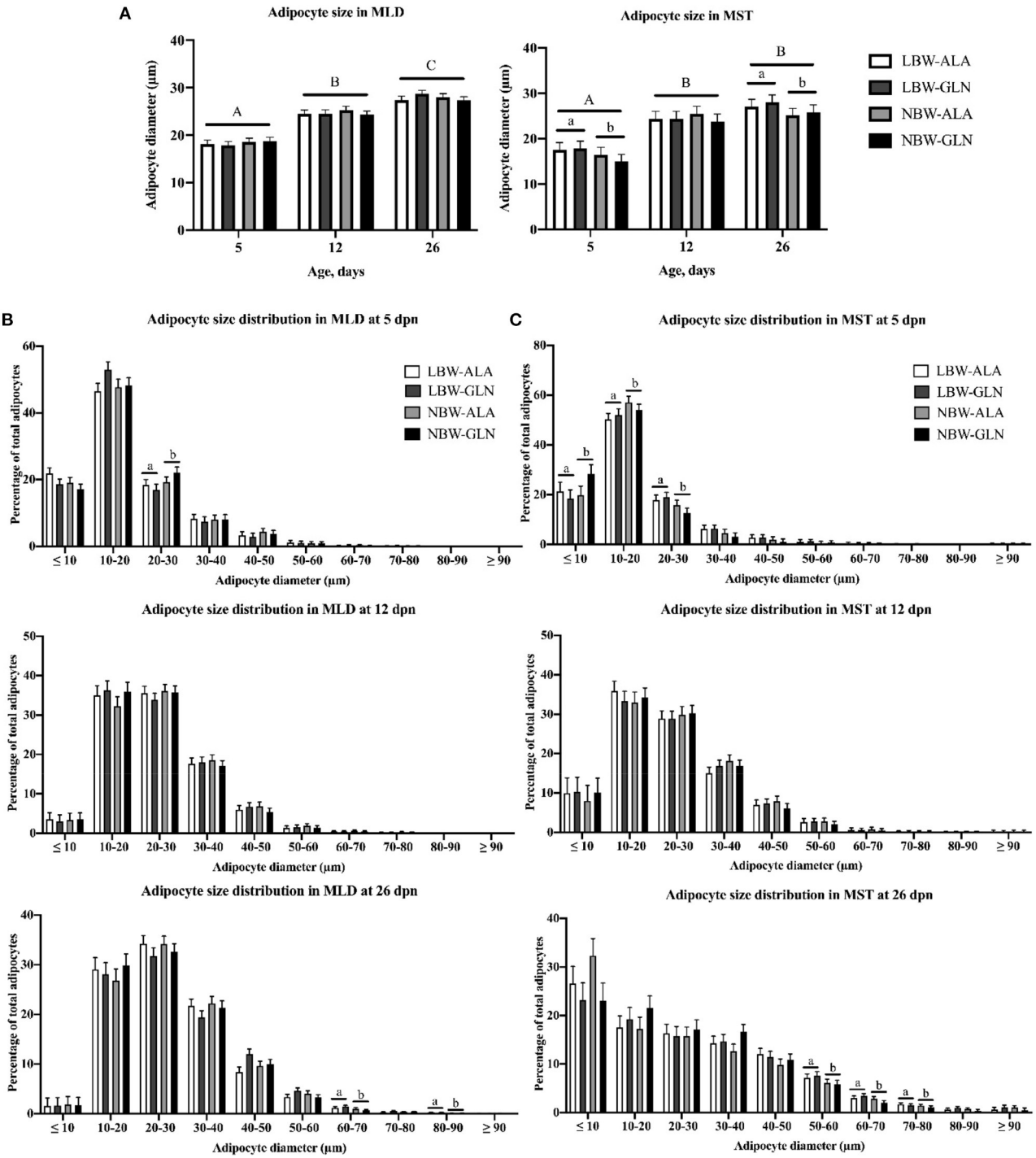

FIGURE 1 | Intramuscular adipocyte diameter and adipocyte size frequency distribution within *M. longissimus* (MLD) and *M. semitendinosus* (MST) of low- (LBW) and normal-birth-weight (NBW) piglets at 5, 12, and 26 dpn, supplemented with glutamine (GLN) or alanine (ALA) ($n = 12$ per group). **(A)** Intramuscular adipocyte diameter within MLD and MST; intramuscular adipocyte size distribution within **(B)** MLD and **(C)** MST. Values represent LSmeans and SE in error bars. ^{a,b}Significant differences between LBW and NBW piglets; $^{A-C}$Significant differences among ages ($p < 0.05$, Tukey–Kramer test).

with respective blocking peptides, pre-incubated for 30 min (**Supplementary Figure 3**).

Statistical Analysis

Statistical analysis was performed with the analysis of variance (ANOVA) model using the MIXED procedure of SAS statistical software (version 9.4, SAS Inst., Cary, USA). The fixed factors were BiW (LBW or NBW), supplementation (ALA or GLN), and age (5, 12, or 26), and respective interactions and sow were included as random factors. The used model was as follows:

$$Y_{ijksl} = \mu + \mathrm{BiW}_i + \mathrm{Sup}_j + \mathrm{Age}_k + (\mathrm{BiW} \times \mathrm{Sup})_{ij} + (\mathrm{BiW} \times \mathrm{Age})_{ik} + (\mathrm{Sup} \times \mathrm{Age})_{jk} + (\mathrm{BiW} \times \mathrm{Sup} \times \mathrm{Age})_{ijk} + \mathrm{Sow}_s + e_{ijksl},$$

where Y_{ijksl} = dependent variable (animal l from Sow s in BiW group i, Sup group j, and Age group k); μ = overall mean; BiW_i = effect of birth weight i ($i = 1$–2); Sup_j = effect of supplementation j ($j = 1$–2); Age_k = effect of age k ($k = 1$–3); $(\mathrm{BiW} \times \mathrm{Sup})_{ij}$ = effect of interaction; $(\mathrm{BiW} \times \mathrm{Age})_{ik}$ = effect of interaction; $(\mathrm{Sup} \times \mathrm{Age})_{jk}$ = effect of interaction; $(\mathrm{BiW} \times \mathrm{Sup} \times \mathrm{Age})_{ijk}$ = effect of interaction; Sow_s = random effect of sow s ($s = 49$); and e_{ijksl} = random residual error.

Least-square means (LSmeans) and standard errors (SE) were calculated for each fixed effect, and pairwise differences were tested by the Tukey–Kramer test. The SLICE statement of the MIXED procedure was used for partitioned analysis of the LSmeans for the interaction between BiW and supplementation within ages. Differences were considered significant if Tukey–Kramer adjusted $p < 0.05$ and a trend if $0.1 > p \geq 0.05$. The CORR procedure of SAS was used to calculate Spearman correlation coefficients. Correlations were regarded as low ($0.3 < r < 0.5$), moderate ($0.5 < r < 0.7$), high ($0.7 < r < 0.9$), and very high ($r > 0.9$) as described by Mukaka et al. (32).

RESULTS

Lipid Droplets and Adipocyte Size in *M. longissimus* and *M. semitendinosus*

Results of total lipid droplet area in muscle fibers and in adipocytes were reported in our former publication (5). We observed more lipid droplets in LBW piglets than in their NBW littermates at 5 dpn. Differences disappeared in older animals, and an influence of Gln supplementation was not detected. In the current study, we measured the size of individual intramuscular adipocytes. Adipocyte size distributions in MLD and MST are presented in **Figure 1**. The adipocyte size was mainly influenced by age and BiW, but no significant interaction effect among BiW, supplementation, and age was observed ($p > 0.05$). In both muscles, the mean adipocyte diameter was larger in piglets at 12 ($p \leq 0.001$) or 26 dpn ($p < 0.001$) compared with animals at 5 dpn (**Figure 1A**). Size histograms showed that piglets at 26 dpn had more large adipocytes than at 5 or 12 dpn (**Figures 1B,C**). Comparing the adipocyte size distribution of MLD revealed more small-diameter adipocytes (20–30 μm, $p = 0.03$) at 5 dpn in NBW piglets and more large-diameter adipocytes (60–70 μm, $p = 0.016$ and 80–90 μm, $p < 0.001$) at 26 dpn in LBW piglets (**Figure 1B**). In addition, we found more medium-diameter fat cells (40–50 μm) in Gln-supplemented piglets at 26 dpn than in Ala-supplemented animals, independent of BiW groups. In MST, the mean diameter of adipocytes of LBW piglets was greater than that of their NBW littermates at 5 ($p = 0.038$) and 26 dpn ($p = 0.03$), which was not observed in MLD. Furthermore, NBW piglets had more small-size adipocytes (<20 μm, $p < 0.05$), whereas LBW animals had more medium-size adipocytes (20–30 μm, $p = 0.012$ and 30–40 μm, $p = 0.077$) at 5 dpn. At 26 dpn, LBW piglets had more large-diameter fat cells (50–80 μm, $p < 0.05$) in MST than NBW piglets. Fewer adipocytes with a diameter smaller than 10 μm were observed in GLN-supplemented piglets in comparison with Ala-supplemented animals ($p = 0.037$), regardless of BiW group.

Relative mRNA Abundance of PLIN Family Members and Interacting Lipolysis-Related Genes in *M. longissimus*

The abundance of *PLIN1–5* and interacting lipolysis-related genes was quantified with RT-qPCR (**Figure 2**) to elucidate their contribution to the observed differences in lipid deposition between LBW and NBW piglets. The statistical analyses revealed no interaction effect among BiW, supplementation, and age for the mRNA abundances of the investigated genes ($p > 0.05$). Age and BiW were also the main influencing factors for the mRNA abundances of the investigated genes. The *PLIN1* mRNA level was overall higher in LBW than in NBW piglets at 5 dpn ($p = 0.033$), and in particular, it was higher in LBW-GLN piglets than in NBW-GLN piglets ($p = 0.017$, **Figure 2A**). However, no significant effects of supplementation ($p = 0.53$) or age ($p = 0.127$) were observed. Relative mRNA expression of *PLIN2* was higher in piglets at 5 dpn in comparison with animals at 12 ($p < 0.001$) or 26 dpn ($p = 0.04$, **Figure 2B**). Furthermore, LBW-ALA piglets had more *PLIN2* mRNA compared with their NBW-ALA littermates at 5 dpn ($p = 0.008$). Independent of supplementation, *PLIN2* mRNA abundance was greater in LBW piglets than in NBW piglets at 5 dpn ($p = 0.001$). However, this effect was not observed at 12 ($p = 0.811$) or 26 dpn ($p = 0.949$), and no supplementation effects were detected ($p = 0.462$) independent of ages. The relative mRNA abundance of *PLIN3* was too low to be reliably detected in MLD of piglets in this study. The abundance of *PLIN4* mRNA was lower in piglets at 5 dpn ($p = 0.005$, **Figure 2C**) and 12 dpn ($p = 0.014$) compared with piglets at 26 dpn and was not influenced by BiW ($p = 0.570$) or supplementation ($p = 0.172$). The abundance of *PLIN5* mRNA in piglets at 12 dpn tended to be lower than in piglets at 5 dpn ($p = 0.062$, **Figure 2D**) and was lower than in animals at 26 dpn ($p < 0.001$). Furthermore, LBW-ALA piglets tended to have higher *PLIN5* mRNA levels than NBW-ALA piglets at 5 dpn ($p = 0.074$). Overall, independent of Gln supplementation, LBW piglets had more *PLIN5* mRNA compared with NBW at 5 dpn ($p = 0.042$), but not at 12 ($p = 0.874$) or 26 dpn ($p = 0.538$). The results did not show an effect of Gln supplementation on *PLIN5* mRNA abundance ($p = 0.851$).

Birth weight and Gln supplementation had no effect on mRNA abundance of *LPL* ($p = 0.641$ and $p = 0.29$, respectively). There was only an age effect detected; thus, more *LPL* mRNA was measured in piglets at 26 dpn compared with piglets at 5 ($p < 0.001$, **Figure 2E**) and 12 dpn ($p < 0.001$). Similarly, the

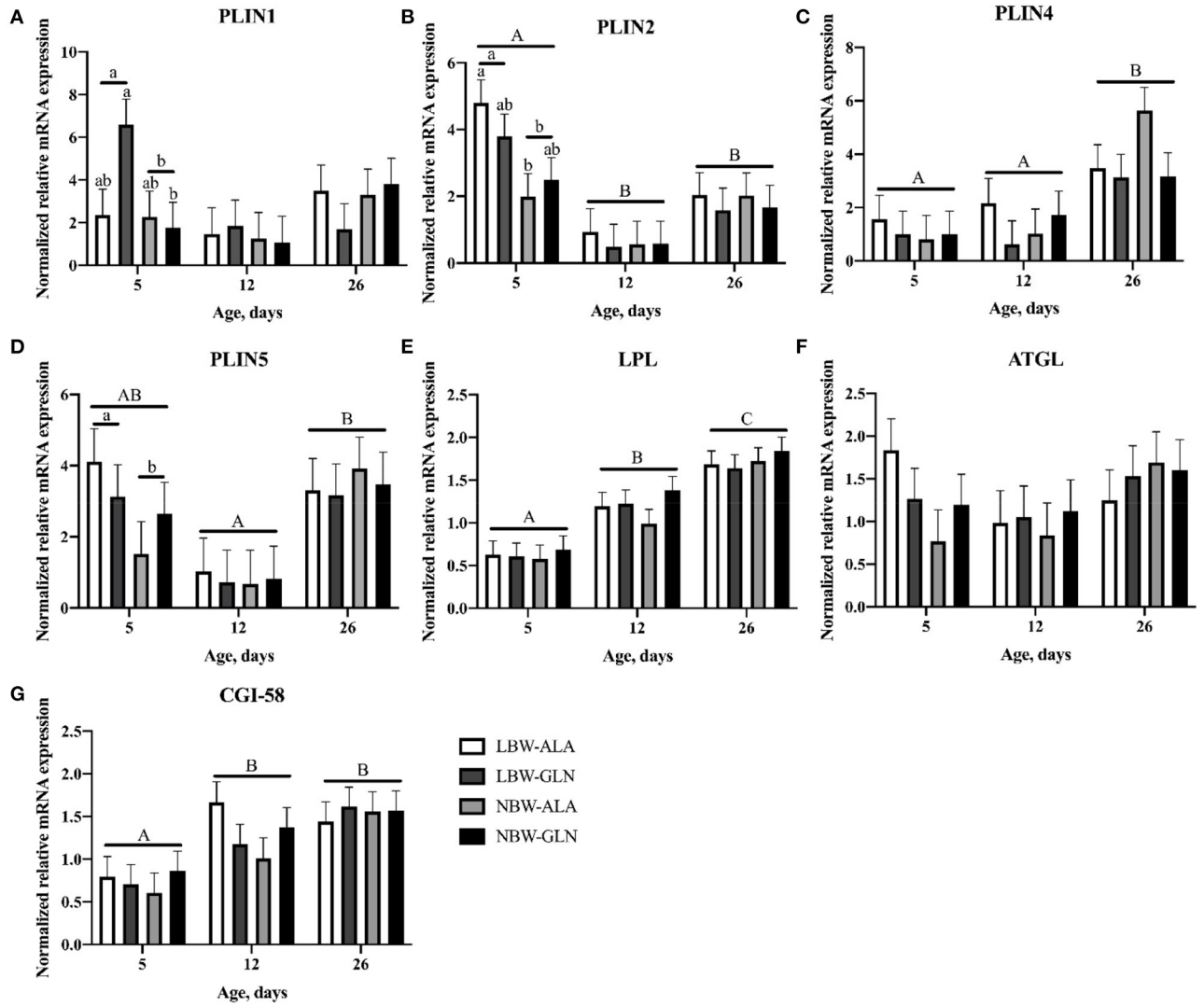

FIGURE 2 | Normalized relative mRNA expression of perilipins and related lipases in *M. longissimus* of low- (LBW) and normal-birth-weight (NBW) piglets at 5, 12, and 26 dpn, supplemented with glutamine (GLN) or alanine (ALA) ($n = 12$ per group). Values represent LSmeans and SE in error bars of PLIN1 **(A)**, PLIN2 **(B)**, PLIN4 **(C)**, PLIN5 **(D)**, LPL **(E)**, ATGL **(F)**, and CGI-58 **(G)** mRNA abundance, normalized to YWHAZ and PPIA. ^{a,b}Significant differences between LBW and NBW piglets at the same age; $^{A-C}$Significant differences among ages ($p < 0.05$, Tukey–Kramer test).

mRNA level of *CGI-58* was higher in piglets at 12 ($p = 0.026$, **Figure 2F**) and 26 dpn ($p < 0.001$) compared with animals at 5 dpn. No BiW ($p = 0.561$) or Gln supplementation ($p = 0.774$) effects were observed. There was a trend for higher level of *ATGL* mRNA in LBW-ALA compared with NBW-ALA piglets at 5 dpn ($p = 0.054$). Moreover, *ATGL* mRNA tended to be higher in LBW piglets than in NBW animals at 5 dpn independent of supplementation ($p = 0.054$), but it was not affected by Gln supplementation ($p = 0.738$) or age ($p = 0.335$).

Localization of PLIN Proteins Within *M. longissimus*

The proteins encoded by the five *PLIN* genes were detected with immunohistochemistry in the MLD of piglets. Different localizations and staining patterns were observed for the individual PLIN proteins. A strong signal was observed for PLIN1 around fat vacuoles in mature and developing adipocytes (**Figures 3A–C**). Additional weak signals in muscle tissue were identified as unspecific (see **Supplementary Figure 1**) by blocking specific antibody bindings with the respective blocking peptide. In contrast, PLIN2 was localized exclusively at intramyocelluar lipid droplets (**Figures 3D–F**). The staining decreased with age according to the reduction of lipid droplets within muscle fibers. Similar staining patterns were observed for PLIN3 and PLIN4, both located at the periphery of muscle fibers and large adipocytes (**Figures 4A–D**), whereas PLIN5 was detected in the cytosol of many small, undefined cells between muscle fibers (**Figures 4E,F**).

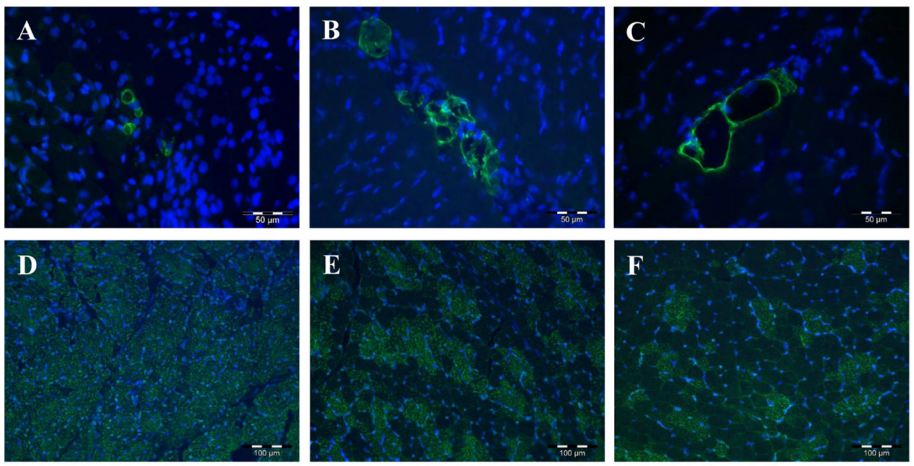

FIGURE 3 | Immunohistochemical localization of PLIN1 **(A–C)** and PLIN2 **(D–F)** in porcine *M. longissimus* at 5, 12, and 26 dpn, respectively. PLIN1 and 2 were stained green. Nuclei were counterstained blue with Hoechst 33258.

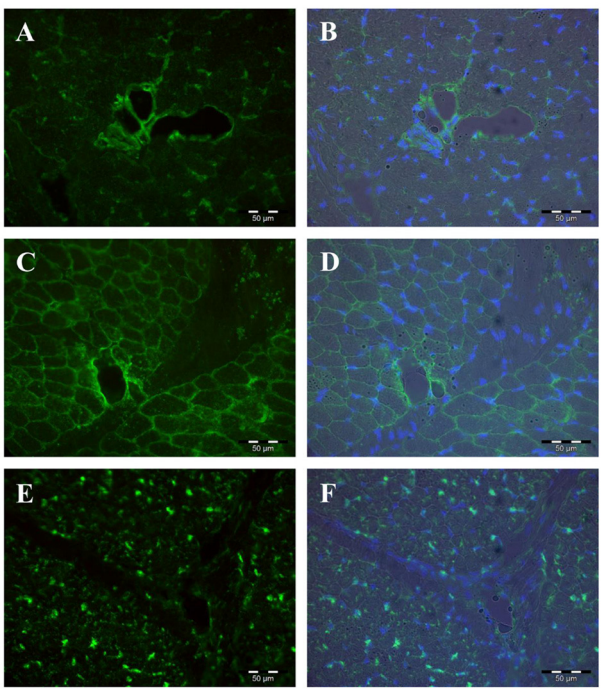

FIGURE 4 | Immunohistochemical localization of PLIN3 **(A,B)**, PLIN4 **(C,D)**, and PLIN5 **(E,F)** in porcine *M. longissimus* at 12 dpn. Nuclei were counterstained blue with Hoechst 33258. The right panel shows merged images of fluorescence (PLIN and Hoechst 33258) and bright field.

Protein Abundance of PLIN1–5 in *M. longissimus*

Normalized protein abundances of PLIN1–5 within MLD were determined with western blots and are shown in **Figure 5**. A significant interaction effect among BiW, supplementation, and age was observed for the protein abundance of PLIN3 ($p = 0.017$), but for no other protein ($p > 0.05$). Age and BiW were the main factors influencing protein abundances of perilipins in MLD of piglets. The protein abundances of all five perilipins (**Figures 5A–E**) were higher in piglets at 5 dpn compared with animals at 12 dpn ($p < 0.01$) and 26 dpn ($p < 0.01$). The protein content of PLIN1 was not influenced by BiW, whereas PLIN3 and 4 protein abundances (**Figures 5C,D**) were higher in LBW-GLN compared with NBW-GLN piglets at 5 dpn ($p < 0.001$ and $p = 0.021$, respectively). Regardless of supplementation, protein abundances of PLIN2–5 (**Figures 5B–E**) were higher in LBW piglets compared with their NBW littermates at 5 dpn ($p = 0.015$, $p = 0.009$, $p = 0.012$, and $p = 0.016$, respectively). However, an influence of Gln supplementation on protein abundances of PLIN1–5 was not observed ($p = 0.642$, $p = 0.522$, $p = 0.578$, $p = 0.460$, and $p = 0.68$, respectively).

Correlations Among Traits

Since most investigated traits were age dependent, Spearman correlation coefficients were calculated for each age group separately. We detected relationships among investigated genes and between gene expression and phenotypic traits (**Supplementary Table 1**). The relative mRNA abundances of *PLIN2*, *4*, and *5* were moderately or highly correlated among each other in all age groups ($r > 0.50$, $p < 0.001$). The *PLIN1* mRNA was moderately correlated with mRNA of *PLIN2*, *4*, and *5* at 12 and 26 dpn ($r > 0.6$, $p < 0.001$). Furthermore, *ATGL* mRNA was closely correlated with *CGI-58* and *PLIN2*, *4*, and *5* mRNA at 5 dpn ($r > 0.4$, $p < 0.001$), whereas *LPL* mRNA was correlated with *ATGL* and *CGI-58* only in piglets at 5 dpn ($r > 0.6$, $p < 0.001$). The protein abundances of the five investigated *PLIN*s were not as closely correlated as mRNA, with only weak-to-high correlation among PLIN2 and PLIN4 and 5 in all age groups ($r > 0.3$, $p < 0.001$). There was no clear relationship between gene expression and intramuscular adipocyte area, except a weak negative correlation between PLIN1, 4, and 5 and adipocyte area at 12 dpn ($r < -0.3$, $p < 0.05$). However, we observed weak

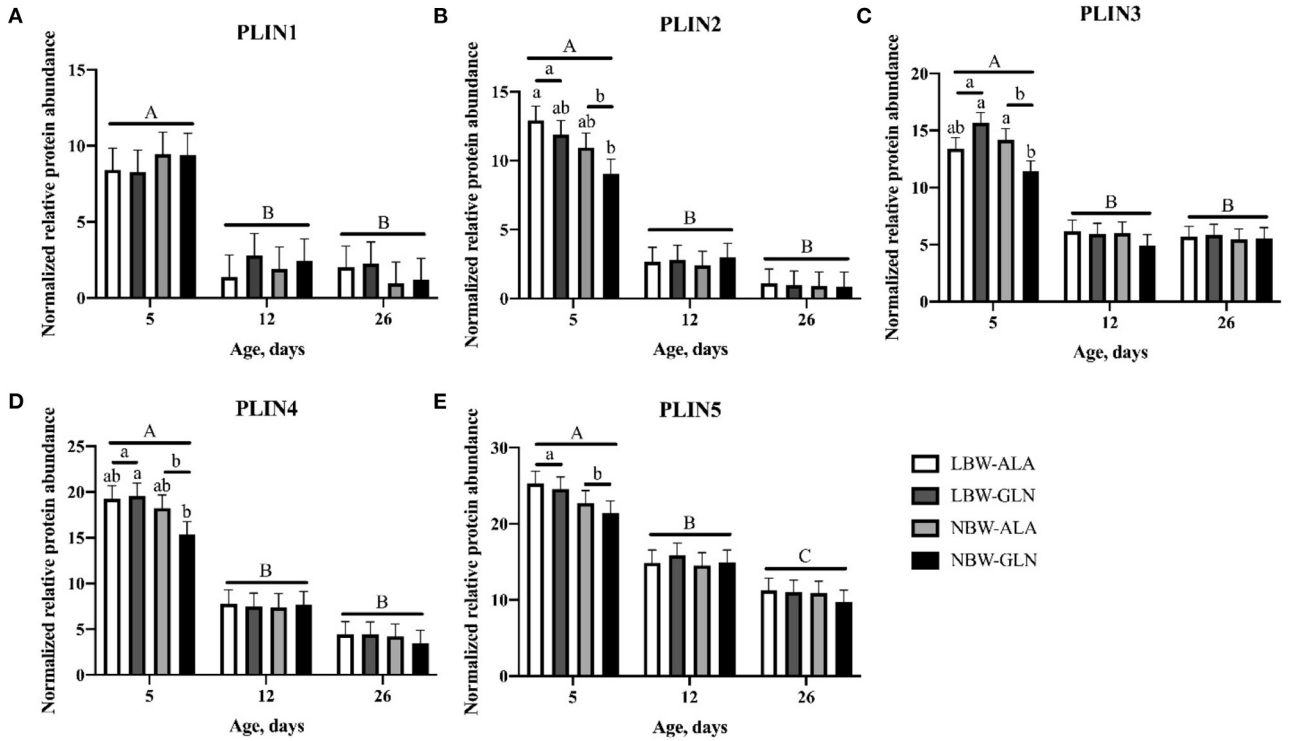

FIGURE 5 | Normalized relative protein abundance of PLIN1 **(A)**, PLIN2 **(B)**, PLIN3 **(C)**, PLIN4 **(D)**, and PLIN5 **(E)** in *M. longissimus* of low- (LBW) and normal-birth-weight (NBW) piglets at 5, 12, and 26 dpn, supplemented with glutamine (GLN) or alanine (ALA) ($n = 12$ per group). Values represent LSmeans and SE in error bars of protein abundances normalized to total protein. ^{a,b}Significant differences between piglets at the same age; $^{A-C}$Significant differences among ages ($p < 0.05$, Tukey–Kramer test).

or moderate correlations between intramyocelluar lipid droplet area and protein abundances of PLIN2–5 ($r > 0.3$, $p < 0.05$) at 12 dpn and mRNA of *PLIN1*, *2*, *4*, and *5* as well as protein abundance of PLIN2 and 5 at 26 dpn ($r = 0.357$, $p < 0.05$). The mean adipocyte diameter showed a low negative correlation with intramuscular adipocyte area ($r = -0.355$, $p < 0.05$) at 12 dpn and with *PLIN4* mRNA ($r = -0.337$, $p < 0.05$) at 26 dpn.

DISCUSSION

Our previous study indicated a clear difference between LBW and NBW piglets in the abundance of lipid droplets within muscle fibers at 5 dpn (5). The area percentage of intramyocellular lipid droplets decreased during the first days of life by more than 80%. The difference between LBW and NBW piglets disappeared with age. At the same time, intramuscular adipocytes started to develop with high individual variation. The current study was conducted to elucidate the process of lipid deposition and redistribution between muscle fibers and developing adipocytes as part of the muscle development and its modulation by Gln. Intramyocellular lipid droplets are vital organelles sequestering lipids, regulating intramyocelluar lipid homeostasis by preventing from lipotoxicity (11, 15). Within skeletal muscle, the perilipin family of proteins plays a vital role in lipid droplet metabolism (33). It is not known whether Gln can directly interact with and modulate perilipin family members, but PLINs are biomarkers for lipid deposition and adipocyte development within skeletal muscle in pigs (25, 26, 34). Therefore, we investigated the expression pattern of the five known members of the perilipin family and their related lipases in skeletal muscle of LBW piglets and their NBW littermates, which were orally supplemented with Gln or Ala during the first 12 days of life.

Larger Intramuscular Adipocytes Were Observed in LBW Piglets

Myogenesis and adipogenesis are competitive processes during muscle development (7, 8). Thus, when the muscle growth is delayed, as reported in LBW piglets (5, 10), nutrients are available for the development of intramuscular adipocytes at the same time. Gondret et al. (10) observed a greater adipocyte diameter in the MST of LBW pigs at 112 kg compared with high birth weight pigs. In agreement with Gondret et al. (10), we observed larger adipocytes in the MST, but not MLD, of LBW compared with NBW piglets during the first weeks of life. In addition, LBW piglets had more large-size adipocytes in both muscles at 26 dpn, whereas NBW animals had more small-size adipocytes at 5 dpn. Together with the result of our previous study that LBW had more intramyocelluar lipid droplets compared with NBW piglets (5), this suggests that LBW piglets stored the lipids in

intramyocellular lipid droplets rather than in adipocytes during the first days of life. Then, with increasing age, the lipids were transferred to intramuscular adipocytes. Overall, LBW piglets had more intramuscular lipid deposition during the suckling period than their NBW littermates.

Different Localizations of Perilipins Within *M. longissimus* Suggest Diverse Functions

All five members of the perilipin family of proteins were detected in MLD of piglets in our study with mainly distinct localizations. The first member, PLIN1, was originally discovered in adipocytes (35) surrounding lipid droplets (36). Other PLINs were consecutively detected. The five members of the perilipin family are proteins associated with the surface of lipid droplets and function in the formation, stabilization, and utilization of lipid droplets (26). Wolins et al. (37) elucidated the process how PLINs mediate lipid droplet formation in cultured 3T3-L1 adipocytes. According to their studies, nascent lipid droplets are coated first by PLIN3 and 4, then PLIN2 is recruited to the surface of growing lipid droplets. Afterwards, PLIN1 starts to bind the mature lipid droplets, stabilizing and protecting them from lipolysis. However, PLIN1 starts to promote triglyceride hydrolysis when it is phosphorylated by protein kinase A (38). In previous experiments, PLIN1 was discovered to be around large adipocytes (35, 39) and was thought to be restricted within white and brown adipose tissue or steroidogenic cells (40, 41). Our results indicate that PLIN1 can also be detected within skeletal muscle at the intramuscular adipocytes, in line with the findings of Gandolfi et al. (34). Furthermore, Skinner et al. (42) reported that PLIN1 can also be detected in the cytosol when it moves from smooth endoplasmic reticulum to mature adipocytes. While PLIN1 is a suitable marker for intramuscular fat deposition in pigs, PLIN2 was traditionally considered a marker for lipid droplets within skeletal muscle as it is located around small lipid droplets (34, 43). MacPherson et al., however, argued this point as the distribution of PLIN2 was only 60–80% parallel to intramuscular lipid droplets in some studies (44–46). Nevertheless, in most investigations, PLIN2 was found ubiquitously, appearing as the most abundant protein of the perilipin family in skeletal muscle (46, 47), which could not be concluded from our study. It shares a similar function and homology with PLIN1 and is able to replace PLIN1 when it is lacking (47, 48). The study of Xu et al. revealed that PLIN2 is competing with PLIN1 for binding at the surface of lipid droplets in adipocytes (49). There was no co-localization of PLIN1 and PLIN2 observed in MLD of piglets in our study. While PLIN1 and PLIN2 share similar functions, PLIN3 and PLIN4, both interacting with nascent lipid droplets, were localized at the periphery of muscle fibers and intramuscular adipocytes in our study. Previous studies have indicated that PLIN3 and 4 were also located cytosolically (21, 33, 50). However, in this study, we did not observe a clear association of PLIN3 and 4 with lipid droplets beside a weak cytosolic signal, which could indicate binding of smaller nascent lipid droplets that could not be detected under the microscope. The last member of this family, PLIN5, was localized within undefined cells between the muscle fibers in our study. It could not be clarified what kind of cells were stained and whether this was a specific binding of the PLIN5 antibody, although blocking the epitope with the respective peptide completely prevented antibody binding and staining. Previous studies found that PLIN5 could be recruited to the mitochondria to supply energy (33, 51); thus, it could be important during skeletal muscle growth. Altogether, the members of the perilipin family have different localizations within skeletal muscle tissue according to their distinct roles in lipid storage and metabolism.

Differences Between LBW and NBW Piglets in Lipid Deposition at 5 dpn Were Associated With the Expression of *PLIN1–5* and Lipolysis-Related Genes

The expression of *PLIN*s and lipolysis-related genes was measured to elucidate whether the observed differences in intramuscular lipid deposition between LBW and NBW piglets are regulated by different *PLIN* family members and whether the availability of free Gln in the muscle was involved. There are many examples in the literature that *PLIN1* mRNA expression is correlated with fat deposition in different species, e.g., pigs (52), cattle (53), and humans (54). Our results indicated a higher *PLIN1* mRNA level, but not a higher protein level, in LBW piglets at 5 dpn compared with their NBW littermates. The lower protein abundance of PLIN1 in piglets at 26 dpn in comparison with animals at 5 dpn was in contrast to the increasing appearance of adipocytes with age (5). However, possible explanations for this expression pattern of PLIN1 are as follows: (i) the size of adipocytes is smaller in younger piglets; hence, more PLIN1 protein is required to enclose lipid droplets of small adipocytes as they have a larger summarized surface. (ii) The intramuscular fat was not evenly distributed in the muscle (5); thus, the results may vary within the same muscle, and different parts were used for histology and mRNA or protein extraction. (iii) The relative protein abundance was normalized to the total protein abundance, which is increasingly dominated by structural muscle proteins (55). This applies also for other PLIN proteins; thus, the age effect will not be discussed in the following.

PLIN2 was previously reported to stimulate uptake of fatty acids in transfected COS-7 cells (56) and promote lipid droplet enlargement in murine fibroblasts (57). Consistent with our published data of intramyocellular lipid droplets (5), we observed higher *PLIN2* mRNA and protein abundance in LBW compared with NBW piglets at 5 dpn in the current study. Thus, this variance of intramuscular lipid droplet content in piglets with different birth weight might result from the different expression pattern of *PLIN2*. Although, we observed weak-to-moderate positive correlations between intramyocellular lipid droplet area and PLIN2 protein abundance only at 12 and 26 dpn.

The protein abundance of PLIN3 and 4 was higher in LBW piglets at 5 dpn in comparison with NBW piglets, and both proteins had similar localizations in muscle tissue. We observed staining of small particles within particular muscle fibers, but different from the PLIN2 staining pattern. This is in accordance with previous studies indicating that PLIN3

functions in the biogenesis of small, nascent lipid droplets together with PLIN4 (21, 37, 58, 59). However, in PLIN3 blots, which were incubated with blocking peptide, the 47-kDa (theoretical size of PLIN3) band was only partially blocked, whereas a 63-kDa (similar to PLIN1) band was completely blocked. Therefore, the PLIN3 antibody possibly non-specifically binds to other members of the PLIN family. Additionally, the PLIN3 protein results should be considered with caution because of the very low mRNA abundance. Interestingly, PLIN4 blocking experiments indicated the size of PLIN4 protein at about 80 kDa (**Supplementary Figure 3**), which was smaller than the theoretical protein size (164 kDa). Whether it is an unknown isoform needs further clarification. Among the perilipin family, PLIN4 is the only protein that does not share the same PAT domain and a four-helix bundle with other PLINs and cannot mediate lipolysis (21, 26). Pourteymour et al. reported PLIN4 was more expressed in slow-twitch than in fast-twitch fibers in humans (60). Even though we did not investigate this specifically, it may also be similar in pigs, since most lipid droplets are located in slow-twitch fibers and are associated with PLINs.

Previous studies have suggested that PLIN5 is correlated with oxidative activities in skeletal muscle. Bosma et al. reported that overexpression of PLIN5 in the tibialis anterior muscle of rats increased oxidative gene expression and intramyocellular lipid content (61). Furthermore, this group reported higher interactivity of lipid droplets and mitochondria in human vastus lateralis muscle, rat tibialis anterior muscle, or cultured HEK293 cells upon overexpression of *PLIN5* (62). In our study, LBW piglets had a higher level of *PLIN5* mRNA and protein than NBW piglets at 5 dpn, regardless of supplementation. This suggests more oxidative activities in skeletal muscle of LBW piglets in the first days of life, probably to generate energy for muscle growth. Furthermore, PLIN5 protein was negatively correlated with adipocyte diameter in piglets at 26 dpn, suggesting PLIN5 is not involved in adipocyte growth and utilization of the lipids stored in intramyocellular lipid droplets.

Altogether, PLIN2–5 were more abundant in muscle tissue of LBW piglets than in NBW animals during their first days of life. A possible explanation for this observation may be that LBW piglets expend fewer fatty acids for their muscle and body growth than their NBW littermates, and the excess fatty acids are synthesized to triglycerides and stored in intramyocellular lipid droplets, preventing lipotoxicity. However, with increasing age, body growth or lipid deposition in adipocytes requires more energy, and the excess lipids in lipid droplets are then utilized. There is no indication from the current study that Gln supplementation alters the expression level of PLINs in porcine skeletal muscle.

The uptake of fatty acids from the blood is an important energy source for skeletal muscle metabolism, and LPL plays an important role in triacylglycerol hydrolysis from lipoproteins (63, 64). It is a rate-limiting lipase during this process and is mainly synthesized in skeletal muscle (64, 65). In a previous study, a tissue-specific over-expression of *LPL* was reported to increase the fatty acid content in mouse skeletal muscle (66, 67). Therefore, in the current study, we hypothesized that *LPL* expression was positively related to intramuscular lipid droplets, which are synthesized *de novo* from fatty acids (16). In the present study, relative *LPL* mRNA expression was significantly higher in piglets at 26 dpn compared with younger animals at 5 and 12 dpn, indicating an increasing demand of fatty acids in porcine skeletal muscle during the early postnatal period. The mRNA level of *LPL* was not influenced by BiW, suggesting that the higher content of intramyocellular lipid droplets in LBW piglets may not result from increased fatty acid uptake.

In addition to promoting lipid droplet formation and stabilization, PLINs were reported to modulate hydrolysis of the main content of lipid droplets, the triglycerides, together with ATGL and its coactivator CGI-58 (44). Moreover, ATGL is a vital lipase in skeletal muscle (41). During lipolysis within adipocytes, PLIN1 is phosphorylated first, then CGI-58 combined with PLIN1 is released from the surface of lipid droplets and activates ATGL (33). Subsequently, ATGL interacts with triacylglycerols of the lipid droplet cores and metabolizes them to diacylglycerols and fatty acids (33). In non-adipose tissue, e.g., myocytes, where PLIN1 is lacking, ATGL and CGI-58 could possibly mediate lipolysis with PLIN2 without being phosphorylated (44, 68, 69). Perilipin 3 and 5 could be both phosphorylated with stimulation to promote lipolysis in skeletal muscle (69). However, few studies have investigated the interaction of PLIN3 and lipases. Additionally, PLIN5 is able to bind CGI-58 or ATGL separately and is the only member of the PLIN family that binds ATGL directly (41, 70, 71). However, the interaction of PLIN5 and ATGL prevents lipolysis unless phosphorylation of PLIN5 (41). Our results indicated that mRNA expression of *CGI-58* was not influenced by BiW or Gln supplementation despite the difference in lipid droplet distribution between LBW and NBW piglets at 5 dpn. Moreover, *CGI-58*, as a regulator of ATGL activity (72), exhibited higher mRNA expression in piglets at 12 and 26 dpn in comparison with piglets at 5 dpn, indicating increased lipolysis activity with increasing age. However, the lipolysis rate of triglycerides in skeletal muscle is controlled by ATGL (69), but its relative mRNA expression in these animals was not influenced by BiW, supplementation, or age. Whether post translationally the regulation of ATGL played a role needs further clarification.

PLINs Were Closely Correlated to Lipases Within *M. longissimus*

Relative mRNA expressions of *PLIN2*, *4*, and *5* were closely correlated among each other within skeletal muscle of piglets in this study, suggesting their similar or interactive roles in intramuscular lipid droplet mobilization during the first weeks of life. Moreover, although *LPL* was not influenced by BiW, supplementation, or age in this study, its mRNA expression showed moderate correlations with the mRNA abundance of *PLIN2*, *PLIN5*, *ATGL*, and *CGI-58* in piglets at 5 dpn. This could be a sign of LPL's function in intramuscular lipid droplet formation together with these genes. In addition, as ATGL-mediated lipolysis requires interactions with PLIN family members (41), close correlations among *ATGL* mRNA and *PLIN*s in animals at 5 and 26 dpn were observed in this study. Consistent with that, the study of MacPherson et al.

(44, 69) revealed distinct roles of PLINs in mediating lipolysis. Overexpression of *PLIN5* correlated with an increase of *ATGL* expression to maintain lipid homeostasis in the study of Bosma et al. (61). All these data revealed that *PLIN* family members are closely correlated with the important lipases in skeletal muscle.

CONCLUSIONS

Perilipins have their distinct roles in regulating the lipid droplet formation, distribution, and mobilization in porcine skeletal muscle. Their expression and function are closely related as indicated by high correlations among *PLIN2–5* at both mRNA and protein level. The results revealed BiW as an important factor influencing their expression pattern, with a higher expression of most *PLIN*s in LBW piglets at 5 dpn. Furthermore, the close interactive correlations among *PLIN* family and related lipases suggested the *PLIN*s play important roles in lipolysis together with *LPL*, *ATGL*, and *CGI-58* within porcine skeletal muscle in the early postnatal phase. Oral supplementation with Gln had only negligible effects on the expression level of *PLIN*s and related lipases.

DATA AVAILABILITY STATEMENT

The raw data supporting the conclusions of this article will be made available by the authors, without undue reservation.

ETHICS STATEMENT

The animal study was reviewed and approved by State Office for Agriculture, Food Safety and Fishing Mecklenburg Western Pomerania, Germany (permission No. 7221.3-1-026/16).

AUTHOR CONTRIBUTIONS

YZ performed most experiments, analyzed the data, and drafted the manuscript. EA designed the study, performed parts of the experiments and analyses, and helped with writing the manuscript. CM designed and supervised the animal experiment, provided resources, acquired funding, and revised the manuscript. QS, ZL, and JS performed the animal experiment, provided resources, and reviewed and edited the manuscript. SM supervised and administered the project, provided resources, and reviewed and edited the manuscript. All authors approved the final submitted manuscript.

FUNDING

YZ was funded by a China Scholarship Council (CSC) grant. The project was partly funded by Deutsche Forschungsgemeinschaft (DFG), Bonn, Germany (grant number ME 1420/10-1). The publication of this article was funded by the Open Access Fund of the FBN.

ACKNOWLEDGMENTS

The authors acknowledge the excellent technical assistance of E. Schwitulla, S. Foß, F. Feldt, and K. Gürtler; Dr. A. Tuchscherer for statistical advice; Dr. R. Pfuhl and the staff of the experimental slaughterhouse; as well as the EAS team.

SUPPLEMENTARY MATERIAL

The Supplementary Material for this article can be found online at: https://www.frontiersin.org/articles/10.3389/fvets.2021.633898/full#supplementary-material

REFERENCES

1. D'Inca R, Gras-Le Guen C, Che LQ, Sangild PT, Le Huerou-Luron I. Intrauterine growth restriction delays feeding-induced gut adaptation in term newborn pigs. *Neonatology*. (2011) 99:208–16. doi: 10.1159/000314919
2. Jamin A, Seve B, Thibault JN, Floc'h N. Accelerated growth rate induced by neonatal high-protein milk formula is not supported by increased tissue protein synthesis in low-birth-weight piglets. *J Nutr Metab*. (2012) 2012:545341. doi: 10.1155/2012/545341
3. Wu G. Amino acids: metabolism, functions, and nutrition. *Amino Acids*. (2009) 37:1–17. doi: 10.1007/s00726-009-0269-0
4. Wu G, Bazer FW, Johnson GA, Knabe DA, Burghardt RC, Spencer TE, et al. Triennial growth symposium: important roles for L-glutamine in swine nutrition and production. *J Anim Sci*. (2011) 89:2017–30. doi: 10.2527/jas.2010-3614
5. Zhao Y, Albrecht E, Sciascia QL, Li Z, Görs S, Schregel J, et al. Effects of oral glutamine supplementation on early postnatal muscle morphology in low and normal birth weight piglets. *Animals (Basel)*. (2020) 10:1976. doi: 10.3390/ani10111976
6. Hausman GJ, Basu U, Du M, Fernyhough-Culver M, Dodson MV. Intermuscular and intramuscular adipose tissues: bad vs. good adipose tissues. *Adipocyte*. (2014) 3:242–55. doi: 10.4161/adip.28546
7. Hocquette JF, Gondret F, Baeza E, Medale F, Jurie C, Pethick DW. Intramuscular fat content in meat-producing animals: development, genetic and nutritional control, and identification of putative markers. *Animal*. (2010) 4:303–19. doi: 10.1017/S1751731109991091
8. Yan X, Zhu MJ, Dodson MV, Du M. Developmental programming of fetal skeletal muscle and adipose tissue development. *J Genomics*. (2013) 1:29–38. doi: 10.7150/jgen.3930
9. Zhao SM, Ren LJ, Chen L, Zhang X, Cheng ML, Li WZ, et al. Differential expression of lipid metabolism related genes in porcine muscle tissue leading to different intramuscular fat deposition. *Lipids*. (2009) 44:1029–37. doi: 10.1007/s11745-009-3356-9
10. Gondret F, Lefaucheur L, Juin H, Louveau I, Lebret B. Low birth weight is associated with enlarged muscle fiber area and impaired meat tenderness of the longissimus muscle in pigs. *J Anim Sci*. (2006) 84:93–103. doi: 10.2527/2006.84193x
11. Walther TC, Farese RV Jr. Lipid droplets and cellular lipid metabolism. *Annu Rev Biochem*. (2012) 81:687–714. doi: 10.1146/annurev-biochem-061009-102430
12. Murphy DJ, Vance J. Mechanisms of lipid-body formation. *Trends Biochem Sci*. (1999) 24:109–15. doi: 10.1016/S0968-0004(98)01349-8
13. Brasaemle DL, Wolins NE. Packaging of fat: an evolving model of lipid droplet assembly and expansion. *J Biol Chem*. (2012) 287:2273–9. doi: 10.1074/jbc.R111.309088
14. Thiam AR, Farese RV Jr, Walther TC. The biophysics and cell biology of lipid droplets. *Nat Rev Mol Cell Biol*. (2013) 14:775–86. doi: 10.1038/nrm3699

15. Kusminski CM, Shetty S, Orci L, Unger RH, Scherer PE. Diabetes and apoptosis: lipotoxicity. *Apoptosis*. (2009) 14:1484–95. doi: 10.1007/s10495-009-0352-8
16. Thiele C, Spandl J. Cell biology of lipid droplets. *Curr Opin Cell Biol*. (2008) 20:378–85. doi: 10.1016/j.ceb.2008.05.009
17. Olofsson SO, Bostrom P, Andersson L, Rutberg M, Levin M, Perman J, et al. Triglyceride containing lipid droplets and lipid droplet-associated proteins. *Curr Opin Lipidol*. (2008) 19:441–7. doi: 10.1097/MOL.0b013e32830dd09b
18. Pol A, Martin S, Fernandez MA, Ingelmo-Torres M, Ferguson C, Enrich C, et al. Cholesterol and fatty acids regulate dynamic caveolin trafficking through the golgi complex and between the cell surface and lipid bodies. *Mol Biol Cell*. (2005) 16:2091–105. doi: 10.1091/mbc.e04-08-0737
19. Lu XY, Gruia-Gray J, Copeland NG, Gilbert DJ, Jenkins NA, Londos C, et al. The murine perilipin gene: the lipid droplet-associated perilipins derive from tissue-specific, mRNA splice variants and define a gene family of ancient origin. *Mammalian Genome*. (2001) 12:741–9. doi: 10.1007/s00335-01-2055-5
20. Londos C, Brasaemle DL, Schultz CJ, Segrest JP, Kimmel AR. Perilipins, ADRP, and other proteins that associate with intracellular neutral lipid droplets in animal cells. *Semin Cell Dev Biol*. (1999) 10:51–8. doi: 10.1006/scdb.1998.0275
21. Wolins NE, Skinner JR, Schoenfish MJ, Tzekov A, Bensch KG, Bickel PE. Adipocyte protein S3-12 coats nascent lipid droplets. *J Biol Chem*. (2003) 278:37713–21. doi: 10.1074/jbc.M304025200
22. Yamaguchi T, Matsushita S, Motojima K, Hirose F, Osumi T. MLDP, a novel PAT family protein localized to lipid droplets and enriched in the heart, is regulated by peroxisome proliferator-activated receptor alpha. *J Biol Chem*. (2006) 281:14232–40. doi: 10.1074/jbc.M601682200
23. Wolins NE, Quaynor BK, Skinner JR, Tzekov A, Croce MA, Gropler MC, et al. OXPAT/PAT-1 is a PPAR-induced lipid droplet protein that promotes fatty acid utilization. *Diabetes*. (2006) 55:3418–28. doi: 10.2337/db06-0399
24. Dalen KT, Dahl T, Holter E, Arntsen B, Londos C, Sztalryd C, et al. LSDP5 is a PAT protein specifically expressed in fatty acid oxidizing tissues. *Biochim Biophys Acta*. (2007) 1771:210–27. doi: 10.1016/j.bbalip.2006.11.011
25. Kimmel AR, Brasaemle DL, McAndrews-Hill M, Sztalryd C, Londos C. Adoption of PERILIPIN as a unifying nomenclature for the mammalian PAT-family of intracellular lipid storage droplet proteins. *J Lipid Res*. (2010) 51:468–71. doi: 10.1194/jlr.R000034
26. Itabe H, Yamaguchi T, Nimura S, Sasabe N. Perilipins: a diversity of intracellular lipid droplet proteins. *Lipids Health Dis*. (2017) 16:83. doi: 10.1186/s12944-017-0473-y
27. Erkens T, Van Poucke M, Vandesompele J, Goossens K, Van Zeveren A, Peelman LJ. Development of a new set of reference genes for normalization of real-time RT-PCR data of porcine backfat and longissimus dorsi muscle, and evaluation with PPARGC1A. *BMC Biotechnol*. (2006) 6:41. doi: 10.1186/1472-6750-6-41
28. Uddin MJ, Cinar MU, Tesfaye D, Looft C, Tholen E, Schellander K. Age-related changes in relative expression stability of commonly used housekeeping genes in selected porcine tissues. *BMC Res Notes*. (2011) 4:441. doi: 10.1186/1756-0500-4-441
29. Liu Y, Albrecht E, Schering L, Kuehn C, Yang R, Zhao Z, et al. Agouti signaling protein and its receptors as potential molecular markers for intramuscular and body fat deposition in cattle. *Front Physiol*. (2018) 9:172. doi: 10.3389/fphys.2018.00172
30. Schering L, Albrecht E, Komolka K, Kuhn C, Maak S. Increased expression of thyroid hormone responsive protein (THRSP) is the result but not the cause of higher intramuscular fat content in cattle. *Int J Biol Sci*. (2017) 13:532–44. doi: 10.7150/ijbs.18775
31. Hellemans J, Mortier G, De Paepe A, Speleman F, Vandesompele J. qBase relative quantification framework and software for management and automated analysis of real-time quantitative PCR data. *Genome Biol*. (2007) 8:R19. doi: 10.1186/gb-2007-8-2-r19
32. Mukaka MM. Statistics Corner: a guide to appropriate use of correlation coefficient in medical research. *Malawi Med J*. (2012) 24:69–71.
33. Morales PE, Bucarey JL, Espinosa A. Muscle lipid metabolism: role of lipid droplets and perilipins. *J Diabetes Res*. (2017) 2017:1789395. doi: 10.1155/2017/1789395
34. Gandolfi G, Mazzoni M, Zambonelli P, Lalatta-Costerbosa G, Tronca A, Russo V, et al. Perilipin 1 and perilipin 2 protein localization and gene expression study in skeletal muscles of European cross-breed pigs with different intramuscular fat contents. *Meat Sci*. (2011) 88:631–7. doi: 10.1016/j.meatsci.2011.02.020
35. Greenberg AS, Egan JJ, Wek SA, Garty NB, Blanchettemackie EJ, Londos C. Perilipin, a major hormonally regulated adipocyte-specific phosphoprotein associated with the periphery of lipid storage droplets. *J Biol Chem*. (1991) 266:11341–6. doi: 10.1016/S0021-9258(18)99168-4
36. Blanchettemackie EJ, Dwyer NK, Barber T, Coxey RA, Takeda T, Rondinone CM, et al. Perilipin is located on the surface-layer of intracellular lipid droplets in adipocytes. *J Lipid Res*. (1995) 36:1211–26. doi: 10.1016/S0022-2275(20)41129-0
37. Wolins NE, Quaynor BK, Skinner JR, Schoenfish MJ, Tzekov A, Bickel P. S3-12, adipophilin, and TIP47 package lipid in adipocytes. *J Biol Chem*. (2005) 280:19146–55. doi: 10.1074/jbc.M500978200
38. Brasaemle DL, Rubin B, Harten IA, Gruia-Gray J, Kimmel AR, Londos C. Perilipin A increases triacylglycerol storage by decreasing the rate of triacylglycerol hydrolysis. *J Biol Chem*. (2000) 275:38486–93. doi: 10.1074/jbc.M007322200
39. Yamaguchi T, Omatsu N, Matsushita S, Osumi T. CGI-58 interacts with perilipin and is localized to lipid droplets - possible involvement of CGI-58 mislocalization in Chanarin-Dorfman syndrome. *J Biol Chem*. (2004) 279:30490–7. doi: 10.1074/jbc.M403920200
40. Dalen KT, Schoonjans K, Ulven SM, Weedon-Fekjaer MS, Bentzen TG, Koutnikova H, et al. Adipose tissue expression of the lipid droplet-associating proteins S3-12 and perilipin is controlled by peroxisome proliferator-activated receptor-gamma. *Diabetes*. (2004) 53:1243–52. doi: 10.2337/diabetes.53.5.1243
41. Wang H, Bell M, Sreenivasan U, Hu H, Liu J, Dalen K, et al. Unique regulation of adipose triglyceride lipase (ATGL) by perilipin 5, a lipid droplet-associated protein. *J Biol Chem*. (2011) 286:15707–15. doi: 10.1074/jbc.M110.207779
42. Skinner JR, Harris LA, Shew TM, Abumrad NA, Wolins NE. Perilipin 1 moves between the fat droplet and the endoplasmic reticulum. *Adipocyte*. (2013) 2:80–6. doi: 10.4161/adip.22864
43. Listenberger LL, Ostermeyer-Fay AG, Goldberg EB, Brown WJ, Brown DA. Adipocyte differentiation-related protein reduces the lipid droplet association of adipose triglyceride lipase and slows triacylglycerol turnover. *J Lipid Res*. (2007) 48:2751–61. doi: 10.1194/jlr.M700359-JLR200
44. MacPherson RE, Peters SJ. Piecing together the puzzle of perilipin proteins and skeletal muscle lipolysis. *Appl Physiol Nutr Metab*. (2015) 40:641–51. doi: 10.1139/apnm-2014-0485
45. MacPherson RE, Herbst EA, Reynolds EJ, Vandenboom R, Roy BD, Peters SJ. Subcellular localization of skeletal muscle lipid droplets and PLIN family proteins OXPAT and ADRP at rest and following contraction in rat soleus muscle. *Am J Physiol Regul Integr Comp Physiol*. (2012) 302:R29–36. doi: 10.1152/ajpregu.00163.2011
46. Shaw CS, Sherlock M, Stewart PM, Wagenmakers AJ. Adipophilin distribution and colocalization with lipid droplets in skeletal muscle. *Histochem Cell Biol*. (2009) 131:575–81. doi: 10.1007/s00418-009-0558-4
47. Brasaemle DL, Barber T, Wolins NE, Serrero G, BlanchetteMackie EJ, Londos C. Adipose differentiation-related protein is an ubiquitously expressed lipid storage droplet-associated protein. *J Lipid Res*. (1997) 38:2249–63. doi: 10.1016/S0022-2275(20)34939-7
48. Jiang HP, Serrero G. Isolation and characterization of a full-length cDNA coding for an adipose differentiation-related protein. *Proc Natl Acad Sci USA*. (1992) 89:7856–60. doi: 10.1073/pnas.89.17.7856
49. Xu G, Sztalryd C, Lu X, Tansey JT, Gan J, Dorward H, et al. Post-translational regulation of adipose differentiation-related protein by the ubiquitin/proteasome pathway. *J Biol Chem*. (2005) 280:42841–7. doi: 10.1074/jbc.M506569200
50. Wolins NE, Rubin B, Brasaemle DL. TIP47 associates with lipid droplets. *J Biol Chem*. (2001) 276:5101–8. doi: 10.1074/jbc.M006775200
51. Wang H, Sreenivasan U, Hu H, Saladino A, Polster BM, Lund LM, et al. Perilipin 5, a lipid droplet-associated protein, provides physical and metabolic linkage to mitochondria. *J Lipid Res*. (2011) 52:2159–68. doi: 10.1194/jlr.M017939
52. Li B, Weng Q, Dong C, Zhang Z, Li R, Liu J, et al. A key gene, PLIN1, can affect porcine intramuscular fat content based on transcriptome analysis. *Genes*. (2018) 9:194. doi: 10.3390/genes9040194

53. Shirouchi B, Albrecht E, Nuernberg G, Maak S, Olavanh S, Nakamura Y, et al. Fatty acid profiles and adipogenic gene expression of various fat depots in Japanese Black and Holstein steers. *Meat Sci*. (2014) 96:157–64. doi: 10.1016/j.meatsci.2013.06.027
54. Gjelstad IM, Haugen F, Gulseth HL, Norheim F, Jans A, Bakke SS, et al. Expression of perilipins in human skeletal muscle in vitro and in vivo in relation to diet, exercise and energy balance. *Arch Physiol Biochem*. (2012) 118:22–30. doi: 10.3109/13813455.2011.630009
55. Fröhlich T, Kemter E, Flenkenthaler F, Klymiuk N, Otte KA, Blutke A, et al. Progressive muscle proteome changes in a clinically relevant pig model of Duchenne muscular dystrophy. *Sci Rep*. (2016) 6:33362. doi: 10.1038/srep33362
56. Gao J, Serrero G. Adipose differentiation related protein (ADRP) expressed in transfected COS-7 cells selectively stimulates long chain fatty acid uptake. *J Biol Chem*. (1999) 274:16825–30. doi: 10.1074/jbc.274.24.16825
57. Imamura M, Inoguchi T, Ikuyama S, Taniguchi S, Kobayashi K, Nakashima N, et al. ADRP stimulates lipid accumulation and lipid droplet formation in murine fibroblasts. *Am J Physiol-Endoc M*. (2002) 283:E775–E83. doi: 10.1152/ajpendo.00040.2002
58. Bulankina AV, Deggerich A, Wenzel D, Mutenda K, Wittmann JG, Rudolph MG, et al. TIP47 functions in the biogenesis of lipid droplets. *J Cell Biol*. (2009) 185:641–55. doi: 10.1083/jcb.200812042
59. Skinner JR, Shew TM, Schwartz DM, Tzekov A, Lepus CM, Abumrad NA, et al. Diacylglycerol enrichment of endoplasmic reticulum or lipid droplets recruits perilipin 3/TIP47 during lipid storage and mobilization. *J Biol Chem*. (2009) 284:30941–8. doi: 10.1074/jbc.M109.013995
60. Pourteymour S, Lee S, Langleite TM, Eckardt K, Hjorth M, Bindesboll C, et al. Perilipin 4 in human skeletal muscle: localization and effect of physical activity. *Physiol Rep*. (2015) 3:12481. doi: 10.14814/phy2.12481
61. Bosma M, Sparks LM, Hooiveld GJ, Jorgensen JA, Houten SM, Schrauwen P, et al. Overexpression of PLIN5 in skeletal muscle promotes oxidative gene expression and intramyocellular lipid content without compromising insulin sensitivity. *Bba-Mol Cell Biol L*. (2013) 1831:844–52. doi: 10.1016/j.bbalip.2013.01.007
62. Bosma M, Minnaard R, Sparks LM, Schaart G, Losen M, de Baets MH, et al. The lipid droplet coat protein perilipin 5 also localizes to muscle mitochondria. *Histochem Cell Biol*. (2012) 137:205–16. doi: 10.1007/s00418-011-0888-x
63. Tan MH, Sata T, Havel RJ. The significance of lipoprotein lipase in rat skeletal muscles. *J Lipid Res*. (1977) 18:363–70. doi: 10.1016/S0022-2275(20)41685-2
64. Wang H, Eckel RH. Lipoprotein lipase: from gene to obesity. *Am J Physiol Endocrinol Metab*. (2009) 297:E271–88. doi: 10.1152/ajpendo.90920.2008
65. Kersten S. Physiological regulation of lipoprotein lipase. *Biochim Biophys Acta*. (2014) 1841:919–33. doi: 10.1016/j.bbalip.2014.03.013
66. Levakfrank S, Radner H, Walsh A, Stolberger R, Knipping G, Hoefler G, et al. Muscle-specific overexpression of lipoprotein-lipase causes a severe myopathy characterized by proliferation of mitochondria and peroxisomes in transgenic mice. *J Clin Invest*. (1995) 96:976–86. doi: 10.1172/JCI118145
67. Kim JK, Fillmore JJ, Chen Y, Yu CL, Moore IK, Pypaert M, et al. Tissue-specific overexpression of lipoprotein lipase causes tissue-specific insulin resistance. *P Natl Acad Sci USA*. (2001) 98:7522–7. doi: 10.1073/pnas.121164498
68. Zechner R, Kienesberger PC, Haemmerle G, Zimmermann R, Lass A. Adipose triglyceride lipase and the lipolytic catabolism of cellular fat stores. *J Lipid Res*. (2009) 50:3–21. doi: 10.1194/jlr.R800031-JLR200
69. MacPherson RE, Ramos SV, Vandenboom R, Roy BD, Peters SJ. Skeletal muscle PLIN proteins, ATGL and CGI-58, interactions at rest and following stimulated contraction. *Am J Physiol Regul Integr Comp Physiol*. (2013) 304:R644–50. doi: 10.1152/ajpregu.00418.2012
70. Granneman JG, Moore HP, Mottillo EP, Zhu Z. Functional interactions between Mldp (LSDP5) and Abhd5 in the control of intracellular lipid accumulation. *J Biol Chem*. (2009) 284:3049–57. doi: 10.1074/jbc.M808251200
71. Granneman JG, Moore HP, Mottillo EP, Zhu Z, Zhou L. Interactions of perilipin-5 (Plin5) with adipose triglyceride lipase. *J Biol Chem*. (2011) 286:5126–35. doi: 10.1074/jbc.M110.180711
72. Sanders Matthew A, Madoux F, Mladenovic L, Zhang H, Ye X, Angrish M, et al. Endogenous and synthetic ABHD5 ligands regulate ABHD5-Perilipin interactions and lipolysis in fat and muscle. *Cell Metab*. (2015) 22:851–60. doi: 10.1016/j.cmet.2015.08.023

Conflict of Interest: The authors declare that the research was conducted in the absence of any commercial or financial relationships that could be construed as a potential conflict of interest.

frontiers in Molecular Biosciences

ORIGINAL RESEARCH
published: 13 August 2021
doi: 10.3389/fmolb.2021.700078

miR-10a-5p Inhibits the Differentiation of Goat Intramuscular Preadipocytes by Targeting KLF8 in Goats

Qing Xu[1,2,3], *Yong Wang*[1,2,3], *Xin Li*[1,2,3], *Yu Du*[1,2], *Yanyan Li*[1,3]*, *Jiangjiang Zhu*[1,2] and *Yaqiu Lin*[1,2,3]*

[1]Key Laboratory of Qinghai-Tibetan Plateau Animal Genetic Resource Reservation and Utilization of Education Ministry, Southwest Minzu University, Chengdu, China, [2]Key Laboratory of Qinghai-Tibetan Plateau Animal Genetic Resource Reservation and Exploitation of Sichuan Province, Southwest Minzu University, Chengdu, China, [3]College of Animal Science and Veterinary, Southwest Minzu University, Chengdu, China

Intramuscular fat contributes to the improvement of meat quality of goats. MicroRNAs (miRNAs) have been reported to regulate adipocyte differentiation and maturation. The aim of our study was to clarify whether miR-10a-5p regulates goat intramuscular preadipocyte (GIPC) differentiation and its direct downstream signaling pathway. GIPCs were isolated from longissimus dorsi, whose miR-10a-5p level was measured at different time point of differentiation induction. Adipogenic differentiation of the GIPCs was evaluated by Oil Red O and BODIPY staining, and the expression changes of adipogenic genes like ACC, ATGL, CEBPβ, PPARγ, etc. Related mechanisms were verified by qPCR, a bioinformatic analysis, a dual-luciferase reporter assay, overexpression, and siRNA transfection. Oil Red O and BODIPY staining both with adipogenic gene detection showed that miR-10a-5p suppressed the accumulation of lipid droplets in GIPCs and inhibited its differentiation. The dual-luciferase reporter assay experiment revealed that miR-10a-5p regulates GIPC differentiation by directly binding to KLF8 3'UTR to regulate its expression. Thus, the results indicated that miR-10a-5p inhibits GIPC differentiation by targeting KLF8 and supply a new target for fat deposition and meat quality improvement.

Keywords: MiR-10a-5p, KLF8, goat, intramuscular preadipocytes, differentiation

OPEN ACCESS

Edited by:
Xiao Li,
Northwest A and F University, China

Reviewed by:
Zhuanjian Li,
Henan Agricultural University, China
Carmela De Marco,
Magna Grãcia University of Catanzaro, Italy

***Correspondence:**
Yaqiu Lin
linyq1999@163.com
Yanyan Li
liyanyan@swun.edu.cn

Specialty section:
This article was submitted to Cellular Biochemistry, a section of the journal Frontiers in Molecular Biosciences

Received: *25 April 2021*
Accepted: *13 July 2021*
Published: *13 August 2021*

Citation:
Xu Q, Wang Y, Li X, Du Y, Li Y, Zhu J and Lin Y (2021) miR-10a-5p Inhibits the Differentiation of Goat Intramuscular Preadipocytes by Targeting KLF8 in Goats. Front. Mol. Biosci. 8:700078. doi: 10.3389/fmolb.2021.700078

INTRODUCTION

Intramuscular fat (IMF) is deposited in skeletal muscle fibers (Hocquette et al., 2010). IMF can be used to store energy and functions during exercise, but an excessive accumulation of IMF in the muscle is related to many diseases in people, such as diabetes, insulin resistance, lipodystrophy, etc. (Goodpaster et al., 2000; Shoelson et al., 2007; Tada et al., 2020; Yamada et al., 2020). The IMF content in animals is not only an important index of high quality of meat but also an important character of good germplasm. IMF is an important factor for meat quality which is connected with meat tenderness, meat flavor, and color (Wood et al., 2004; Chen and Sui, 2018; Liu et al., 2019). The number and size of intramuscular adipocytes mainly determine the IMF contents, and intramuscular adipocytes are very important because they provide sites for later marbling fat deposition. However, the mechanism of preadipocyte differentiation still needs to be further investigated.

MicroRNAs (miRNAs or miRs) are small noncoding RNAs; several studies suggested that they are the negative regulator over the process of target gene expression through degrading mRNAs or inhibiting the translation of mRNAs (Mourelatos, 2008; Li et al., 2014; Schreck et al., 2017; Lin et al.,

2019; van der Kwast et al., 2020). Recently, more and more studies have proved the significance of miRNAs in regulating adipogenic differentiation. However, roles of miRNAs in GIPC differentiation shift fate are still unclear.

In the current study, we explored the action of miR-10a-5p in GIPC differentiation as well as mechanisms during the process. In general, we demonstrated that miR-10a-5p expression was significantly changed during preadipocyte differentiation in goats. MiR-10a-5p inhibits GIPC differentiation by targeting KLF8. Therefore, our conclusion supplied a new idea and theoretical basis for the basic research of improving the quality of meat.

MATERIALS AND METHODS

Isolation and Cell Culture of Goat Intramuscular Preadipocytes

The 7-day-old Jianzhou Daer male goats ($n = 3$) were used as an experimental model. The GIPCs were isolated and cultured, as we previously described (Xu et al., 2018; Ma et al., 2021). Briefly, the isolated longissimus dorsi muscles of goats were washed with PBS for three times and minced and then were digested with an equal volume of collagenase type II at 37°C for 2 h in a shaking water bath every 5 min. Steel mesh filters of 200 and 400 μm were utilized to isolate digested cells. The rinsed filtrated cells by DMEM/F12 medium were centrifuged twice at 2000 r/min for 5 min to collect sediment clumps and then the supernatant was discarded. The viable cells were resuspended in DMEM/F12, including 10% fetal bovine serum and plated in 25-cm^2 flask in a 5% CO_2 atmosphere at 37°C for subsequent culture. Experimentation on goats performed in the present study had been given prior approval by the Ethics Committee of Southwest Minzu University under permit no. SMU20160108, and all of the methods were performed according to the guidelines and regulations.

Preadipocyte Differentiation Induction

We induced GIPCs adipogenic differentiation *in vitro* as before (Xu et al., 2018). Briefly, adipogenesis induction medium [MEM/F12 containing 10% FBS and 50 μmol•L^{-1} oleic acid (Sigma)] was used to culture GIPCs in 12-well plates with a density of 1×10^6 cells per well for the required time point. We changed the culture medium every other day. After induction, Oil Red O staining and BODIPY staining were used to distinguish mature adipocytes from preadipocytes during the process of culture.

Oil Red O and BODIPY Staining

Adipogenic differentiation of the GIPCs was assessed by Oil Red O or BODIPY staining as previously described (Xu et al., 2018). The GIPCs were washed with PBS and fixed in 10% formaldehyde for 10 min, then washed with PBS, and stained using the Oil Red O or BODIPY working solutions for 20 min. The cells were then observed and photographed after washing. After photographing, the cells were destained in 1 ml 100% isopropanol for 15 min and the Oil Red signal was quantified by measuring the absorbance at 490 nm (OD 490) as a semi-quantitative assessment method to determine the extent of differentiation. The stained area of Oil Red O or BODIPY staining was measured using ImageJ (NIH, Bethesda, MD, United States).

qRT-PCR

Total RNA from cells was extracted using the TRIzol reagent (TaKaRa) according to the manufacturer's protocol. The mRNAs were reverse transcribed using the RevertAid First Strand cDNA Synthesis Kit (Thermo) according to the protocol. Then, amplification reactions were performed using amplification primers with the SYBR Green PCR Master Mix (TaKaRa); the reaction volumes were 20 μl. Then 1 μl of cDNA was applied in every set of experiment. The mRNA expression levels were standardized to UXT or U6. Information on primers for qPCR is listed in **Table 1**.

Transfection

Small interfering RNA (siRNA) against KLF8, 5'-CAGACUCUUGUAGUGUCCACUUCAAdTdT-3' was synthesized by Invitrogen. KLF8 expression plasmid was constructed by inserting expanded KLF8 cDNA (KX247671) fragments into pcDNA3.1 vector (sense primer sequence: 5'CGGGGTACCATGGATGAACTCATAAACAACT-3', anti-sense primer sequence: 5'-ATAAGAATGCGGCCGCTTACA CGGTGTCATGGCGC-3'). The KLF8 interference (designated as siKLF8) or negative control (siNC) GIPCs were constructed using siRNA. The KLF8 overexpression (designated as KLF8) GIPCs were constructed using an expression plasmid, and the control cells for the KLF8 overexpression group were designated as a vector. Cells had been pre-cultured for 2 h in a serum-free medium for transfection. Then plasmid or siRNA was introduced into the cells using a Lipofectamine 3000 transfection reagent, in accordance with the manufacturer's instruction (Invitrogen, Carlsbad, United States).

The miR-10a-5p mimics (designated as mimics: UACCCU GUAGAUCCGAAUUUGU), an inhibitor (designated as inhibitor: ACAAAUUCGGAUCUACAGGGUA), and a respective negative control (designated as mock: UUGUAC UACACAAAAGUACUG, NC: CAGUACUUUUGUGUAGUA CAA) (Genepharma, Shanghai, China) as needed were transfected into the GIPCs by Lipofectamine 3000 (Invitrogen, Carlsbad, United States) and opti-MEM (Gibco BRL Co., LTD) culture medium according to the manufacturer's instruction.

After 12-h transfection, the original medium was replaced by a fresh differentiation medium to induce GIPC differentiation. After 48-h induction, the cells were used for Oil red O or BODIPY staining or collected to extract RNA for qPCR detection.

Luciferase Reporter Assay

For the luciferase reporter assay, the 3'UTR of KLF8 containing the wild or mutant miR-10a-5p target sites was cloned using primers with *Not*I and *Xho*I (Thermo, MA, United States) cleavage sites. The wild or mutant type 3'UTR fragment was inserted into the corresponding site of the psiCHECK vector and then co-transfected into 293T cells with miR-10a-5p mimics/mock. After 48 h transfection, the cells were harvested and the Dual-Luciferase Reporter Assay System Kit (Promega, Madison,

TABLE 1 | The sequences information of specificity primers.

Gene/miRNA (Accession number in GenBank)	Sequence
ACC (XM_018064169.1)	GGAGACAAACAGGGACCATT
	ATCAGGGACTGCCGAAAC
ATGL (NM_001285739.1)	GGTGCCAATATCATCGAGGT
	CACACCCGTGGCAGTCAG
AP2 (NM_001285623.1)	TGAAGTCACTCCAGATGACAGG
	TGACACATTCCAGCACCAGC
*CEBP*α (XM_018062278)	CCGTGGACAAGAACAGCAAC
	AGGCGGTCATTGTCACTGGT
*CEBP*β (XM_018058020.1)	CAAGAAGACGGTGGACAAGC
	AACAAGTTCCGCAGGGTG
DGAT2 (NM_001314305.1)	CAATAGGTCCAAGGTAGA
	GAAGC
	ACCAGCCAGGTGAAGTAGAGC
GLUT4 (NM_001314227.1)	TGCTCATTCTTGGACGGTTCT
	CATGGATTCCAAGCCTAGCAC
FASN (NM_001285629.1)	TGTGCAACTGTGCCCTAG
	GTCCTCTGAGCAGCGTGT
HSL (XM_018062484.1)	AGGGTCATTGCCGACTTCC
	GTCTCGTTGCGTTTGTAGTGC
LPL (NM_001285607.1)	TCCTGGAGTGACGGAATCTGT
	GACAGCCAGTCCACCACGAT
PPARγ (NM_001285658)	AAGCGTCAGGGTTCCACTATG
	GAACCTGATGGCGTTATGAGAC
*Pref*1 (KP686197.1)	CCGGCTTCATGGATAAGACCT
	GCCTCGCACTTGTTGAGGAA
*SREBP*1 (NM_001285755)	AAGTGGTGGGCCTCTCTGA
	GCAGGGGTTTCTCGGACT
*KLF*8 (KX247671)	GACTACAGCAAGAACCAG
	CAGC
	CTCCTGTATGGATTCTGCGGT
UXT (XM_005700842.2)	GCAAGTGGATTTGGGCTGTAAC
	ATGGAGTCCTTGGTGAGGTTGT
U6 (NR_138,085.1)	TGGAACGCTTCACGAATTTGCG
	GGAACGATACAGAGAAGA
	TTAGC
miR-10a-5p	CAGCTGTACCCTGTAGATCCGA
	GTGCAGGGTCCGAGGT

WI, United States) was used for detecting dual-luciferase activity, according to the manufacturer's instructions.

Statistical Analysis

All data were presented as "mean ± SD." The variance of data was analyzed by SPSS 17.0, followed by Duncan's multiple comparisons test. * indicates the p values were < 0.05, ≥ 0.01, whereas ** indicates p values < 0.01. All experiments in our study were carried out for three times at least.

RESULTS

miR-10a-5p Expression Changed During GIPCs Differentiation

MicroRNAs have been reported to regulate adipogenic differentiation (Hamam et al., 2015; Tang et al., 2017; Ai et al., 2019; Li et al., 2019); however, the role of miR-10a-5p in goat intramuscular adipogenesis has not been reported. The differential expression of miR-10a-5p after GIPC differentiation has been observed by miRNA sequencing technology in our previous study (data not shown). In order to clarify the role of miR-10a-5p in the differentiation of GIPCs, we first isolated intramuscular preadipocytes from goat longissimus dorsi and induced them to adipogenic differentiation. Oil red O staining was used to ascertain the extent of differentiation; our obtained results showed that the lipid droplets accumulation increased with the extension of induction time, and the GIPCs were differentiated completely after 60-h induction (**Figure 1A**). Then qRT-PCR was implemented to research the role of miR-10a-5p in adipogenic differentiation of GIPCs. The test result showed an obvious alteration in the expression of miR-10a-5p during differentiation when compared to 0 h (**Figure 1B**). All above indicate that miR-10a-5p may regulate the adipogenic differentiation of GIPCs.

miR-10a-5p Inhibits the Adipogenic Differentiation of GIPCs

To clarify the effect of miR-10a-5p on GIPC adipogenic differentiation, miR-10a-5p mimics (named as miR-10a-5p) or its control (named as mock) was transfected to GIPCs to overexpress miR-10a-5p. The expression of miR-10a-5p in GIPCs increased ~ 10,000 times caused by mimic transfection than the same amount of control vector transfected cells (**Figure 2A**). Preadipocyte differentiation is associated with lipid droplets accumulation in the cells. Oil red O and BODIPY stainings were utilized as lipid droplet detection methods. In our study, after miR-10a-5p overexpression, the lipid droplet accumulation was significantly decreased in the group of mimic-transfected cells than the control group (**Figures 2B–E**). Oil red O and BODIPY staining results showed about 20–30% reduction of lipid droplets with miR-10a-5p overexpression (**Figures 2B–E**). Additionally, there are representative of the genes upregulated during the differentiation process from preadipocytes to mature adipocytes. Indeed, the mRNA expression levels of representative genes AP2, DGAT2, FASN, HSL, LPL, and Pref1 were obviously inhibited due to the overexpression of miR-10a-5p in GIPCs (**Figure 2F**). All these results implied that miR-10a-5p may weaken the adipogenic differentiation of GIPCs.

For further validating the suppression effect of miR-10a-5p on GIPC adipogenic differentiation, miR-10a-5p inhibitor (named as inhibitor) or its control (named as NC) was transfected to GIPCs to silence miR-10a-5p expression. About 80% of the interference efficiency was caused by inhibitor transfection compared to the NC group (**Figure 3A**). Oil red O and BODIPY staining results showed that compared with the control group, miR-10a-5p knockdown significantly promoted the about 10–20% of lipid droplet accumulation (**Figures 3B–E**). Coincidently, the mRNA levels of important markers of adipocyte differentiation like ACC, ATGL, CEBPβ, GLUT4, HSL, PPARγ, and Pref1 were upregulated due to the knockdown of miR-10a-5p in GIPCs (**Figure 3F**). Therefore, miR-10a-5p inhibits adipogenic differentiation of GIPCs.

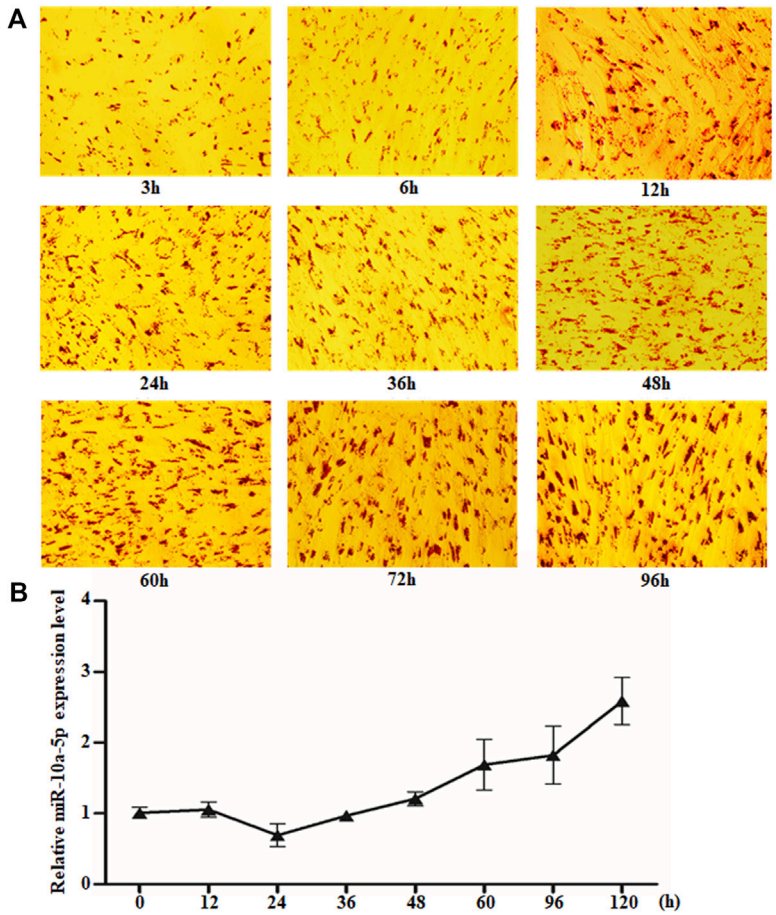

FIGURE 1 | miR-10a-5p expression changed obviously during GIPC differentiation. **(A)** Representative images of Oil O staining of GIPCs cultured in oleic acid induction medium for different hours. **(B)** qRT-PCR analysis of the relative level of miR-10a-5p expression in GIPCs cultured in oleic acid induction medium for the hours as indicated. N > or = 3 for A and B.

miR-10a-5p Targets the 3'UTR of KLF8 mRNA

It has been well known that miRNA binds to the 3'-UTR of target mRNA's complementary sequences, so the target gene's mRNA expression can be inhibited (Redis and Calin, 2017; Rouleau et al., 2017; Sun et al., 2017). TargetScan (Garcia et al., 2011), microRNAseq (Yan et al., 2018), miRDB (Wong and Wang, 2015), and DIANA-microT (Maragkakis et al., 2009) were the tools used for predicting the miR-10a-5p possible target genes. Among all the potential target genes predicted in both databases, we chose KLF8, as it is a positive regulator of 3T3-L1 differentiation and knocking down its expression can reduce RXRα overexpression-caused GIPC differentiation (Lee et al., 2012; Xu et al., 2020). Also, its family members are important regulators for adipogenic differentiation (Kinoshita et al., 2010; Pei et al., 2011; Tahmasebi et al., 2013; Shen et al., 2018; Chen J. et al., 2020). By sequence analysis, there is potential binding site of miR-10a-5p in the 3'UTR of KLF8 in goat (**Figure 4A**). First, we measured the mRNA level of KLF8 in miR-10a-5p mimics or inhibitor-transfected cells. As expected, the mimics of miR-10a-5p significantly downregulated the mRNA level of KLF8, while miR-10a-5p inhibitor upregulated its mRNA expression when compared with each control group, respectively (**Figure 4B**). In order to make sure whether miR-10a-5p can directly target KLF8 3'UTR, we mutated miR-10a-5p–binding sites in the KLF8 3'UTR area (**Figure 4C**). Luciferase report vectors were constructed with wild-type KLF8 3'UTR (KLF8 3'UTR WT) and mutated KLF8 3'UTR (KLF8 3'UTR MT). The KLF8 luciferase activity was measured for describing miR-10a-5p function on luciferase translation. The results showed that luciferase activity of wild-type KLF8 3'UTR was significantly inhibited by miR-10a-5p overexpression, yet mutated KLF8 3'UTR terminated this effect (**Figure 4D**). Taken together, we confirmed that KLF8 is the direct target of miR-10a-5p. Then, we got the conclusion that miR-10a-5p targets KLF8 and regulates KLF8 expression.

KLF8 Promotes the Adipogenic Differentiation of GIPCs

Since KLF8 is the target of miR-10a-5p and plenty of studies have shown that KLF8 and its family members are regulators of

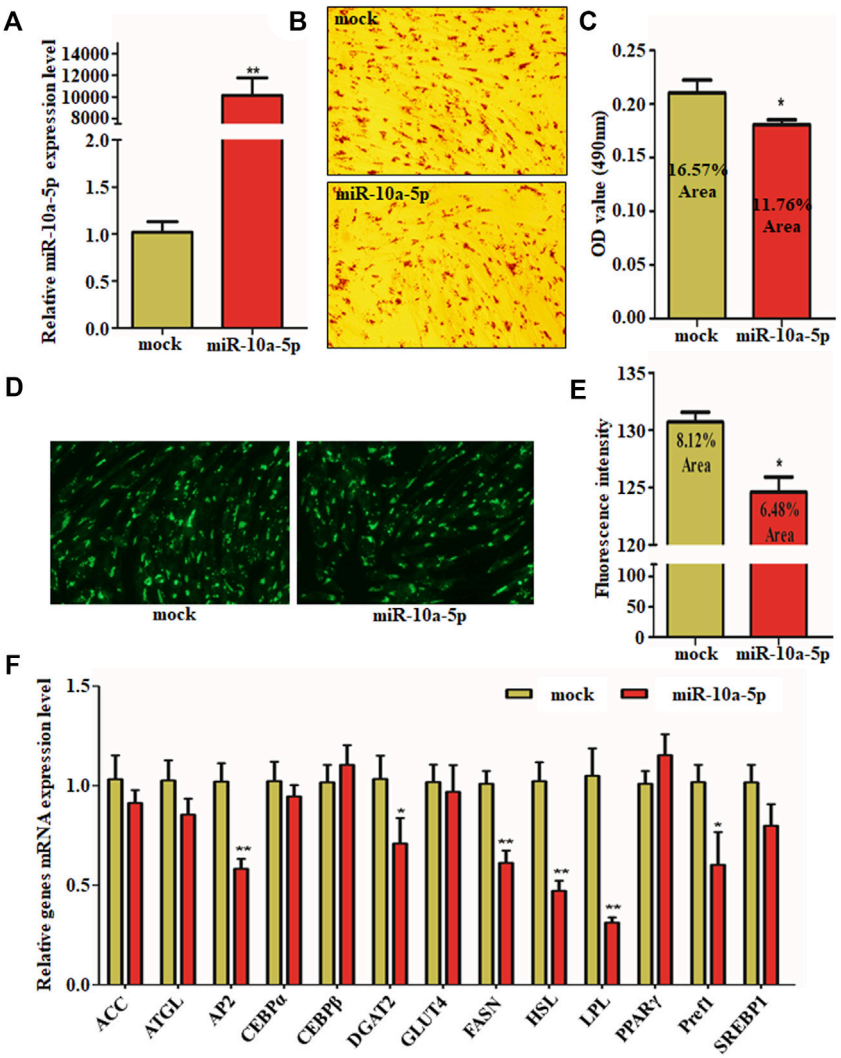

FIGURE 2 | Overexpression of miR-10a-5p inhibits GIPC differentiation. **(A)** qRT-PCR analysis of levels of miR-10a-5p expression in GIPCs with mimics or control transfected for 24 h. **(B)** Representative images of Oil Red O staining of GIPCs with miR-10a-5p mimics or control and **(C)** semi-quantitative assessment of Oil Red O content absorbance detection at 490 nm. **(D)** Representative images of mature adipocytes stained with BODIPY and **(E)** stained area was measured using ImageJ. **(F)** qRT-PCR analysis of levels of genes expression in GIPCs with miR-10a-5p mimics or control. N > or = 3, * indicates p values < 0.05 and ≥ 0.01, ** indicates p values < 0.01.

adipogenic differentiation, we further explored the relationship between KLF8 expression and GIPCs differentiation. We first synthesized KLF8 siRNA (named as siKLF8 and its control named as siNC) and constructed its expression plasmid (named as KLF8 and its control named as vector). Both the expression plasmid and siRNA were effective that cells transfected with the KLF8 expression plasmid can upregulate its expression about 5,000 times, and KLF8 siRNA can downregulate its expression about 60 times (**Figure 5A**). Oil red O and BODIPY staining results showed that KLF8 overexpression could contribute to the lipid droplet accumulation; nevertheless, KLF8 knockdown can inhibit the lipid droplet accumulation when compared with each control group, respectively (**Figures 5B–E**). qPCR was used to detect relative adipogenic gene expression, and the crucial adipocyte differentiation markers DGAT2, ACC, and LPL were markedly promoted by KLF8 overexpression (**Figure 5F**). Also, LPL, PPARγ, and C/EBPβ as adipocyte differentiation genes were obviously inhibited by KLF8 interference (**Figure 5F**). In summary, our results indicated that KLF8 confers GIPCs with more properties of adipogenic differentiation.

DISCUSSION

Preadipocytes differentiate into adipocytes, which improve the color and flavor of meat in animals. According to the results we obtained, we expounded that miR-10a-5p is involved in regulating GIPCs adipogenic differentiation.

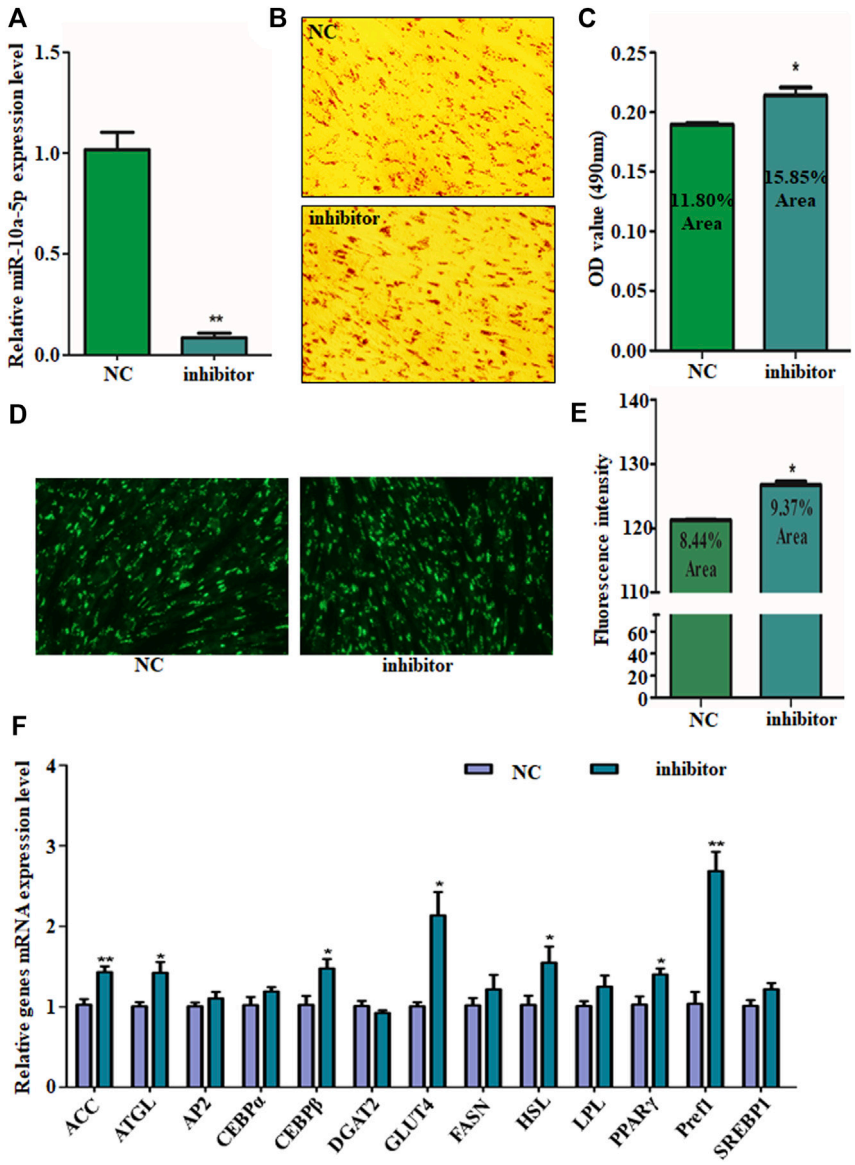

FIGURE 3 | Silence of miR-10a-5p promotes GIPC differentiation. **(A)** qRT-PCR analysis of levels of miR-10a-5p expression in GIPCs with inhibitor or control transfected for 24 h. **(B)** Representative images of Oil Red O staining of GIPCs with miR-10a-5p inhibitor or control and **(C)** semi-quantitative assessment of Oil Red O content absorbance detection at 490 nm. **(D)** Representative images of mature adipocytes stained with BODIPY and **(E)** stained area was measured using ImageJ. **(F)** qRT-PCR analysis of levels of genes expression in GIPCs with miR-10a-5p inhibitor or control. N > or = 3, * indicates p values < 0.05 and ≥ 0.01, ** indicates p values < 0.01.

miR-10a-5p directly targets the 3'UTR of KLF8 to inhibit its expression which promotes adipogenic differentiation. Furthermore, miR-10a-5p inhibits the accumulation of lipid droplets and the expression of relative adipogenic genes. Our results indicate that miR-10a-5p regulates alteration and lineage fate in GIPCs at the adipogenic differentiation process.

Accumulation of lipid droplets in the cells is associated with the differentiation of preadipocytes (Lee et al., 2017; Peng et al., 2018). This was verified by Oil red O and BODIPY staining in our study. Additionally, the differentiation of adipocytes is featured with genes expression alteration such as PPARγ, LPL, HSL, and C/EBP, and so on (Rosen and MacDougald, 2006; Kim et al., 2015; Lee et al., 2017; Peng et al., 2018; Chen X. et al., 2020). Indeed, during the differentiation process from preadipocytes to mature adipocytes, ACC, ATGL, CEBPβ, GLUT4, HSL, PPARγ, and Pref1 are the representative upregulated genes. It is interesting that the adipogenic genes expression in miR-10a-5p overexpression GIPCs are not consistent with miR-

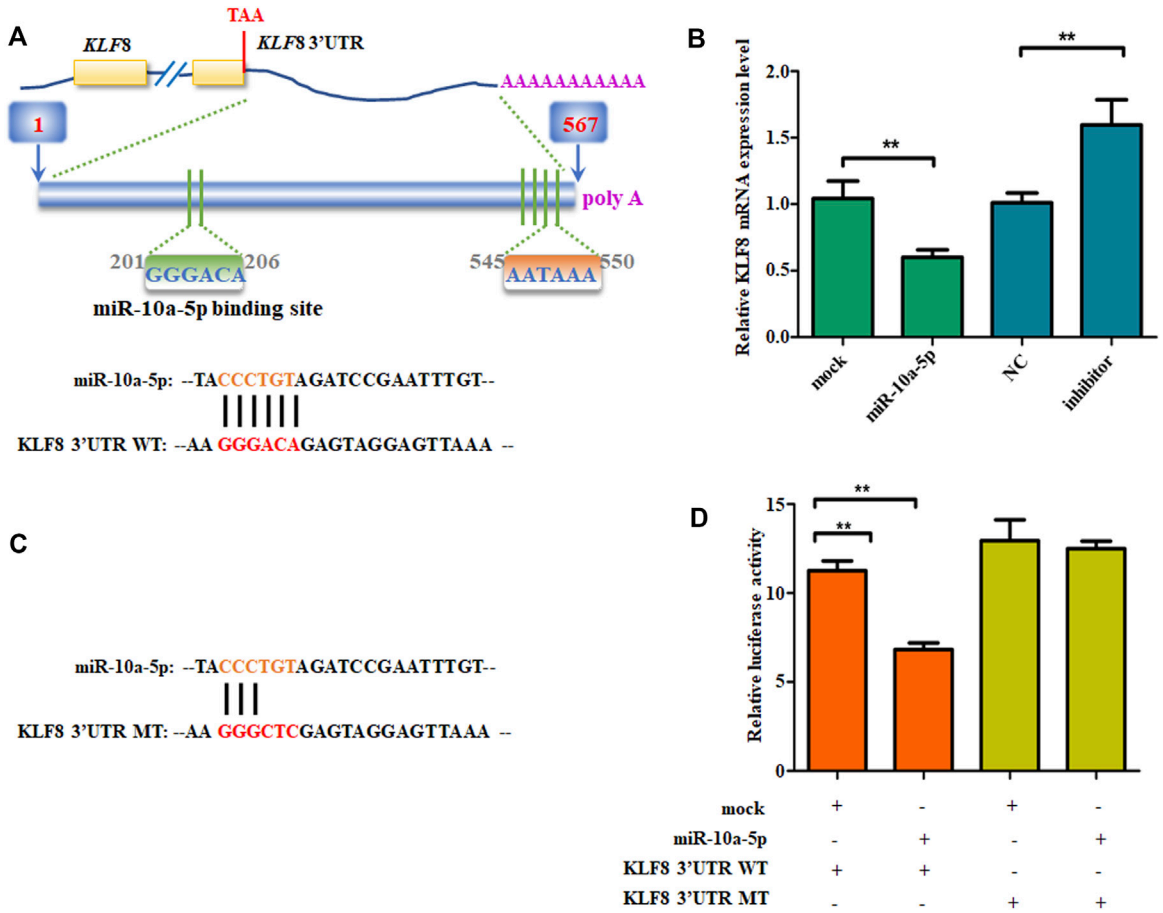

FIGURE 4 | miR-10a-5p directly bind to KLF8 3'UTR. **(A)** The predicted miR-10a-5p binding site in KLF8 3'UTR. **(B)** qRT-PCR analysis of levels of genes expression in GIPCs with miR-10a-5p mimics, inhibitor, or each control. **(C)** mutant miR-10a-5p binding site in KLF8 3'UTR. **(D)** Luciferase assay of transfected with wild-type or mutant KLF8 3'UTR plasmid in 293T cells. N >or = 3 for B and D, * indicates p values < 0.05 and ≥0.01, ** indicates p values < 0.01.

10a-5p knockdown cells (**Figures 2F**, **3F**). KLF8 overexpression and knockdown cells showed the same phenomenon (**Figure 5F**). Here, we confirmed that KLF8 was the target of miR-10a-5p, but the knockdown of KLF8 causing the expression tendency of differentiation-related genes was not completely consistent with miR-10a-5p overexpression (**Figures 2F**, **5F**). Also, the expression trend of differentiation-related genes did not present the same consistency in both KLF8 overexpression cells and miR-10a-5p knockdown cells (**Figures 3F**, **5F**). One possible explanation for this observed deviation is that the differentiation of GIPCs was regulated by more complex mechanisms, and this deviation might be referred to other regulation pathways for which further investigation would be need.

miRNAs are known as endogenous small noncoding RNAs that have been identified as gene expression post-transcriptional regulators, and miRNAs bind mainly to the target mRNA's 3' untranslated regions (UTRs), resulting in the blockade of mRNA translation or mRNA degradation (Kerr et al., 2011; Callegari et al., 2013). Thus, miRNAs play vital roles in the differentiation and maturation of adipocytes, as shown in the findings of the present studies (Kato et al., 2012; Kobayashi et al., 2013; Miyoshi et al., 2014; Fujita et al., 2015a; Fujita et al., 2015b; Fujihara et al., 2015; Fujimori et al., 2015; Kato et al., 2016). Several miRNAs have been reported to contribute to lipid synthesis, metabolism, transportation, and storage. miR-10a-5p was reported to be relevant to proliferation, metastasis, invasive, drug resistance, inflammation, and other behaviors in cancer cells. In a previous investigation, miR-10a-5p was shown to restrain adipogenic differentiation in primary mouse preadipocytes. In the current study, up- or downregulation of miR-10a-5p was found to be involved in the differentiation of preadipocytes in goats. We also found that miR-10a-5p binds to the 3'UTR of KLF8 to perform its functions in an KLF8-dependent pathway. Taken together, our studies show that miR-10a-5p is critical for GIPC differentiation.

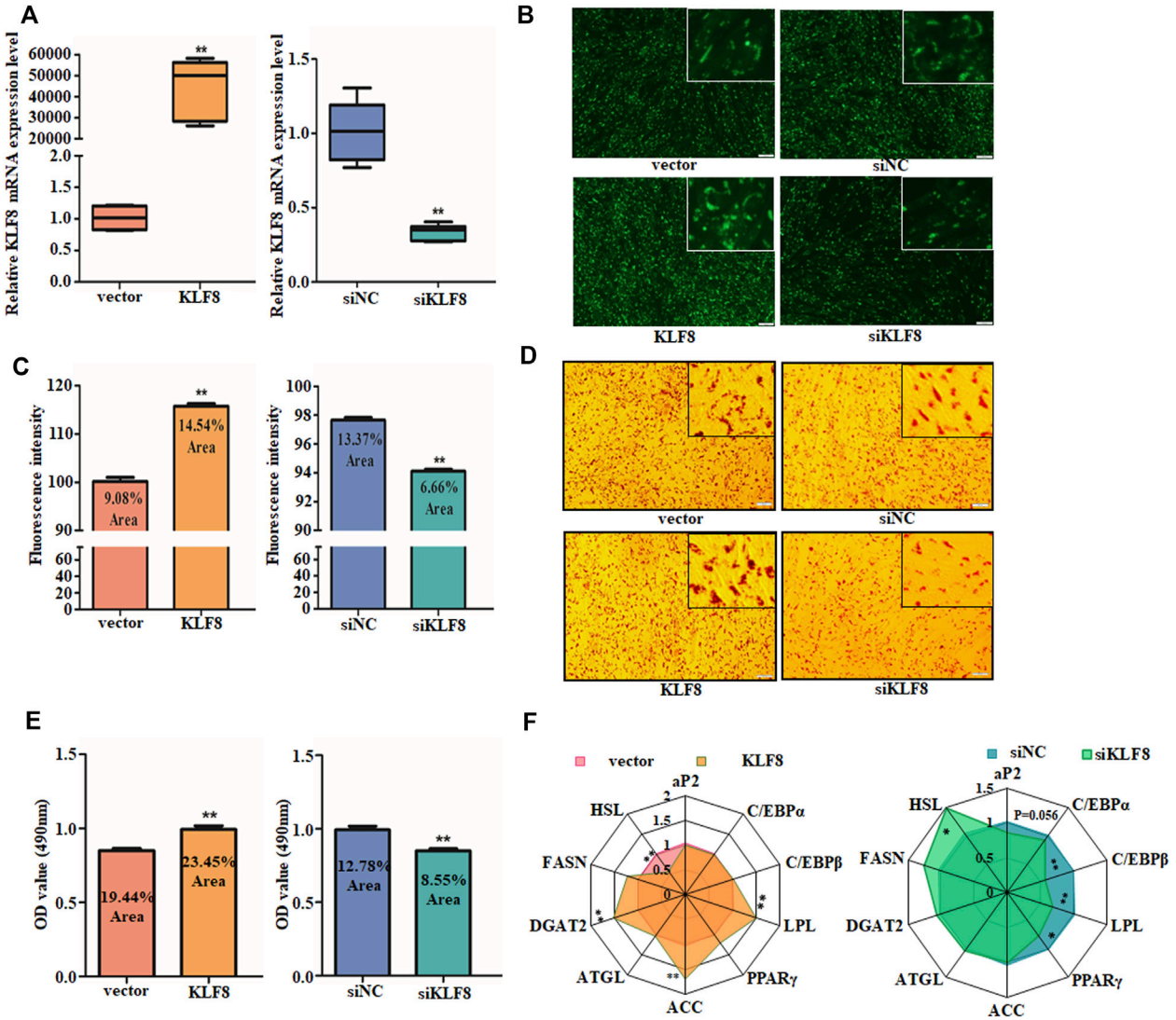

FIGURE 5 | KLF8 promotes GIPC differentiation. **(A)** qRT-PCR analysis of levels of KLF8 with KLF8 siRNA, expression plasmid, or each control transfected for 24 h. **(B)** Representative images of mature adipocytes stained with BODIPY and **(C)** stained area was measured using ImageJ. **(D)** Representative images of Oil Red O staining of GIPCs with miR-10a-5p inhibitor or control and **(E)** semi-quantitative assessment of Oil Red O content absorbance detection at 490 nm. **(F)** qRT-PCR analysis of genes expression in GIPCs with KLF8 up- or downregulation, the result was showed by a network diagram. N >or = 3 for B and D, * indicates p values < 0.05 and ≥ 0.01, ** indicates p values < 0.01.

CONCLUSION

Our results show that miR-10a-5p acts as an inhibitor of GIPC differentiation by targeting KLF8. This finding supplied a new target and possible mechanism for the basic research of meat quality improvement.

DATA AVAILABILITY STATEMENT

The raw data supporting the conclusions of this article will be made available by the authors, without undue reservation.

ETHICS STATEMENT

The animal study was reviewed and approved by the Ethics Committee of Southwest Minzu University.

AUTHOR CONTRIBUTIONS

Concept and design: QX, YW, XL, YD, YL, JZ, and YQL; development of methodology: QX, YL, YW, and YQL;

acquisition of data: QX and YQL; analysis and interpretation of data: QX; writing, review, and/or revision of the manuscript: QX, YL, YW, and YQL; administrative, technical, or material support: YL, YW, and JZ; study supervision: YW and YQL.

FUNDING

This study was supported by grants from the National Natural Sciences Foundation of China (31672395) and the Applied Basic Research Program Key Project of Sichuan Province (2018JY0036).

REFERENCES

Ai, G., Meng, M., Wang, L., Shao, X., Li, Y., Cheng, J., et al. (2019). microRNA-196a Promotes Osteogenic Differentiation and Inhibit Adipogenic Differentiation of Adipose Stem Cells via Regulating β-catenin Pathway. *Am. J. Transl Res.* 11, 3081–3091.

Callegari, E., Elamin, B. K., Sabbioni, S., Gramantieri, L., and Negrini, M. (2013). Role of microRNAs in Hepatocellular Carcinoma: A Clinical Perspective. *Onco Targets Ther.* 6, 1167–1178. doi:10.2147/OTT.S36161

Chen, G., and Sui, Y. (2018). Production, Performance, slaughter Characteristics, and Meat Quality of Ziwuling Wild Crossbred Pigs. *Trop. Anim. Health Prod.* 50, 365–372. doi:10.1007/s11250-017-1441-2

Chen, J., Yang, Y., Li, S., Yang, Y., Dai, Z., Wang, F., et al. (2020). E2F1 Regulates Adipocyte Differentiation and Adipogenesis by Activating ICAT. *Cells* 9, 1024. doi:10.3390/cells9041024

Chen, X., Raza, S. H. A., Cheng, G., Ma, X., Wang, J., and Zan, L. (2020). Bta-miR-376a Targeting KLF15 Interferes with Adipogenesis Signaling Pathway to Promote Differentiation of Qinchuan Beef Cattle PreadipocytesKLF15 Interferes With Adipogenesis Signaling Pathway to Promote Differentiation of Qinchuan Beef Cattle Preadipocytes. *Animals* 10, 2362. doi:10.3390/ani10122362

Fujihara, S., Kato, K., Morishita, A., Iwama, H., Nishioka, T., Chiyo, T., et al. (2015). Antidiabetic Drug Metformin Inhibits Esophageal Adenocarcinoma Cell Proliferation *In Vitro* and *In Vivo*. *Int. J. Oncol.* 46, 2172–2180. doi:10.3892/ijo.2015.2903

Fujimori, T., Kato, K., Fujihara, S., Iwama, H., Yamashita, T., Kobayashi, K., et al. (2015). Antitumor Effect of Metformin on Cholangiocarcinoma: *In Vitro* and *In Vivo* Studies. *Oncol. Rep.* 34, 2987–2996. doi:10.3892/or.2015.4284

Fujita, K., Iwama, H., Oto, T., Okura, R., Kobayashi, K., Takano, J., et al. (2015a). Galectin-9 Suppresses the Growth of Hepatocellular Carcinoma via Apoptosis *In Vitro* and *In Vivo*. *Int. J. Oncol.* 46, 2419–2430. doi:10.3892/ijo.2015.2941

Fujita, K., Kobara, H., Mori, H., Fujihara, S., Chiyo, T., Matsunaga, T., et al. (2015b). Differences in miRNA Expression Profiles Between GIST and Leiomyoma in Human Samples Acquired by Submucosal Tunneling Biopsy. *Endosc. Int. Open* 03, E665–E671. doi:10.1055/s-0034-1393077

Garcia, D. M., Baek, D., Shin, C., Bell, G. W., Grimson, A., and Bartel, D. P. (2011). Weak Seed-Pairing Stability and High Target-Site Abundance Decrease the Proficiency of Lsy-6 and Other microRNAs. *Nat. Struct. Mol. Biol.* 18, 1139–1146. doi:10.1038/nsmb.2115

Goodpaster, B. H., Thaete, F. L., and Kelley, D. E. (2000). Thigh Adipose Tissue Distribution Is Associated with Insulin Resistance in Obesity and in Type 2 Diabetes Mellitus. *Am. J. Clin. Nutr.* 71, 885–892. doi:10.1093/ajcn/71.4.885

Hamam, D., Ali, D., Kassem, M., Aldahmash, A., and Alajez, N. M. (2015). microRNAs as Regulators of Adipogenic Differentiation of Mesenchymal Stem Cells. *Stem Cell Dev.* 24, 417–425. doi:10.1089/scd.2014.0331

Hocquette, J. F., Gondret, F., Baéza, E., Médale, F., Jurie, C., and Pethick, D. W. (2010). Intramuscular Fat Content in Meat-Producing Animals: Development, Genetic and Nutritional Control, and Identification of Putative Markers. *Animal* 4, 303–319. doi:10.1017/S1751731109991091

Kato, K., Gong, J., Iwama, H., Kitanaka, A., Tani, J., Miyoshi, H., et al. (2012). The Antidiabetic Drug Metformin Inhibits Gastric Cancer Cell Proliferation *In Vitro* and *In Vivo*. *Mol. Cancer Ther.* 11, 549–560. doi:10.1158/1535-7163.MCT-11-0594

Kato, K., Iwama, H., Yamashita, T., Kobayashi, K., Fujihara, S., Fujimori, T., et al. (2016). The Anti-Diabetic Drug Metformin Inhibits Pancreatic Cancer Cell Proliferation *In Vitro* and *In Vivo*: Study of the microRNAs Associated With the Antitumor Effect of Metformin. *Oncol. Rep.* 35, 1582–1592. doi:10.3892/or.2015.4496

Kerr, T. A., Korenblat, K. M., and Davidson, N. O. (2011). MicroRNAs and Liver Disease. *Transl. Res.* 157, 241–252. doi:10.1038/jhg.2016.5310.1016/j.trsl.2011.01.008

Kim, M., Park, J.-E., Song, S.-B., and Cha, Y.-S. (2015). Effects of Black Adzuki Bean (Vigna Angularis) Extract on Proliferation and Differentiation of 3T3-L1 Preadipocytes into Mature AdipocytesVigna Angularis) Extract on Proliferation and Differentiation of 3T3-L1 Preadipocytes into Mature Adipocytes. *Nutrients* 7, 277–292. doi:10.3390/nu7010277

Kinoshita, M., Ono, K., Horie, T., Nagao, K., Nishi, H., Kuwabara, Y., et al. (2010). Regulation of Adipocyte Differentiation by Activation of Serotonin (5-HT) Receptors 5-HT2AR and 5-HT2CR and Involvement of MicroRNA-448-Mediated Repression of KLF5. *Mol. Endocrinol.* 24, 1978–1987. doi:10.1210/me.2010-0054

Kobayashi, M., Kato, K., Iwama, H., Fujihara, S., Nishiyama, N., Mimura, S., et al. (2013). Antitumor Effect of Metformin in Esophageal Cancer: *In Vitro* Study. *Int. J. Oncol.* 42, 517–524. doi:10.3892/ijo.2012.1722

Lee, H., Kim, H. J., Lee, Y. J., Lee, M.-Y., Choi, H., Lee, H., et al. (2012). Krüppel-Like Factor KLF8 Plays a Critical Role in Adipocyte Differentiation. *Plos One* 7, e52474. doi:10.1371/journal.pone.0052474

Lee, H., Kim, J., Park, J. Y., Kang, K. S., Park, J. H., and Hwang, G. S. (2017). Processed Panax Ginseng , Sun Ginseng, Inhibits the Differentiation and Proliferation of 3T3-L1 Preadipocytes and Fat Accumulation in *Caenorhabditis elegans*. *J. Ginseng Res.* 41, 257–267. doi:10.1016/j.jgr.2016.04.004

Li, X.-H., Qu, J.-Q., Yi, H., Zhang, P.-F., Yi, H.-M., Wan, X.-X., et al. (2014). Integrated Analysis of Differential miRNA and mRNA Expression Profiles in Human Radioresistant and Radiosensitive Nasopharyngeal Carcinoma Cells. *PLoS One* 9, e87767. doi:10.1371/journal.pone.0087767

Li, X., Zhao, Y., Li, X., Wang, Q., Ao, Q., Wang, X., et al. (2019). MicroRNA-150 Modulates Adipogenic Differentiation of Adipose-Derived Stem Cells by Targeting Notch3. *Stem Cell Int.* 2019, 1–12. doi:10.1155/2019/2743047

Lin, Z., He, H., Wang, M., and Liang, J. (2019). MicroRNA-130a Controls Bone Marrow Mesenchymal Stem Cell Differentiation towards the Osteoblastic and Adipogenic Fate. *Cell Prolif* 52, e12688. doi:10.1111/cpr.12688

Liu, K., Yu, W., Wei, W., Zhang, X., Tian, Y., Sherif, M., et al. (2019). Melatonin Reduces Intramuscular Fat Deposition by Promoting Lipolysis and Increasing Mitochondrial Function. *J. Lipid Res.* 60, 767–782. doi:10.1194/jlr.M087619

Ma, J., Lin, Y., Zhu, J., Huang, K., and Wang, Y. (2021). MiR-26b-5p Regulates the Preadipocyte Differentiation by Targeting FGF21 in Goats. *In Vitro Cell.Dev.Biol.-Animal* 57, 257–263. doi:10.1007/s11626-020-00493-y

Maragkakis, M., Alexiou, P., Papadopoulos, G. L., Reczko, M., Dalamagas, T., Giannopoulos, G., et al. (2009). Accurate microRNA Target Prediction Correlates with Protein Repression Levels. *BMC Bioinformatics* 10, 295. doi:10.1186/1471-2105-10-295

Miyoshi, H., Kato, K., Iwama, H., Maeda, E., Sakamoto, T., Fujita, K., et al. (2014). Effect of the Anti-diabetic Drug Metformin in Hepatocellular Carcinoma *In Vitro* and *In Vivo*. *Int. J. Oncol.* 45, 322–332. doi:10.3892/ijo.2014.2419

Mourelatos, Z. (2008). The Seeds of Silence. *Nature* 455, 44–45. doi:10.3892/ijo.2013.223310.1038/455044a

Pei, H., Yao, Y., Yang, Y., Liao, K., and Wu, J.-R. (2011). Krüppel-like Factor KLF9 Regulates PPARγ Transactivation at the Middle Stage of Adipogenesisγ Transactivation at the Middle Stage of Adipogenesis. *Cell Death Differ* 18, 315–327. doi:10.1038/cdd.2010.100

Peng, S.-g., Pang, Y.-l., Zhu, Q., Kang, J.-h., Liu, M.-x., and Wang, Z. (2018). Chlorogenic Acid Functions as a Novel Agonist of PPARγ2 during the Differentiation of Mouse 3T3-L1 Preadipocytesγ2 During the Differentiation of Mouse 3T3-L1 Preadipocytes. *Biomed. Res. Int.* 2018, 8594767. doi:10.1155/2018/8594767

Redis, R. S., and Calin, G. A. (2017). SnapShot: Non-coding RNAs and Metabolism. *Cel Metab.* 25, 220. doi:10.1016/j.cmet10.1016/j.cmet.2016.12.012

Rosen, E. D., and MacDougald, O. A. (2006). Adipocyte Differentiation From the Inside Out. *Nat. Rev. Mol. Cel Biol.* 7, 885–896. doi:10.1038/nrm2066

Rouleau, S., Glouzon, J.-P. S., Brumwell, A., Bisaillon, M., and Perreault, J.-P. (2017). 3′ UTR G-Quadruplexes Regulate miRNA Binding. *RNA* 23, 1172–1179. doi:10.1261/rna.06096210.1261/rna.060962.117

Schreck, C., Istvánffy, R., Ziegenhain, C., Sippenauer, T., Ruf, F., Henkel, L., et al. (2017). Niche WNT5A Regulates the Actin Cytoskeleton During Regeneration of Hematopoietic Stem Cells. *J. Exp. Med.* 214, 165–181. doi:10.1084/jem.20151414

Shen, L., Li, Q., Wang, J., Zhao, Y., Niu, L., Bai, L., et al. (2018). miR-144-3p Promotes Adipogenesis Through Releasing C/EBPα from Klf3 and CtBP2. *Front. Genet.* 9, 677. doi:10.3389/fgene.2018.00677

Shoelson, S. E., Herrero, L., and Naaz, A. (2007). Obesity, Inflammation, and Insulin Resistance. *Gastroenterology* 132, 2169–2180. doi:10.1053/j.gastro10.1053/j.gastro.2007.03.059

Sun, M., Ding, J., Li, D., Yang, G., Cheng, Z., and Zhu, Q. (2017). NUDT21 Regulates 3′-UTR Length and microRNA-Mediated Gene Silencing in Hepatocellular Carcinoma. *Cancer Lett.* 410, 158–168. doi:10.1016/j.canlet.2017.09.026

Tada, A., Kober, A. H., Islam, M. A., Igata, M., Takagi, M., Suzuki, M., et al. (2020). Evaluation of Fat Accumulation and Adipokine Production during the Long-Term Adipogenic Differentiation of Porcine Intramuscular Preadipocytes and Study of the Influence of Immunobiotics. *Cells* 9, 1715. doi:10.3390/cells9071715

Tahmasebi, S., Ghorbani, M., Savage, P., Yan, K., Gocevski, G., Xiao, L., et al. (2013). Sumoylation of Krüppel-like Factor 4 Inhibits Pluripotency Induction but Promotes Adipocyte Differentiation. *J. Biol. Chem.* 288, 12791–12804. doi:10.1074/jbc.M113.465443

Tang, R., Ma, F., Li, W., Ouyang, S., Liu, Z., and Wu, J. (2017). miR-206-3p Inhibits 3T3-L1 Cell Adipogenesis via the C-Met/PI3K/Akt Pathway. *Ijms* 18, 1510. doi:10.3390/ijms18071510

van der Kwast, R. V. C. T., Quax, P. H. A., and Nossent, A. Y. (2020). An Emerging Role for isomiRs and the microRNA Epitranscriptome in Neovascularization. *Cells* 9, 61. doi:10.3390/cells9010061

Wong, N., and Wang, X. (2015). miRDB: an Online Resource for microRNA Target Prediction and Functional Annotations. *Nucleic Acids Res.* 43, D146–D152. doi:10.1093/nar/gku1104

Wood, J. D., Nute, G. R., Richardson, R. I., Whittington, F. M., Southwood, O., Plastow, G., et al. (2004). Effects of Breed, Diet and Muscle on Fat Deposition and Eating Quality in Pigs. *Meat Sci.* 67, 651–667. doi:10.1016/j.meatsci.2004.01.007

Xu, Q., Lin, S., Wang, Y., Zhu, J., and Lin, Y. (2018). Fibroblast Growth Factor 10 (FGF10) Promotes the Adipogenesis of Intramuscular Preadipocytes in Goat. *Mol. Biol. Rep.* 45, 1881–1888. doi:10.1007/s11033-018-4334-1

Xu, Q., Wang, Y., Zhang, Y., Zhu, J., and Lin, Y. (2020). RXRα Cooperates with KLF8 to Promote the Differentiation of Intramuscular Preadipocytes in Goat. *Anim. Biotechnol.* 27, 1–11. doi:10.1080/10495398.2020.1732397

Yamada, T., Kamiya, M., and Higuchi, M. (2020). Fat Depot-specific Effects of Body Fat Distribution and Adipocyte Size on Intramuscular Fat Accumulation in Wagyu Cattle. *Anim. Sci. J.* 91, e13449 doi:10.1111/asj.13449

Yan, Z., Guo, Y., Wang, Y., Li, Y., and Wang, J. (2018). MicroRNA Profiles of BMSCs Induced into Osteoblasts with Osteoinductive Medium. *Exp. Ther. Med.* 15, 2589–2596. doi:10.3892/etm.2018.5723

Conflict of Interest: The authors declare that the research was conducted in the absence of any commercial or financial relationships that could be construed as a potential conflict of interest.

Publisher's Note: All claims expressed in this article are solely those of the authors and do not necessarily represent those of their affiliated organizations, or those of the publisher, the editors and the reviewers. Any product that may be evaluated in this article, or claim that may be made by its manufacturer, is not guaranteed or endorsed by the publisher.

frontiers in Veterinary Science

ORIGINAL RESEARCH
published: 16 December 2021
doi: 10.3389/fvets.2021.788316

Interference With *ACSL1* Gene in Bovine Adipocytes: Transcriptome Profiling of mRNA and lncRNA Related to Unsaturated Fatty Acid Synthesis

*Yanbin Bai[1], Xupeng Li[1], Zongchang Chen[1], Jingsheng Li[1], Hongshan Tian[1], Yong Ma[1], Sayed Haidar Abbas Raza[2], Bingang Shi[1], Xiangmin Han[1], Yuzhu Luo[1], Jiang Hu[1], Jiqing Wang[1], Xiu Liu[1], Shaobin Li[1] and Zhidong Zhao[1]**

[1] College of Animal Science and Technology & Gansu Key Laboratory of Herbivorous Animal Biotechnology, Gansu Agricultural University, Lanzhou, China, [2] College of Animal Science and Technology, Northwest A&F University, Xianyang, China

OPEN ACCESS

Edited by:
Min Du,
Washington State University,
United States

Reviewed by:
Ran Di,
Institute of Animal Sciences, Chinese Academy of Agricultural Sciences (CAAS), China
Zexi Cai,
Aarhus University, Denmark

***Correspondence:**
Zhidong Zhao
zhaozd@gsau.edu.cn

Specialty section:
This article was submitted to Livestock Genomics, a section of the journal Frontiers in Veterinary Science

Received: 02 October 2021
Accepted: 17 November 2021
Published: 16 December 2021

Citation:
Bai Y, Li X, Chen Z, Li J, Tian H, Ma Y, Raza SHA, Shi B, Han X, Luo Y, Hu J, Wang J, Liu X, Li S and Zhao Z (2021) Interference With ACSL1 Gene in Bovine Adipocytes: Transcriptome Profiling of mRNA and lncRNA Related to Unsaturated Fatty Acid Synthesis. Front. Vet. Sci. 8:788316. doi: 10.3389/fvets.2021.788316

The enzyme long-chain acyl-CoA synthetase 1 (ACSL1) is essential for lipid metabolism. The *ACSL1* gene controls unsaturated fatty acid (UFA) synthesis as well as the formation of lipid droplets in bovine adipocytes. Here, we used RNA-Seq to determine lncRNA and mRNA that regulate UFA synthesis in bovine adipocytes using RNA interference and non-interference with *ACSL1*. The corresponding target genes of differentially expressed (DE) lncRNAs and the DE mRNAs were found to be enriched in lipid and FA metabolism-related pathways, according to GO and KEGG analyses. The differentially expressed lncRNA- differentially expressed mRNA (DEL-DEM) interaction network indicated that some DELs, such as TCONS_00069661, TCONS_00040771, TCONS_ 00035606, TCONS_00048301, TCONS_001309018, and TCONS_00122946, were critical for UFA synthesis. These findings assist our understanding of the regulation of UFA synthesis by lncRNAs and mRNAs in bovine adipocytes.

Keywords: lncRNA, ACSL1, bovine adipocytes, unsaturated fatty acids, RNA-Seq

INTRODUCTION

As a member of the ACSL family (ACSL1, 3, 4, 5, and 6), long-chain acyl-CoA synthase 1 (ACSL1) is needed for the activation, transportation, and degradation of fatty acids (FAs), as well as lipid synthesis (1, 2). ACSL1 is found on the outer mitochondrial membrane (2) and converts long-chain FAs into fatty acyl-CoA to synthesize triglycerides (3), stimulate FA deposition, activate FAs (1), and finally to enter the β-oxidation pathway (4). Previous research has found that the presence of long-chain unsaturated FAs in beef, such as DHA (22: 6, $n-3$) and EPA (20: 5, $n-3$), aids in the prevention of cardiovascular disease, atherosclerosis, and the promotion of fetal brain and visual growth (5–8). A quantitative trait locus (QTL) study revealed that *ACSL1* influences the relative content of UFAs, omega-3 FAs, polyunsaturated FAs, docosapentaenoic acid, and DHA (9). Furthermore, overexpression of *ACSL1* activates and transports FA for the synthesis of diglycerides and phospholipids rather than cholesterol esters (10). In adipocytes, the arachidonic acid levels were further stimulated by the overexpression of *ACSL1* (11). Furthermore, four transcription

factors, E2F1, E2F4, Sp1, and KLF15, symbiotically control *ACSL1* expression, suggesting that *ACSL1* controls UFA synthesis in cells (12). We have also observed, using RNA interference (13) and gene overexpression (14), that *ACSL1* controlled UFA synthesis and the formation of lipid droplets in bovine adipocytes.

Long non-coding RNAs (lncRNAs) are noncoding RNA molecules > 200 nt that are found in the nucleus/cytoplasm and undergo eukaryotic transcription (15). Earlier, lncRNAs were regarded as a byproduct of the transcription of RNAP II and thought to have minimal physiological activity. However, numerous studies have shown that they act as multi-level regulators of protein-coding gene expression, by epigenetic (16, 17), transcriptional (18, 19), and post-transcriptional regulation (20, 21). RNA-seq is effective for identifying differentially expressed (DE) genes as well as quantifying transcriptomes (22, 23). This technique has been frequently used in the functional analysis of lncRNAs/mRNAs in adipose tissue in cattle (24–27), sheep (28), pigs (29), and chickens (30). Jiang et al. (25) isolated 3,716 candidate lncRNAs from fat samples from calves and adult cattle and confirmed their crucial role in cattle of various ages. Liu et al. (26) demonstrated that genes, such as *PLIN1, PLIN2*, and *PPARGC1A* regulated various lipid-related pathways. Cai et al. (31) identified a novel lncRNA, *BADLNCR1*, that suppressed bovine adipogenesis by inhibiting *GLRX5* expression. However, the roles of lncRNA/mRNAs in UFA synthesis in bovine adipocytes are poorly understood. Here, we used RNA-Seq to examine the lncRNAs/mRNA levels in bovine adipocytes by RNA interference and non-interference of *ACSL1*. We screened both lncRNAs and mRNAs in terms of UFA synthesis to understand their role in the regulation of UFA synthesis in bovine adipocytes.

MATERIALS AND METHODS

Ethics Statements

A healthy 1-day-old calf was born and raised at the animal farm of Gansu Agricultural University (LanZhou, China) and humanely slaughtered in a slaughterhouse, followed by the collection of the perirenal adipose tissue along with heart, spleen, kidney, liver, lung, and leg muscle tissues. The study protocol was approved by the Gansu Agricultural University, China, as well as the Ministry of Science and Technology of the People's Republic of China (Approval number 2006–398). Animal experimentation, including sample collection, was performed in agreement with the ethical commission's guidelines of Gansu Agricultural University. Furthermore, the experimental protocol complied with the local animal welfare guidelines.

Sample Collection and Cell Culture

The perirenal adipose tissue of 1-day-old calf (from the animal farm of Gansu Agricultural University) was collected and shredded in PBS, followed by the addition of type I collagenase (200 U/mL). The solution was shaken at 37°C for 1 h, and enzymatic digestion was stopped by the addition of an equal volume of complete medium. The digested product was serially filtered through 100 μm and 40 μm mesh filters, followed by centrifugation (1,500 rpm, 10 min). The erythrocyte lysate was mixed with the pellet and centrifuged (1,500 rpm, 10 min). After discarding the supernatant, a complete medium was added to the pellet, mixed, and centrifuged twice (1,500 rpm, 10 min). The pellet was resuspended, and the cells were seeded in a 10 cm cell culture dish and cultured in 5% CO_2 at 37°C. The medium was refreshed after 12 h to remove the non-adherent cells and was refreshed every 48 h. At 90% confluence, the cells were removed with trypsin and frozen in liquid nitrogen.

ACSL1 Expression

Bovine pre-adipocytes were grown and passaged to the F3 generation, and cells were isolated on differentiation days 0, 2, 4, 6, and 8. We performed qRT-PCR to assess *ACSL1* expression at different stages of differentiation.

Synthesis and Screening of *ACSL1* siRNA

The complete sequence of bovine *ACSL1* (GenBank No. 537161) was used to design and synthesize three siRNA sequences (Guangzhou Ruibo Biological Company). **Table 1** shows the sequence information.

Next, the synthesized siRNA-ACSL1 and the corresponding siRNA-Non-specific Control (siRNA-NC) were transfected into bovine adipocytes. After 48 h of culture, we performed qRT-PCR to determine *ACSL1* mRNA expression to screen the siRNA-ACSL1 with the highest interference efficiency.

Next, we sequenced the bovine adipocytes in which *ACSL1* expression was silenced and those that exhibited normal expression.

RNA Quantification

We used TRIzol reagent to isolate total RNA from siRNA-ACSL1 or siRNA-NC bovine adipocytes, followed by strict quality control of the RNA samples. First, 1% agarose gel electrophoresis (AGE) was used to analyze RNA integrity and the presence of DNA contamination. RNA purity was measured using an IMPLEN NanoPhotometer® spectrophotometer and quantified using an RNA analysis kit and a Qubit®2.0 Fluorometer. Finally, the RNA Nano 6000 Assay Kit was used to assess RNA integrity using the Agilent Bioanalyzer 2100 system.

Library Preparation for Transcriptome Sequencing

The cDNA library was prepared using the NEBNext Ultra Directional RNA Library Prep Kit for Illumina sequencing using a combination of equal amounts of total RNA of two parallel bovine adipocytes cultures in equal ratios of siRNA-ACSL1/siRNA-NC. The total RNA was from 6 dishes of bovine

TABLE 1 | Target sequences of siRNAs for bovine *ACSL1*.

siRNA No.	Target sequence
ACSL1 siRNA-1	GGATAGAGGAGTACCTGTA
ACSL1 siRNA-2	CCCTATGAATGGCTTTCAT
ACSL1 siRNA-3	ACTCTTCTCTATCGACAAT

adipocytes, of which 3 dishes were treated with ACSL1 gene interference, and the other 3 dishes were the control group. The Epicenter Ribo-zero rRNA Removal kit was used for the removal of the rRNA, followed by the construction of six libraries, which were labeled si_ACSL1_1, si_ACSL1_2, si_ACSL1_3, NC_ACSL1_1, NC_ACSL1_2, and NC_ACSL1_3, respectively. Briefly, poly-T oligo-attached magnetic beads were used to obtain mRNA, followed by fragmentation using divalent cations at high temperatures in NEBNext First Strand Synthesis Reaction Buffer (5X). First-strand cDNA was prepared using a random hexamer primer and M-MuLV Reverse Transcriptase (RNaseH-), followed by the application of DNAPI and RNase H. These activities facilitated the conversion of the remaining overhangs into blunt ends. The NEBNext adaptor with hairpin loop structure was ligated to prepare for hybridization after adenylation of the 3′ ends of the DNA fragments. The Beckman Coulter AMPure XP system was used to obtain cDNA fragments of 150 ∼ 200 bp in length. These fragments were treated with 3 μL of USER Enzyme at 37°C for 15 min, followed by 5 min at 95°C before PCR. Next, Phusion High-Fidelity DNA polymerase, Universal PCR primers, and Index (X) Primer were used for PCR analysis. Finally, the Agilent Bioanalyzer 2100 system was used to assess the quality of the library generated. The index-coded samples were clustered using a cBot Cluster Generation System for TruSeq PE Cluster Kit v3-cBot-HS (Illumina). An Illumina HiSeq PE150 platform was used to sequence the library at Novogene Bioinformatics Institute (Beijing, China), resulting in the generation of data on the 150 bp paired-end reads.

Analysis of Sequencing Data

In-house Perl scripts were used to analyze the raw reads. Clean reads were obtained after filtering the raw data for low-quality reads/adaptors/polyNs, and at the same time, we obtained the Q20, Q30, and GC information. The STAR (v2.5.1b) software (32) was used to create a list of the reference genome, and the corresponding paired-end clean reads were aligned to the cattle reference genome (Bos_taurus_Ensembl_94). We used HTSeq v0.6.0 to assess the read counts mapped to each gene. The gene lengths and read counts aligned to the genes were calculated using FPKM. Normalization of the expression of lncRNAs/mRNAs removed the impact of sequencing depth, gene length, and sample difference on gene expression. The R package DESeq2 was used to identify DE-lncRNAs (DELs) and protein-coding genes (33) following a negative binomial distribution. Genes and lncRNAs with an adjusted $P < 0.05$ (P-adjust) were labeled as differentially expressed.

Prediction of lncRNA

Cuffcompare software was used to screen the lncRNA transcripts. The assembled transcripts were filtered to determine probable lncRNAs to reduce the false-positive rate using the following steps: (1) New transcripts were identified by comparison with reference annotations; (2) Transcripts with exon numbers ≥ 2 and lengths > 200 nt were selected for the exon number screening and transcript length screening of the transcripts; (3) Transcripts were assessed for coding potential by integration using coded potential calculator 2 (CPC2) (34), Pfam (35), and Coding-Non-Coding-Index (CNCI) (36) to predict the coding potential and the intersection of the non-coding transcripts, allowing selection of the candidate lncRNA dataset; (4) The candidate novel lncRNAs were finally screened using the HUGO Gene Nomenclature Committee (HGNC) naming guidelines for long non-coding RNA (37) and named based on their positional relationships with coding genes.

Target Gene Prediction of lncRNAs

The target genes for the lncRNAs in the RNA-seq results were predicted based on cis-and trans-regulation. We investigated the coding genes within 100 kb of the lncRNAs to determine their target genes (38). The trans role implied an expression-based association between the lncRNA and target genes. We determined the correlation between the lncRNAs and coding genes with custom scripts, and the genes with Pearson correlation coefficient > 0.95 were identified as the target genes of the lncRNAs (39).

GO and KEGG Analyses of the DEMs and lncRNA Target Genes

The GOseq R package was used to perform Gene Ontology (GO) analysis of the target genes of differentially expressed mRNAs (DEMs)/lncRNA target genes, with corrected gene length bias (40). The KEGG database was used to evaluate the functional significance of the biological systems (cells, organisms, and the ecosystem) based on genome sequencing and other high-throughput experimental data. The cluster Profiler R package was used for KEGG pathway analysis of the DEMs/lncRNA target genes. A $P < 0.05$ indicated a significant relationship between the terms and the DE-lncRNA target genes.

The DEL-DEM Co-expression Network

Next, we obtained the differentially expressed lncRNAs (DELs) and their target genes from the cis and trans prediction results, respectively, to further explore the interactions between the DEMs and DELs. These were incorporated with the DEMs from the sequencing results. We screened the lipogenic-related mRNAs based on literature searches to improve the visibility of the results and finally constructed a DEL-DEM co-expression network using Cytoscape (v3.6.0) (41).

Experimental Verification of mRNAs and lncRNAs

We randomly selected 12 significant DEMs and 7 DELs and analyzed their expression using qRT-PCR. The Evo-MLV kit was used to synthesize the RNA extracted from bovine adipocytes. First, we used Primer 5.0 to design specific primers for mRNAs and lncRNAs. **Tables 2**, **3** show the primers of DEMs and DELs used, respectively. The PCR products were analyzed using 1.5% AGE and then sequenced using the Sanger method. Then, we verified the mRNAs/lncRNAs from bovine adipocytes by comparing the amplified sequences of the PCR products with the sequences of the specific mRNAs and lncRNAs obtained from RNA-Seq using MEGA 5.0. Second, the Applied Biosystems QuantStudio®6 Flex was used to perform qRT-PCR using the TB Green® Premix Ex Taq™ II, and the bovine *GAPDH* gene as

TABLE 2 | mRNAs' primers used in the qRT-PCR.

mRNAs	Forward (5′→ 3′)	Reverse (5′→ 3′)
NELL2	ACAATAGTGGCGACACCTGG	CGTCCAGGCAAGTTTTGGTG
ACSL1	TGCTGCCTGACTGTTGCT	ACCACTTGCCAATGTCCC
SLC26A7	TGGAGTGGGCGACACATTAC	TGACAGAACAGCAAAGGCCA
FABP4	TTCCTTCAAATTGGGCCAGGA	AGTTCGATGCAAACGTCATCC
TMEM87B	AGCCTCGTCTAGGAACCGT	ATCAAGAAGAGACAGAGGGAGG
OLR1	CTTTGTCTGGGATTACTGG	GTGGGCAAGGGTTTCTAT
TGFBI	CCCCGTGGAGAACTGAACAA	ATGTCCACCTCAGCAACAGG
PTGIS	TCCTGGGCCGTGGTCTT	TAGGAGTGGGGATCCAGGAG
VCAN	GATTACGGGTGGCTGTTGGA	GATTACGGGTGGCTGTTGGA
FMOD	ACAGCCATGTACTGCGACAA	TCACTGGTGATCTGGTTGCC
IDH3A	ACCTGTGTGCGGGATTGATT	CTTCGCAGCGTGGTCAAAAA
EMP3	GCCCTCCACATCCTCATT	CTTCAGCCAGCCGTTCTC
GAPDH	AGTTCAACGGCACAGTCAAGG	ACCACATACTCAGCACCAGCA

TABLE 3 | lncRNAs' primers used in the qRT-PCR.

lncRNAs	Forward (5′→ 3′)	Reverse (5′→ 3′)
TCONS_00069661	TGCCATTCCTTTCGTT CTTCT	TCCTCTGCTTTCCCA CTGTTT
TCONS_00139018	CGTACTCCTTTCCCA ATT	TGCCTCCTGAGAAAT CTG
TCONS_00057814	TGGGTCTGTGCGTTT GCG	TCTGGTGGAGGTCCG TAGCG
TCONS_00050038	GCCCTGACAACGGC TACCT	TGGGATTCCAGGCCC TTCC
TCONS_00002149	CCTGCCTTGACTGTT TGA	CCTGTTGAGATGCCT CTTT
TCONS_00057808	CACTAGGCACTCGCA TTCC	GCAAACGCACAGAC CCAC
TCONS_00040771	AAGAGGGCTTTGGAG TGA	TTCTGCCATAAGGGT GGT
GAPDH	AGTTCAACGGCACAG TCAAGG	ACCACATACTCAGCA CCAGCA

the internal reference. The $2^{-\Delta\Delta CT}$ method was used to calculate relative expression with *GAPDH* as the internal control (42). Also, the expression of mRNAs and lncRNAs from both the techniques were expressed as Log_2 (fold change) for the si-treated group in comparison with the NC-treated group. Paired *t*-tests using GraphPad Prism v6 were used for data analysis. Data were expressed as the mean ± SE deviation of triplicate experiments. A $P < 0.05$ indicated a significant difference.

Next, the lncRNA levels were determined in various bovine tissues to further verify the role of lncRNA in the production of bovine UFAs. Briefly, we used TRIzol to isolate total RNA from the collected heart, spleen, lung, liver, kidney, leg muscle, and perinephric fat, followed by reverse transcription to generate cDNA. Finally, the expression of lncRNAs was determined using qRT-PCR. The $2^{-\Delta\Delta CT}$ method was used to determine the relative expression using *GAPDH* as the internal control. The paired *t*-test using GraphPad Prism v6 was done for data analysis. Data were expressed as the mean ± SE deviation of triplicate experiments.

RESULTS

Temporal Expression of *ACSL1* During the Differentiation of Bovine Adipocytes

The cultured F3 generation bovine pre-adipocytes were collected on differentiation days 0, 2, 4, 6, and 8, and qRT-PCR was performed to determine the relative expression of *ACSL1*. The rise in *ACSL1* levels was followed by a reduction, with the maximum expression on day 4 ($P < 0.01$). Therefore, day-4 bovine adipocytes were used for subsequent experiments (13).

Screening of Effective siRNA for *ACSL1*

We transfected three pairs of siRNAs into the bovine adipocytes and determined their expression after 48 h to screen the most efficient siRNA fragments for silencing *ACSL1*. There was a >70% reduction in the mRNA expression of *ACSL1*, with si3-ACSL1 showed the highest efficiency of interference (86%; $P < 0.01$). Therefore, si3-ACSL1 was selected for subsequent experiments (13). Next, we transfected differentiation day 4 adipocytes with si3-ACSL1 (si-treated group) (13), followed by sequencing of both the si-treated cells and NC-treated cells.

Sequencing Data Summary

We constructed six cDNA libraries for the NC-treated group ($n = 3$) and si-treated group ($n = 3$) to explore the regulation of UFA synthesis by mRNAs and lncRNAs. After sequencing, the raw reads were acquired using the Illumina HiSeq PE150 Platform and deposited in GenBank (accession numbers: SRR13358757-13358762). Next, we tested the correlation between the expression of different samples (**Figure 1A**). In total, we obtained 98,462,108–117,507,866 and 93,238,078–110,700, 276 raw reads from the libraries from the NC-treated group and si-treated group, respectively, which resulted in 96,857,744–115,542,046 and 91,106,662–109,206,440 clean reads after removing low-quality/adaptor sequences, resulting in ∼15 GB data/sample. The GC contents were 51.54–56.29%. Q20 was >96%, and Q30 was >90% (**Table 4**). More than 87.76% of clean reads aligned to the reference genome, resulting in 173,090 assembled transcripts (**Supplementary File 1**). Our study identified 5,432 putative lncRNAs, which included 65.2% lincRNAs, 20.7% antisense lncRNAs, and 14.1% sense_overlapping lncRNAs (**Figures 1B,C**). At the transcriptional level, 15,547 mRNAs were obtained, of which 454 were novel mRNAs.

Genomic Expression of lncRNAs and mRNAs

We analyzed the gene structure and expression to determine the dissimilarities between the lncRNAs and mRNAs obtained by RNA-seq. The results showed that mRNAs were expressed at a relatively higher degree with the lncRNAs, based on the FPKM values (**Figure 2A**). The mRNAs (5,321 bp on average) were substantially longer than the lncRNAs (1,813 bp on average)

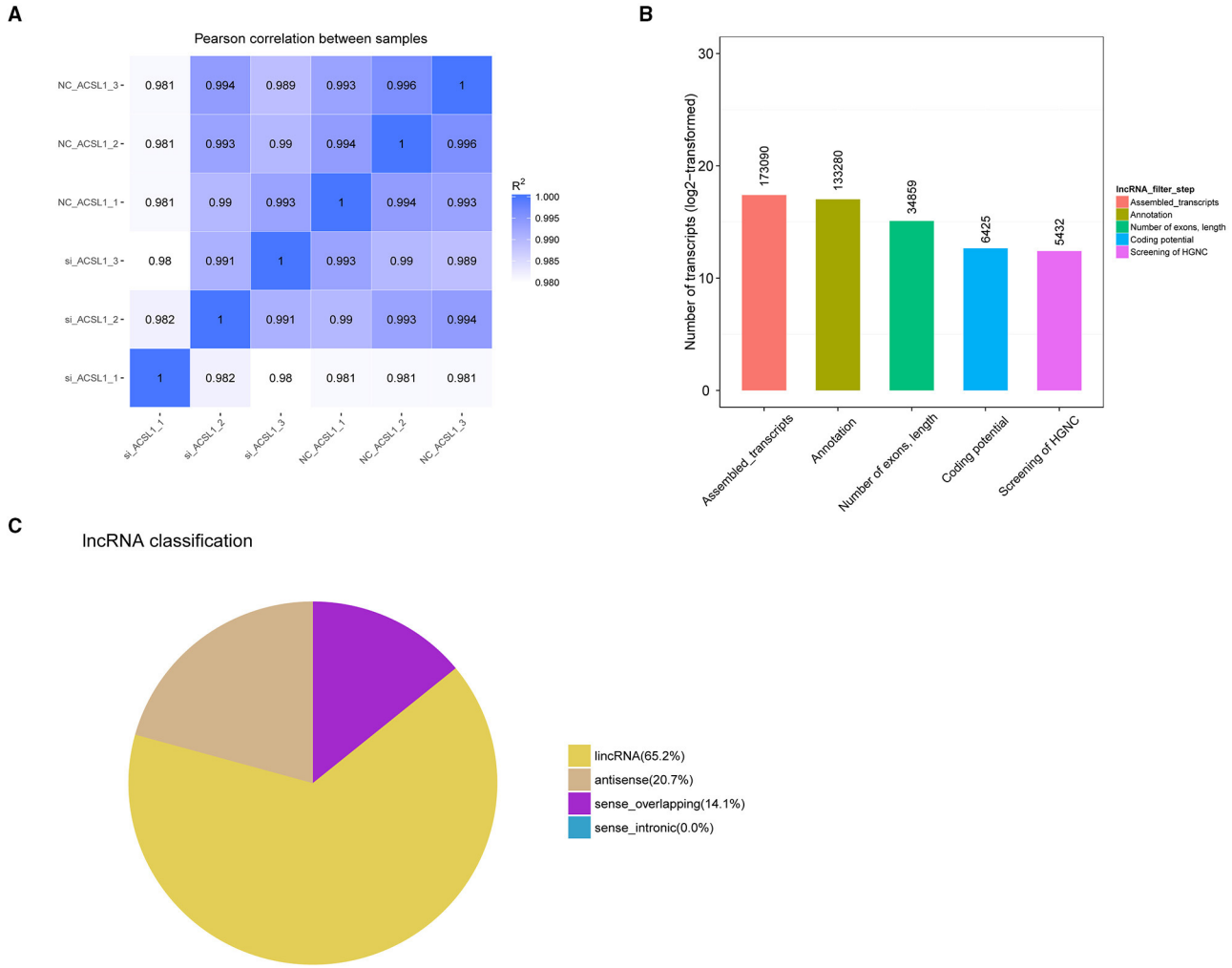

FIGURE 1 | Sequencing data after manipulation of *ACSL1* expression in bovine adipocytes. **(A)** Pearson correlation coefficients between samples. **(B)** LncRNA were screened using Cuffcompare software. **(C)** Classification of lncRNA.

TABLE 4 | Summary of the sequencing data.

Sample_name	Raw_reads	Clean_reads	Raw_bases (G)	Clean_bases (G)	Q20 (%)	Q30 (%)	GC_content (%)
NC_ACSL1_1	117,507,866	115,542,046	17.63	17.33	97.49	93.04	55.28
NC_ACSL1_2	98,462,108	96,857,744	14.77	14.53	97.65	93.44	53.35
NC_ACSL1_3	103,447,506	101,411,748	15.52	15.21	97.73	93.64	53.64
si_ACSL1_1	110,700,276	109,206,440	16.61	16.38	97.05	92.25	56.29
si_ACSL1_2	100,037,150	98,632,486	15.01	14.79	97.76	93.68	52.87
si_ACSL1_3	93,238,078	91,106,662	13.99	13.67	96.38	90.86	51.54

(**Figure 2B**). The mRNAs had a higher number of exons (6.04 on average) than those of the lncRNAs (2.91 on average). Also, 61.23% of mRNAs had four or more exons, while 81.41% of lncRNAs had three or fewer exons (**Figure 2C**). Furthermore, most of the mRNAs (402 bp on average) had longer ORFs than the lncRNAs (147 bp on average) (**Figure 2D**).

We detected 75 DELs and 107 DEMs in the si-treated group compared with the NC-treated group (P-adjusted < 0.05). We performed differential mRNA cluster analysis to examine the clustering pattern of DEMs under varying experimental conditions. We found that the same group of DEMs was clustered together (**Figure 2E**), supporting the accuracy and

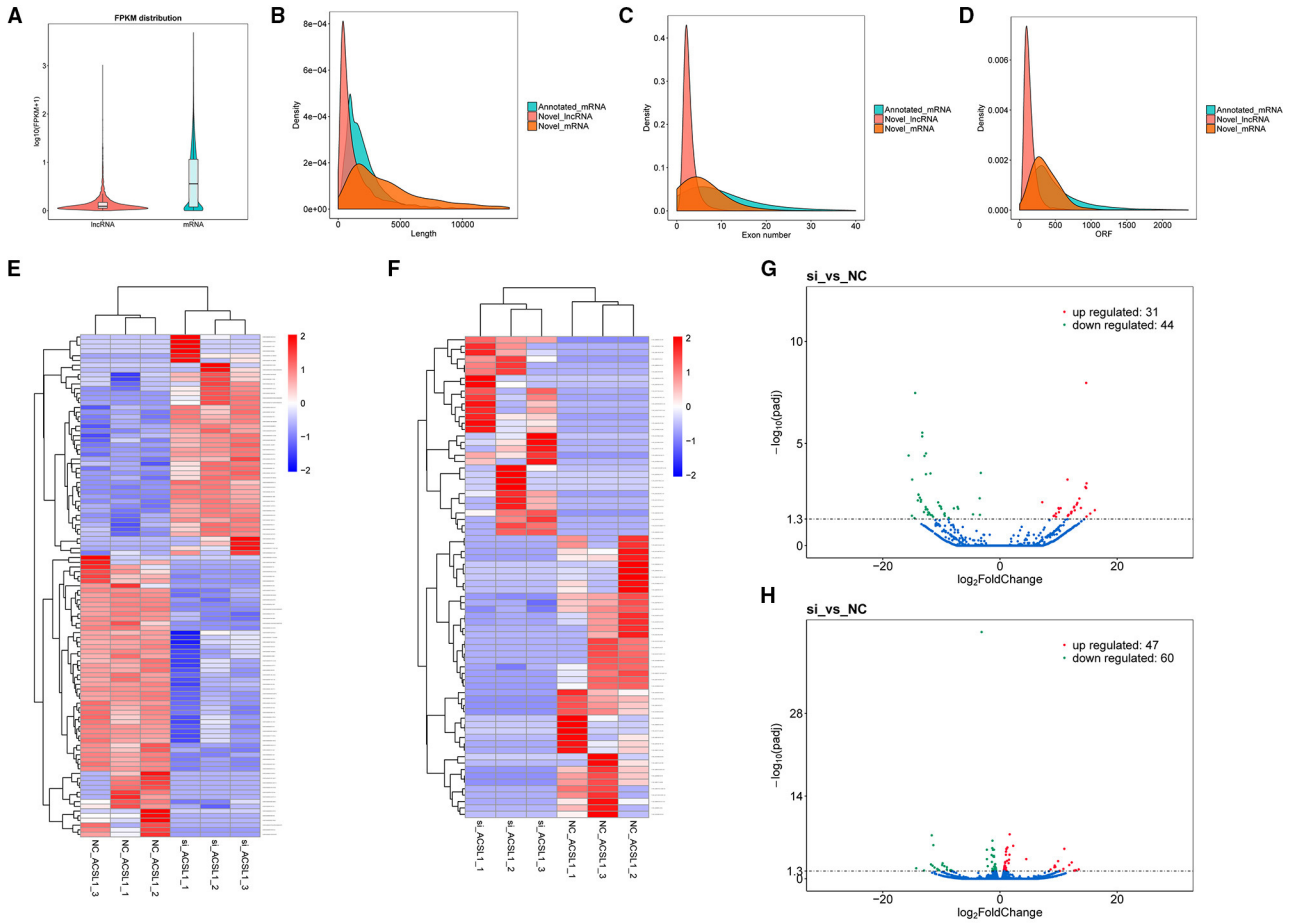

FIGURE 2 | Genomic expression of lncRNAs and mRNAs. **(A)** The expression of lncRNA and mRNA. **(B–D)** Comparison of length, exon count, and ORF length between lncRNAs and mRNAs. **(E,F)** Cluster heatmap of DEMs and DELs. The FPKM array was centered and scaled in the row direction by R package pheatmap (v1.0.8). Red indicates higher expression and blue represents lower expression. The $\log_{10}$ (FPKM+1) value was converted (scale number) and clustered. **(G,H)** Volcano plot of DELs and DEMs.

reliability of the samples. Furthermore, we found that in the si-treated group, 31 lncRNAs were significantly upregulated, and 44 lncRNAs were significantly downregulated (P-adjusted < 0.05). **Figure 2F** shows the clustering results. Similarly, we observed significantly upregulated expression of 47 mRNAs and downregulated expression of 60 mRNAs in the si-treated group (P-adjusted < 0.05). The volcano plots (**Figures 2G,H**) and the **Supplementary Files 2, 3** show the DEL and DEMs, respectively.

GO and KEGG Analyses of the DEMs

The results of the GO analysis revealed that the significant DEMs were classified into 386 functional groups ($P < 0.05$; **Supplementary File 4**). Of these, 64 terms were significantly enriched in molecular function (GO-MF), and metalloendopeptidase inhibitor activity (GO: 0008191; $P = 0.0017$) was the most significantly enriched GO term, followed by EP4 subtype prostaglandin E2 receptor binding (GO: 0031867; $P = 0.0019$) and oxidoreductase activity (GO: 0016671; $P = 0.0034$). For the cellular component (GO-CC), 33 terms were significantly enriched, with the extracellular region (GO: 0005576; $P = 0.0001$) the most significantly enriched, followed by the invadopodium membrane (GO: 0071438; $P = 0.0004$). For the biological processes (GO-BP), 289 GO terms were related to various processes or regulation, such as glycosaminoglycan metabolic process (GO: 0030203; $P = 0.0009$), aminoglycan metabolic process (GO: 0006022; $P = 0.0014$), and positive regulation of MAPK cascade (GO: 0043410; $P = 0.0055$). **Figure 3A** shows the top 50 functional GO annotations for the DEMs. The KEGG pathway analysis showed that the DEMs were involved in 116 signaling pathways (**Supplementary File 5**). **Figure 3B** shows the top 20 signaling pathways, and the PPAR signaling pathway showed the highest level of significance ($P < 0.05$), followed by the Rap1 signaling pathway and PI3K-Akt signaling pathway. Our results indicated that these pathways were probably involved in UFA synthesis.

Cis-/Trans-Regulation of the lncRNAs Target Genes

We identified 20,724 protein-coding genes as the nearest neighbors of 5,423 out of 5,432 lncRNAs using 100 kb as

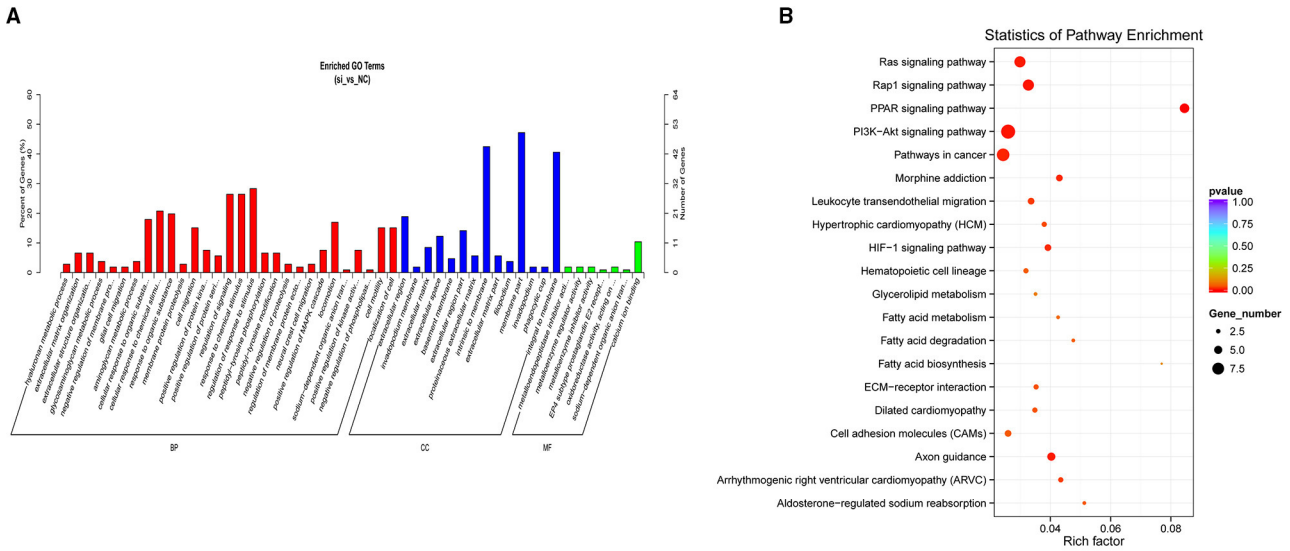

FIGURE 3 | GO and KEGG analysis of DEMs. **(A)** GO analysis of DEMs showing the relevant categories. **(B)** Top 20 of KEGG pathways of DEMs.

the cutoff (**Supplementary File 6**). Subsequent GO analysis revealed 435 significantly enriched GO terms ($P < 0.05$; **Supplementary File 7**). **Figure 4A** shows the top 50 GO functional annotations of the DEL target genes. The top five GO terms were embryonic skeletal system development, anterior/posterior pattern specification, sequence-specific DNA binding, regionalization, and embryonic skeletal system morphogenesis. The results of KEGG analysis indicated the involvement of seven pathways ($P < 0.05$; **Supplementary File 8**), and **Figure 4B** shows the top 20 KEGG pathways, such as MAPK signaling pathway, PPAR signaling pathway, Ribosome biogenesis in eukaryotes, and ether lipid metabolism.

Next, we identified 5,432 lncRNAs and 698,719 genes to investigate the trans target genes of lncRNAs using the Pearson correlation ≥ 0.95 as the cutoff (**Supplementary File 9**). **Figure 4C** shows the top 50 GO functional annotations of the DEL target genes. GO analysis identified 1,154 significantly enriched GO terms (**Supplementary File 10**), and the top five GO terms were enzyme binding, kinase regulator activity, rRNA binding, G-protein coupled nucleotide receptor activity, and G-protein coupled purinergic nucleotide receptor activity. We also found that 274 KEGG pathways were involved in the trans-target genes for lncRNAs (**Supplementary File 11**), such as the Ribosome, Citrate cycle (TCA cycle), protein digestion and absorption, FA metabolism, and FA degradation (**Figure 4D**).

Network Construction Based on DEMs and DELs

We obtained the DELs and their targets from the cis and trans prediction results, respectively, and incorporated them with the DEMs from the sequencing results (**Supplementary File 12**). Then, we screened lipogenic-related mRNAs based on literature searches and finally constructed a DEL-DEM co-expression network (**Supplementary File 13**). The DEL-DEM co-expression network involved 14 DELs and 22 trans-targets (**Figure 5A**), as well as 2 DELs and 2 cis-targets (**Figure 5B**). The co-expression network results showed that some lncRNAs interacted with multiple DEMs; for example, 14 DEMs co-expressed with *TCONS_00069661*, and 2 DEMs co-expressed with *TCONS_00142457*, *TCONS_00040771*, and *TCONS_00074138*, respectively, indicating that these lncRNAs and mRNAs belonged to the core non-coding/coding RNAs and had important regulatory effects on the synthesis of UFAs.

qRT-PCR of RNA-Seq Data

We randomly chose 12 and 7 genes from DEMs and DELs, respectively, to analyze the validity of the RNA-seq data by qRT-PCR. The results were comparable to the results of mRNA and lncRNA expression derived from the RNA-seq data (**Figures 6A,B**). Furthermore, the sequence of the qRT-PCR-amplified fragments of the specific primers were consistent with the sequences obtained by RNA-seq (**Supplementary File 14**).

We used qRT-PCR to study the expression of lncRNA *TCONS_00069661*, located at the center of the co-expression network and expressed in the kidney, spleen, heart, liver, lung, leg muscle, and perirenal fat of cattle. We found that *TCONS_00069661* was highly expressed in the adipose tissue of cattle (**Figure 6C**). Moreover, our previous studies showed that *ACSL1* gene was also highly expressed in bovine adipose tissue (12). Thus, these results substantiated the reliability of the co-expression network, and suggested the regulatory roles played by DELs and DEMs in UFA synthesis.

DISCUSSION

In recent years, transcriptome sequencing has been frequently used for gene expression analysis and to reveal biological

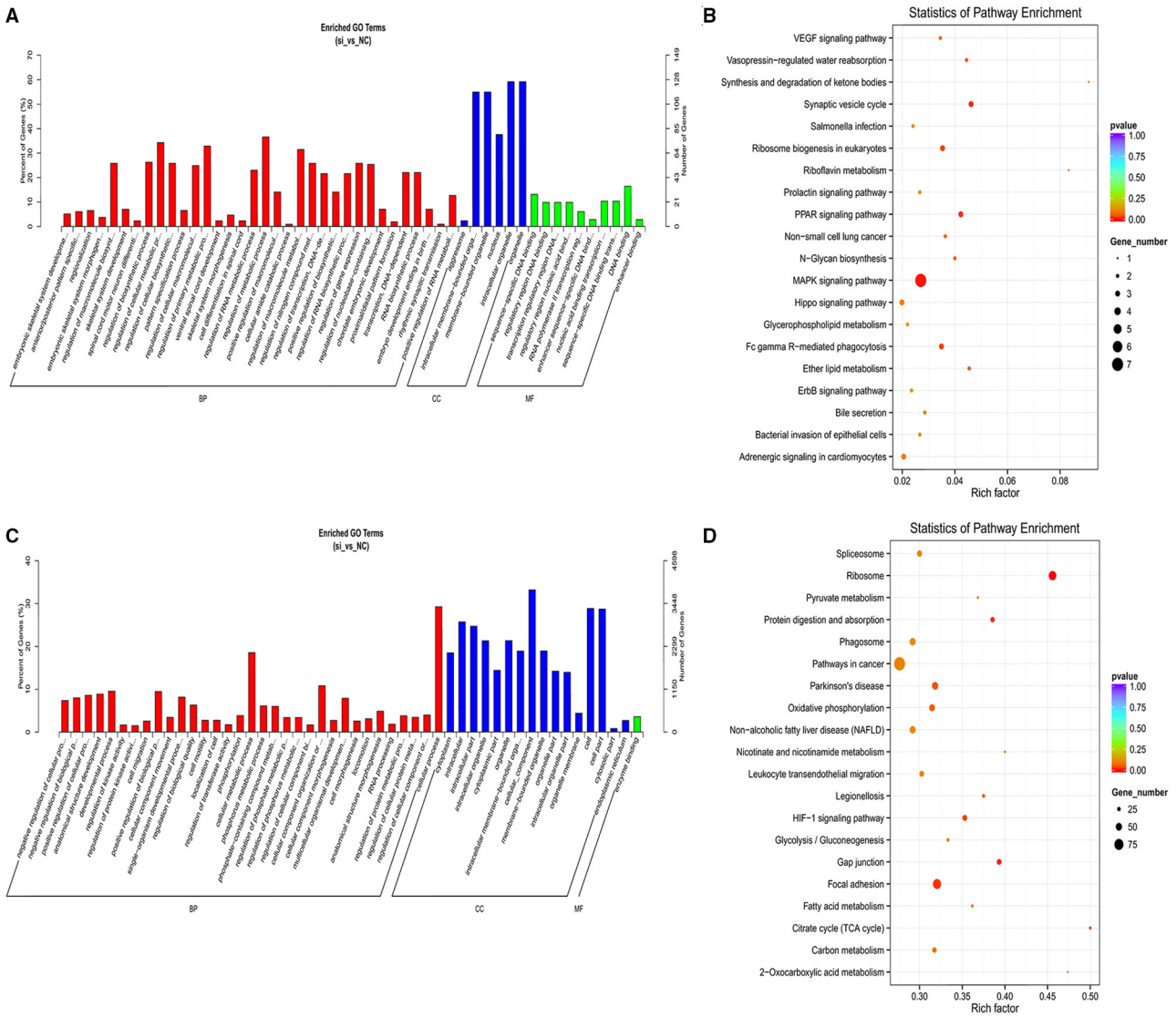

FIGURE 4 | GO and KEGG analyses of cis and trans target genes of DELs. **(A)** The GO analysis of top 50 cis target genes with the corresponding categories. **(B)** Top 20 of KEGG pathways analysis of cis target genes. **(C)** Top 50 GO analysis of trans target genes along with the categories of BP, CC, and MF. **(D)** The KEGG pathways of the top 20 trans target genes.

characteristics. Here, we investigated the expression of *ACSL1*, a key gene involved in the production of UFAs in adipocytes, to explore the molecular mechanism of UFAs synthesis. After different manipulations of *ACSL1*, we performed strand-specific RNA sequencing to identify mRNAs and lncRNAs in bovine adipocytes systematically.

In this study, 15,547 mRNAs and 5,432 lncRNA transcripts were identified in the NC-treated group and si-treated group, of which 107 mRNAs and 75 lncRNA transcripts were differentially expressed, respectively. The qRT-PCR results confirmed the strong correlation between lncRNA and mRNA expression and the transcriptome data. Compared with other transcriptomic studies in beef cattle, fewer mRNAs and lncRNAs were identified in this study. We speculated that it was probably because our study focused specifically on bovine adipocytes. Most of the current research on beef cattle has used specific tissues for sequencing; however, the results were not sufficiently targeted (24, 43). Fewer exons were tested within the 5,432 lncRNAs identified here, which had a lower expression and shorter lengths compared to those of mRNAs. Our results are consistent with the results of other recent studies in other mammals (24, 28, 44). These results on lncRNA expression suggest conservative regulation in mammals.

Next, GO and KEGG analyses were used for determining the biological functions of the mRNAs identified by our sequencing data. The GO analysis classified the significantly enriched DEMs into 386 functional groups (including 289 BPs ($P < 0.05$), 33 CCs, and 64 MFs). Some GO terms were closely related to

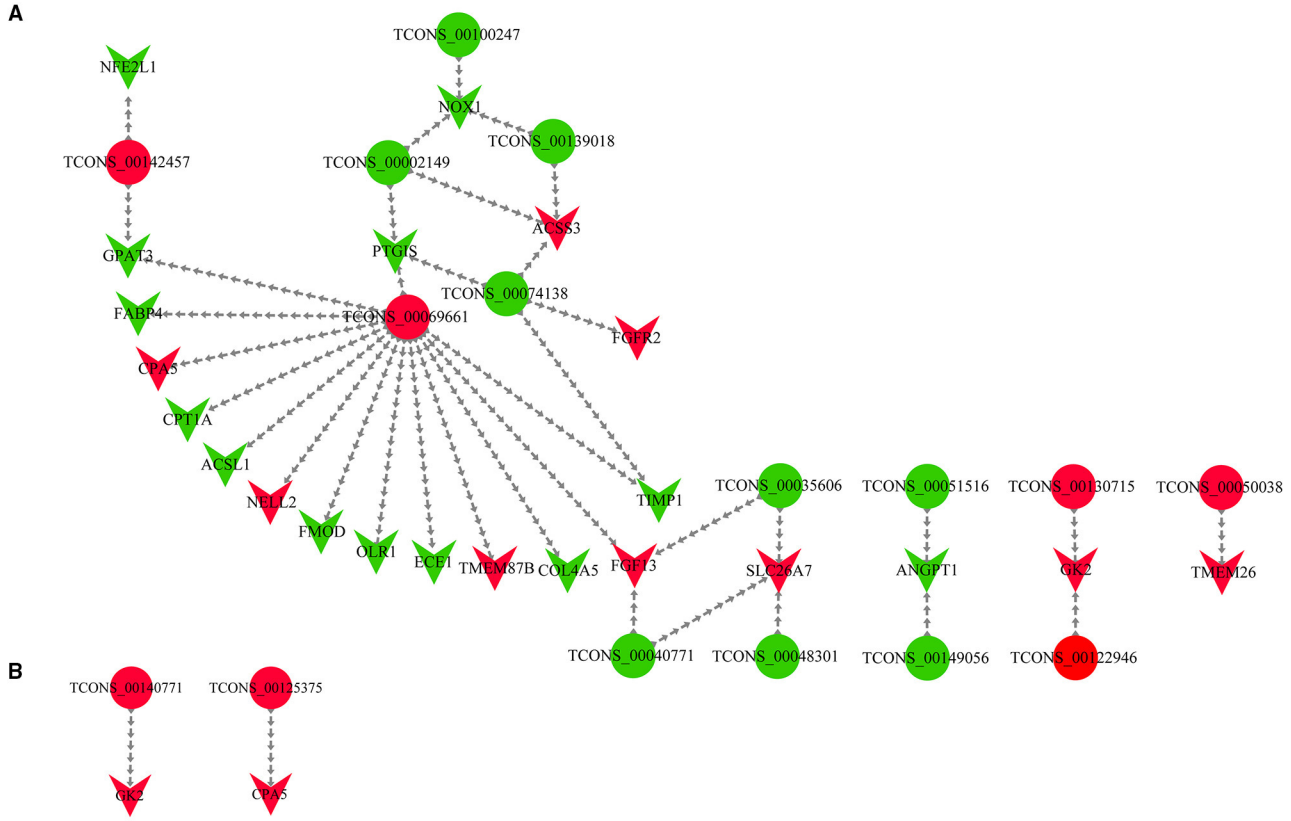

FIGURE 5 | The DEL-DEM interaction network. **(A)** DEL and trans-target interaction network. The trans-target was a DEM as well. **(B)** DEL and cis-target interaction network. The cis-target was a DEM as well. The circle type and inverted triangles type represent a lncRNA and mRNA, respectively. Red represents upregulation, and the green represents downregulation.

the production of UFAs and fats, such as positive regulation of MAPK cascade (GO: 0043410; $P = 0.00545$), adiponectin-mediated signaling pathway (GO: 0033211; $P = 0.025288$), long-chain FA transport (GO: 0015909; $P = 0.030592$), and positive regulation of PPAR signaling pathway (GO: 0035360; $P = 0.031822$).

MAPK signaling pathways have been shown to control various biological processes via various cellular mechanisms and might involve activation/inhibition of the molecules involved (45). Wu et al. identified C1qTNF-related factor as one of the adipokines Protein 6 (*CTRP6*), which promoted the differentiation of subcutaneous fat in pigs through the MAPK signaling pathway (46). Adiponectin (*APN*) is a hormone protein that is specifically secreted from human and animal adipose tissue and plays an important role in adipogenesis (47, 48). Only after specific binding of adiponectin to its receptor, can it activate the intracellular signaling cascade to exert its biological effects (49). Additionally, *ADIPOQ* is also known to play a critical role in adipocyte development, which affects the composition of UFAs and lipid production (50). The GO analysis also identified various candidate genes, several of which were demonstrated to be related to UFA synthesis, such as *ACSL1*, *FABP4*, and *PTGIS*. Additionally, the positive regulation of the MAPK cascade identified eight background genes, including *BMPER*, *FGFR2*, and *CSPG4*. Although they are not marker genes of UFA synthesis, the regulatory effect of MAPK on adipogenesis indicated that they were probably potential candidates for UFA synthesis.

The results of the KEGG pathway analysis showed that the DEMs were substantially enriched in 13 pathways ($P < 0.05$). Some DEMs were considerably enriched in the PPAR signaling pathway, PI3K-Akt signaling pathway, Rap1 signaling pathway, Ras signaling pathway, and ECM-receptor interaction. The PPAR signaling pathway is a crucial pathway closely related to FA and sterol metabolism as well as adipogenic differentiation (51). The PPAR family involves three subtypes *PPAR-α/-β/-δ/-γ*, with variable roles (52). PPARα activates FA oxidation; *PLIN1*, *PLIN3*, *LIPE*, and *FABP4* are the known targets of *PPAR* (53). FA-binding protein 4 (*FABP4*) has the ability to predict marbling (54). *PPARβ/δ* participates in adipogenic differentiation and adipogenesis (52). In this study, the PPAR signaling pathway was significantly enriched with 6 DEMs: *ACSL1*, *CPT1A*, *FABP4*, *GK2*, *OLR1*, and *PTGIS*. These genes were all known to be essential genes for lipid production (1, 55).

The PI3K-Akt signaling pathway is a classic insulin-related signaling pathway (56). PI3Ks are involved in the

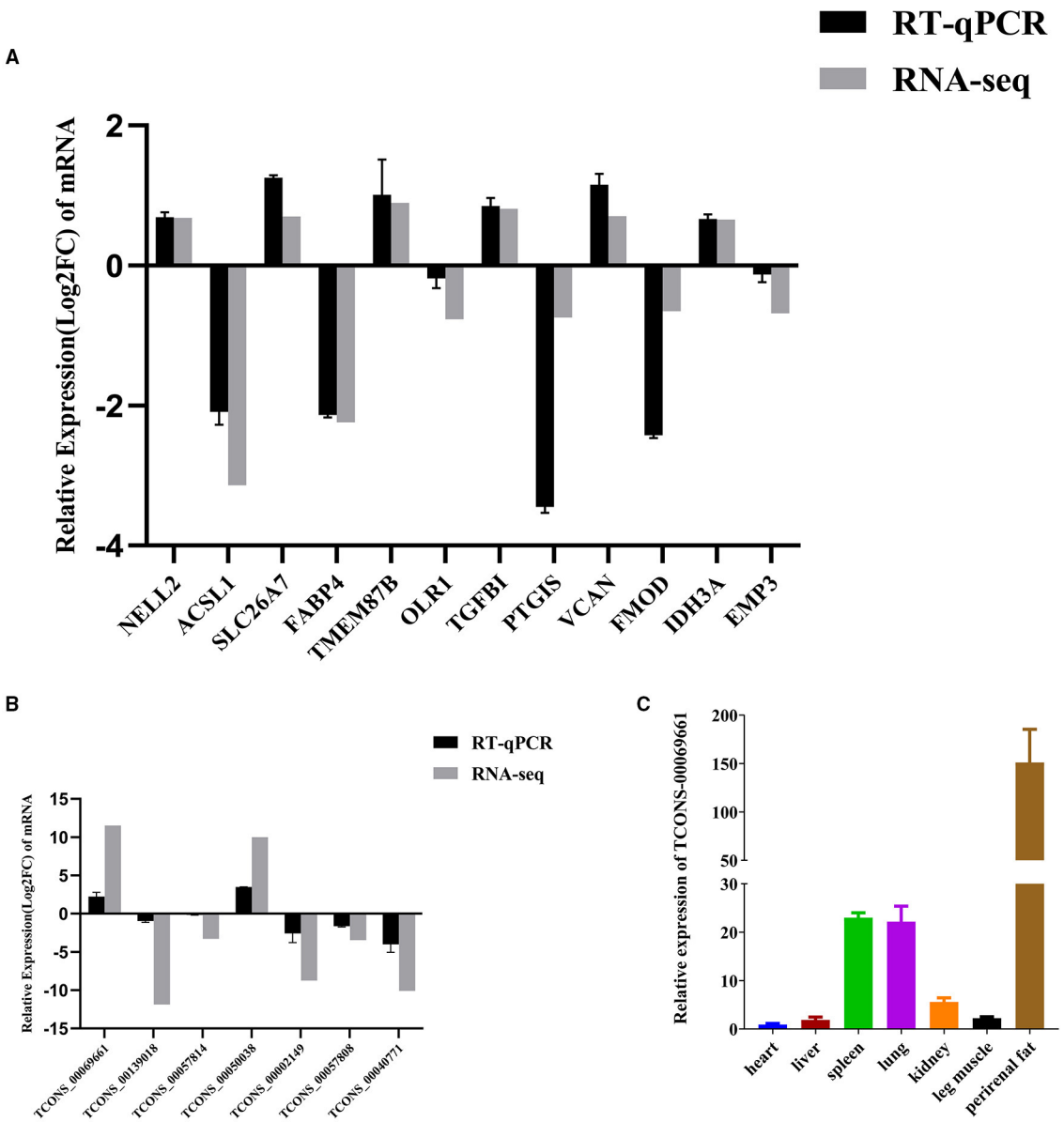

FIGURE 6 | qRT-PCR of DEMs and DELs. **(A)** Changes in mRNA expression between the NC and si-treated groups. **(B)** qRT-PCR verification of changes in lncRNA expression between the NC and si-treated groups. **(C)** qRT-PCR analysis of DEL *TCONS-00069661* in heart, liver, spleen, lung, kidney, leg muscles, and perirenal fat. Three biological and technical replicates were used for each group. The qRT-PCR data were determined using the $2^{-\Delta\Delta Ct}$ method with *GAPDH* as the internal reference. The verification data of mRNA and lncRNA sequencing results were further normalized to $\log_2$ (foldchange). Data represent means ± standard error.

phosphorylation of proteins and the PI3K-Akt pathway might also be involved in adipogenesis (57–59). The insulin-mediated PI3K/AKT signaling pathway plays a vital role within adipocytes of obese patients and leads to an excess of lipids that has to be appropriately stored in the fat tissue (57). In the present study, *ANGPT1*, *COL4A5*, *EFNA5*, *FGF13*, *FGFR2*, *ITGA3*, *ITGA4*, *KITLG*, and *XLOC_000377* were all considerably enriched in the PI3K-Akt signaling pathway, suggesting that differential expression of these genes might induce the FA-related metabolism pathway in beef cattle.

Rap1, a small G protein, is known to be involved in regulating cell survival/proliferation via the regulation of the PI3-AKT pathway (60). Studies have shown that Ras proteins act as molecular switches to play various regulatory functions in cell growth and survival (61). The Ras signaling pathway has been shown to activate the MAPK cascade; also, the PI3K-Akt pathway is known to regulate cell growth and apoptosis (60). We obtained a total of 14 DEMs from the Rap1 and Ras signaling pathways, which were observed to play vital roles in UFA synthesis. The ECM is essential for tissue architecture and has an important

role in adipogenesis (62). ECM is substantially enriched in bovine adipose tissue and may regulate specific genes to participate in adipogenesis (63). In this study, the ECM-receptor interaction was substantially enriched in 3 DEMs, including *ITGA3*, *ITGA4*, and *COL4A5*. These three genes were more closely related to diseases (64–66), but studies have found that *ITGA3*, *ITGA4*, and *COL4A1* may be involved in the composition of adipocyte extracellular matrix and the differentiation of adipocytes (67).

For a more in-depth understanding of the DELs potential function, we performed GO and KEGG analyses of its cis and trans target genes. In this study, we identified 75 DELs and predicted their target genes, which were primarily enriched in the GO terms associated with the regulation of FA biosynthesis and metabolism ($P < 0.05$), such as glycerol-3-phosphate biosynthetic process (GO: 0046167), negative regulation of plasma membrane long-chain FA transport (GO: 0010748), FA catabolic process (GO: 0009062), lipid oxidation (GO: 0034440), and FA oxidation (GO: 0019395). These findings suggested that the DELs' target genes are involved in functions from the synthesis to metabolism of FAs, indicating the influence the DELs may have on the synthesis and metabolism of UFAs and lipid. Similarly, some lncRNAs are known to play important roles in lipid synthesis in cattle (25, 31, 68). The KEGG analysis results of the target genes of DELs also showed significant involvement ($P < 0.05$) of pathways related to UFA synthesis, such as the PPAR signaling pathway, MAPK signaling pathway, Ether lipid metabolism, and Citrate cycle (TCA cycle). The TCA cycle involves various critical metabolic steps, and ether lipid metabolism is another vital FA metabolism-related pathway (69, 70).

To improve the screening out of lncRNAs and mRNAs that may be related to UFA synthesis more intuitively and in-depth, we constructed a DEL-DEM co-expression network. The DEL-DEM co-expression network involved 14 DELs and 22 trans-targets, as well as two DELs and two cis-targets to demonstrate their potential in UFAs production. In the results of the co-expression network, lncRNA TCONS_00069661 was of particular interest, as it was predicted to simultaneously target 14 DEMs including *ACSL1*, such as *FABP4*, *OLR1*, and *COL4A5*. We found that *FABP4* was a downregulated DEM, which not only regulated the differentiation of bovine adipocytes in the PPAR signaling pathway and supported the transport of extracellular FAs but was also involved in lipolysis and FA transport in different tissues (71, 72). A recent study on the *FABP4* gene of Yanbian cattle showed that a SNP in *FABP4* substantially affected the fat content, protein content, and marbling level (73). Li et al. (74) found that with increasing age, the concentration of SFA in Yanbian cattle decreased, and the concentration of MUFA increased proportionally with an increase in the percentage of intramuscular lipids leading, in turn, to an increase in the expression of the *FABP4* gene. A SNP (g.8232C > A) in the oxidized low-density lipoprotein receptor 1 (*OLR1*) has been shown to be related to rump fat thickness and weaning weight in Nelore cattle (75–78), indicating its importance in regulating fat deposition. In our study, the upregulated lncRNA *TCONS_00069661* was predicted to target the downregulated gene *OLR1*. We speculate that *TCONS_00069661* targets the 3'-UTR of *OLR1*, thereby preventing its translation. Current research on *COL4A5* has been related to disease, and some of the genes in this family have been studied in cattle. Previous studies have confirmed the role of *COL5A3*, *COL6A2*, and *COL3A1* in inducing *CD44* expression, followed by upregulation of the cellular expression of docosanoic acid, palmitic acid, and trans-oleic acid and downregulation of the cellular expression of tridecanoic acid, stearic acid, and cis-5, 8, 11, 14-EPA (79). Liu et al. (26) found that *COL6A1*, *COL6A2*, *COL4A2*, *COL1A1*, *COL4A6*, *COL4A5*, *COL6A3*, *COL1A2*, and other genes were strongly related to fat metabolism in the transcriptomic study of the muscles of Shandong black cattle and Luxi cattle.

Additionally, our co-expression network results showed that not only did one lncRNA target multiple mRNAs but multiple lncRNAs targeted one mRNA. For example, *TCONS_00040771*, *TCONS_00035606*, and *TCONS_00048301* simultaneously targeted *SLC26A7*, and *TCONS_00130715* and *TCONS_00122946* simultaneously targeted *GK2*. However, our results of the co-expression network diagram showed dissimilar upward and downward trends of lncRNAs and mRNAs. Thus, we speculate that there is a direct relation between some lncRNAs and mRNAs (21, 31), with some combining with miRNAs to perform the function of ceRNA, leading to the degradation of mRNA targets or translational repression, and the mode of action involved lncRNA-miRNA-mRNA network (80, 81). Further studies should involve the verification of the lncRNA-mRNA targeting relationship pairs that might exist in subsequent studies to explore their mode of action and specific roles in the synthesis of UFAs.

CONCLUSION

This study used RNA-seq to determine lncRNA and mRNA levels by interference and comparing *ACSL1* expression with controls in bovine adipocytes. GO and KEGG analyses showed that the target genes of the DELs and DE-genes were enriched in the relevant FA and lipogenesis-related pathways. Based on the above results, we constructed a DEL-DEM interaction network. The results of this study expand our knowledge of the molecular mechanisms used by lncRNAs as well as the genes involved in the regulation of UFA synthesis in bovine adipocytes.

DATA AVAILABILITY STATEMENT

The datasets presented in this study can be found in online repositories. The names of the repository/repositories and accession number(s) can be found in the article/**Supplementary Material**.

ETHICS STATEMENT

The animal study was reviewed and approved by Ethical Commission of Gansu Agricultural University as well as the

Ministry of Science and Technology of the People's Republic of China.

AUTHOR CONTRIBUTIONS

YB, HT, and ZZ: conceptualization. YB, HT, BS, and ZZ: methodology. YB, XLi, JL, YM, and ZC: validation. YB, BS, XLiu, and SL: formal analysis. ZZ, HT, and YB: investigation. YL, JH, and JW: resources. YB: writing—original draft preparation. YB, ZZ, and SR: writing—review and editing. ZZ and XH: supervision. ZZ: project administration. ZZ and JH: funding acquisition. All authors have read and agreed to the published version of the manuscript.

FUNDING

This research was supported by the National Natural Science Foundation (31860631), Young Doctor Fund Project of Gansu Provincial Department of Education (2021QB-027), and Scientific research start-up funds for openly-recruited doctors (GSAU-RCZX201711).

ACKNOWLEDGMENTS

We thank LetPub (www.letpub.com) for its linguistic assistance during the preparation of this manuscript.

SUPPLEMENTARY MATERIAL

The Supplementary Material for this article can be found online at: https://www.frontiersin.org/articles/10.3389/fvets.2021.788316/full#supplementary-material

Supplementary File 1 | The sequencing results were compared to the reference genome.

Supplementary Files 2, 3 | Details of DELs and DEMs.

Supplementary File 4 | Details of GO analysis of DEMs.

Supplementary File 5 | Details of KEGG pathway analysis of DEMs.

Supplementary File 6 | Cis-regulation of the lncRNAs target genes.

Supplementary File 7 | GO analysis of DELs cis-regulated target genes.

Supplementary File 8 | KEGG pathway analysis of DELs cis-regulated target genes.

Supplementary File 9 | Trans-regulation of the lncRNAs target genes.

Supplementary File 10 | GO analysis of DELs trans-regulated target genes.

Supplementary File 11 | KEGG pathway analysis of DELs trans-regulated target genes.

Supplementary File 12 | The cis-regulated target genes and the trans-regulated target genes of DELs intersect with DEMs, respectively.

Supplementary File 13 | Literature screening information on lipogenesis-related mRNAs.

Supplementary File 14 | The result of the alignment between the sequence of the amplified fragments of qRT-PCR and the sequence in RNA-Seq.

REFERENCES

1. Coleman RA, Lewin TM, Muoio DM. Physiological and nutritional regulation of enzymes of triacylglycerol synthesis. *Annu Rev Nutr.* (2000) 20:77–103. doi: 10.1146/annurev.nutr.20.1.77
2. Soupene E, Kuypers FA. Mammalian long-chain acyl-coa synthetases. *Exp Biol Med.* (2008) 233:507–21. doi: 10.3181/0710-MR-287
3. Zhan T, Poppelreuther M, Ehehalt R, Fullekrug J. Overexpressed fatp1, acsvl4/fatp4 and acsl1 increase the cellular fatty acid uptake of 3t3-l1 adipocytes but are localized on intracellular membranes. *PLoS ONE.* (2012) 7:e45087. doi: 10.1371/journal.pone.0045087
4. Ellis JM, Li LO, Wu PC, Koves TR, Ilkayeva O, Stevens RD, et al. Adipose acyl-coa synthetase-1 directs fatty acids toward beta-oxidation and is required for cold thermogenesis. *Cell Metab.* (2010) 12:53–64. doi: 10.1016/j.cmet.2010.05.012
5. Lopez-Huertas E. Health effects of oleic acid and long chain omega-3 fatty acids (epa and dha) enriched milks. A review of intervention studies. *Pharmacol Res.* (2010) 61:200–7. doi: 10.1016/j.phrs.2009.10.007
6. Russo GL. Dietary n-6 and n-3 polyunsaturated fatty acids: from biochemistry to clinical implications in cardiovascular prevention. *Biochem Pharmacol.* (2009) 77:937–46. doi: 10.1016/j.bcp.2008.10.020
7. Simopoulos AP. Omega-3 fatty acids in health and disease and in growth and development. *Am J Clin Nutr.* (1991) 54:438–63. doi: 10.1093/ajcn/54.3.438
8. Barcelo-Coblijn G, Murphy EJ. Alpha-linolenic acid and its conversion to longer chain n-3 fatty acids: benefits for human health and a role in maintaining tissue n-3 fatty acid levels. *Prog Lipid Res.* (2009) 48:355–74. doi: 10.1016/j.plipres.2009.07.002
9. Widmann P, Nuernberg K, Kuehn C, Weikard R. Association of an acsl1 gene variant with polyunsaturated fatty acids in bovine skeletal muscle. *BMC Genet.* (2011) 12:96. doi: 10.1186/1471-2156-12-96
10. Li LO, Mashek DG, An J, Doughman SD, Newgard CB, Coleman RA. Overexpression of rat long chain acyl-coa synthetase 1 alters fatty acid metabolism in rat primary hepatocytes. *J Biol Chem.* (2006) 281:37246–55. doi: 10.1074/jbc.M604427200
11. Cao Y, Wang S, Liu S, Wang Y, Jin H, Ma H, et al. Effects of long-chain fatty acyl-coa synthetase 1 on diglyceride synthesis and arachidonic acid metabolism in sheep adipocytes. *Int J Mol Sci.* (2020) 21:2044. doi: 10.3390/ijms21062044
12. Zhao ZD, Zan LS, Li AN, Cheng G, Li SJ, Zhang YR, et al. Characterization of the promoter region of the bovine long-chain acyl-coa synthetase 1 gene: roles of e2f1, sp1, klf15, and e2f4. *Sci Rep.* (2016) 6:19661. doi: 10.1038/srep19661
13. Tian HS, Su XT, Han XM, Zan LS, Luo YZ, Wang JQ, et al. Effects of silencing ACSL1 gene by siRNA on the synthesis of unsaturated fatty acids in adipocytes of qinchuan beef cattle. *J Agric Biotechnol.* (2020) 10:1722–32. doi: 10.3969/j.issn.1674-7968.2020.10.002
14. Zhao Z, Abbas RS, Tian H, Shi B, Luo Y, Wang J, et al. Effects of overexpression of acsl1 gene on the synthesis of unsaturated fatty acids in adipocytes of bovine. *Arch Biochem Biophys.* (2020) 695:108648. doi: 10.1016/j.abb.2020.108648
15. Anderson DM, Anderson KM, Chang CL, Makarewich CA, Nelson BR, McAnally JR, et al. A micropeptide encoded by a putative long noncoding rna regulates muscle performance. *Cell.* (2015) 160:595–606. doi: 10.1016/j.cell.2015.01.009
16. Bertani S, Sauer S, Bolotin E, Sauer F. The noncoding rna mistral activates hoxa6 and hoxa7 expression and stem cell differentiation by recruiting mll1 to chromatin. *Mol Cell.* (2011) 43:1040–6. doi: 10.1016/j.molcel.2011.08.019
17. Zhao J, Sun BK, Erwin JA, Song JJ, Lee JT. Polycomb proteins targeted by a short repeat rna to the mouse x chromosome. *Science.* (2008) 322:750–6. doi: 10.1126/science.1163045
18. Sheik MJ, Gaughwin PM, Lim B, Robson P, Lipovich L. Conserved long noncoding rnas transcriptionally regulated by oct4 and nanog modulate pluripotency in mouse embryonic stem cells. *RNA.* (2010) 16:324–37. doi: 10.1261/rna.1441510
19. Xiao T, Liu L, Li H, Sun Y, Luo H, Li T, et al. Long noncoding rna adinr regulates adipogenesis by transcriptionally activating c/ebpalpha. *Stem Cell Rep.* (2021) 16:1006–8. doi: 10.1016/j.stemcr.2021.03.024
20. Cai R, Tang G, Zhang Q, Yong W, Zhang W, Xiao J, et al. A novel lnc-rna, named lnc-ora, is identified by rna-seq analysis, and its knockdown inhibits

adipogenesis by regulating the pi3k/akt/mtor signaling pathway. *Cells*. (2019) 8:477. doi: 10.3390/cells8050477
21. Li H, Yang J, Jiang R, Wei X, Song C, Huang Y, et al. Long non-coding rna profiling reveals an abundant mdncr that promotes differentiation of myoblasts by sponging mir-133a. *Mol Ther Nucleic Acids.* (2018) 12:610–25. doi: 10.1016/j.omtn.2018.07.003
22. Mortazavi A, Williams BA, McCue K, Schaeffer L, Wold B. Mapping and quantifying mammalian transcriptomes by rna-seq. *Nat Methods.* (2008) 5:621–8. doi: 10.1038/nmeth.1226
23. Miao X, Qin QL. Genome-wide transcriptome analysis of mrnas and micrornas in dorset and small tail han sheep to explore the regulation of fecundity. *Mol Cell Endocrinol.* (2015) 402:32–42. doi: 10.1016/j.mce.2014.12.023
24. Gao Y, Li S, Lai Z, Zhou Z, Wu F, Huang Y, et al. Analysis of long non-coding rna and mrna expression profiling in immature and mature bovine (bos taurus) testes. *Front Genet.* (2019) 10:646. doi: 10.3389/fgene.2019.00646
25. Jiang R, Li H, Huang Y, Lan X, Lei C, Chen H. Transcriptome profiling of lncrna related to fat tissues of qinchuan cattle. *Gene.* (2020) 742:144587. doi: 10.1016/j.gene.2020.144587
26. Liu R, Liu X, Bai X, Xiao C, Dong Y. Different expression of lipid metabolism-related genes in shandong black cattle and luxi cattle based on transcriptome analysis. *Sci Rep.* (2020) 10:21915. doi: 10.1038/s41598-020-79086-4
27. Song C, Huang Y, Yang Z, Ma Y, Chaogetu B, Zhuoma Z, et al. Rna-seq analysis identifies differentially expressed genes insubcutaneous adipose tissuein qaidamford cattle, cattle-yak, angus cattle. *Animals.* (2019) 9:1077. doi: 10.3390/ani9121077
28. Ma L, Zhang M, Jin Y, Erdenee S, Hu L, Chen H, et al. Comparative transcriptome profiling of mrna and lncrna related to tail adipose tissues of sheep. *Front Genet.* (2018) 9:365. doi: 10.3389/fgene.2018.00365
29. Xing K, Zhao X, Ao H, Chen S, Yang T, Tan Z, et al. Transcriptome analysis of mirna and mrna in the livers of pigs with highly diverged backfat thickness. *Sci Rep.* (2019) 9:16740. doi: 10.1038/s41598-019-53377-x
30. Xing S, Liu R, Zhao G, Liu L, Groenen M, Madsen O, et al. Rna-seq analysis reveals hub genes involved in chicken intramuscular fat and abdominal fat deposition during development. *Front Genet.* (2020) 11:1009. doi: 10.3389/fgene.2020.01009
31. Cai H, Li M, Jian W, Song C, Huang Y, Lan X, et al. A novel lncrna badlncr1 inhibits bovine adipogenesis by repressing glrx5 expression. *J Cell Mol Med.* (2020) 24:7175–86. doi: 10.1111/jcmm.15181
32. Dobin A, Davis CA, Schlesinger F, Drenkow J, Zaleski C, Jha S, et al. Star: ultrafast universal rna-seq aligner. *Bioinformatics.* (2013) 29:15–21. doi: 10.1093/bioinformatics/bts635
33. Anders S, Huber W. Differential expression analysis for sequence count data. *Genome Biol.* (2010) 11:R106. doi: 10.1186/gb-2010-11-10-r106
34. Kang YJ, Yang DC, Kong L, Hou M, Meng YQ, Wei L, et al. Cpc2: a fast and accurate coding potential calculator based on sequence intrinsic features. *Nucleic Acids Res.* (2017) 45:W12–6. doi: 10.1093/nar/gkx428
35. Finn RD, Bateman A, Clements J, Coggill P, Eberhardt RY, Eddy SR, et al. Pfam: the protein families database. *Nucleic Acids Res.* (2014) 42:D222–30. doi: 10.1093/nar/gkt1223
36. Sun L, Luo H, Bu D, Zhao G, Yu K, Zhang C, et al. Utilizing sequence intrinsic composition to classify protein-coding and long non-coding transcripts. *Nucleic Acids Res.* (2013) 41:e166. doi: 10.1093/nar/gkt646
37. Wright MW. A short guide to long non-coding rna gene nomenclature. *Hum Genomics.* (2014) 8:7. doi: 10.1186/1479-7364-8-7
38. Ghanbarian AT, Hurst LD. Neighboring genes show correlated evolution in gene expression. *Mol Biol Evol.* (2015) 32:1748–66. doi: 10.1093/molbev/msv053
39. Liao Q, Liu C, Yuan X, Kang S, Miao R, Xiao H, et al. Large-scale prediction of long non-coding rna functions in a coding-non-coding gene co-expression network. *Nucleic Acids Res.* (2011) 39:3864–78. doi: 10.1093/nar/gkq1348
40. Young MD, Wakefield MJ, Smyth GK, Oshlack A. Gene ontology analysis for rna-seq: accounting for selection bias. *Genome Biol.* (2010) 11:R14. doi: 10.1186/gb-2010-11-2-r14
41. Shannon P, Markiel A, Ozier O, Baliga NS, Wang JT, Ramage D, et al. Cytoscape: a software environment for integrated models of biomolecular interaction networks. *Genome Res.* (2003) 13:2498–504. doi: 10.1101/gr.1239303
42. Livak KJ, Schmittgen TD. Analysis of relative gene expression data using real-time quantitative pcr and the 2(-delta delta c(t)) method. *Methods.* (2001) 25:402–8. doi: 10.1006/meth.2001.1262
43. Li H, Wei X, Yang J, Dong D, Huang Y, Lan X, et al. Developmental transcriptome profiling of bovine muscle tissue reveals an abundant gosb that regulates myoblast proliferation and apoptosis. *Oncotarget.* (2017) 8:32083–100. doi: 10.18632/oncotarget.16644
44. Huang W, Zhang X, Li A, Xie L, Miao X. Differential regulation of mrnas and lncrnas related to lipid metabolism in two pig breeds. *Oncotarget.* (2017) 8:87539–53. doi: 10.18632/oncotarget.20978
45. Yue J, Lopez JM. Understanding mapk signaling pathways in apoptosis. *Int J Mol Sci.* (2020) 21:2346. doi: 10.3390/ijms21072346
46. Wu W, Zhang J, Zhao C, Sun Y, Pang W, Yang G. Ctrp6 regulates porcine adipocyte proliferation and differentiation by the adipor1/mapk signaling pathway. *J Agric Food Chem.* (2017) 65:5512–22. doi: 10.1021/acs.jafc.7b00594
47. Ghadge AA, Khaire AA, Kuvalekar AA. Adiponectin: a potential therapeutic target for metabolic syndrome. *Cytokine Growth Factor Rev.* (2018) 39:151–8. doi: 10.1016/j.cytogfr.2018.01.004
48. Katsiki N, Mantzoros C, Mikhailidis DP. Adiponectin, lipids and atherosclerosis. *Curr Opin Lipidol.* (2017) 28:347–54. doi: 10.1097/MOL.0000000000000431
49. Deepa SS, Zhou L, Ryu J, Wang C, Mao X, Li C, et al. Appl1 mediates adiponectin-induced lkb1 cytosolic localization through the pp2a-pkczeta signaling pathway. *Mol Endocrinol.* (2011) 25:1773–85. doi: 10.1210/me.2011-0082
50. Gao Y, Li F, Zhang Y, Dai L, Jiang H, Liu H, et al. Silencing of adipoq efficiently suppresses preadipocyte differentiation in porcine. *Cell Physiol Biochem.* (2013) 31:452–61. doi: 10.1159/000343381
51. Farmer SR. Regulation of ppargamma activity during adipogenesis. *Int J Obes.* (2005) 29 (Suppl. 1):S13–6. doi: 10.1038/sj.ijo.0802907
52. Khan WS, Adesida AB, Tew SR, Longo UG, Hardingham TE. Fat pad-derived mesenchymal stem cells as a potential source for cell-based adipose tissue repair strategies. *Cell Prolif.* (2012) 45:111–20. doi: 10.1111/j.1365-2184.2011.00804.x
53. Gaudel C, Schwartz C, Giordano C, Abumrad NA, Grimaldi PA. Pharmacological activation of pparbeta promotes rapid and calcineurin-dependent fiber remodeling and angiogenesis in mouse skeletal muscle. *Am J Physiol Endocrinol Metab.* (2008) 295:E297–304. doi: 10.1152/ajpendo.00581.2007
54. Cai G, Zhang X, Weng W, Shi G, Xue S, Zhang B. Associations between pparg polymorphisms and the risk of essential hypertension. *PLoS ONE.* (2017) 12:e181644. doi: 10.1371/journal.pone.0181644
55. Chmurzynska A. The multigene family of fatty acid-binding proteins (fabps): function, structure and polymorphism. *J Appl Genet.* (2006) 47:39–48. doi: 10.1007/BF03194597
56. Pessin JE, Saltiel AR. Signaling pathways in insulin action: molecular targets of insulin resistance. *J Clin Invest.* (2000) 106:165–9. doi: 10.1172/JCI10582
57. Sharma BR, Kim HJ, Rhyu DY. Caulerpa lentillifera extract ameliorates insulin resistance and regulates glucose metabolism in c57bl/ksj-db/db mice via pi3k/akt signaling pathway in myocytes. *J Transl Med.* (2015) 13:62. doi: 10.1186/s12967-015-0412-5
58. Kim SP, Ha JM, Yun SJ, Kim EK, Chung SW, Hong KW, et al. Transcriptional activation of peroxisome proliferator-activated receptor-gamma requires activation of both protein kinase a and akt during adipocyte differentiation. *Biochem Biophys Res Commun.* (2010) 399:55–9. doi: 10.1016/j.bbrc.2010.07.038
59. Yun J, Jin H, Cao Y, Zhang L, Zhao Y, Jin X, et al. Rna-seq analysis reveals a positive role of htr2a in adipogenesis in yan yellow cattle. *Int J Mol Sci.* (2018) 19:1760. doi: 10.3390/ijms19061760
60. Yang C, Zhang J, Wu T, Zhao K, Wu X, Shi J, et al. Multi-omics analysis to examine gene expression and metabolites from multisite adipose-derived mesenchymal stem cells. *Front Genet.* (2021) 12:627347. doi: 10.3389/fgene.2021.627347
61. Goodsell DS. The molecular perspective: the ras oncogene. *Oncologist.* (1999) 4:263–264 doi: 10.1634/theoncologist.4-3-263
62. Mariman EC, Wang P. Adipocyte extracellular matrix composition, dynamics and role in obesity. *Cell Mol Life Sci.* (2010) 67:1277–92. doi: 10.1007/s00018-010-0263-4

63. Lee HJ, Jang M, Kim H, Kwak W, Park W, Hwang JY, et al. Comparative transcriptome analysis of adipose tissues reveals that ecm-receptor interaction is involved in the depot-specific adipogenesis in cattle. *PLoS ONE.* (2013) 8:e66267. doi: 10.1371/journal.pone.0066267
64. Attia HR, Ibrahim MH, El-Aziz S, Hassan NM, Osman RA, Hagag HA, et al. Itga4 gene methylation status in chronic lymphocytic leukemia. *Future Sci OA.* (2020) 6:O583. doi: 10.2144/fsoa-2020-0034
65. Naylor RW, Morais M, Lennon R. Complexities of the glomerular basement membrane. *Nat Rev Nephrol.* (2021) 17:112–27. doi: 10.1038/s41581-020-0329-y
66. Tian L, Chen M, He Q, Yan Q, Zhai C. Microrna199a5p suppresses cell proliferation, migration and invasion by targeting itga3 in colorectal cancer. *Mol Med Rep.* (2020) 22:2307–17. doi: 10.3892/mmr.2020.11323
67. Ullah M, Sittinger M, Ringe J. Extracellular matrix of adipogenically differentiated mesenchymal stem cells reveals a network of collagen filaments, mostly interwoven by hexagonal structural units. *Matrix Biol.* (2013) 32:452–65. doi: 10.1016/j.matbio.2013.07.001
68. Li M, Sun X, Cai H, Sun Y, Plath M, Li C, et al. Long non-coding rna adncr suppresses adipogenic differentiation by targeting mir-204. *Biochim Biophys Acta.* (2016) 1859:871–82. doi: 10.1016/j.bbagrm.2016.05.003
69. Huang Y, Zhang C, Wang Y, Sun X. Identification and analysis of mirnas in the normal and fatty liver from the holstein dairy cow. *Anim Biotechnol.* (2020) 24:1–12. doi: 10.1080/10495398.2020.1804919
70. Salleh MS, Mazzoni G, Hoglund JK, Olijhoek DW, Lund P, Lovendahl P, et al. Rna-seq transcriptomics and pathway analyses reveal potential regulatory genes and molecular mechanisms in high- and low-residual feed intake in nordic dairy cattle. *BMC Genomics.* (2017) 18:258. doi: 10.1186/s12864-017-3622-9
71. Goszczynski DE, Papaleo-Mazzucco J, Ripoli MV, Villarreal EL, Rogberg-Munoz A, Mezzadra CA, et al. Genetic variation in fabp4 and evaluation of its effects on beef cattle fat content. *Anim Biotechnol.* (2017) 28:211–19. doi: 10.1080/10495398.2016.1262868
72. Guo B, Kongsuwan K, Greenwood PL, Zhou G, Zhang W, Dalrymple BP. A gene expression estimator of intramuscular fat percentage for use in both cattle and sheep. *J Anim Sci Biotechnol.* (2014) 5:35. doi: 10.1186/2049-1891-5-35
73. Yin BZ, Fang JC, Zhang JS, Zhang LM, Xu C, Xu HY, et al. Correlations between single nucleotide polymorphisms in fabp4 and meat quality and lipid metabolism gene expression in yanbian yellow cattle. *PLoS ONE.* (2020) 15:e234328. doi: 10.1371/journal.pone.0234328
74. Li XZ, Yan CG, Gao QS, Yan Y, Choi SH, Smith SB. Adipogenic/lipogenic gene expression and fatty acid composition in chuck, loin, and round muscles in response to grain feeding of yanbian yellow cattle. *J Anim Sci.* (2018) 96:2698–709. doi: 10.1093/jas/sky161
75. Chen KC, Hsieh IC, Hsi E, Wang YS, Dai CY, Chou WW, et al. Negative feedback regulation between microrna let-7g and the oxldl receptor lox-1. *J Cell Sci.* (2011) 124:4115–24. doi: 10.1242/jcs.092767
76. Fonseca PD, de Souza FR, de Camargo GM, Gil FM, Cardoso DF, Zetouni L, et al. Association of adipoq, olr1 and ppargc1a gene polymorphisms with growth and carcass traits in nelore cattle. *Meta Gene.* (2015) 4:1–7. doi: 10.1016/j.mgene.2015.02.001
77. Kaneda M, Lin BZ, Sasazaki S, Oyama K, Mannen H. Allele frequencies of gene polymorphisms related to economic traits in bos taurus and bos indicus cattle breeds. *Anim Sci J.* (2011) 82:717–21. doi: 10.1111/j.1740-0929.2011.00910.x
78. Kataoka H, Kume N, Miyamoto S, Minami M, Morimoto M, Hayashida K, et al. Oxidized ldl modulates bax/bcl-2 through the lectinlike ox-ldl receptor-1 in vascular smooth muscle cells. *Arterioscler Thromb Vasc Biol.* (2001) 21:955–60. doi: 10.1161/01.ATV.21.6.955
79. Hu ZL, Park CA, Reecy JM. Developmental progress and current status of the animal qtldb. *Nucleic Acids Res.* (2016) 44:D827–33. doi: 10.1093/nar/gkv1233
80. Yue B, Li H, Liu M, Wu J, Li M, Lei C, et al. Characterization of lncrna-mirna-mrna network to reveal potential functional cernas in bovine skeletal muscle. *Front Genet.* (2019) 10:91. doi: 10.3389/fgene.2019.00091
81. Zhu M, Liu J, Xiao J, Yang L, Cai M, Shen H, et al. Lnc-mg is a long non-coding rna that promotes myogenesis. *Nat Commun.* (2017) 8:14718. doi: 10.1038/ncomms14718

Conflict of Interest: The authors declare that the research was conducted in the absence of any commercial or financial relationships that could be construed as a potential conflict of interest.

Publisher's Note: All claims expressed in this article are solely those of the authors and do not necessarily represent those of their affiliated organizations, or those of the publisher, the editors and the reviewers. Any product that may be evaluated in this article, or claim that may be made by its manufacturer, is not guaranteed or endorsed by the publisher.

frontiers in Veterinary Science

REVIEW
published: 24 February 2022
doi: 10.3389/fvets.2022.819605

Genetic and Environmental Determinants of Beef Quality—A Review

Tomasz Sakowski[1], *Grzegorz Grodkowski*[2], *Marcin Gołebiewski*[2], *Jan Slósarz*[2], *Piotr Kostusiak*[2], *Paweł Solarczyk*[2] *and Kamila Puppel*[2]*

[1] *Department of Biotechnology and Nutrigenomics, Institute of Genetics and Animal Biotechnology, Jastrzebiec, Poland,*
[2] *Department of Animal Breeding, Institute of Animal Sciences, Warsaw University of Life Sciences, Warsaw, Poland*

The flavor, quality, and composition of beef changes with the cattle diet regimen. The quality of meat varies, and that variability is determined by both individual and environmental factors: age, breed, live weight, fatness degree, plane of nutrition, and concentrate/roughage ratio. The strategy for the rearing and feeding of cattle for slaughter should therefore aim at reducing the saturated fatty acid content and increasing the polyunsaturated fatty acid and monounsaturated fatty acid levels. Many diseases in humans, like atherosclerosis and cardiovascular diseases, are associated with dietary fat, and their development process could take a year, the results of which can be a shorter life and its lower quality. The objective of this review was to describe the factors affecting the meat quality and fatty acid profile of the intramuscular fat of European cattle fed various diets.

Keywords: red meat, quality, beef, fatty acid composition, breed

OPEN ACCESS

Edited by:
Min Du,
Washington State University, United States

Reviewed by:
Paulina Pogorzelska-Przybyłek, University of Warmia and Mazury in Olsztyn, Poland
Monika Sobczuk-Szul, University of Warmia and Mazury in Olsztyn, Poland

***Correspondence:**
Kamila Puppel
kamila_puppel@sggw.edu.pl

Specialty section:
This article was submitted to Livestock Genomics, a section of the journal Frontiers in Veterinary Science

Received: *21 November 2021*
Accepted: *12 January 2022*
Published: *24 February 2022*

Citation:
Sakowski T, Grodkowski G, Gołebiewski M, Slósarz J, Kostusiak P, Solarczyk P and Puppel K (2022) Genetic and Environmental Determinants of Beef Quality—A Review. Front. Vet. Sci. 9:819605. doi: 10.3389/fvets.2022.819605

INTRODUCTION

According to Directive 2001/101/EC[1], products containing more connective tissue and fat should be labeled as "mechanically separated meat." In the case of beef, the term "good quality of meat" means that the meat is free from all quality defects and that it is originated from healthy animals. All changes occurred correctly at an appropriate pace both in the living animals and in the slaughtered carcasses. It also means that the meat has been cut from the carcass and delivered for consumption or processing after reaching a sufficient degree of ripeness. Listrad et al. (1) pointed out that the quality of the meat can be described by 4 terms: security, healthiness (nutritional quality), sensory quality, and serviceability.

Meat is a mixture of several compounds, but its basic ingredients include water (70–76%), protein (18–23%), nitrogen compounds (1–3%), carbohydrates (0.5–2%), muscle fat (0.7–10%), and mineral components (0.5–2%). The development of the basic chemical composition of meat and thus the development of its nutritional quality are influenced by many factors, both genetic and environmental (1–5).

Water is the predominant component of beef, accounting for ∼70–76%. It occurs in a bound form (indistinguishable by centrifugation and pressure) and in the free form. Differences in water concentration in muscle tissue result primarily from the different content of intramuscular fat.

[1]Dyrektywa Komisji 2001/101/WE z dnia 26 listopada 2001 r. zmieniajaca dyrektywe 2000/13/WE Parlamentu Europejskiego i Rady w sprawie zblizenia ustawodawstw Państw Członkowskich odnoszacych sie do etykietowania, p., Ed.

In addition, the age of the animals also shapes the level of this parameter, because the water content decreases with the age of the animals (6).

The total protein content of meat is in the range of 15–23% (7–9). It is believed that white meat is healthier than red meat. However, when assessing the healthiness of meat, protein content in particular types of meat is important, but not the most important factor. Beef is characterized by a better amino acid profile compared to other meats. It contains significantly more branched-chain amino acids, including valine, leucine, and isoleucine. Beef is also a rich source of amino acids that pass through the blood/cerebrospinal fluid barrier (10).

Beef meat is characterized by moderate and quite varied fat content, ranging between 0.6 and 23.3% weight of tissue (11). Fat content changes with age and intensity of nutrition (12). In late-maturing (large caliber) animals, the growth phase, which is characterized by high fat deposition, is shifted over time, so it is possible to link it to high body weight without worrying about lowering the carcass quality. Individual breeds differ from each other in the composition of intramuscular fat as well as the ratio between the different types of fibers. Late-maturing breeds such as Belgian Blue, Limousine, and Blonde d'Aquitaine are characterized by a better muscle tone and less fat (13) compared to those achieved by early-maturing breeds such as Angus. In addition, studies have shown a relationship of single-nucleotide polymorphism in candidate genes (calpastatin) with tenderness (14).

A unique feature of meat is its hydrophilicity, that is, the ability to bind and add water. Water absorption is a factor shaping the organoleptic characteristics of meat. During the ripening process, the ability of meat to bind water increases as a result of loosening the muscle protein grid (15).

The color of meat is one of the meat characteristics that are firstly evaluated by the consumer and, on this basis, shapes the image of the culinary applications of the meat (16). The color is a factor of the age of the animal, its nutrition, the conditions of keeping the animals before slaughtering, and the conditions of ripening. Meat becomes darker with age, changing color from red to dark red (15). Fresh beef should have a bright red color, which is mainly formed by the concentration and form of myoglobin and, to a lesser extent, by hemoglobin (the content in meat ranges from 6 to 16% of total heme coloration and mainly depends on the anatomical origin of the meat) and cytochrome c (17). Myoglobin (Mb) is a water-soluble hemoprotein that occurs in skeletal and cardiac muscles. Myoglobin concentration is determined by the species, breed, age, sex, feeding system, and physical activity of the animal. Cow muscles contain more myoglobin than heifers, bulls, or wolves. Myoglobin is at the level of 1–3 mg/g in muscles in calves, 6–10 mg/g in young cattle for slaughter, and 16–20 mg/g in cows for slaughter (18). Myoglobin occurs in three forms of redox: deoxymyoglobin (DMb), oxymyoglobin, and metmyoglobin (MMb). In turn, the redox form depends on the presence of a ligand connected to the iron atom of hem and on the value of iron (Fe^{2+}, Fe^{3+}). Deoxymyoglobin is a purple-red pigment which retains its form in fresh meat only at a low partial oxygen pressure of $<$1.4 mmHg. In the presence of oxygen, DMb is spontaneously oxidized to oxymyoglobin (19). When both ferrous myoglobin derivatives are oxidized to iron (Fe^{3+}), it is transformed into metmyoglobin. MMb is the most undesirable form of heme pigment in muscles both in the vital period and in the post-mortem period (20). The formation of MMb is maximal when the partial pressure of oxygen is about 4 mmHg (18). Metmyoglobin is reduced by a complex of MMb reductase, cytochrome b5, and NADH. It should be noted that higher physical activity in the vital period increases the reductase activity (19). The stabilization of meat color in the post-mortem period depends on the activity of MMb reductase, which is the highest in the temperature range of 30–37°C. Both the higher antioxidant potential of the meat and its storage in the dark increase its activity (18). In addition, the muscles differ in color stability, where the highest stability is attributed to m. longissimus dorsi, followed by m. semimembranosus and m. gluteus medium, and the lowest to m. psoas major. The structure of the muscle proteins is also important and is a function of pH values; a dark color is accompanied by higher pH values (18, 21).

The pH value of the meat reflects the changes that occur after slaughter, i.e., the degree of maturity of the meat and its durability and usefulness. The lactic acid formed during anaerobic glycogenolysis acidifies the environment, and this process may last until the glycogen stores are exhausted or glycolytic enzymes are inactivated by a low pH. During these transformations, the pH of meat decreases from 7.0 to 5.5–5.6. The glycogen content significantly determines the final pH of the meat and the degree of protein proteolysis. In addition, it significantly affects water absorption, fat emulsifiability, tenderness and juiciness, taste, and smell. If the pH value is lowered too quickly, meat with a watery structure (piles, soft, exudative meat) will occur (18). However, the slower rate of glycolysis and changes in pH is the reason for the occurrence of dark, firm, dry (DFD) meat. Post-mortem proteolysis during meat maturation is a function of pH and temperature (16). The degree of acidification of the meat mainly affects the extent of the proteolysis, while the temperature of the environment influences its rate. Transport and pre-slaughter stress are factors that significantly increase the glycogen levels in the muscles after slaughter. At pH24 (24 h after slaughter), values above 6.0 are considered to be typical of DFD meat. This meat has a limited shelf-life (it may spoil after 7 days of refrigerated storage), is susceptible to bacterial spoilage, and is not suitable for the production of durable products (18). In addition, the dark, unnatural color negatively affects the appearance of the meat. Too advanced processes of meat maturation accompanied by the multiplication of microflora lead to its rotting decomposition—such meat is not fit for consumption. The characteristic features of this process are the appearance of stickiness and mucus on the surface of the meat, a change in smell (the release of unpleasant gases with a scent of hydrogen sulfide and ammonia), a visible change in color to dark red with a greenish or yellow tinge, and a meat pH exceeding 6.5 (16–18). Additionally, Rutherford et al. (22) reported that the rumen temperature can be used as a predictor of meat quality. Bulls with a greater rumen temperature during the pre-slaughter phase produced meat with a significantly higher pH_{ult}. The flavor, quality, and composition

of beef changes with cattle diet regimen (2). The types of forage fed to cattle affect both the carcass characteristics and gains. Beef quality, including its fatty acid composition, has recently been the focus of the interest of many researchers and customers. The genetic variability in beef quality has been linked to differences between lines or breeds, variations due to the crossing of breeds, and variations between animals (23). Differences between many breeds of cattle have been reported for Red Angus and Simmental steers (24), Aberdeen Angus, Belgian Blue, and Limousine bulls (25) and for different double-muscle genotype bulls (26).

Structural changes in the connective tissue are associated with the activity of cathepsin enzymes (21). Calpaine activity is responsible for the alteration of the proteolytic cytoskeletal and regulatory proteins of myofiber (27). In the skeletal muscle of the animals, 3 major types of calpains have been identified: m-calpain, μ-calpain, and calpaina 3; μ-calpain activity decreases sharply in the first days after slaughter, while m-calpain activity is stable (28). The National Institutes of Health issued detailed recommendations on the intake of long-chain n-3 fatty acids, recommending that at least 650 mg/day C20:5 n-3 and C22:6 n-3, 2.22 g/day C18:3 n-3, and 4.44 g/day C18:2 n-6 should help reduce the risk of cardiovascular diseases (29). Although seafood is the main source of polyunsaturated fatty acid (PUFA) n-3 fatty acids in the human diet, studies clearly indicate that red meat can also be an excellent source.

It is the intent of this review to synthesize and summarize the currently available information about beef quality as well as to discuss the interpretation of the results.

DIETETIC PROPERTIES OF BEEF

The share of individual fatty acid families in bovine intramuscular fat is as follows: 38–44% are saturated fatty acids (SFA), 46% are monounsaturated fatty acids (MUFA), and 10% are PUFA (18). Studies have shown that C12:0, C14:0, and C16:0 have atherogenic properties, while C14:0, C16:0, and C18:0 have thrombogenic properties (30). MUFA as well as fatty acids from the families PUFA n-3 and PUFA n-6 have anti-atherogenic and antithrombogenic effects. The quality of meat varies, and that variability is determined by both individual and environmental factors: age, live weight, fatness degree, plane of nutrition, and concentrate/roughage ratio (18, 29, 31). Barton et al. (32) revealed that supplementation of sunflower seed increased the proportions of C18:2 n-6 and C18:2 *cis*-9 *trans*-11 and PUFA/SFA ratio and decreased the fatty acid atherogenicity in meat lipids. Pasture-finished cattle produce beef with a greater concentration of PUFA n-3 fatty acids than concentrate-fed cattle (33–35).

Crude glycerin can be used as a long-term substitute for barley meal in concentrations of up to 10% of dry matter in the diets of finishing bulls (36). The different quantities of glycerin in ruminants might be either converted to volatile fatty acids, especially butyrate and propionate at the expense of acetate, or directly absorbed from the digestive system and act as a gluconeogenesis precursor in the liver (37, 38). Glycerin supplementation may also improve forage digestibility and increase the production of microbial proteins in the rumen in a dose-dependent manner (39). Glycerin addition in ruminant diet has also been estimated in several studies with cattle (40–42), but the results for carcass characteristics and growth performance were inconclusive and ambiguous. The study of Barton et al. (36) showed that the partial replacement of barley with crude glycerine did not have a significant influence on the feed conversion ratio and daily gain of bulls. Similar to these results, Mach et al. (41) concluded that glycerine is a good energy ingredient replacement in the finishing diet of bulls, with no negative impact on feed efficiency and daily gains. Positive effects on feed efficiency and daily gains have been noted when dietary glycerin supplementation in steer and heifer finishing diets was included at <10% of dry matter (40, 42). Conversely, reduced feed efficiency and daily gains were noted when a diet containing 16% glycerin was used (42). Dietary glycerin supplementation did not change the carcass composition, slaughter characteristic, and chemical composition of musculus longissimus lumborum (MLL). However, it is noteworthy that all the fatness characteristics (internal fats, carcass separable fat, carcass fatness score, fat thickness on MLL, and petroleum ether extract of MLL) were numerically higher in glycerin-fed cattle (36).

The formation of the fatty acid profile is also related to the type of muscle. Studies have shown that the SFA concentration in femorsis biceps is more than 3 times higher than in semimembranous biceps. When analyzing the MUFA and PUFA contents, we can also see the advantage of biceps femorsis over semimembranous biceps (31).

INFLUENCE OF BREED ON BEEF AND CARCASS PROPERTIES

Breed differences in the muscle lipid fatty acid profile are often affected by the intramuscular fat content (due to differences in the fatty acid composition of the major muscle lipid fractions) (12, 16). Differences in the fatty acid composition of crossbred cattle were determined by genetic differences, rather than by differences in the content of intramuscular fat (43). Iwanowska and Pospiech (44) revealed that variations in cattle slaughter value can be as high between breeds as within a single breed; they found that the culinary meat amount obtained from carcasses may be increased by a modification in the carcass cutting system.

The musculature of an animal is influenced by many genes, one of which is the gene coding myostatin, whose polymorphism is associated with the occurrence of a double-muscled phenotype in Belgian Blue and Piemontese cattle. The Piemontese breed has a deletion of 11 nucleotides in exon 3 of the gene located on chromosome 2. This mutation caused the loss of 3 amino acids (275–277) in the polypeptide protein chain. Exon 3 has an open reading frame; the deletion caused it to move and create a stop codon after 287 amino acids. This led to a shortening of the protein chain and thus a loss of protein function (45). The relative increase in the number of fibers is observed in early pregnancy (46), with the results in the calf having almost twice as many muscle fibers at the time of birth. Belgian Blue animals have an

increased ability to convert feed into lean muscle and produce a higher percentage of the most desirable cuts of meat. These animals have less bone, less fat, and on average 20% more muscle compared with double-muscled (DBM) and normal Belgian Blue bulls, and it was found that the meat of DBM bulls contained about 3 times more PUFA content (27.5 vs. 11.3 g/100 g of FA) compared with normal animals (47).

The dietary and healthy benefits to humans are determined by the long-chain PUFA traits due to their anti-atherogenic, anti-inflammatory, and antithrombotic effects. Meat is one of the most nourishing dietary sources (48). The n-6/n-3 ratio is considered as a risk factor in coronary heart disease and cancer disease when it is higher than 4 (49). This indicator was significantly lower in the LCS (based on lucerne silage and legume–cereal mixture silage) bulls and well below the recommended maximum (34). A number of reports showed variations in beef cattle performance and carcass characteristics under similar production conditions due to breed effects in crossbreeding experiments (50–53). Barton et al. (5) evaluated the effects of breed on live weight gain, carcass composition, and slaughter characteristics, comparing these with those of Aberdeen Angus, Charolais, Hereford, and Simmental bulls. The target slaughter live weights were fixed at 550 kg for earlier-maturing breeds, i.e., Aberdeen Angus and Hereford, and at 630 kg for later-maturing breeds, i.e., Charolaise and Simmental. Charolaise and Simmental gained faster than Aberdeen Angus, while Hereford was intermediate. More valuable cuts were in Charolaise and Simmental. Hereford breed was characterized by the highest separable fat percentage. The thinnest subcutaneous fat over m. longissimus lumborumet thoracis was recorded in Charolaise and Simmental than in Aberdeen Angus and Hereford. The results of the experiment showed that earlier-maturing bulls had a lower live weight and produced more fat and less percentage of meat from high-priced cuts in comparison with later-maturing breeds.

Nogalski et al. (54) defined the impact of genotype and carcass conformation class on the slaughter quality of 200 young bulls. In this group were 108 crossbred bulls and 92 Holstein-Friesians (HF). They were slaughtered at the age of 21–22 months. The results of the classification placed 61.11% of crossbred beef bulls in R class (in EUROP system), and 56.53% of HF bulls were classified as O. Using the same conformation classes, the HF bulls were characterized by a lower slaughter quality than the crossbred beef bulls which had a higher content of fat by 0.42% and also better fatty acid composition of meat. The carcasses from too young cattle were characterized by a lower content of muscles, only slight marbling, and poor subcutaneous fat cover. According to Kaczmarek (55), early-maturing breeds like Hereford and Aberdeen Angus tend to deposit fat earlier and are intensively feed with concentrates, which causes their carcasses to be fatter. The late-maturing breeds, like Chianina, Charolaise, Limousine, or Piemontese, manifest a higher tendency to accumulate protein rather than fat. Those breeds are predisposed for intensive fattening due to their impressive daily weight gains. On the other hand, Nogalski et al. (34) concluded that crossbred animals had an advantage over HF bulls as exposed by the higher content of functional fatty acids in meat fat.

The physiological groups have a strong influence on the composition of carcass tissues (56). Heifers reach the finishing phase before steers, who, in turn, reach the finishing phase before bulls (57). Pogorzelska-Przybyłek et al. (58) reported that, in semi-intensive production systems, steers performed better than bulls, and HF × HH crosses were more suitable than HF × Limousin and HF × Charolais crosses. The quality of carcasses is influenced by two important factors, e.g., final body weight and age of the animals. Based on the slaughter value, Nogalski et al. (54) determined the most efficient finishing weight of young Polish Holstein Friesian × Limousine crossbred bulls and steers. Upon comparing the slaughter results of bulls and steers, it was shown that bulls have a better slaughter value, 1.07–2.60% higher percentage of carcass dressing, lower carcass fatness, and higher carcass conformation. On the other hand, Sharman et al. (59) showed that a moderate level of energy intake and lower sensitivity to changes in dietary protein levels weigh in favor of steers. Additionally, Blanco et al. (60) reported that fattening steers and especially heifers can lead to improved fat-related meat quality traits in lean breeds.

The slaughter performance and fattening of Polish Red Cattle bulls were investigated by Łappa et al. (61). They reported that the carcasses of animals 12 months of age contained 68.12% meat and 13.25% fat, while 15-month-old animals had 66.61% meat and 15.12% fat, respectively. Nahlik (62) reported that the carcasses of 15-month-old Polish Red bulls reached 71.01% meat and 12.24% fat. Oprzadek et al. (63) reported newer results for tissue composition of 12-month-old Polish Red bull carcasses which had 71.91% meat and 9.76% fat. The analysis of the Polish Red Cattle slaughter value shows similar traits to the Limousine breed (amount and quality of meat) and that it strongly exceeds that of the Hereford breed. Additionally, Pogorzelska-Przybyłek et al. (58) reported that dairy–beef crosses should be slaughtered at 21 months of age to improve the carcass quality.

The study carried out by Daszkiewicz and Wajda (64) showed that the dressing percentages of Black and White breed and Limousine breed were respectively, 50.22 and 61.84%. Monsón et al. (65) reported a similar result (61.40%) for the Limousine breed. Both results of Daszkiewicz and Wajda (66) and Monsón et al. (65) have been confirmed by Oprzadek et al. (63) in a study on 12-month-old bulls. The dressing percentage of Limousine was higher (59.25%) than the values obtained for Black and White (50.94%) and Hereford breeds (54.92%). Miciński et al. (67) reported 63.86% dressing percentage of the Limousine breed and 55.30% of the Hereford breed. As shown by Malau-Aduli et al. (68), in the adipose tissue of Limousine and Jersey cattle, the total MUFA content tended to increase with age.

Many researchers provide that the best moment to terminate the fattening of a herd is when the animals attain the so-called slaughtering maturity, i.e., best musculature and carcass tissue composition and developed culinary elements (66, 69). Feeds rich in proteins should be used during the most intensive muscle tissue development. It is not recommended to slaughter animals too early before they attain appropriate slaughter maturity.

INFLUENCE OF FEEDING SYSTEM ON BEEF AND CARCASS PROPERTIES

Differences in carcass composition between animals fed different diets can be attributed to the diet composition or the effect of growth rate. Bulls and steers fed concentrates, forage *ad libitum*, or finished on concentrates after grazing were slaughtered at a similar weight and had a similar dressing percentage and degree of fat cover (16). Garcia et al. (70) reported total CLA values in the longissimus dorsi muscle of 5.8 vs. 3.1 mg/g FAs in steers fed on pasture supplemented with cracked corn grain (1% live weight) compared to a corn-based concentrate with alfalfa hay. Additionally, Rutherford et al. (71) reported that a production system including a grazing period within bull beef production may be a more sustainable approach to producing Holstein bulls.

Other factors, such as nutrition, have also been found to influence the meat quality due to their regulatory effect on biological processes in muscle and on fat deposition (29, 32, 72). Various feeding strategies are often used to increase the content of PUFA n-3 fatty acid and to improve beef intramuscular PUFA n-6/PUFA n-3 ratio (2, 4, 73–77). The strategy for the rearing and feeding of cattle for slaughter should therefore aim at reducing the SFA content and increasing the PUFA and MUFA levels (18, 30). Cattle forage typically contain 1–4% lipids, mostly PUFA, including α-linoleic and acid linoleic acid (29). Fredriksson-Eriksson and Pickova (31) reported that a higher α-linoleic concentration in meat from pasture-fed bulls can be enhanced by its association with the thylakoid membranes in chloroplasts that can protect against ruminal biohydrogenation. Ground grass-fed beef had a greater concentration of C18:2 *cis*-9 *trans*-11 and C18:1 *trans*-11 (29, 31). French et al. (78) reported that decreasing the proportion of concentrate in the diet, which effectively increased grass intake, caused a linear decrease in the concentration of SFA and in the n-6/n-3 ratio and a linear increase in the PUFA/SFA ratio.

Replacement maize silage with alfalfa silage and legume–cereal mixture silage conspicuously increased the C18:3n-3 dietary intake (32). Nogalski et al. (34) reported that the low proportion of PUFA in the FA profile could be related to the age of bulls at slaughter (21–22 months). The PUFA content of intramuscular fat in m. longissimus dorsi decreases with age, reaching 25.5% at 7 months, 18.4% at 14 months, and 13.6% at 19 months (79). The recommended PUFA n-6/PUFA n-3 ratio by the FAO and WHO is around 5.0 (15). The introduction of supplements rich in PUFA (80–82) prevents or minimizes biohydrogenation and affects the carcass characteristics (83). Albertí et al. (84) found that addition of 5% linseed decreased the dressing rate without changing the daily gain or classification of carcasses. Additionally, a lower n-6/n-3 fatty acid ratio has been observed in muscle from grass-fed animals compared to that in concentrate-fed animals (32).

Murphy et al. (85) reported that increased toe net growth does not adversely affect the walking ability. Despite the greater toe net growth in bulls accommodated on rubber flooring, there was no effect of floor type on locomotion score, suggesting that the increased toe net growth does not adversely affect the walking ability.

EFFECT OF SEX ON BEEF AND CARCASS QUALITY

The research carried out by Bureš and Barton (86) showed the impact of the sex and age of slaughtered animals on carcass composition, feed intake, growth, and quality of MLL meat on Simmental × Charolaise heifers and bulls. The results showed that the body weight of the bulls increased, while the daily dry matter consumption was higher. They obtained a significant interaction between sex × slaughter age and feed conversion ratio which decreased in older heifers. The bull carcasses were leaner with a higher total meat proportion. Bull carcasses obtained a higher proportion of the high-priced shoulder meat, and heifer carcasses had a better meat proportion of loin and rump. The proportion of bones and high-priced meat has decreased with the age of animals, whose carcasses were also fatter. Bulls had less dry matter, proteins, and intramuscular fat and more collagen than heifers.

Richardson and Herd (87) indicate differences between age and sex groups in terms of feed conversion ratio, which is caused by a few biological mechanisms, e.g., protein turnover, different body composition, or tissue metabolism of animals. The higher internal fat deposition in the heifer group determined a lower killing-out proportion. The same conclusions were reported by Steen (88), Frickh et al. (89), and Velik et al. (90). The fatness characteristics were affected by slaughter age and sex. Bulls had a lower proportion of fat in their body composition than heifers. Both groups produced more fat with increasing age; however, this trend was more intense for heifers.

The different meat distribution in bull and heifer carcasses showed a more intensive meat expansion in the forequarter in bulls and hindquarter in heifers. The respective research of Steen and Kilpatrick (91) and Link et al. (92) comparing the carcasses of different breeds of bulls and heifers were in agreement with the results of Bureš and Barton (86). With age, the proportions of high-value meat are decreasing, causing a fall of high/low-priced meat ratio, e.g., the MLL content per 100 kg of slaughter weight is smaller; the fat content is also higher with age. Harper and Pethick (93) documented the influence of sex hormones on intramuscular adipocyte development. This study showed almost twice higher intramuscular fat content in heifers (petroleum ether extract) than in bulls of the same age. The papers discussed have shown significant differences between both sexes slaughtered at two fixed ages in terms of performance, parameters of meat quality, and carcass traits. The heifers grew slower and less effectively, had a lower killing-out proportion, and produced fatter carcasses with a lower total meat proportion than the bulls. The MLL of bulls compared to heifers contained more intramuscular fat, less protein, less dry matter, and more total collagen, which was assessed by the sensory panel as more acceptable. The increase of slaughter age by 4 months resulted, especially in heifers, in reduced daily gain and feed conversion ratio as well as markedly higher fatness characteristics. Therefore,

such an extension of the finishing period could not be considered advantageous for Charolaise × Simmental heifers fed a high-energy diet. Shifting the term of slaughter for 4 months caused a decrease of feed conversion and daily gains, especially in the heifer group. Therefore, application of high-energy diet in the finishing period was not efficient to Charolaise × Simmental heifers. Additionally, Prado et al. (94) reported that the finishing of young bulls in feedlot is to be recommended since the animals produce carcasses with higher amounts of edible meat and higher yields of commercial cuts, thus allowing for a better price for the carcass.

Many researchers (6, 95, 96) indicate sex as an important factor causing differences in meat quality. Additionally, heifer carcasses also have a higher fat/meat proportion (97, 98).

CONCLUSION

There is a well-recognized impact of breed on lipid metabolism in tissues and dietary fatty acid content in bovine muscles. Based on the literature reviewed, it can be concluded that the quality of beef is largely related to sex, age of the slaughtered animals, and feeding system. All of these factors must be taken into consideration when addressing improvements to the nutritional quality of beef.

AUTHOR CONTRIBUTIONS

TS: contributed to conceptualization, searching of literature, writing—original draft, writing—review and editing, project administration, and supervision. KP: contributed to conceptualization, writing—original draft, and writing—review and editing. MG, JS, PK, and PS: contributed to searching of literature. GG: contributed to visualization. All authors read and approved the final manuscript.

FUNDING

The authors acknowledge the financial support for this project provided by transnational funding bodies, being partners of the FP7 ERA-net project, CORE Organic Plus, and European Commission co-fund.

REFERENCES

1. Listrat A, Lebret B, Louveau I, Astruc T, Bonnet M, Lefaucheur L, et al. How muscle structure and composition influence meat and flesh quality. *Sci World J.* (2016) 2016:3182746. doi: 10.1155/2016/3182746
2. Chail A. *Effects of Beef Finishing Diets and Muscle Type on Meat Quality, Fatty Acids and Volatile Compounds*. Master of Science, Utah State University Logan, Utah (2015).
3. Domaradzki P, Florek M, Litwińczuk A. Czynniki kształtujace jakość miesa wołowego. *Wiadom. Zootech.* (2016). p. 160–70.
4. Barton L, Marounek M, Kudrna V, Bureš D, Zahradkova R. Growth performance and fatty acid profiles of intramuscular and subcutaneous fat from Limousin and Charolais heifers fed extruded linseed. *Meat Sci.* (2007) 76:517–23. doi: 10.1016/j.meatsci.2007.01.005
5. Barton L, Rehak D, Teslik V, Bures D, Zahradkova R. Effect of breed on growth performance and carcass composition of Aberdeen Angus, Charolais, Hereford and Simmental bulls. *Czech J Anim Sci.* (2006) 51:47–53. doi: 10.17221/3908-CJAS
6. Jurczak ME. *Towaroznawstwo produktów* zwierzecych: ocena jakości miesa. Wydaw. SGGW (2004).
7. Gigli S, Failla S, Iacurto M, Contò M, Sañudo C, Olleta J, et al. Performance at slaughter and beef quality characteristics of some Mediterranean beef breeds compared to Central and North European breeds (GemQual EU Project). In: *Proceedings of Seminar of the Scientific Professional Network on Mediterranean Livestock Farming (RME)*. (2006). p. 173–82.
8. Pesonen M, Honkavaara M, Huuskonen AK. of breed on production, carcass traits and meat quality of Aberdeen Angus, Limousin and Aberdeen Angus × Limousin bulls offered a grass silage-grain-based diet. *Agric Food Sci.* (2012) 21:361–9. doi: 10.23986/afsci.6520
9. Duckett S, Neel J, Lewis RM, Fontenot J, Clapham W. Effects of forage species or concentrate finishing on animal performance, carcass and meat quality. *J Anim Sci.* (2013) 91:1454–67. doi: 10.2527/jas.2012-5914
10. Wu G, Cross H, Gehring K, Savell J, Arnold A, McNeill S. Composition of free and peptide-bound amino acids in beef chuck, loin, round cuts. *J Anim Sci.* (2016) 94:2603–13. doi: 10.2527/jas.2016-0478
11. Listrat A, Pissavy AL, Micol D, Jurie C, Lethias C, David P, et al. Collagens XII and XIV: two collagen types both associated with bovine muscle and intramuscular lipid metabolism. *Livestock Sci.* (2016) 187:80–6. doi: 10.1016/j.livsci.2016.02.009
12. De Smet S, Raes K, Demeyer D. Meat fatty acid composition as affected by fatness and genetic factors: a review. *Anim Res.* (2004) 53:81–98. doi: 10.1051/animres:2004003
13. Keane MG. *Relative Tissue Growth Patterns and Carcass Composition in Beef Cattle; Teagasc*. (2011). Available online at: http://hdl.handle.net/11019/1183
14. Calvo JH, Iguacel LP, Kirinus JK, Serrano M, Ripoll G, Casasus I, et al. A new single nucleotide polymorphism in the calpastatin (CAST) gene associated with beef tenderness. *Meat Sci.* (2014) 96:775–82. doi: 10.1016/j.meatsci.2013.10.003
15. Kołczak T. *Beef Quality. Zywność. Nauka. Technologia. Jakość*. (2008) 56, 5–22.
16. Przysucha T, Abramowicz P, Balcerak M, Brzozowski P, Gołebiewski M, Grodzki H, et al. *Miesne uzytkowanie bydła; Wydawnictwo* SGGW,Warszawa (2018).
17. Hunt M, Hedrick H. Chemical, physical and sensory characteristics of bovine muscle from four quality groups. *J Food Sci.* (1977) 42:716–20. doi: 10.1111/j.1365-2621.1977.tb12586.x
18. Mohan A. *Myoglobin Redox Form Stabilization: Role of Metabolic Intermediates and NIR Detection*. Kansas State University (2009).
19. Mancini R, Hunt M. Research in meat color. *Meat Sci.* (2005) 71:100–21. doi: 10.1016/j.meatsci.2005.03.003
20. McKenna D, Mies P, Baird B, Pfeiffer K, Ellebracht J, Savell J. Biochemical and physical factors affecting discoloration characteristics of 19 bovine muscles. *Meat Sci.* (2005) 70:665–82. doi: 10.1016/j.meatsci.2005.02.016
21. Khan MI, Jung S, Nam KC, Jo C. Postmortem aging of beef with a special reference to the dry aging. *Kor J Food Sci Anim Resour.* (2016) 36:159–69. doi: 10.5851/kosfa.2016.36.2.159
22. Rutherford NH, Lively FO, Arnott G. Evaluation of rumen temperature as a novel indicator of meat quality: rumen temperature, and haematological indicators of stress during the pre-slaughter period as predictors of instrumental meat quality in bulls. *Meat Sci.* (2019) 158:107913. doi: 10.1016/j.meatsci.2019.107913
23. Garcia PT, Casal JJ. Effect of dietary plant lipids on conjugated linoleic acid (CLA) concentrations in beef and lamb meats. In: El-Shemy HA, editor. *Soybean—Bio-Active Compounds*. Vienna: InTech (2013). p. 135–59. doi: 10.5772/52608
24. Laborde FL, Mandell IB, Tosh JJ, Wilton JW, Buchanan-Smith JG. Breed effects on growth performance, carcass characteristics, fatty acid composition, and palatability attributes in finishing steers. *J Anim Sci.* (2001) 79:355–65. doi: 10.2527/2001.792355x

25. Cuvelier C, Clinquart A, Hocquette JF, Cabaraux JF, Dufrasne I, Istasse L, et al. Comparison of composition and quality traits of meat from young finishing bulls from Belgian Blue, Limousin and Aberdeen Angus breeds. *Meat Sci.* (2006) 74:522–31. doi: 10.1016/j.meatsci.2006.04.032
26. Aldai N, Dugan MER, Najera AI, Osoro K. N-6 and n-3 fatty acids in different beef adipose tissues depending on the presence or absence of the gene responsible for double-muscling. *Czech J Anim Sci.* (2008) 53:515–22. doi: 10.17221/365-CJAS
27. Sensky P, Parr T, Bardsley R, Buttery P. The relationship between plasma epinephrine concentration and the activity of the calpain enzyme system in porcine longissimus muscle. *J Anim Sci.* (1996) 74:380–7. doi: 10.2527/1996.742380x
28. Pandurangan M, Hwang I. The role of calpain in skeletal muscle. *Anim Cells Syst.* (2012) 16:431–7. doi: 10.1080/19768354.2012.724708
29. Leheska J, Thompson L, Howe J, Hentges E, Boyce J, Brooks J, et al. Effects of conventional and grass-feeding systems on the nutrient composition of beef. *J Anim Sci.* (2008) 86:3575–85. doi: 10.2527/jas.2007-0565
30. de Almeida JC, Perassolo MS, Camargo JL, Bragagnolo N, Gross JL. Fatty acid composition and cholesterol content of beef and chicken meat in Southern Brazil. *Revist Brasileira Ciênc Farmacêut.* (2006) 42:109–17. doi: 10.1590/S1516-93322006000100012
31. Fredriksson-Eriksson SF, Pickova J. Fatty acids and tocopherol levels in M. Longissimus dorsi of beef cattle in Sweden–A comparison between seasonal diets. *Meat Sci.* (2007) 76:746–54. doi: 10.1016/j.meatsci.2007.02.021
32. Barto,n L, Marounek M, Kudrna V, Bures D, Zahradkova R. Growth, carcass traits, chemical composition and fatty acid profile in beef from Charolais and Simmental bulls fed different types of dietary lipids. *J Sci Food Agric.* (2008) 88:2622–30. doi: 10.1002/jsfa.3381
33. Dewhurst RJ, Scollan ND, Lee MR, Ougham HJ, Humphreys MO. Forage breeding and management to increase the beneficial fatty acid content of ruminant products. *Proc Nutr Soc.* (2003) 62:329–36. doi: 10.1079/PNS2003241
34. Nogalski Z, Wroński M, Wielgosz-Groth Z, Purwin C, Sobczuk-Szul M, Mochol M, et al. The Effect of Carcass Conformation Class (Europ System) on the Slaughter Quality of Young Crossbred Beef Bulls and Holstein-Friesians/Porównanie wartości rzeznej buhajków mieszańców miesnych i holsztyno-fryzów w zalezności od klasy uformowania w systemie EUROP. *Ann Anim Sci.* (2013) 13:121–31. doi: 10.2478/v10220-012-0064-9
35. Barto,n L, Bures D, Kudrna V. Meat quality and fatty acid profile of the musculus longissimus lumborum in Czech Fleckvieh, Charolais and Charolais x Czech Fleckvieh bulls fed different types of silages. *Czech J Anim Sci.* (2010) 55:479–87. doi: 10.17221/1713-CJAS
36. Barton L, Bures D, Homolka P, Jancik F, Marounek M, Rehak D. Effects of long-term feeding of crude glycerine on performance, carcass traits, meat quality, and blood and rumen metabolites of finishing bulls. *Livestock Sci.* (2013) 155:53–9. doi: 10.1016/j.livsci.2013.04.010
37. Krehbiel C. Ruminal and physiological metabolism of glycerin. *J Anim Sci.* (2008) 86:392.
38. Rémond B, Souday E, Jouany J. *In vitro* and *in vivo* fermentation of glycerol by rumen microbes. *Anim Feed Sci Technol.* (1993) 41:121–32. doi: 10.1016/0377-8401(93)90118-4
39. Wang C, Liu Q, Huo W, Yang W, Dong K, Huang Y, et al. Effects of glycerol on rumen fermentation, urinary excretion of purine derivatives and feed digestibility in steers. *Livestock Sci.* (2009) 121:15–20. doi: 10.1016/j.livsci.2008.05.010
40. Pyatt N, Doane P, Cecava M. Effect of crude glycerin in finishing cattle diets. *Proc J Dairy Sci.* (2007) 85:412.
41. Mach N, Bach A, Devant M. Effects of crude glycerin supplementation on performance and meat quality of Holstein bulls fed high-concentrate diets. *J Anim Sci.* (2009) 87:632–8. doi: 10.2527/jas.2008-0987
42. Parsons G, Shelor M, Drouillard J. Performance and carcass traits of finishing heifers fed crude glycerin. *J Anim Sci.* (2009) 87:653–7. doi: 10.2527/jas.2008-1053
43. Graham J, Bernaud E, Deland M. Sire and dam breed effects on fatty acid profiles in the longissimus dorsi muscle and subcutaneous fat of beef cattle. *Aust J Exp Agric.* (2006) 46:913–9. doi: 10.1071/EA05301
44. Iwanowska A, Pospiech E. Comparison of slaughter value and muscle properties of selected cattle breeds in Poland–Review. *Acta Sci Polonor Tech Alimentar.* (2010) 9:7–22.
45. Dunner S, Miranda ME, Amigues Y, Cañón J, Georges M, Hanset R, et al. Haplotype diversity of the myostatin gene among beef cattle breeds. *Genet Sel Evol.* (2003) 35:103–18. doi: 10.1186/1297-9686-35-1-103
46. Swatland H, Kieffer NM. Fetal development of the double muscled condition in cattle. *J Anim Sci.* (1974) 38:752–7. doi: 10.2527/jas1974.384752x
47. Raes K, De Smet S, Demeyer D. Effect of double-muscling in Belgian Blue young bulls on the intramuscular fatty acid composition with emphasis on conjugated linoleic acid and polyunsaturated fatty acids. *Anim Sci.* (2001) 73:253–60. doi: 10.1017/S1357729800058227
48. Givens DI, Khem KE, Gibbs RA. The role of meat as a source of n-3 polyunsaturated fatty acids in the human diet. *Meat Sci.* (2006) 74:209–18. doi: 10.1016/j.meatsci.2006.04.008
49. Webb EC, O'Neill H. The animal fat paradox and meat quality. *Meat Sci.* (2008) 80:28–36. doi: 10.1016/j.meatsci.2008.05.029
50. Kogel J, Pickl M, Rott J, Hollwich W, Sarreiter R, Mehler N. Crossbreeding trial with Charolais, Blond d'Aquitaine and Limousin on Fleckvieh cows - 2nd communication: Carcass yield and carcass quality. *Zuchtungskun.* (2000) 72:201–16.
51. Wheeler T, Cundiff L, Shackelford S, Koohmaraie M. Characterization of biological types of cattle (Cycle VII): Carcass, yield, and longissimus palatability traits. *J Anim Sci.* (2005) 83:196–207. doi: 10.2527/2005.831196x
52. Hyslop JJ, Keatinge R, Chapple DG. Voluntary food intake, live-weight gain, carcass quality and food conversion in contrasting genotypes of weaned suckler-bred bulls finished intensively on a cereal-based diet. *Anim Sci.* (2006) 82:117–24. doi: 10.1079/ASC20054
53. Steinwidder A, Guggenberger T, Schauer A, Roemer A, Ibi G, Frickh J. Effect of ration, sex and breeding on fattening performance of cattle from suckler cow systems. *Zuchtungskun.* (2007) 79:128–41.
54. Nogalski Z, Wielgosz-Groth Z, Purwin C, Sobczuk-Szul M, Mochol M, Pogorzelska-Przybylek P, et al. Effect of slaughter weight on the carcass value of young crossbred ('Polish Holstein Friesian' x 'Limousin') steers and bulls. *Chilean J Agric Res.* (2014) 74:59–66. doi: 10.4067/S0718-58392014000100010
55. Kaczmarek A. *Hodowla i chów bydła*. Poznań AR: Poznań (1994).
56. Aricetti JA, Rotta, P. P.;,Prado RM, Perotto D, Moletta JL, Matsushita M, et al. Carcass characteristics, chemical composition and fatty acid profile of Longissimus muscle of bulls and steers finished in a pasture system bulls and steers finished in pasture systems. *Asian Australas. J Anim. Sci.* (2008) 21:1441–8. doi: 10.5713/ajas.2008.80061
57. Rotta PP, Prado RM, Prado IN, Valero MV, Visentainer JV, Silva RR. The effects of genetic groups, nutrition, finishing systems and gender of Brazilian cattle on carcass characteristics and beef composition and appearance: a review. *Asian Austr J Anim Sci.* (2009) 22:1718–34. doi: 10.5713/ajas.2009.90071
58. Pogorzelska-Przybyłek P, Nogalski Z, Sobczuk-Szul M, Purwin C, Momot M. Carcass characteristics of grass-fed crossbred bulls and steers slaughtered at two different ages. *Can J Anim Sci.* (2018) 98:376–85. doi: 10.1139/cjas-2017-0148
59. Sharman ED, Lancaster PA, McMurphy CP, Garmyn AJ, Pye BJ, Mafi GG, et al. Effect of rate of body weight gain in steers during the stocker phase. I. Growth, partitioning of fat among depots, and carcass characteristics of growing-finishing beef cattle. *J Anim Sci.* (2013) 91:4322–35. doi: 10.2527/jas.2012-5440
60. Blanco M, Ripoll G, Delavaud C, Casasús I. Performance, carcass and meat quality of young bulls, steers and heifers slaughtered at a common body weight. *Livest Sci.* (2020) 240:104156. doi: 10.1016/j.livsci.2020.104156
61. Lappa H, Romer J, Lewinska L. Porownanie przydatnosci opasowej i rzeznej buhajkow rasy czarno-bialej, czerwono-bialej, polskiej czerwonej i mieszancow dc X pc opasanych do wieku 12 i 15 miesiecy. *Rocz Nauk Rol.* (1975) 96-B-4:23–39.
62. Nahlik KJ. *Wpływ krzyzowania bydła polskiego czerwonego z bydłem czerwono-białym i simentalskim na przydatność opasowa i rzezna mieszańców pokolenia F1*. (1973). Państwowe Wydawnictwo Rolnicze i Leśne.
63. Oprzadek J, Dymnicki E, Reklewski Z. Zmiany tempa wzrostu i skladu tkankowego tuszy mlodego bydla w zaleznosci od rasy. *Rocz Nauk Polskiego Tow Zootech.* (2007) 3:103–9.

64. Daszkiewicz T, Wajda S. Masa przedubojowa buhajkow a ich wydajnosc rzezna i jakosc miesa. *Gospodar Mies*. (2002) 54:16–8.
65. Monson F, Sanudo C, Sierra I. Influence of breed and ageing time on the sensory meat quality and consumer acceptability in intensively reared beef. *Meat Sci.* (2005) 71:471–9. doi: 10.1016/j.meatsci.2005.04.026
66. Daszkiewicz T, Wajda S. Wartość rzezna oraz jakość miesa buhajków rasy czarno-białej i limousine. *Rocz Instyt Przem Miesn Tłuszcz*. (2002) 39:57–65.
67. Micinski J, Klupczynski J, Ostoja H, Cierach M, Dymnicka M, Lozicki A, et al. Wplyw rasy i zywienia buhajkow na wyniki klasyfikacji ich tusz w systemie EUROP oraz na ocene tekstury miesa. *Zywn Nauk Tech Jak Sup*. (2005) 3:147–56.
68. Malau-Aduli A, Siebert B, Bottema C, Pitchford W. A comparison of the fatty acid composition of triacylglycerols in adipose tissue from Limousin and Jersey cattle. *Aust J Agric Res.* (1997) 48:715–22. doi: 10.1071/A96083
69. Brzozowski P. *Technologie produkcji zywca wołowego*. Hortpress, Warszawa (2006).
70. Garcia PT, Pensel NA, Sancho AM, Latimori NJ, Kloster AM, Amigone MA, et al. Beef lipids in relation to animal breed and nutrition in Argentina. *Meat Sci.* (2008) 79:500–8. doi: 10.1016/j.meatsci.2007.10.019
71. Rutherford NH, Gordon AW, Arnott G, Lively FO. The effect of beef production system on the health, performance, carcass characteristics, and meat quality of Holstein Bulls. *Animals.* (2020) 10:1922. doi: 10.3390/ani10101922
72. Scollan N, Hocquette JF, Nuernberg K, Dannenberger D, Richardson I, Moloney A. Innovations in beef production systems that enhance the nutritional and health value of beef lipids and their relationship with meat quality. *Meat Sci.* (2006) 74:17–33. doi: 10.1016/j.meatsci.2006.05.002
73. French P, O'riordan E, Monahan F, Caffrey P, Vidal M, Mooney M, et al. Meat quality of steers finished on autumn grass, grass silage or concentrate-based diets. *Meat Sci*. (2000) 56:173–80. doi: 10.1016/S0309-1740(00)00037-1
74. Choi N, Enser M, Wood J, Scollan N. Effect of breed on the deposition in beef muscle and adipose tissue of dietary n-3 polyunsaturated fatty acids. *Anim Sci.* (2000) 71:509–19. doi: 10.1017/S1357729800055417
75. Vatansever L, Kurt E, Enser M, Nute G, Scollan N, Wood J, et al. Shelf life and eating quality of beef from cattle of different breeds given diets differing in n-3 polyunsaturated fatty acid composition. *Anim Sci.* (2000) 71:471–82. doi: 10.1017/S135772980005548X
76. French P, O'riordan E, Monahan F, Caffrey P, Mooney M, Troy D, et al. The eating quality of meat of steers fed grass and/or concentrates. *Meat Sci.* (2001) 57:379–86. doi: 10.1016/S0309-1740(00)00115-7
77. Lourenco M, Van Ranst G, Vlaeminck B, De Smet S, Fievez V. Influence of different dietary forages on the fatty acid composition of rumen digesta as well as ruminant meat and milk. *Anim Feed Sci Technol.* (2008) 145:418–37. doi: 10.1016/j.anifeedsci.2007.05.043
78. French P, Stanton C, Lawless F, O'riordan E, Monahan F, Caffrey P, et al. Fatty acid composition, including conjugated linoleic acid, of intramuscular fat from steers offered grazed grass, grass silage, or concentrate-based diets. *J Anim Sci*. (2000) 78:2849–55. doi: 10.2527/2000.78112849x
79. Lengyel Z, Husvéth F, Polgár P, Szabó F, Magyar L. Fatty acid composition of intramuscular lipids in various muscles of Holstein-Friesian bulls slaughtered at different ages. *Meat Sci.* (2003) 65:593–8. doi: 10.1016/S0309-1740(02)00252-8
80. Puppel K. *The Influence of Fish Oil and Linseed Supplementation on the Fat and the Protein Fraction Content of Cow's Milk*. Doctoral Thesis, SGGW, Warszawa (2011).
81. Puppel K, Nalecz-Tarwacka T, Kuczynska B, Golebiewski M, Kordyasz M, Grodzki H. The age of cows as a factor shaping the antioxidant level during a nutritional experiment with fish oil and linseed supplementation for increasing the antioxidant value of milk. *J Sci Food Agric.* (2012) 92:2494–9. doi: 10.1002/jsfa.5658
82. Puppel K, Kuczynska B, Nalecz-Tarwacka T, Grodzki H. Influence of linseed variety on fatty acid profile in cow's milk. *J Sci Food Agric.* (2013) 93:2276–80. doi: 10.1002/jsfa.6037
83. Castro T, Manso T, Mantecón A, Guirao J, Jimeno V. Fatty acid composition and carcass characteristics of growing lambs fed diets containing palm oil supplements. *Meat Sci.* (2005) 69:757–64. doi: 10.1016/j.meatsci.2004.11.008
84. Albert,í P, Beriain MJ, Ripoll G, Sarriés V, Panea B, Mendizabal JA, et al. Effect of including linseed in a concentrate fed to young bulls on intramuscular fatty acids and beef color. *Meat Sci.* (2014) 96:1258–65. doi: 10.1016/j.meatsci.2013.11.009
85. Murphy VS, Lowe DE, Lively FO, Gordon AW. The impact of floor type on lameness and hoof health of dairy origin bulls. *Animal.* (2018) 12:2382–90. doi: 10.1017/S1751731118000095
86. Bures D, Barton L. Growth performance, carcass traits and meat quality of bulls and heifers slaughtered at different ages. *Czech J Anim Sci.* (2012) 57:34–43. doi: 10.17221/5482-CJAS
87. Richardson E, Herd R. Biological basis for variation in residual feed intake in beef cattle. 2. Synthesis of results following divergent selection. *Aust J Exp Agric.* (2004) 44:431–40. doi: 10.1071/EA02221
88. Steen R. The effect of plane of nutrition and slaughter weight on growth and food efficiency in bulls, steers and heifers of three breed crosses. *Livestock Prod Sci.* (1995) 42:1–11. doi: 10.1016/0301-6226(95)00002-3
89. Frickh J, Steinwidder A, Baumung R. Effect of ration, sex and slaughter weight on slaughtering performance of Simmental cattle. *Zuchtungskun.* (2002) 74:362–75.
90. Velik M, Forschungszentrum LR, Steinwidder A, Frickh J. Effect of ration, sex, and breed on carcass performance and meat quality of cattle from suckler cow systems. In: *Proceedings of 17 International Science Symposium on Nutrition of Domestic Animals' Zadravec-Erjavec Days' (17. Mednarodno znanstveno posvetovanje o prehrani domaèih ¾ivali'Zadravèevi-Erjavèevi dnevi')*, Radenci, 13-14 Nov 2008 (2008).
91. Steen RW, Kilpatrick DJ. Effects of pasture grazing or storage feeding and concentrate input between 5.5 and 11 months of age on the performance and carcass composition of bulls and on subsequent growth and carcass composition at 620 kg live weight. *Anim Sci.* (1998) 66:129–41. doi: 10.1017/S1357729800008900
92. Link G, Willeke H, Golze M, Bergfeld U. Fattening- and slaughter performance of bulls and heifers of beef breeds and the cross PF breed German Angus x Simmental. *Archiv Tierzucht-Archiv Anim Breed.* (2007) 50:356–62. doi: 10.5194/aab-50-356-2007
93. Harper G, Pethick D. How might marbling begin? *Aust J Exp. Agric.* (2004) 44:653–62. doi: 10.1071/EA02114
94. Prado IN, Passetti RA, Rivaroli DC, Ornaghi MG, de Souza KA, Carvalho CB, et al. Carcass composition and cuts of bulls and steers fed with three concentrate levels in the diets. *Asian-Australas J Anim Sci.* (2015) 28:1309–16. doi: 10.5713/ajas.15.0021
95. Cepin S, Cepon M. Genetic and environmental influences on carcass and meat quality of beef. *Tehnol Mesa.* (2001) 42:283–94.
96. Wajda S, Daszkiewicz T. Kulinarne mieso wolowe i ocena jego wlasciwosci organoleptycznych. *Gospod Mięs.* (2001) 53:18–22.
97. Sack E, Scholz W. Schlachtkörperzusammensetzung beim Rind. *Kulmbacher Reihe.* (1987) 7:87–117.
98. Pisula A, Tyburcy A, Dasiewicz K. Czynniki decydujace o jakości miesa wołowego. *Gospod Mies.* (2007) 1:4–11.

Conflict of Interest: The authors declare that the research was conducted in the absence of any commercial or financial relationships that could be construed as a potential conflict of interest.

Publisher's Note: All claims expressed in this article are solely those of the authors and do not necessarily represent those of their affiliated organizations, or those of the publisher, the editors and the reviewers. Any product that may be evaluated in this article, or claim that may be made by its manufacturer, is not guaranteed or endorsed by the publisher.

frontiers in Genetics

ORIGINAL RESEARCH
published: 31 March 2022
doi: 10.3389/fgene.2022.844833

Comparative Transcriptome Analysis Provides Insight into Spatio-Temporal Expression Characteristics and Genetic Regulatory Network in Postnatal Developing Subcutaneous and Visceral Fat of Bama Pig

Yingying Zhang[1,2], Hongyang Wang[1,2], Weilong Tu[1,2], Sayed Haidar Abbas Raza[3], Jianguo Cao[1,2], Ji Huang[1,2], Huali Wu[1,2], Chun Fan[4], Shengchang Wang[4], Ying Zhao[4] and Yongsong Tan[1,2]**

[1]Institute of Animal Husbandry and Veterinary Science, Shanghai Academy of Agricultural Sciences, Shanghai, China, [2]Shanghai Engineering Research Center of Breeding Pig, Shanghai, China, [3]College of Animal Science and Technology, Northwest A&F University, Yangling, China, [4]Shanghai Laboratory Animal Research Center, Shanghai, China

OPEN ACCESS

Edited by:
Min Du,
Washington State University,
United States

Reviewed by:
Chengchi Fang,
Huazhong Agricultural University,
China
Ali Raza Jahejo,
Shanxi Agricultural University, China
Rui-Si Hu,
University of Electronic Science and Technology of China, China
Rajwali Khan,
University of Agriculture, Pakistan
Yalan Yang,
Agricultural Genomics Institute at Shenzhen (CAS), China

***Correspondence:**
Yingying Zhang
zyy686868@163.com
Yongsong Tan
typine@163.com

Specialty section:
This article was submitted to Livestock Genomics, a section of the journal Frontiers in Genetics

Received: 28 December 2021
Accepted: 04 March 2022
Published: 31 March 2022

Citation:
Zhang Y, Wang H, Tu W, Abbas Raza SH, Cao J, Huang J, Wu H, Fan C, Wang S, Zhao Y and Tan Y (2022) Comparative Transcriptome Analysis Provides Insight into Spatio-Temporal Expression Characteristics and Genetic Regulatory Network in Postnatal Developing Subcutaneous and Visceral Fat of Bama Pig. Front. Genet. 13:844833. doi: 10.3389/fgene.2022.844833

The depot differences between Subcutaneous Fat (SAF) and Visceral Fat (VAF) are critical for human well-being and disease processes in regard to energy metabolism and endocrine function. Miniature pigs (*Sus scrofa*) are ideal biomedical models for human energy metabolism and obesity due to the similarity of their lipid metabolism with that of humans. However, the regulation of differences in fat deposition and development remains unclear. In this study, the development of SAF and VAF was characterized and compared in Bama pig during postnatal development (infancy, puberty and adulthood), using RNA sequencing techniques (RNA-Seq). The transcriptome of SAF and VAF was profiled and isolated from 1-, 3- and 6 months-old pigs and identified 23,636 expressed genes, of which 1,165 genes were differentially expressed between the depots and/or developmental stages. Upregulated genes in SAF showed significant function and pathway enrichment in the central nervous system development, lipid metabolism, oxidation-reduction process and cell adhesion, whereas genes involved in the immune system, actin cytoskeleton organization, male gonad development and the hippo signaling pathway were preferentially expressed in VAF. Miner analysis of short time-series expression demonstrated that differentiation in gene expression patterns between the two depots corresponded to their distinct responses in sexual development, hormone signaling pathways, lipid metabolism and the hippo signaling pathway. Transcriptome analysis of SAF and VAF suggested that the depot differences in adipose tissue are not

Abbreviations: DEGs, differentially expressed genes; FPKM, fragments per kilobase of exon model per Million mapped fragments; GO, gene ontology; HSL, hormone sensitive lipase; IL-6, interleukin-6; IL-8, interleukin-8; IMF, intramuscular fat; Ips, pluripotent stem; IPA, ingenuity pathway analysis; KEGG, Kyoto Encyclopedia of Genes and Genomes; MCP-1, macrophage chemoattractant protein-1; Qrt-PCR, quantitative real-time polymerase chain reaction; RNA-Seq, RNA sequencing technologies; STEM, Short time-series expression miner; SAF, subcutaneous fat; VAF, visceral fat.

only related to lipid metabolism and endocrine function, but are closely associated with sexual development and organ size regulation.

Keywords: Bama pig, subcutaneous fat, visceral fat, transcriptome analysis, insulin response, organ size regulation

INTRODUCTION

There is an increasing understanding that adipose tissue contributes to both human well-being and disease processes (Pradat, 2021). Moderate amounts of adipose tissue are essential for health. In addition to its main function in thermogenesis, in energy storage, release and regulation, and in homeostasis, research has shown the potential beneficial effects of adipose tissue in the evolution of the human brain (Aiello and Wheeler, 1995). On the other hand, excess fat mass in body can be harmful. Adipose tissue development results in obesity and related comorbidities; it is an important endocrine organ that secretes a number of pro- and anti-inflammatory adipokines, which can increase the risk for multiple metabolic diseases, such as type 2 diabetes, cardiovascular disease and cancer (Lee et al., 2013; Pradat, 2021).

According to adipose tissue anatomy and distribution, these can be divided into two main categories, subcutaneous fat (SAF) and visceral fat (VAF), which are intrinsically different as a result of genetic or developmental events. Heterogeneity among SAF and VAF include depot differences in morphology and cellular composition (Van Harmelen et al., 2004; Tchkonia et al., 2005), metabolism (Wang et al., 2003; Bartness and Song, 2007; Fried et al., 2010; Koutsari et al., 2011) and production (Varma et al., 2007; Harvey et al., 2020), which collectively form the "microenvironment" within each depot contributing to differences in metabolism and endocrine function (Pradat, 2021). For instance, the number of stromal cells per gram of tissue is fewer in abdominal SAF than in omental VAF (Van Harmelen et al., 2004), but contains greater numbers of preadipocytes in SAF (Tchkonia et al., 2005; Karpe and Pinnick, 2015). Expression of hormone-sensitive lipase (HSL) and perilipinn, two lipid droplet-associated proteins, are differentially expressed between SAF and VAF (Wang et al., 2003), glucose uptake in VAF being greater than in SAF (Virtanen et al., 2002). Expression of proinflammatory cytokines (interleukin-6, IL-6, interleukin-8, IL-8, and macrophage chemoattractant protein-1, MCP-1) were generally higher in VAF, whereas leptin and IP-10 expression was higher in SAT (Harvey et al., 2020). Moreover, molecules that are involved in innate immunity, acute phase response and complement factors are overexpressed in VAT (Madani et al., 2009). However, the molecular mechanism of heterogeneity between SAF and VAF is not completely clear so that further research is needed. The factors affecting adipose tissue distribution include race, sex, age and other factors (Pradat, 2021). Age has been considered one of the complex factors determining fatness and fat distribution. Fat accumulates in the central area of both SAF and VAF during aging (Kuk et al., 2009), and there is evidence showing that obesity increases risk for morbidity and mortality in young people, whereas its effect in the elderly is much more complex (Bosello and Vanzo, 2021). Nevertheless, the mechanisms involved are poorly understood.

The domestic pig (*Sus scrofa*), particularly the miniature breeds, has served widely as an important model organism for studies of human disease and comparative genome studies, not only because swine are similar in organ size, anatomical structure, physiological indicators, organ development and disease progression with those of humans, but because of their high genomic sequence and chromosome structure homology with humans (Rothschild, 2004; Schook et al., 2005; Groenen et al., 2012; Alföldi and Lindblad-Toh, 2013). Adipocyte biology is pivotal in the regulation of fat metabolism, glucose absorption, energy metabolism and innate immune responses in pigs (Lunney, 2007; Gabler et al., 2009). Differential deposition and its regulatory mechanisms between SAF and intramuscular fat (IMF) have been proved (Tous et al., 2013; Wu et al., 2020). Bama pig, a Chinese indigenous miniature pig breed inhabiting the Guangxi province, is being increasingly developed as an animal model for medical research, for example, in human drug evaluation, xenotransplantation and a range of diseases, and the development of induced pluripotent stem (Ips) cell lines (Li et al., 2006; Liu et al., 2008; Chen et al., 2009; Esteban et al., 2009; Liu et al., 2009; Liu et al., 2010; Zhang et al., 2011; Zhang et al., 2012). Although they have a crucial role, our knowledge of patterns of transcriptome divergence between different postnatal developmental stages within and between SAF and VAF are poorly studied.

To help improve this situation, we have examined gene expression profiles in SAF and VAF of pigs during postnatal development using RNA sequencing techniques (RNA-Seq). This allowed us to identify the differential dynamics of gene expression of SAF and VAF, and investigate the underlying functional differences in differentially expressed genes (DEGs) during postnatal development, and between the two depots, and should improve our understanding of SAF and VAF deposition.

MATERIAL AND METHODS

Animal and Ethics Statements

Animals used were conducted according to the Regulations for the Administration of Affairs Concerning Experimental Animals (Ministry of Science and Technology, China, June 2004) and approved by the Institutional Animal Care and Use Committee (IACUC) of Shanghai Academy of Agricultural Sciences (approved ID: SAASPZ0520012, Shanghai, China, 24 December 2020). Male Bama pigs with similar genetic backgrounds produced by one sire were born and raised under the same environmental and nutritional conditions, housed at Taizhou experimental miniature pig breeding case managed by

Taihe Biotechnology Co., Ltd., in Taizhou, Jiangsu Province, China. Animals were fasted 24 h prior to slaughter. Fasting blood samples were collected. Animals were then euthanized with pentobarbital sodium (150 mg/kg). The adipose tissues were sampled immediately after death.

Biological Material and RNA-Seq Experiments

Nine Bama male pigs were included in this study 3 groups, 3 of them were 1 months old (infancy, weight = 4.70 ± 0.17 kg, 20 October 2019), 3 being 3 months-old (puberty, weight = 7.57 ± 0.32 kg, 18 August 2019), and 3 were 6 months-old (adulthood, weight = 17.83 ± 3.01 kg, 12 May 2019). SAF on the back between the third and fourth last ribs and VAF adjacent to kidney deposition were isolated from pigs and frozen immediately in liquid nitrogen until lipid extraction. A portion of fresh SAF and VAF were cut into about a cubic centimeter of tissue and fixed in 4% paraformaldehyde for histological analysis.

Total RNA was extracted from adipose tissues using TRIzol reagent (Invitrogen, Carlsbad, CA, United States). The samples were purified using a Rneasy Mini Kit (Qiagen, Hilden, Germany). RNA integrity was assessed with a 2200 Bioanalyzer (Agilent Technologies, Inc., Santa Clara, CA, United States) and agarose gel electrophoresis.

RNA integrity number (RIN) of the samples range from 6.6 to 9.4. The RNA sequence libraries were prepared with a TruSeq RNA Sample Preparation Kit (Illumina, San Diego, CA, United States). The quality of Cdna libraries was checked using an Agilent 2200 TapeStation system (Agilent, Palo Alto, CA, United States). The cDNA libraries were sequenced with an Illumina HiSeq X ten Illumina, San Diego, CA, United States which generated paired-end raw reads of approximately 150 bp in size. The fastq-formatted RNA-seq datasets have been deposited in the National Center for Biotechnology Information (NCBI) Gene Expression Omnibus database (GEO: GSE184038).

The fastp were used for removing the adaptor sequence and discarding the low-quality reads to achieve the clean data (Chen et al., 2018). A read will be discarded when it does not meet requirements of the following parameters, reads length ≥50 bp, the Nbase number ≤5 and less than 40 percent of bases are unqualified (quality score ≥ 15). The clean reads were aligned to 9,823(NCBI Taxonomy ID)genomes (version: sscrofa11.1) using the Hisat2 (Kim et al., 2019). The RNA-seq count was calculated by Htseq-count and the expression data were normalized using fragments per kilobase of exon model per Million mapped fragments (FPKM). The DEGs were filtered by using DESeq2 algorithm under the following criteria: 1) log2FC >0.585 or <−0.585; ii), FDR <0.05 (Love et al., 2014)

Functional Enrichment Analysis

ClusterProfiler was used for GO and Pathway enrichment (Yu et al., 2012). We downloaded the GO annotations from the Gene Ontology (http://www.geneontology.org/) and Pathway annotation from Kyoto Encyclopedia of Genes and Genomes (KEGG) (https://www.kegg.jp/). The *p*-value can be calculated by hypergeometric distribution, which corresponded to a one-sided version of Fisher's exact test. FDR was used to correct *p*-values (*p*-values < 0.05) (Ashburner et al., 2000). GO and Pathway enrichment was also applied to the genes belonging to specific profiles. Significant profiles were identified using Fisher's exact test and multiple comparisons.

QRT-PCR

QRT-PCR were analyzed using an Applied Biosystems StepOnePlus Real-Time PCR System (Applied Biosystems, Foster City, CA, United States). Total RNA from SAF and VAF tissues were isolated using TRIzol® Reagent (Invitrogen, Carlsbad, CA, United States); cDNAs were synthesized using a Thermo Scientific RevertAid First Strand Cdna Synthesis Kit; and QRT-PCR analyses were carried by using Roche FastStart Universal SYBR Green Master (Rox). Mrna primers were designed using Primer 5.0 software (Primer-E Ltd., Plymouth, United Kingdom) and their sequences are listed in **Supplementary Tables S1–S2**. Parallel reactions using *GAPDH* were performed to normalize the amount of templated cDNA. Each of the amplifications was triplicated and the mean value was calculated using the △△C*t* method. The results (FC) were expressed as $2^{\triangle\triangle Ct}$: $\triangle\triangle \mathbf{C}t = (Ct_{ij} - Ct_{GAPDHj}) - (Ct_{i1} - Ct_{GAPDH1})$, where Ct_{ij} and Ct_{GAPDHj} are the C*t* values for gene I and for GAPDH in a sample (named j); Ct_{i1} and Ct_{GAPDH1} are the Ct values in sample 1, expressed as the standard. A Student's *t*-test of independent data was used to assess the statistical significance of differential expression levels of each gene within the samples.

Short Time-Series Expression Miner Analysis

STEM analysis is a commonly used bioinformatics method used to determine statistically significant time-dependent gene expression profiles (Ernst and Bar-Joseph, 2006). Expression profiles of DEGs were determined by cluster analysis based on the STEM method (http://www.cs.cmu.edu/~jernst/st/) (Draghici et al., 2007; Ehrenkaufer et al., 2013). it assumes the values of gene expression represent log ratios relative to the expression at the first time-point. The approach selects a set of predetermined temporal model profiles and determines the statistical significance of the number of genes assigned to each profile compared to the number of genes expected based on chance. This method was used to explore mRNAs that might be correlated with fat development. Significant profiles were identified using Fisher's exact test and multiple comparisons. GO and Pathway enrichment was also applied to the genes belonging to specific profiles.

Construction of Molecular Interaction Network

One of the advanced bioinformatic tools, Ingenuity Pathway Analysis (IPA) software program was used to construct a molecular interaction network for better interpretation of the gene expression profiles as revealed by RNA-seq on the strength of a build-in scientific literature-based database (IPA Ingenuity

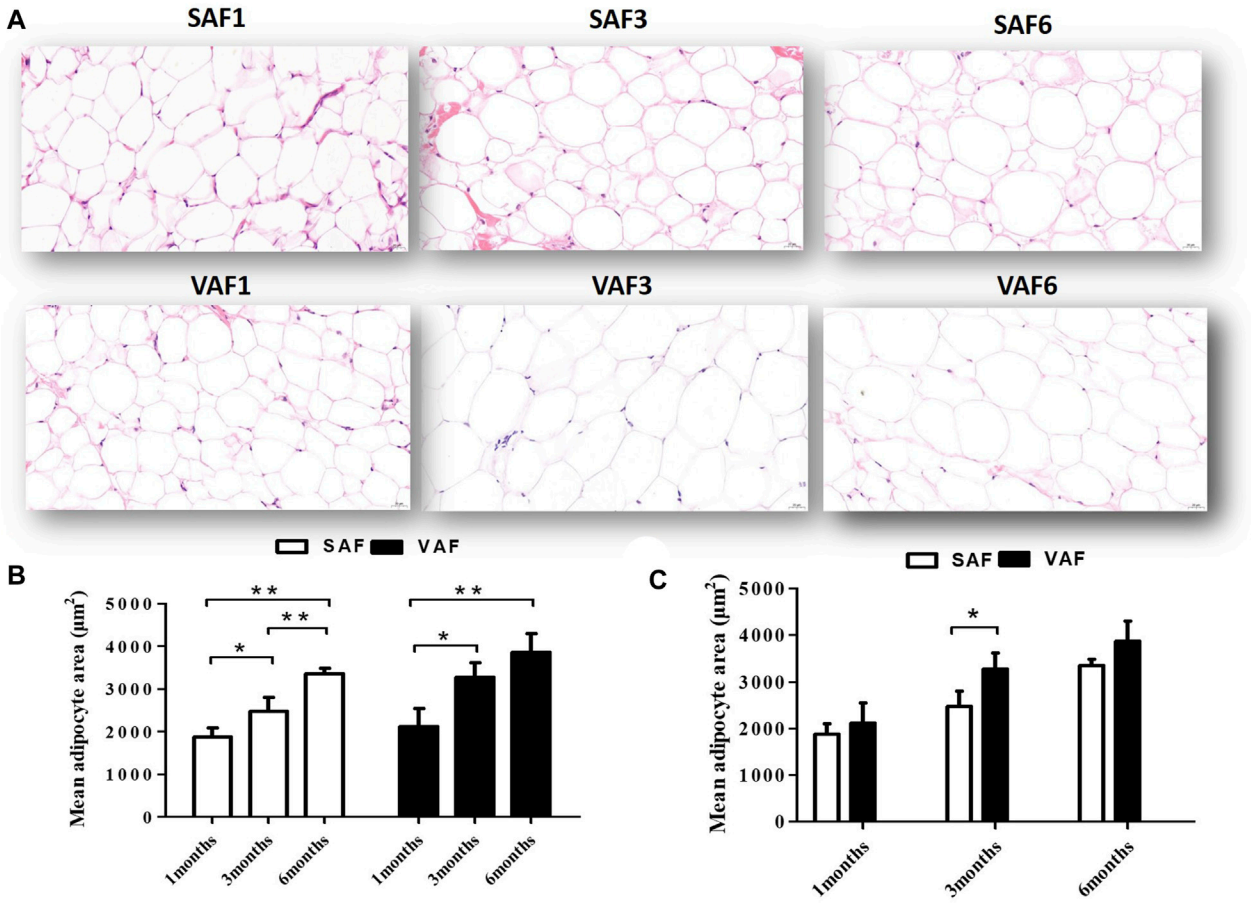

FIGURE 1 | Histological sections of SAF tissue and VAF tissue of pigs during the postnatal stage. **(A)**. H&E staining of SAF tissue and VAF tissue at 1, 3 and 6 months (x400 magnification, scale bar: 20μm); **(B,C)**. Mean adipocyte size of SAF and VAF tissues at the postnatal stage; areas were measured by Images J software for 3 different animals per group (0.122 mm^2 total area for each sample). $^*p < 0.05$, $^{**}p < 0.01$.

Web Site, www.ingenuity.com), a very convenient software program to classify the pathways, molecular networks and functions most relevant to genes of interest or experimental datasets (Calvano et al., 2005; Mayburd et al., 2006).

RESULTS

Genome-Wide Identification of the Expressed Genes in Subcutaneous Fat and Visceral Fat

Nine male pigs were included in this study measuring the body fatness traits at 1, 3 and 6 months of age (**Supplementary Table S3**). At 6 months, all measured indicators were significantly higher than those at 1 and 3 months ($p < 0.05$). Body fat rate, backfat thickness, perirenal, mesenteric fat and greater omentum weights at 3 months were significantly higher than at 1 month ($p < 0.05$), but weights were similar between 1 and 3 months ($p > 0.05$). This corresponds to the larger adipocyte size in pigs at 1 month compared with 3 and 6 months (**Figures 1A–C**). Histological examination showed that size significantly increased during the postnatal stage for both SAF and VAF ($p < 0.05$, $p < 0.01$). In addition, sizes in VAF were significantly bigger than SAF at 3 months ($p < 0.05$), whereas differences were insignificant at 1 and 6 months ($p > 0.05$). We hypothesize that SAF and VAF in the pigs were systemically differentiating at 3 months and fat development was distinct between the depositions of SAF and VAF. On this basis, we investigated the SAF and VAF transcriptome at 3 representative stages: infancy (1 month), juvenile (3 months) and adulthood (6 months) using RNA-seq techniques to establish a general overview of the differential dynamics of gene expression in the SAF and VAF, and gain further insight into functional differences in DEGs among the postnatal developmental stages and between the fat depositions.

SAF and VAF samples from pig were isolated from 1-, 3- and 6 months-old pigs to profile spatiotemporal changes of the adipose transcriptome by RNA-seq using 3 replicates. A statistical table for raw and clean data sets of all RNA-seq libraries were listed in **Supplementary Table S4**. About

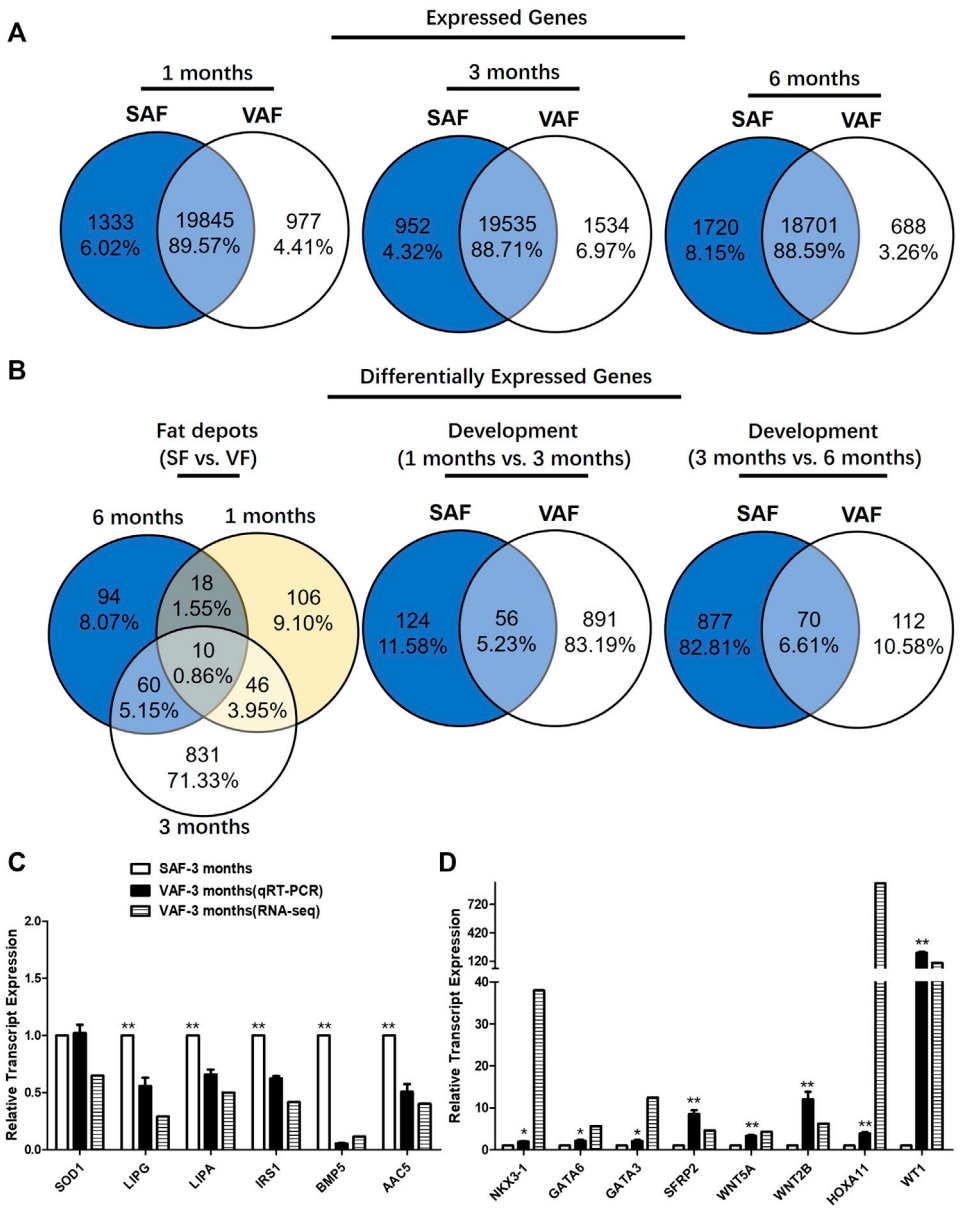

FIGURE 2 | Gene identification and differentially expressed genes (DEGs) in SAF and VAF tissue from Bama pigs during the postnatal stage. **(A)** Expressed genes in each fat depot. **(B)** DEGs in each fat depot (fragments per kilobase of exon model per Million mapped fragments, FPKM) fold-change >2; $p < 0.05$). **(C)** Experimental verification of gene expression level using qRT-PCR. Relative expression levels (SAF/VAF) of 10 DEGs verified in 3 months pigs. **(D)** Experimental verification of gene expression level using qRT-PCR. Relative expression levels (SAF/VAF) of 5 DEGs verified in 3 months-old pigs ($n = 3$). *Significant ($p \leq 0.05$). **Significant ($p \leq 0.01$).

45–60 million sequencing raw reads were obtained for the 9 SAF and 9 VAF libraries respectively. ~90% of the total clean reads were uniquely mapped to swine genome sequences in the samples (**Supplementary Table S5**). Using the Htseq method (Wen, 2017), the number of genes was calculated and expression data were standardized by FPKM. There were ~23,600 expressed genes (normalized read count >3 in at least one sample) were identified, about 88.6–89.6% were detected in both fat depots (**Figure 2A**).

Analysis of Consistency Within Samples

Although there is little difference among individuals in the SAF and VAF with each group, samples from each may differ in hereditary characters. Comparing the consistency within samples, those that deviated too much from the norm could be excluded from subsequent screening of DEGs, making analysis more reliable and credible. Sample correlation analysis showed that, except for VAF6-3, they were more consistent in each group. VAF6-3 deviated too much from the other VAF6 samples by

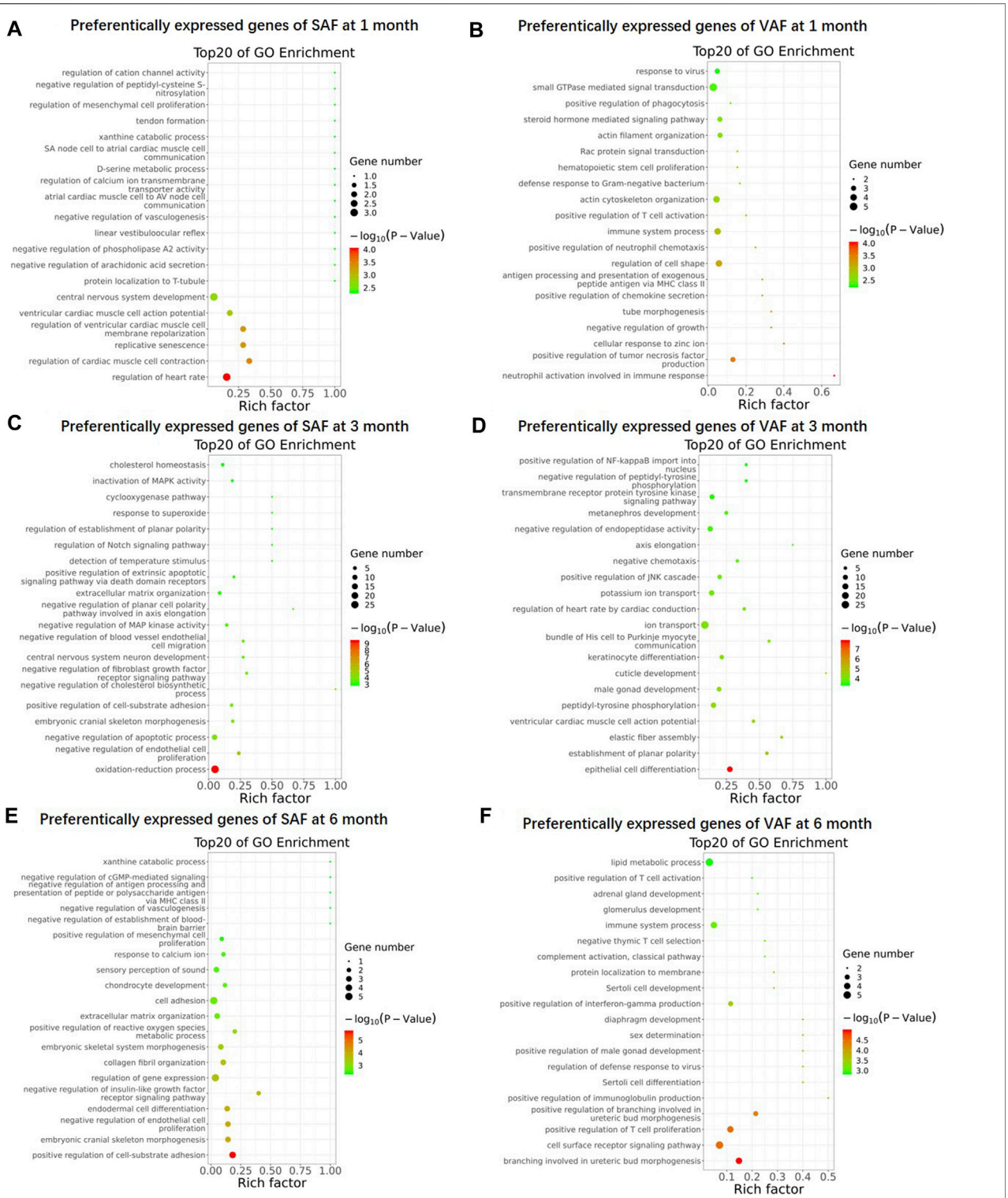

FIGURE 3 | Gene Ontology (GO) enrichment of upregulated genes. GO enrichment of upregulated genes in 1 month SAF **(A)**, 1 month-old VAF **(B)**, 3 months SAF **(C)**, 3 months-old VAF **(D)**, 6 months SAF **(E)**, 6 months VAF **(F)** groups. The X-axis provides the richness factor, calculated by dividing the upregulated gene number in a given GO term by the total gene number in the term of genome. The size and color of the bubbles represent gene number and enrichment significance according to hypergeometric testing, respectively.

using Pearson correlation coefficient ($p < 0.65$), so it was excluded from screening (results are shown in **Supplementary Figure S1**).

Spatiotemporal Expression of Subcutaneous Fat and Visceral Fat Adipose-Associated Genes

There were significantly DEGs with clear fat depots, and/or age-based expression patterns. Of them, 1165 DEGs were differentially expressed between the SAF and VAF (**Figure 2B**). There were 180 DEGs between SAF and VAF depots at 1 month, 947 at 3 months and 182 at 6 months. Only 10 (0.86%) DEGs were shared between the SAF and VAF. Within each fat depot, there were 180 and 947 (1 vs. 3 months), 947 and 182 (3 vs. 6 months) age-based DEGs in the SAF and VAF depots, respectively, with only 56 (5.23%) and 70 (6.61%) being shared. The upregulated and downregulated genes are given in **Supplementary Tables S6–S12**. In each comparison, 50% were upregulated in 1 month compared to 3 months SAF; and 71% were upregulated in 3 compared to 6 months SAFs; 28% were upregulated in 1 month VAF compared to 3 months VAF; 69% were upregulated in 3 compared to 6 months VAF; 47% were upregulated in 1 month SAF compared to 1 month VAF; 23% were upregulated in 3 months SAF compared to 3 months VAF; 45% were upregulated in 6 months SAF compared to 6 months VAF.

For gene expression levels by RNA-seq, a quantitative real-time polymerase chain reaction (Qrt-PCR) was used in determining expression levels of the genes associated with lipid metabolism and the hippo signaling pathway. Regarding the Qrt-PCR used to validate relative gene expression of the 14 selected mRNAs, it is shown in **Figures 2C,D** that *lipase, endothelial* (*LIPG*), *lipase A, lysosomal acid, cholesterol esterase* (*LIPA*), *insulin receptor substrate 1*(*IRS1*), *bone morphogenetic protein 5* (*BMP5*), *acetoacetyl-CoA synthetase* (*AACS*) were upregulated and the expression of *NK3 homeobox 1* (*NKX3-1*), *transcription factor GATA-6* (*GATA6*), *GATA binding protein 3* (*GATA3*), *secreted frizzled-related protein 2* (*SFRP2*), *wingless-type MMTV integration site family, member 5A* (*WNT5A*), *wingless-type MMTV integration site family, member 2B* (*WNT2B*), *homeobox A11* (*HOXA11*) *and Wilms tumor 1* (*WT1*) decreased in SAF at 3 months. The tendency for changes was consistent between the RNA-seq and qRT-PCR results, except for *SOD1*. This indicates that their gene regulation networks are developmentally distinct regarding fat deposition, suggesting different functioning with age.

Functional Enrichment Analysis

To gain an overview on the functions of the DEGs, we carried out Gene Ontology (GO) enrichment analysis between SAF and VAF at the same developmental stage, and identified 243, 359, 332 and 455 significantly enriched GO terms for upregulated DEGs in 1-, 3- and 6 months SAF, as also in 1-, 3- and 6 months VAF, respectively (**Supplementary Tables S13–S18**). **Figure 3** shows the top 20 most significantly enriched GO items in each group. At 1 month, GO terms including "central nervous system development" and "regulation of heart rate" were significantly enriched in upregulated DEGs in SAF (**Figure 3A**); GO terms including "regulation of cell shape," "immune system process" and "actin cytoskeleton organization" were significantly enriched in upregulated DEGs in VAF (**Figure 3B**). At 3 months, GO terms including "oxidation-reduction process," "negative regulation of apoptotic process," "cholesterol homeostasis" and "lipid metabolic process" were significantly enriched in upregulated DEGs in SAF (**Figure 3C**); GO terms included "epithelial cell differentiation," "male gonad development," "ion transport" and "positive regulation of JNK cascade" were significantly enriched in the upregulated DEGs in VAF (**Figure 3D**); at 6 months, GO terms including "positive regulation of cell-substrate adhesion," "regulation of gene expression," "cell adhesion" and "collagen fibril organization" were significantly enriched in upregulated DEGs in SAF (**Figure 3E**); GO terms including "cell surface receptor signaling pathway" and "immune system process" were significantly enriched in upregulated DEGs in VAF (**Figure 3F**).

KEGG analysis of the DEGs obtained significantly enriched pathways for upregulated genes in 1-, 3- and 6 months SAF or VAF groups (**Supplementary Tables S19–S21**). The enriched pathways between SAF and VAF at 1 and 6 months mainly related to diseases (**Supplementary Tables S19, S21**). At 3 months, pathways included "oxidative phosphorylation," "TNF signaling pathway," "PI3K-Akt signaling pathway," "ECM-receptor interaction" and "focal adhesion" were significantly enriched in upregulated DEGs in SAF (**Supplementary Table S20**); pathways including "Hippo signaling pathway," "thyroid hormone synthesis," "oxytocin signaling pathway," "calcium signaling pathway," "focal adhesion," "regulation of actin cytoskeleton" and "MAPK signaling pathway" were significantly enriched in upregulated DEGs in VAF (**Supplementary Table S20**). Deposit-specific DEGs enrichment in the lipid metabolism (SAF-specific), sexual development (VAF-specific), hormone signaling pathway (VAF-specific) and the hippo signaling pathway (VAF-specific) at 3 months are shown in **Table 1**.

In summary, functional enrichment analysis uncovered some unexpected results: 1) A number of the genes preferentially expressed in SAF and VAF did not overlap, especially at 3 months. 2) Enriched terms related to lipid metabolism were seen in 3 months SAF, suggesting that smaller body sizes were likely the result of their relatively high lipid metabolic rate. 3) Genes associated with sexual development were upregulated in the 3 months VAF, indicating that these pigs were at the juvenile-to-adult growth stage, consistent with the characteristics of precocious puberty in miniature pigs. 4) Genes related to the hormone signaling pathway were already highly expressed in 3-months VAF, indicating that hormone levels are different between SAF and VAF, which directly affects the metabolism of adipose tissue, as well as its accumulation and distribution. 5) Genes related to the Hippo signaling pathway were upregulated in 3 months VAF, suggesting it is important in regulating the balance of cell proliferation and apoptosis regarding organ and tissue size at 3 months.

TABLE 1 | Deposit-specific DEGs enrichment in the lipid metabolic process (SAF-specific), sexual development (VAF-specific), hormone signaling pathway (VAF-specific) and Hippo signaling pathway (VAF-specific) at 3 months.

Gene ID	Gene symbol	Gene title	log2FC (SF/VAF)	*p*-value	FDR
SAF-specific DEGs enrichment in the lipid metabolic process					
448,985	CYP7A1	cytochrome P450, family 7, subfamily A, polypeptide 1	3.91	0	0
100,157,318	APOD	apolipoprotein D-like	3.03	0	0
396,832	LEP	leptin	2.18	0	0
100,516,456	LIPG	lipase, endothelial	1.78	0	0
100,155,736	AACS	acetoacetyl-CoA synthetase	1.32	0	0.01
100,142,668	APOE	apolipoprotein E	1.53	0	0
404,693	IRS1	insulin receptor substrate 1	1.26	0	0.05
397,576	CAV1	caveolin 1, caveolae protein, 22 kDa	1.03	0	0.03
100,156,545	LIPA	lipase A, lysosomal acid, cholesterol esterase	1.00	0	0.04
100,512,686	TWIST1	twist basic helix-loop-helix transcription factor 1	0.91	0	0.02
VAF-specific DEGs enrichment in sexual development					
100,521,236	HOXA11	homeobox A11	−9.88	0	0
397,338	WT1	Wilms tumor 1	−6.66	0	0
100,738,625	NKX3-1	NK3 homeobox 1	−5.25	0	0.02
733,631	GATA3	GATA binding protein 3	−3.64	0	0
100,520,560	WNT2B	wingless-type MMTV integration site family, member 2B	−2.65	0	0
397,600	GATA-6	transcription factor GATA-6	−2.50	0	0
100,516,027	SFRP2	secreted frizzled-related protein 2	−2.21	0	0.02
100,627,056	WNT5A	wingless-type MMTV integration site family, member 5A	−2.09	0	0
100,155,189	TESC	tescalcin	−1.12	0	0.01
VAF-specific DEGs enrichment in the hormone signaling pathway					
1.01E+08	KCNN4	potassium intermediate/small conductance calcium-activated channel, subfamily N, member 4	−8.84	0	0.01
1E+08	ASGR2	asialoglycoprotein receptor 2	−7.29	0	0.04
1E+08	CACNG6	calcium channel, voltage-dependent, gamma subunit 6	−6.66	0	0.01
396,828	KCNMB1	potassium large conductance calcium-activated channel, subfamily M, beta member 1	−4.56	0	0.01
397,081	PLA2G4F	phospholipase A2, group IVF	−4.43	0	0.04
1.01E+08	ADCY8	adenylate cyclase 8 (brain)	−4.26	0	0
1.01E+08	CACNA1D	calcium channel, voltage-dependent, L type, alpha 1D subunit	−3.73	0	0
396,898	FXYD2	FXYD domain containing ion transport regulator 2	−3.52	0	0
396,856	MYL9	myosin, light chain 9, regulatory	−3.31	0	0
1E+08	CACNA2D2	calcium channel, voltage-dependent, alpha 2/delta subunit 2	−3.25	0	0.01
1.01E+08	DUOXA2	dual oxidase maturation factor 2	−2.89	0	0
1.01E+08	MYLK	myosin light chain kinase	−2.88	0	0
1E+08	CAMK1G	calcium/calmodulin-dependent protein kinase IG	−2.83	0	0
1.01E+08	ATP1B2	ATPase, Na+/K+ transporting, beta 2 polypeptide	−1.93	0	0.01
541,593	ATP1A2	ATPase, Na+/K+ transporting, alpha 2 polypeptide	−1.89	0	0.04
1.01E+08	ATP1B1	ATPase, Na+/K+ transporting, beta 1 polypeptide	−1.76	0	0
396,848	MYL6B	myosin light chain 6B-like	−1.56	0	0.04
1.01E+08	RYR2	ryanodine receptor 2 (cardiac)	−1.51	0	0.02
VAF-specific DEGs enrichment in the Hippo signaling pathway					
1.01E+08	WWC1	WW and C2 domain containing 1	−8.84	0	0
1E+08	CDH1	cadherin 1, type 1, E-cadherin (epithelial)	−7.78	0	0
1.01E+08	WNT16	wingless-type MMTV integration site family, member 16	−7.05	0	0
1.01E+08	RASSF6	Ras association (RalGDS/AF-6) domain family member 6	−6.27	0	0
397,668	AREG	amphiregulin	−6.27	0	0
1.01E+08	DLG3	discs, large homolog 3	−3.86	0	0
1.01E+08	WNT2B	wingless-type MMTV integration site family, member 2B	−2.65	0	0
1.01E+08	PRKCZ	protein kinase C, zeta	−2.48	0	0.01
1E+08	WNT10B	wingless-type MMTV integration site family, member 10B	−2.1	0	0
1.01E+08	WNT5A	wingless-type MMTV integration site family, member 5A	−2.09	0	0
492,315	BMP7	bone morphogenetic protein 7	−2	0	0

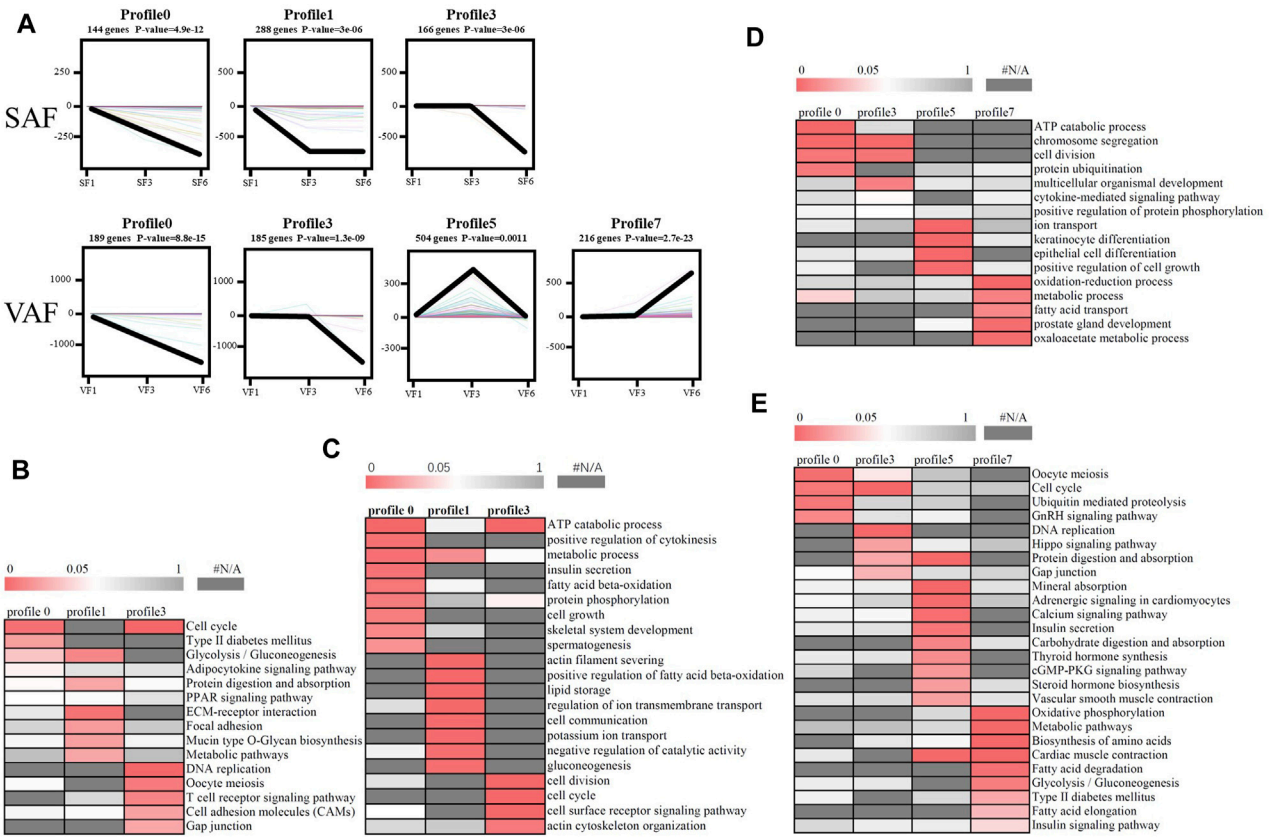

FIGURE 4 | Patterns of gene expression and GO or pathway enrichment across the points in SAF and VAF. **(A)** Patterns across 3 time-points in SAF and VAF inferred by STEM analysis. In each frame, the color lines represent the expression patterns of each gene, whereas the black line represents the expression tendency of all the genes. The number of genes belonging to each pattern was labeled above the frame. **(B)** GO enrichment analysis of 3 significant clusters in SAF. **(C)** KEGG enrichment analysis of 3 significant clusters in SAF. **(D)** GO enrichment analysis of 4 significant clusters in VAF. **(E)** KEGG enrichment analysis of 4 significant clusters in VAF. The significance of the most represented GO-slims in each main cluster is indicated by *p*-value. The red areas represented the significant *p*-value, wheaeas the dark gray represented the nonsignificant values.

Short Time-Series Expression Miner Analysis

According to STEM analysis, all DGEs in SAF or VAF at the 3 ages were classified into 8 clusters according to their degree of expression. Among them, the *p* values of 3 clusters for SAF and 4 clusters for VAF were statistically significant (**Figure 4A**). The number of DGEs in the 3 clusters for SAF ranged from 144 in cluster 0 to 288 in cluster 1, while these in the 4 clusters for VAF ranged from 185 in cluster 3 to 504 in cluster 5.

To determine the significance of the transcriptional changes in each group, GO and KEGG classifications were implemented for the genes belonging to the overrepresented profiles. In SAF, genes involved in lipid storage, the PPAR signaling pathway was overrepresented in Profile 1, whereas genes involved in cell division and cycle were enriched in Profile 0 and 3 (**Figures 4B,C**; **Supplementary Table S22**). In VAF, however, the genes involved in the hippo signaling pathway were enriched in Profile 3 (**Figures 4D,E**; **Supplementary Table S23**), where expression stays the same at 1 and 3 months, but decreased at 6 months (**Figure 4A**), suggesting that these genes are key in regulating the size of organs and tissues during the early phase. The genes involved in the GnRH signaling pathway were enriched in Profile 0 (**Figures 4D,E**; **Supplementary Table S23**), where expression gradually decreased with age, indicating genes involved in sexual development starts at early stage (**Figure 4A**). In profile 5, the overrepresented GO and pathway included insulin secretion, thyroid and steroid hormone synthesis (**Figures 4D,E**; **Supplementary Table S23**). Expression levels of these genes peaked at 3 months and subsequently decreased (**Figure 4A**). Genes involved in lipid metabolism were enriched in profile 7(**Figures 4D,E**; **Supplementary Table S23**), where expression was lower and then peaked at 6 months (**Figure 4A**). These results suggested a variation in genes and pathways between SAF and VAF. Obviously, the differentiation in gene expression patterns between the two deposits corresponded to their distinct responses in sexual development, hormone signaling pathways, lipid metabolism, as well as the hippo signaling pathway. A total of 9 genes in profile 7 of VAF and profile 0, 1 and 3 of SAF were randomly selected for Qrt-PCR verification (**Figure 5**); the RNA-seq and Qrt-PCR patterns were consistent.

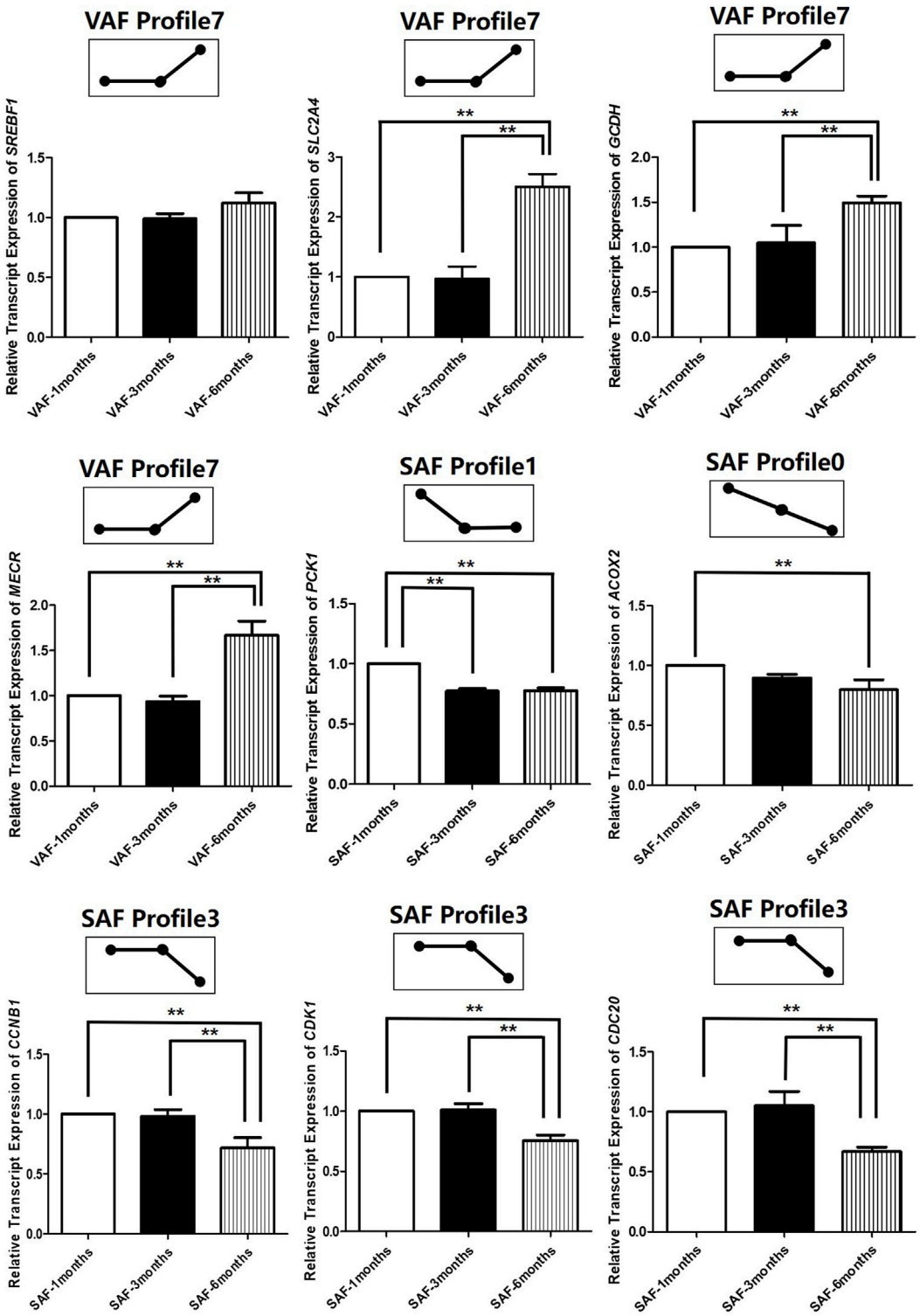

FIGURE 5 | Experimental verification of gene expression level in across 3 time-points in SAF and VAF using qRT-PCR($n = 3$). A total of 9 genes in profile 7 of VAF and profile 0, 1 and 3 of SAF were randomly selected for qRT-PCR verification. **Difference is extremely significant ($p \leq 0.01$).

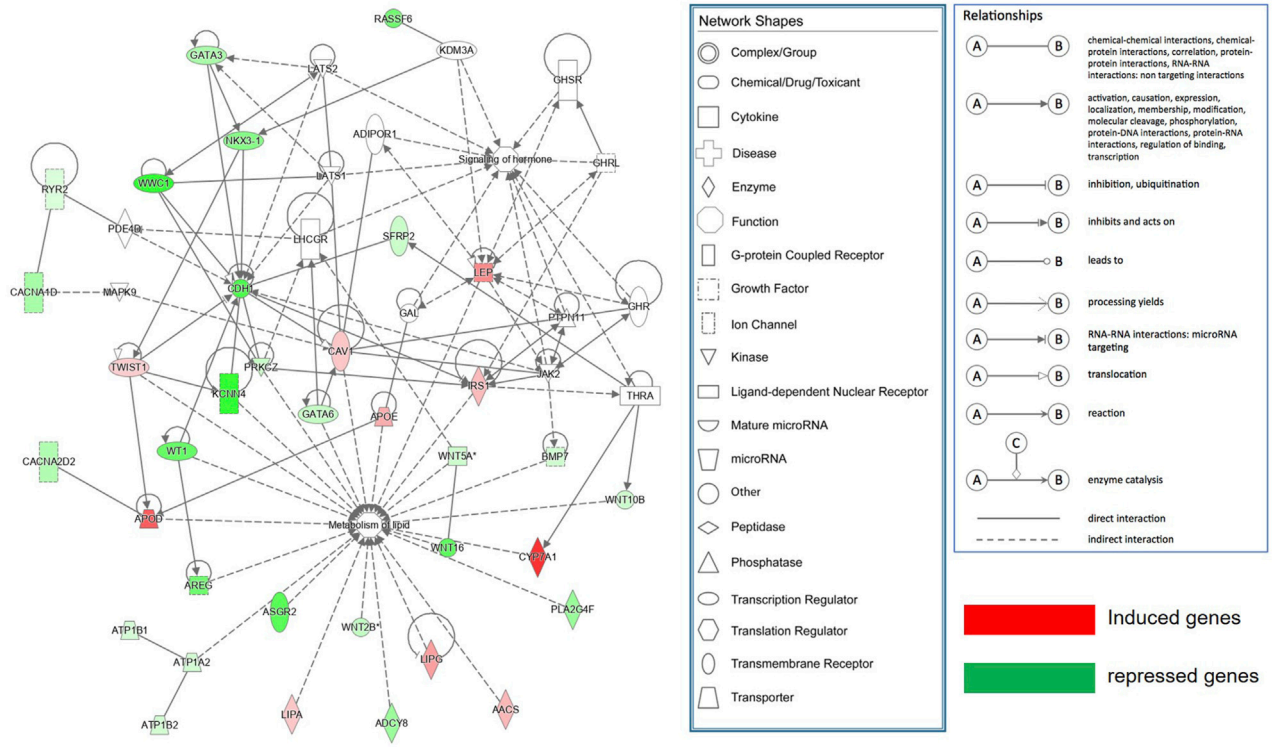

FIGURE 6 | Molecular networks functionally associated with lipid metabolism and hormone signaling identified by Ingenuity Pathway Analysis (IPA).

Molecular Network in Pig Adipose Tissues Potentially Regulates Tissue Deposit-Differences

The DEGs (log2FC >0.585 or <-0.585; ii), FDR <0.05 between SAF-3 and VAF-3 groups were used to construct a gene interaction network in the IPA system, **Figure 6** showing that 35 DEGs were found. Using IPA software, function analysis of these genes showed that the most important functions of this network consisted of lipid metabolism and hormone signaling.

DISCUSSION

Many factors affect fat deposition, including genetics, nutrition, exercise, location of deposition, age, etc., (Lee et al., 2013; Bosello and Vanzo, 2021). Location and age are important factors affecting fat accumulation and obesity-related diseases. Miniature pigs are similar to humans in physiological characteristics, making them suitable for medical research. Our object was to study the histological differences of SAT and VAT cells at 3 ages (1, 3 and 6 months), to the follow them through development. At 1 month they have been weaned, the diet structure changes, and the organism also changes, making them the fastest growth period. At 3 months, they reach sexual maturity, the endocrine levels of hormones and other hormones change greatly, and organs are still developing. At 6 months of age, the pigs are basically mature and fully developed.

The biological functions of the adipocytes are not only being inert storage depots releasing fuel as fatty acids and glycerol in time of fasting or starvation, but also endocrine glands secreting important hormones, cytokines, vasoactive substances, and other peptides (Kahn and Flier, 2000). It is reported that the association of insulin resistance (IR) with obesity involves more than fat mass per se, including adipose location and the degree of dysfunction associated with it (Westphal, 2008). Regional differences exist in the morphological characteristics and metabolic functions of adipose tissue (Lee et al., 2013). Our findings of the adipocyte volume of SAT and VAT increasing significantly with age, being significantly larger in VAT than SAT at 3 months, consistent with available data (Hoffstedt et al., 2010). In addition, the metabolic effects of adipose depots depend on their location and whether they are characterized as VAF or SAF (Westphal, 2008). Centrally located VAT has more influence on IR than does centrally located SAT (Westphal, 2008). Fat cell size is also strongly correlated with molecular level of adipose tissue homeostasis and IR. Small fat cells are the "buffer pool" of human fat, with higher insulin sensitivity and higher absorption rate of TG and FFA, which are considered to have a protective effect (Pausova et al., 2010). However, with the gradual increase of adipocyte volume, these small adipocytes gradually changed into larger ones, with the function of IR restrained to the anti-lipopolysis effect of insulin and possessing high rate lipopolysis (Pausova et al., 2010). Several researches reported that VAT containing more fat cells with large size has stronger decomposition metabolic activity than SAT fat cells (Hoffstedt et al., 2010; Pausova et al., 2010; Lima-Martínez

et al., 2013). Therefore, the total amount of VAT is generally considered to be closely associated to IR (Hoffstedt et al., 2010).

The metabolic differences of adipose tissues in different parts are mainly: lipolysis, triglyceride synthesis and storage, and also differences in adipokines secreted (Lee et al., 2013). To understand the molecular mechanism of SAF and VAF deposition differences with age, we used RNA-Seq to study the transcriptional expression of SAF and VAF at the 3 ages, and mechanisms behind then. Consistent with phenotypic differences, the most DEGs were found in VAF and SF at 3 months. Further functional enrichment analysis of DEGs in adipose tissue of VAF and SAF showed that the expression levels of genes related to lipid metabolism and cholesterol dynamic balance, which were significantly higher in SAF than IN VAF, including *APOE*(*Apolipoprotein E*), *LEPG* (*lipase, olease*), *AACS*, *APOD* (*Apolipoprotein D-like*), *CYP741* (*Cytochrome P450, Family 7, Subfamily A, Polypeptide 1*), *Caveolin 1*(*Caveolin 1, Caveolae protein, 22kDa*), and *CYP7A1* (*Cytochrome P450, Family 7, Subfamily A, Polypeptide 1*), DGEs involved in positive regulation of fatty acid β oxidation; *IRS1* and *TWIST1* (*Twist Basic helix-loop-Helix transcription factor 1*) were also highly expressed in SAF at 3 months. APOE is an enzyme involved in the activation of hydrolyzed fat and the transformation and metabolism of lipoprotein. Its concentration is positively correlated with plasma triglyceride content, and is an apolipoprotein that regulates lipid metabolism and cholesterol balance. It has an anti-atherosclerosis effect by inhibiting the formation of foam cells (Getz and Reardon, 2018). APOD is an apolipoprotein in plasma HDL and VHDL, and has the function of binding and transporting lipids by associating with APOA-I, and lecithin Cholesterol acyl transferase (LCAT) forms a "cholesterol ester transport complex" that helps regulate cholesterol metabolism (Thomas et al., 2003). *Endothelial lipase* (*EL*) gene, a member of lipase family, is expressed at a low level in normal endothelial cells, and its expression being significantly increased by various atherosclerosis (AS) factors (McCoy et al., 2002), which suggests that at 3 months, the cholesterol dynamic balance of SAT is higher than that of VAT, which is associated with higher TG and FFA absorbability and higher small-volume fat cells in SAT (Pausova et al., 2010). Other studies have shown that differences in expression of *HSL* and *perilipin*, encoding a lipid droplet protein that regulates lipolysis, in omental adipose tissue and SAT may be one of the molecular mechanisms underlying the differences between sites of lipolysis (Arner, 1995; Wang et al., 2003). However, the expression levels of these two genes were not significantly different between SAT and VAT, which may be due to the different species and parts of the subjects examined.

Adipose tissue is not only an energy storage organ, but has the potential to release a large number of peptide hormones and active adipocytes through autocrine, paracrine and endocrine forms. Adipokines secreted by SAF and VAF are involved in a number of physiological and pathological processes, including appetite and energy metabolism, IR, reproductive and endocrine system, bone metabolism, immunity and inflammation (Al-Gareeb et al., 2016); the characteristics of these adipokines are different (De Oliveira Leal and Mafra, 2013). Therefore, the study the molecular mechanism of functional differences in adipose tissue of different parts in the prevention and treatment of obesity and obesity-related diseases is important. We found a significant difference in insulin sensitivity between SAT and VAT at 3 months. Insufficient secretion and action of insulin are two important factors leading to IR and diabetes. IR has decreased efficiency of insulin in promoting glucose uptake and utilization for several reasons, and the body produces hyperinsulinemia through compensatory secretion of excessive insulin to maintain the stability of blood glucose (Lebovitz, 2001). We identified *Leptin* (*LEP*) and *IRS1* genes associated with insulin response through analysis of DEGs in SAT and VAT at 3 months. *IRS1* expression in SAT was significantly higher than in VAT. However, the expression levels of 9 genes related to insulin secretion in VAT were significantly higher than those in SAT, such as *ATPase, Na^+/K^+ buffer, beta 2 polypeptide, ATP1B2*; *ATPase, Na^+/K^+ buffer, beta 1 polypeptide, ATP1B1*; *ATPase, Na^+/K^+ buffer, Alpha 2 polypeptide, ATP1A2; Adenylate cyclase 8* (*brain*), *ADCY8*; *Ryanodine receptor 2* (*Cardiac*), *RYR2*; *FXYD domain containing ion Transport Regulator 2, FXYD2*, etc., IRS1 is an important molecule in intracellular insulin signaling (Tamemoto et al., 1994). Leptin is a protein-like circulating factor, mainly involved in body weight regulation by reducing food intake (Halaas et al., 1995), increasing energy consumption (Pelleymounter et al., 1995), strengthening substance metabolism and other ways. The mechanism is through receptors on the target cell membrane and the corresponding signal transduction system. Signal transduction through bidirectional activated kinase J tyrosine protein kinase (JAK) and its transduction and the transcriptional activation protein (STAT) pathway affects the secretion of neuroendocrine hormones, such as neuropeptide Y (NPY), resulting in decreased appetite, increased energy consumption and loss of weight (Bjorbæk and Kahn, 2004). Powe et al. (2019) reported that LEP was significantly positively correlated with insulin response, insulin sensitivity and fat mass during the first trimester. LEP has a bidirectional effect on β cell function and glucose-stimulated insulin secretion (Kulkarni et al., 1997; Highman et al., 1998; Covey et al., 2006). We found that the expression of ATPase gene related to insulin secretion pathway was significantly higher in VAT than in SAT. ATP is a major signal of pancreatic IR (Ye, 2021). In obesity, ATP overproduction promotes systemic IR through a several mechanisms, such as inhibition of AMPK, Mtor induction, hyperinsulinemia, hyper glucagon and mitochondrial dysfunction. Preventing overproduction is a key strategy for insulin sensitization, which suggests that SAT is significantly more responsive and sensitive to insulin than VAT at 3 months, and the molecular basis of VAT's higher metabolic activity determines that this site is closely related to IR (Hardy et al., 2012).

We found that some genes involved in gonadal development and endocrine function were significantly different in SAF and VAF expression at 3 months. Through DEGs pathway analysis, expression of 9 genes related to male sexual development in 3 months VAF was significantly higher than in 3 months SAF, such as *Nkx3-1*, *GATA-6*, *transcription factor GATA-3* (*GATA-3*), *SFRP2*, etc. *Nkx3.1* gene is one of the new NK family homeobox

genes that has a regulatory role in embryonic development (Tanaka et al., 2000), and is one of the key regulatory genes involved in prostatic genesis. Expression of *Nkx3.1* is highly specific to prostatic epithelium (Gelmann et al., 2003), and in the development of embryos, its expression is parallel to the level of androgens. Studies on adult male mice showed that its mRNA expression is significantly increased during sexual maturation, but significantly decreased after castration, *Nkx3.1* being maintained at high expression in a time and concentration dependent manner by androgen (Prescott et al., 1998). GATA-3 and GATA-6 are members of a group of zinc finger-containing transcriptional regulatory factors important in the mammalian reproductive system, including sex determination and reproductive function regulation (De Rooij, 1998; Tremblay and Viger, 2001). GATA-3 is mainly expressed in the pituitary gland, whereas Gata-6 is mainly expressed in endocrine organs and heart, and is highly expressed in testis of human and other vertebrates. It affects the growth and development of testis of mice, promotes the proliferation of stromal and spermatogonial cells, and synthesizes androgens (Bennett et al., 2013; Convissar et al., 2015; Jahromi et al., 2016). The data shows that pigs are in the stage of puberty and sexual maturity. SAF and VAF are important in regulating gonad development in male pigs and there are obvious molecular differences. The results of expression trend analysis also supported this conclusion. We found that genes related to the GnRH signaling pathway were enriched in VAF significant expression trend Profile 0. With increasing age, expression of these genes was highest at 1 month, and gradually decreased by 3 and 6 months. Gonad development and sexual maturation initiation in mammals are regulated by the hypothalamic-pituitary-gonad axis. GnRH, a hormone secreted by the hypothalamus to regulate reproductive function, is critical in sexual maturation initiation. These results indicate that genes involved in pituitary-gonad axis in pigs are highly expressed in the early stage of VAF, which to some extent reveals the molecular mechanism of precocity and reproduction.

We also found that thyroid hormone synthesis and the prolactin signaling pathway related genes were highly expressed in 3 months VAF. Gene expression trend analysis also showed that, in Profile5, gene expression of insulin secretion, oxytocin signaling, thyroid hormone synthesis and steroid hormone biology pathways peaked at 3 months, being lower at 1 and 6 months. Oxytocin helps to reduce weight by reducing food intake and increasing energy expenditure and fat breakdown. Oxytocin signaling is closely related to visceral fat deposition, such that animals without it show significantly increased abdominal fat, the weight of fat pads in perirenal, mesenteric and epididymal regions being significantly increased (Wu et al., 2012). Obesity is closely related to thyroid function, and produces an important regulatory neurohormone that affects cell differentiation and development on one hand, but on the other hand it regulates various metabolic functions in the body, especially of fat and blood sugar. Decomposition of thyroid hormone on fat and blood sugar is often stronger than the synthesis effect of fat and blood sugar, which may be an important reason for the high metabolic activity of VAT (Pausova et al., 2010). The data suggest that prolactin signaling and thyroxine synthesis signaling pathways help regulate VAF energy balance; in particular, during sexual maturation, VAF adipose tissue development is closely related to reproductive and endocrine functions, including insulin secretion, gonadal axis development and the thyroid hormone, etc.

Because miniature pigs are small body size, one can determine how accurately control of the organ size is in maintaining tissue homeostasis and normal body function, issues that are being widely studies. We found that 11 genes involved in the Hippo signaling pathway were significantly higher in 3-months VAF than in SAF, including *bone Morphogenetic protein 7*(*BMP7*), *wingless-type MMTV integration site family member 16* (*WNT16*), Ras association (*RalGDS/AF-6*) *domain family member 6*(*RASSF6*), *amphiregulin* (*AREG*), *WNT5A, wingless-type MMTV integration site family, member 10B*(*WNT10B*), *WNT2B*, *WW and C2 domain containing 1* (*WWC1*), *discs, large homolog 3*(*DLG3*), *Protein kinase Cζ Zeta* (*PRKCZ*), etc., BMP7 is an important member of the Transforming growth factor-β (TGF-β) family (Bragdon et al., 2011), and is a secreted multifunctional protein. The heterodimer of BMP2/BMP7 and BMP4/BMP7 involved in the formation of BMP2/BMP7 and BMP4/BMP7 have good osteogenic bioactivity; it is prominent in promoting osteogenesis and cartilage. The Wingless-type MMTV Integration site family member (WNT) is a class of proteins that are important in growth and development, as well as in physiological and pathological processes. It can initiate intracellular WNT signal transduction pathways and conduct growth stimulus signals; it is also involved in different developmental mechanisms including cell proliferation, polarity, movement, differentiation, survival, self-renewal and calcium balance (Logan and Nusse, 2004; Mohammed et al., 2016; Doumpas et al., 2019). WNT5A, WNT16, WNT10B and WNT2B are important members of the WNT family, with their signal transduction pathways falling into classical pathways that determine cell fate and non-classical pathways that control cell movement and tissue polarity (Mohammed et al., 2016). The classical signaling pathway is involved in skeletal muscle development, affecting the fusion of myoblast cells (Suzuki et al., 2018) and mediating the regulation of Yes-associated protein (YAP) on bone homeostasis (Pan et al., 2018). In conclusion, VAT can be important role in bone and muscle development of Bama pigs by expressing BMP and WNT protein genes and activating the WNT signaling pathway. The Hippo signaling pathway is a growth mechanism that precisely controls organ size and maintains tissue homeostasis by balancing cell proliferation and apoptosis. Its core member is composed of the upstream kinase complex mammalian Sterile 20-like kinase (MST) MPS One Binder kinase, MOB) and the downstream transcription complex-YAP/ PDZ-binding motif, YAP/ TAZ-TEADS regulate cell fate by controlling the expression of time- and space-specific target genes (Zhou et al., 2016). He et al. (2020) first discovered *YAP* and *nuclear receptor subfamily 4, Group A, member 1* (*NR4A1*) in the Hippo signaling pathway, which can precisely determine the balance between cell proliferation and apoptosis to control organ size and maintain tissue homeostasis (He et al., 2020). Based on the high expression of genes involved

in the Hippo signaling pathway in 3 months VAT, we speculate that adipose tissue may be helpful in regulating the balance of cell proliferation and apoptosis controlling organ and tissue size through the Hippo and the WNT signaling pathways, and VAF could be more important than SAF. The functions and molecular mechanisms of the Hippo pathway and WNT adipose tissue expression related genes in pigs are worth further study.

IPA molecular network analysis has also shown that there are 35 DEGs involved in metabolism of lipid and signaling of hormones (**Figure 6**). 11 genes involved in the Hippo signaling pathway analyzed by KEGG were also included in this network, indicating that adipose metabolism and its endocrine function have a role in controlling the organ size. It is also suggested that regional differences of adipose not only influence body metabolism, but affect growth and development, regulating organ size. Those findings are consistent with the findings during *Drosophila* development where fat restricts organ size via the Salvador/Warts/Hippo pathway (Bennett and Harvey, 2006). STEM analysis integrated with the Gene Ontology also was used to explore the expression pattern of the DEGs in SAF and VAF among the three groups of pigs. Expression levels of the genes related to the cell cycle and the Hippo signaling pathway were downregulated in VAF as the pigs reached 6 months, including 15 genes (**Supplementary Table S23**). The findings suggested that VAF is involved in the regulation of organ size at the early stages of postnatal development. This novel finding demonstrates that adipose tissues genes expressed in different regions are closely associated with regulation of the size of a miniature pig. Further molecular validation is needed to elucidate the exact function of relevant adipose tissue genes in controlling the body size.

CONCLUSION

Through transcriptional analysis of the genes expressed in the SAF and VAF tissues of 1-, 3- and 6 months pigs, we identified the genes and pathways that are preferentially expressed in SAF or VAF tissues. These DGEs were functionally related to sexual development, hormone signaling pathways, lipid metabolism and the hippo signaling pathway, suggesting the importance of the signaling pathways contributing to significant regional and developmental stage differences. The findings highlight the essential functions of the molecular network in adipose tissues that potentially regulate adipose tissue deposition differences. Combining the molecular network and DGEs expression analysis, a molecular network that includes 35 DEGs involved in lipid metabolism and hormone signaling has been constructed in the IPA system. Our findings will help in further studies with genes relevant these differences between SAF and VAF during postnatal development. The data provides greater insight into the molecular mechanism of heterogeneity between SAF and VAF critical for health and disease processes of perhaps other living beings by the regulation of energy metabolism and endocrine function.

DATA AVAILABILITY STATEMENT

The datasets presented in this study can be found in online repositories. The names of the repository/repositories and accession number(s) can be found in the article/ **Supplementary Material**.

ETHICS STATEMENT

The animal study was reviewed and approved by All experimental actions were permitted by Committee of Experimental Animal Management at the Institute of Animal Husbandry and Veterinary Science, Shanghai Academy of Agricultural Sciences, Shanghai 201106, China (IACUS, SAASPZ 0520012). Written informed consent was obtained from the owners for the participation of their animals in this study.

AUTHOR CONTRIBUTIONS

YZ: Conceptualization, Validation, Formal analysis, Writing-Original Draft, Funding acquisition SR: Writing, Review and Editing HW: Visualization WT: Investigation JC: Investigation JH: Validation HW: Formal analysis CF: Resources SW: Resources YZ: Resources YT: Funding acquisition, Resources

FUNDING

This work was supported by the National Natural Science Foundation of China (Grant No. 31501937) and the Fund program of Shanghai Science and Technology Committee (Grant No. 18140900500).

ACKNOWLEDGMENTS

The authors thank all of the investigators, research assistants and laboratory technicians who contributed to this study.

SUPPLEMENTARY MATERIAL

The Supplementary Material for this article can be found online at: https://www.frontiersin.org/articles/10.3389/fgene.2022.844833/full#supplementary-material

REFERENCES

Aiello, L. C., and Wheeler, P. (1995). The Expensive-Tissue Hypothesis: The Brain and the Digestive System in Human and Primate Evolution. *Curr. Anthropol.* 36, 199–221. doi:10.1086/204350

Al-Gareeb, A., Alrubai, H., and Suliaman, S. (2016). Effects of Gliclazide Add on Metformin on Serum Omentin-1 Levels in Patients with Type 2 Diabetes Mellitus. *Indian J. Endocr. Metab.* 20, 195. doi:10.4103/2230-8210.176355

Alföldi, J., and Lindblad-Toh, K. (2013). Comparative Genomics as a Tool to Understand Evolution and Disease. *Genome Res.* 23, 1063–1068. doi:10.1101/gr.157503.113

Arner, P. (1995). Differences in Lipolysis between Human Subcutaneous and Omental Adipose Tissues. *Ann. Med.* 27, 435–438. doi:10.3109/07853899709002451

Ashburner, M., Ball, C. A., Blake, J. A., Botstein, D., Butler, H., Cherry, J. M., et al. (2000). Gene Ontology: Tool for the Unification of Biology. *Nat. Genet.* 25 (1), 25–29.

Bartness, T. J., and Song, C. K. (2007). Thematic Review Series: Adipocyte Biology. Sympathetic and Sensory Innervation of white Adipose Tissue. *J. Lipid Res.* 48, 1655–1672. doi:10.1194/jlr.r700006-jlr200

Bennett, F. C., and Harvey, K. F. (2006). Fat Cadherin Modulates Organ Size in Drosophila via the Salvador/Warts/Hippo Signaling Pathway. *Curr. Biol.* 16, 2101–2110. doi:10.1016/j.cub.2006.09.045

Bennett, J., Baumgarten, S. C., and Stocco, C. (2013). GATA4 and GATA6 Silencing in Ovarian Granulosa Cells Affects Levels of mRNAs Involved in Steroidogenesis, Extracellular Structure Organization, IGF-I Activity, and Apoptosis. *Endocrinology* 154, 4845–4858. doi:10.1210/en.2013-1410

Bjorbæk, C., and Kahn, B. B. (2004). Leptin Signaling in the Central Nervous System and the Periphery. *Recent Prog. Horm. Res.* 59, 305–332. doi:10.1210/rp.59.1.305

Bosello, O., and Vanzo, A. (2021). Obesity Paradox and Aging. *Eat. Weight Disord.* 26, 27–35. doi:10.1007/s40519-019-00815-4

Bragdon, B., Moseychuk, O., Saldanha, S., King, D., Julian, J., and Nohe, A. (2011). Bone Morphogenetic Proteins: A Critical Review. *Cell Signal.* 23, 609–620. doi:10.1016/j.cellsig.2010.10.003

Calvano, S. E., Xiao, W., Xiao, W., Richards, D. R., Felciano, R. M., Baker, H. V., et al. (2005). A Network-Based Analysis of Systemic Inflammation in Humans. *Nature* 437, 1032–1037. doi:10.1038/nature03985

Chen, H., Liu, Y.-Q., Li, C.-H., Guo, X.-M., and Huang, L.-J. (2009). The Susceptibility of Three Strains of Chinese Minipigs to Diet-Induced Type 2 Diabetes Mellitus. *Lab. Anim.* 38, 355–363. doi:10.1038/laban1109-355

Chen, S., Zhou, Y., Chen, Y., and Gu, J. (2018). Fastp: An Ultra-Fast All-In-One FASTQ Preprocessor. *Bioinformatics* 34 (17), i884–i890. doi:10.1093/bioinformatics/bty560

Convissar, S. M., Bennett, J., Baumgarten, S. C., Lydon, J. P., DeMayo, F. J., and Stocco, C. (2015). GATA4 and GATA6 Knockdown during Luteinization Inhibits Progesterone Production and Gonadotropin Responsiveness in the Corpus Luteum of Female Mice. *Biol. Reprod.* 93 (133), 133–110. doi:10.1095/biolreprod.115.132969

Covey, S. D., Wideman, R. D., McDonald, C., Unniappan, S., Huynh, F., Asadi, A., et al. (2006). The Pancreatic β Cell Is a Key Site for Mediating the Effects of Leptin on Glucose Homeostasis. *Cel Metab.* 4, 291–302. doi:10.1016/j.cmet.2006.09.005

De Oliveira Leal, V., and Mafra, D. (2013). Adipokines in Obesity. *Clinica Chim. Acta* 419, 87–94. doi:10.1016/j.cca.2013.02.003

De Rooij, D. G. (1998). Stem Cells in the Testis. *Int. J. Exp. Pathol.* 79, 67–80. doi:10.1046/j.1365-2613.1998.00057.x

Doumpas, N., Lampart, F., Robinson, M. D., Lentini, A., Nestor, C. E., Cantù, C., et al. (2019). TCF/LEF Dependent and Independent Transcriptional Regulation of Wnt/β-Catenin Target Genes. *Embo J.* 38, e98873. doi:10.15252/embj.201798873

Draghici, S., Khatri, P., Tarca, A. L., Amin, K., Done, A., Voichita, C., et al. (2007). A Systems Biology Approach for Pathway Level Analysis. *Genome Res.* 17, 1537–1545. doi:10.1101/gr.6202607

Ehrenkaufer, G. M., Weedall, G. D., Williams, D., Lorenzi, H. A., Caler, E., Hall, N., et al. (2013). The Genome and Transcriptome of the Enteric Parasite Entamoeba Invadens, a Model for Encystation. *Genome Biol.* 14, R77. doi:10.1186/gb-2013-14-7-r77

Ernst, J., and Bar-Joseph, Z. (2006). STEM: A Tool for the Analysis of Short Time Series Gene Expression Data. *BMC Bioinformatics* 7, 191. doi:10.1186/1471-2105-7-191

Esteban, M. A., Xu, J., Yang, J., Peng, M., Qin, D., Li, W., et al. (2009). Generation of Induced Pluripotent Stem Cell Lines from Tibetan Miniature Pig. *J. Biol. Chem.* 284, 17634–17640. doi:10.1074/jbc.m109.008938

Fried, S. K., Tittelbach, T., Blumenthal, J., Sreenivasan, U., Robey, L., Yi, J., et al. (2010). Resistance to the Antilipolytic Effect of Insulin in Adipocytes of African-American Compared to Caucasian Postmenopausal Women. *J. Lipid Res.* 51, 1193–1200. doi:10.1194/jlr.p000935

Gabler, N. K., Radcliffe, J. S., Spencer, J. D., Webel, D. M., and Spurlock, M. E. (2009). Feeding Long-Chain N–3 Polyunsaturated Fatty Acids during Gestation Increases Intestinal Glucose Absorption Potentially via the Acute Activation of AMPK. *J. Nutr. Biochem.* 20, 17–25. doi:10.1016/j.jnutbio.2007.11.009

Gelmann, E. P., Bowen, C., and Bubendorf, L. (2003). Expression of NKX3.1 in Normal and Malignant Tissues. *Prostate* 55, 111–117. doi:10.1002/pros.10210

Getz, G., and Reardon, C. (2018). Apoprotein E and Reverse Cholesterol Transport. *Int. J. Mol. Sci.* 19, 3479. doi:10.3390/ijms19113479

Groenen, M. A., Archibald, A. L., Uenishi, H., Tuggle, C. K., Takeuchi, Y., Rothschild, M. F., et al. (2012). Analyses of Pig Genomes Provide Insight into Porcine Demography and Evolution. *Nature* 491, 393–398. doi:10.1038/nature11622

Halaas, J. L., Gajiwala, K. S., Maffei, M., Cohen, S. L., Chait, B. T., Rabinowitz, D., et al. (1995). Weight-Reducing Effects of the Plasma Protein Encoded by the Obese Gene. *Science* 269, 543–546. doi:10.1126/science.7624777

Hardy, O. T., Czech, M. P., and Corvera, S. (2012). What Causes the Insulin Resistance Underlying Obesity? *Curr. Opin. Endocrinol.* 19, 81–87. doi:10.1097/med.0b013e3283514e13

Harvey, I., Boudreau, A., and Stephens, J. M. (2020). Adipose Tissue in Health and Disease. *Open Biol.* 10, 200291. doi:10.1098/rsob.200291

He, L., Yuan, L., Yu, W., Sun, Y., Jiang, D., Wang, X., et al. (2020). A Regulation Loop between YAP and NR4A1 Balances Cell Proliferation and Apoptosis. *Cel Rep.* 33, 108284. doi:10.1016/j.celrep.2020.108284

Highman, T. J., Friedman, J. E., Huston, L. P., Wong, W. W., and Catalano, P. M. (1998). Longitudinal Changes in Maternal Serum Leptin Concentrations, Body Composition, and Resting Metabolic Rate in Pregnancy. *Am. J. Obstet. Gynecol.* 178, 1010–1015. doi:10.1016/s0002-9378(98)70540-x

Hoffstedt, J., Arner, E., Wahrenberg, H., Andersson, D. P., Qvisth, V., Löfgren, P., et al. (2010). Regional Impact of Adipose Tissue Morphology on the Metabolic Profile in Morbid Obesity. *Diabetologia* 53, 2496–2503. doi:10.1007/s00125-010-1889-3

Jahromi, M. S., Tehrani, F. R., Noroozzadeh, M., Zarkesh, M., Ghasemi, A., and Zadeh-Vakili, A. (2016). Elevated Expression of Steroidogenesis Pathway Genes; CYP17, GATA6 and StAR in Prenatally Androgenized Rats. *Gene* 593, 167–171. doi:10.1016/j.gene.2016.07.067

Kahn, B. B., and Flier, J. S. (2000). Obesity and Insulin Resistance. *J. Clin. Invest.* 106 (4), 473–481. doi:10.1172/jci10842

Karpe, F., and Pinnick, K. E. (2015). Biology of Upper-Body and Lower-Body Adipose Tissue-Link to Whole-Body Phenotypes. *Nat. Rev. Endocrinol.* 11, 90–100. doi:10.1038/nrendo.2014.185

Kim, D., Paggi, J. M., Park, C., Bennett, C., and Salzberg, S. L. (2019). Graph-Based Genome Alignment and Genotyping with HISAT2 and HISAT-Genotype. *Nat. Biotechnol.* 37, 907–915. doi:10.1038/s41587-019-0201-4

Koutsari, C., Ali, A. H., Mundi, M. S., and Jensen, M. D. (2011). Storage of Circulating Free Fatty Acid in Adipose Tissue of Postabsorptive Humans. *Diabetes* 60, 2032–2040. doi:10.2337/db11-0154

Kuk, J. L., Saunders, T. J., Davidson, L. E., and Ross, R. (2009). Age-Related Changes in Total and Regional Fat Distribution. *Ageing Res. Rev.* 8, 339–348. doi:10.1016/j.arr.2009.06.001

Kulkarni, R. N., Wang, Z. L., Wang, R. M., Hurley, J. D., Smith, D. M., Ghatei, M. A., et al. (1997). Leptin Rapidly Suppresses Insulin Release from Insulinoma Cells, Rat and Human Islets and, *In Vivo*, in Mice. *J. Clin. Invest.* 100, 2729–2736. doi:10.1172/jci119818

Lebovitz, H. (2001). Insulin Resistance: Definition and Consequences. *Exp. Clin. Endocrinol. Diabetes* 109, S135–S148. doi:10.1055/s-2001-18576

Lee, M.-J., Wu, Y., and Fried, S. K. (2013). Adipose Tissue Heterogeneity: Implication of Depot Differences in Adipose Tissue for Obesity Complications. *Mol. Aspects Med.* 34, 1–11. doi:10.1016/j.mam.2012.10.001

Li, J., Liu, Y., Zhang, J. W., Wei, H., and Yang, L. (2006). Characterization of Hepatic Drug-Metabolizing Activities of Bama Miniature Pigs (*Sus scrofa* Domestica): Comparison with Human Enzyme Analogs. *Comp. Med.* 56, 286–290.

Lima-Martínez, M. M., Blandenier, C., and Iacobellis, G. (2013). Epicardial Adipose Tissue: More Than a Simple Fat Deposit? *Endocrinología y Nutrición (English Edition)* 60, 320–328. doi:10.1016/j.endoen.2012.08.013

Liu, H.-B., Lv, P.-R., He, R.-G., Yang, X.-G., Qin, X.-E., Pan, T.-B., et al. (2010). Cloned Guangxi Bama Minipig (*Sus Scrofa*) and its Offspring Have normal Reproductive Performance. *Cell Reprogramming* 12, 543–550. doi:10.1089/cell.2009.0094

Liu, H.-B., Lv, P.-R., Yang, X.-G., Qin, X.-E., Pi, D.-Y., Lu, Y.-Q., et al. (2009). Fibroblasts from the New-Born Male Testicle of Guangxi Bama Mini-Pig (*Sus Scrofa*) Can Support Nuclear Transferred Embryo Development *In Vitro*. *Zygote* 17, 147–156. doi:10.1017/s0967199408005145

Liu, Y., Zeng, B. H., Shang, H. T., Cen, Y. Y., and Wei, H. (2008). Bama Miniature Pigs (*Sus Scrofa* Domestica) as a Model for Drug Evaluation for Humans: Comparison of *In Vitro* Metabolism and *In Vivo* Pharmacokinetics of Lovastatin. *Comp. Med.* 58, 580–587.

Logan, C. Y., and Nusse, R. (2004). The Wnt Signaling Pathway in Development and Disease. *Annu. Rev. Cel Dev. Biol.* 20, 781–810. doi:10.1146/annurev.cellbio.20.010403.113126

Love, M. I., Huber, W., and Anders, S. (2014). Moderated Estimation of Fold Change and Dispersion for RNA-Seq Data with DESeq2. *Genome Biol.* 15 (12), 550. doi:10.1186/s13059-014-0550-8

Lunney, J. K. (2007). Advances in Swine Biomedical Model Genomics. *Int. J. Biol. Sci.* 3, 179–184. doi:10.7150/ijbs.3.179

Madani, R., Karastergiou, K., Ogston, N., Miheisi, N., Bhome, R., Haloob, N., et al. (2009). RANTES Release by Human Adipose Tissue *In Vivo* and Evidence for Depot-specific Differences. *Am. J. Physiol-endoc M.* 296, E1262–E1268. doi:10.1152/ajpendo.90511.2008

Mayburd, A. L., Martlínez, A., Sackett, D., Liu, H., Shih, J., Tauler, J., et al. (2006). Ingenuity Network-Assisted Transcription Profiling: Identification of a New Pharmacologic Mechanism for MK886. *Clin. Cancer Res.* 12, 1820–1827. doi:10.1158/1078-0432.ccr-05-2149

McCoy, M. G., Sun, G.-S., Marchadier, D., Maugeais, C., Glick, J. M., and Rader, D. J. (2002). Characterization of the Lipolytic Activity of Endothelial Lipase. *J. Lipid Res.* 43, 921–929. doi:10.1016/s0022-2275(20)30466-1

Mohammed, M. K., Shao, C., Wang, J., Wei, Q., Wang, X., Collier, Z., et al. (2016). Wnt/β-Catenin Signaling Plays an Ever-Expanding Role in Stem Cell Self-Renewal, Tumorigenesis and Cancer Chemoresistance. *Genes Dis.* 3, 11–40. doi:10.1016/j.gendis.2015.12.004

Pan, J. X., Xiong, L., Zhao, K., Zeng, P., Wang, B., Tang, F. L., et al. (2018). YAP Promotes Osteogenesis and Suppresses Adipogenic Differentiation by Regulating β-Catenin Signaling. *Bone Res.* 6, 18. doi:10.1038/s41413-018-0018-7

Pausova, Z., Abrahamowicz, M., Mahboubi, A., Syme, C., Leonard, G. T., Perron, M., et al. (2010). Functional Variation in the Androgen-Receptor Gene Is Associated with Visceral Adiposity and Blood Pressure in Male Adolescents. *Hypertension* 55, 706–714. doi:10.1161/hypertensionaha.109.146720

Pelleymounter, M. A., Cullen, M. J., Baker, M. B., Hecht, R., Winters, D., Boone, T., et al. (1995). Effects of the Obese Gene Product on Body Weight Regulation in Ob / Ob Mice. *Science* 269, 540–543. doi:10.1126/science.7624776

Powe, C. E., Huston Presley, L. P., Locascio, J. J., and Catalano, P. M. (2019). Augmented Insulin Secretory Response in Early Pregnancy. *Diabetologia* 62 (8), 1445–1452.

Pradat, P.-F. (2021). The Cerebellum in ALS: Friend or Foe? *J. Neurol. Neurosurg. Psychiatry* 92 (11), 1137. doi:10.1136/jnnp-2021-327216

Prescott, J. L., Blok, L., and Tindall, D. J. (1998). Isolation and Androgen Regulation of the Human Homeobox cDNA,NKX3.1. *Prostate* 35, 71–80. doi:10.1002/(sici)1097-0045(19980401)35:1<71::aid-pros10>3.0.co;2-h

Rothschild, M. F. (2004). Porcine Genomics Delivers New Tools and Results: This Little Piggy Did More Than Just Go to Market. *Genet. Res.* 83, 1–6. doi:10.1017/s0016672303006621

Schook, L., Beattie, C., Beever, J., Donovan, S., Jamison, R., Zuckermann, F., et al. (2005). Swine in Biomedical Research: Creating the Building Blocks of Animal Models. *Anim. Biotechnol.* 16, 183–190. doi:10.1080/10495390500265034

Suzuki, A., Minamide, R., and Iwata, J. (2018). WNT/β-Catenin Signaling Plays a Crucial Role in Myoblast Fusion through Regulation of Nephrin Expression during Development. *Development* 145, dev168351. doi:10.1242/dev.168351

Tamemoto, H., Kadowaki, T., Tobe, K., Yagi, T., Sakura, H., Hayakawa, T., et al. (1994). Insulin Resistance and Growth Retardation in Mice Lacking Insulin Receptor Substrate-1. *Nature* 372, 182–186. doi:10.1038/372182a0

Tanaka, M., Komuro, I., Inagaki, H., Jenkins, N. A., Copeland, N. G., and Izumo, S. (2000). Nkx3.1, a Murine Homolog of Drosophila Bagpipe, Regulates Epithelial Ductal Branching and Proliferation of the Prostate and palatine Glands. *Dev. Dyn.* 219, 248–260. doi:10.1002/1097-0177(2000)9999:9999<::aid-dvdy1054>3.3.co;2-5

Tchkonia, T., Tchoukalova, Y. D., Giorgadze, N., Pirtskhalava, T., Karagiannides, I., Forse, R. A., et al. (2005). Abundance of Two Human Preadipocyte Subtypes with Distinct Capacities for Replication, Adipogenesis, and Apoptosis Varies Among Fat Depots. *Am. J. Physiology-Endocrinology Metab.* 288, E267–E277. doi:10.1152/ajpendo.00265.2004

Thomas, E. A., Dean, B., Scarr, E., Copolov, D., and Sutcliffe, J. G. (2003). Differences in Neuroanatomical Sites of apoD Elevation Discriminate between Schizophrenia and Bipolar Disorder. *Mol. Psychiatry* 8, 167–175. doi:10.1038/sj.mp.4001223

Tous, N., Lizardo, R., Vilà, B., Gispert, M., Font-i-Furnols, M., and Esteve-Garcia, E. (2013). Effect of a High Dose of CLA in Finishing Pig Diets on Fat Deposition and Fatty Acid Composition in Intramuscular Fat and Other Fat Depots. *Meat Sci.* 93, 517–524. doi:10.1016/j.meatsci.2012.10.005

Tremblay, J. J., and Viger, R. S. (2001). GATA Factors Differentially Activate Multiple Gonadal Promoters through Conserved GATA Regulatory Elements. *Endocrinology* 142, 977–986. doi:10.1210/endo.142.3.7995

Van Harmelen, V., Röhrig, K., and Hauner, H. (2004). Comparison of Proliferation and Differentiation Capacity of Human Adipocyte Precursor Cells from the Omental and Subcutaneous Adipose Tissue Depot of Obese Subjects. *Metabolism* 53, 632–637. doi:10.1016/j.metabol.2003.11.012

Varma, V., Yao-Borengasser, A., Rasouli, N., Bodles, A. M., Phanavanh, B., Lee, M.-J., et al. (2007). Human Visfatin Expression: Relationship to Insulin Sensitivity, Intramyocellular Lipids, and Inflammation. *J. Clin. Endocr. Metab.* 92, 666–672. doi:10.1210/jc.2006-1303

Virtanen, K. A., Lönnroth, P., Parkkola, R., Peltoniemi, P., Asola, M., Viljanen, T., et al. (2002). Glucose Uptake and Perfusion in Subcutaneous and Visceral Adipose Tissue during Insulin Stimulation in Nonobese and Obese Humans. *J. Clin. Endocr. Metab.* 87, 3902–3910. doi:10.1210/jcem.87.8.8761

Wang, Y., Sullivan, S., Trujillo, M., Lee, M.-J., Schneider, S. H., Brolin, R. E., et al. (2003). Perilipin Expression in Human Adipose Tissues: Effects of Severe Obesity, Gender, and Depot. *Obes. Res.* 11, 930–936. doi:10.1038/oby.2003.128

Wen, G. (2017). "A Simple Process of RNA-Sequence Analyses by Hisat2, Htseq and DESeq2," in Proceedings of the 2017 International Conference on Biomedical Engineering and Bioinformatics, Bangkok, Thailand, September 14–16, 2017 (Bangkok, Thailand: Association for Computing Machinery), 11–15. doi:10.1145/3143344.3143354

Westphal, S. A. (2008). Obesity, Abdominal Obesity, and Insulin Resistance. *Clin. Cornerstone* 9 (1), 23–31. doi:10.1016/s1098-3597(08)60025-3

Wu, W., Ji, M., Xu, K., Zhang, D., Yin, Y., Huang, X., et al. (2020). Knockdown of CTRP6 Reduces the Deposition of Intramuscular and Subcutaneous Fat in Pigs via Different Signaling Pathways. *Biochim. Biophys. Acta (Bba) - Mol. Cel Biol. Lipids* 1865, 158729. doi:10.1016/j.bbalip.2020.158729

Wu, Z., Xu, Y., Zhu, Y., Sutton, A. K., Zhao, R., Lowell, B. B., et al. (2012). An Obligate Role of Oxytocin Neurons in Diet Induced Energy Expenditure. *Plos One* 7, e45167. doi:10.1371/journal.pone.0045167

Ye, J. (2021). Mechanism of Insulin Resistance in Obesity: A Role of ATP. *Front. Med.* 15 (3), 372–382. doi:10.1007/s11684-021-0862-5

Yu, G., Wang, L. G., Han, Y., and He, Q. Y. (2012). Cluster Profiler: An R Package for Comparing Biological Themes Among Gene Clusters. *Omics* 16 (5), 284–287.

Zhang, N., Jing, W., Cheng, J., Cui, W., Mu, Y., Li, K., et al. (2011). Molecular Characterization and NF-κB-Regulated Transcription of Selenoprotein S from

the Bama Mini-Pig. *Mol. Biol. Rep.* 38, 4281–4286. doi:10.1007/s11033-010-0551-y

Zhang, T.-Y., Dai, J.-J., Wu, C.-F., Gu, X.-L., Liu, L., Wu, Z.-Q., et al. (2012). Positive Effects of Treatment of Donor Cells with Aphidicolin on the Preimplantation Development of Somatic Cell Nuclear Transfer Embryos in Chinese Bama Mini-Pig (*Sus Scrofa*). *Anim. Sci. J.* 83, 103–110. doi:10.1111/j.1740-0929.2011.00926.x

Zhou, Y., Guo, H., Yang, Y., Wang, Z., Li, X., Zhou, R., et al. (2016). Facile Synthesis of Silicon/Carbon Nanospheres Composite Anode Materials for Lithium-Ion Batteries. *Mater. Lett.* 168, 138–142. doi:10.1016/j.matlet.2016.01.009

Conflict of Interest: The authors declare that the research was conducted in the absence of any commercial or financial relationships that could be construed as a potential conflict of interest.

Publisher's Note: All claims expressed in this article are solely those of the authors and do not necessarily represent those of their affiliated organizations, or those of the publisher, the editors, and the reviewers. Any product that may be evaluated in this article, or claim that may be made by its manufacturer, is not guaranteed or endorsed by the publisher.

frontiers | Frontiers in Cell and Developmental Biology

ORIGINAL RESEARCH
published: 06 April 2022
doi: 10.3389/fcell.2022.856881

Transdifferentiation of Myoblasts Into Adipocytes by All-*Trans*-Retinoic Acid in Avian

Dong-Hwan Kim[1], *Joonbum Lee*[1,2], *Yeunsu Suh*[1], *Jae-Kyun Ko*[3] *and Kichoon Lee*[1,2]*

[1]*Department of Animal Sciences, The Ohio State University, Columbus, OH, United States,* [2]*The Ohio State University Interdisciplinary Human Nutrition Program, The Ohio State University, Columbus, OH, United States,* [3]*Department of Surgery, Davis Heart and Lung Research Institute, The Ohio State University, Columbus, OH, United States*

Increased adipogenesis in muscle tissues is related to metabolic syndromes and muscle weakness in humans and improvement of meat quality in animal production. With growing evidence for pro-adipogenic functions of all-*trans*-retinoic acid (atRA), the current study investigated whether atRA can transdifferentiate myoblasts into adipocytes using a quail myogenic cell line (QM7) and avian primary myoblasts. atRA increased cytoplasmic lipid droplet accumulation and mRNA expression for adipogenic genes in these cells. An acute induction of Pparγ expression by atRA under cycloheximide treatment indicated a direct regulation of Pparγ by atRA. In addition, the induction of Pparγ expression was mediated by retinoic acid receptors . At high levels of Pparγ by atRA, BADGE, an antagonist of Pparγ, inhibited, and rosiglitazone, an agonist of Pparγ, further enhanced atRA-induced transdifferentiation. However, at very low levels of Pparγ in the absence of atRA treatment, rosiglitazone could not induce transdifferentiation of avian myoblasts. These data suggest that the induction of Pparγ expression by atRA is an essential molecular event in myoblasts for atRA-induced transdifferentiation into adipocytes. Based on our findings, atRA can be a new transdifferentiation factor of myoblasts to adipocytes, providing a potential nutrient to enhance marbling in poultry.

Keywords: transdifferentiation, myoblast, adipocyte, all-trans retinoic acid, Ppar gamma, avian

OPEN ACCESS

Edited by:
Min Du,
Washington State University, United States

Reviewed by:
Xing Fu,
Louisiana State University Agricultural Center, United States
Eric Testroet,
University of Vermont, United States
Marcio Duarte,
University of Guelph, Canada

***Correspondence:**
Kichoon Lee
lee.2626@osu.edu

Specialty section:
This article was submitted to Cellular Biochemistry, a section of the journal Frontiers in Cell and Developmental Biology

Received: *17 January 2022*
Accepted: *07 March 2022*
Published: *06 April 2022*

Citation:
Kim D-H, Lee J, Suh Y, Ko J-K and Lee K (2022) Transdifferentiation of Myoblasts Into Adipocytes by All-Trans-Retinoic Acid in Avian. Front. Cell Dev. Biol. 10:856881. doi: 10.3389/fcell.2022.856881

1 INTRODUCTION

Intramuscular adipose tissues (IMAT; also termed as marbling fat) are found within muscles. In meat animals, the amount of IMAT is an important criterion to decide the meat quality including flavor, tenderness, and juiciness (Albrecht et al., 2006). Similar to ruminants, including cattle and sheep, amounts of IMAT in poultry breast are generally related to juiciness and tenderness suggesting an importance of IMAT in poultry meat quality (Lonergan et al., 2003). Therefore, identification of new factors increasing IMAT and understanding of their functions lead to developing potential strategies for enhancing marbling fat and improving meat quality in poultry.

Adipogenesis is a process of converting mesodermal precursor cells into adipocytes (Farmer 2006), being accompanied by the initiation of expression of adipogenic transcription factors including peroxisome proliferator-activated receptor γ (Pparγ). These precursor cells have abilities to be differentiated into myocytes with the expression of myogenic transcriptional factors (Rosen and MacDougald 2006; Rodeheffer et al., 2008). Especially, Pparγ has been served as a well-known indicator for adipogenic differentiation in mammals (Tamori et al., 2002; Liang et al., 2016) and avian species (Kim et al., 2020a, Kim et al., 2020b, Kim et al., 2021a, Kim et al., 2021b;

Lee et al., 2021). In addition, over-expression or activation of Pparγ can convert myogenic cells to adipocytes (Hu et al., 1995; Teboul et al., 1995). Supplementation of vitamin D in adipogenic media induced transdifferentiation of the C2C12 myogenic cell line to adipocytes, which is accompanied with the expression of Pparγ (Ryan et al., 2013). Pparγ has served as an important differentiation marker and a potential inducer for transdifferentiation of myocytes to adipocytes in cultures of rodent myogenic cell lines.

All-*trans*-retinoic acid (atRA) which is as a metabolite of vitamin A (retinol) functions as a regulatory molecule in cell differentiation and development including adipogenesis both *in vitro* and *in vivo*. Previous studies showed that adipogenic differentiation can be induced by the supplementation of atRA. Ob1771 cells were differentiated into adipogenic cells by the supplementation of 10 nM of atRA (Safonova et al., 1994). Adipogenic differentiation of 3T3-L1 cells was negatively or positively regulated by supplementation of high- or low-doses of atRA, respectively (Kim et al., 2019). In various avian cell types, chicken embryonic fibroblasts which are isolated at embryonic day (E) 5, stromal vascular cells isolated from fat tissues of chicken embryos, and a DF-1 chicken embryonic fibroblast cell line can be induced to adipogenic cells in the culture condition supplementing atRA (Kim D.-H. et al., 2020; Lee et al., 2021). Furthermore, direct *in ovo* injection of atRA increased adipose weight and size during embryonic development (Kim et al., 2021a). Although atRA has positive regulatory effects on adipogenic differentiation of various avian cell types, it has not been specifically investigated whether atRA can induce transdifferentiation of myoblasts into adipocytes in poultry. In this study, a quail myogenic cell line (QM7) and primary myoblasts from chicken and quail embryos were used to investigate the effects of atRA on transdifferentiation from myogenic to adipogenic cells and the involvement of Pparγ in this process.

2 MATERIALS AND METHODS

2.1 Induction of Adipogenic or Myogenic Differentiation

The quail muscle clone 7 (QM7, ATCC, #CRL-1962, Rockville, MD, United States) cell line was cultured in medium 199 supplemented with 10% fetal bovine (#F4135, Sigma-Aldrich, St. Louis, MO, United States), 10% tryptose phosphate broth (#T8159, Sigma-Aldrich), and 1% antibiotic-antimycotic solution (#15240062, Gibco, Grand Island, NY, United States). Primary myoblasts were isolated from pectoralis muscles of each quail embryo at E12, and each chicken embryo at E13, totaling eight embryos per species in four independent experimental trials, as followed from our previous study (Hassan et al., 2014). Muscle tissues were digested in DMEM containing 1.6 mg/ml collagenase II (#17101015, Sigma-Aldrich) at 37°C with a shaking incubator for 1 h. Then, the tissues were filtered through a 70 mm cell strainer (#352350, BD Falcon, Ahn Arbor, MI, United States) and seeded on a collagen (#A1048301, Thermo Fisher Scientific, Waltham, MA, United States) coated 12-well plate after washing with PBS. The primary myoblasts were cultured in Dulbecco's modified Eagle's medium (DMEM, #11965, Gibco) supplemented with 10% fetal bovine serum (FBS, #F4135, Sigma-Aldrich), and 1% antibiotic–antimycotic solution (#15240062, Gibco). To test the potential effect of atRA on adipogenic differentiation of myoblasts, different concentrations of atRA (0 μM, 100 μM, 150 μM, or 200 μM, #R2625, Sigma-Aldrich) were supplemented to the basic adipogenic media, DMEM containing only 10% chicken serum (CS, #C5405, Sigma-Aldrich) (Kim et al., 2021b), for 48 h. Due to similar viability of the cells between the two groups, 0 and 100 μM of atRA (**Supplementary Figure S1**), 100 μM of atRA was mainly used in this study. Myogenic differentiation was induced by 1% horse serum (HS, #16050, Gibco) for 48 h.

2.2 Lipid Droplet Formation Assay

To examine lipid accumulation, after inducing adipogenic differentiation of the cells for 48 h, they were stained by Oil-Red-O (ORO) to visualize and quantify the formatted lipid droplets as followed from our previous study (Kim D. H. et al., 2020). For quantifying lipid accumulation, ORO was extracted with 100% isopropanol and absorbance values were measured at 490 nm by a spectrophotometer (SpectraMax Plus384, Molecular Devices, Sunnyvale, CA, United States). Undifferentiated cells were used as a negative control. Stained cells were visualized using a microscope (EVOS cell imaging system, Thermo Fisher Scientific).

2.3 RNA Isolation and Reverse-Transcription Quantitative PCR

Total RNA was isolated using TRIzol (#15596026, Invitrogen, Waltham, MA, United States) and cDNA was synthesized by Moloney murine leukemia virus reverse transcriptase (#28020513, Invitrogen) by the methods described in our previous study (Kim D. H. et al., 2020). qPCR was conducted by using AmpliTaq Gold polymerase (#N8080241, Applied Biosystems, Foster City, CA, United States) and SYBR green as detection dyes on an ABI 7300 Real-Time PCR instrument (Applied Biosystems). To quantify gene expression levels involved in adipogenesis and myogenesis, over three independent experiments were performed and each experiment was duplicated. qPCR was performed in duplicate with specific primer sets (**Supplementary Table S1**). The expression levels were normalized to those of endogenous glyceraldehyde-3-phosphate dehydrogenase (Gapdh) and the data were analyzed using the ddCt method (Livak and Schmittgen 2001).

2.4 Chemical Treatments

All chemicals, atRA, AGN194310 (AGN, #SML2665, Sigma-Aldrich), cycloheximide (CHX, #C7698, Sigma-Aldrich), bisphenol A diglycidyl ether (BADGE, #D3415, Sigma-Aldrich), and rosiglitazone (Rosi, #R2408, Sigma-Aldrich), were dissolved in dimethyl sulfoxide (DMSO). In order to examine the acute changes of expression levels of Pparγ after supplementation of atRA in myogenic cells, chicken or quail

primary myoblasts, and QM7 cells, the cells were incubated with different concentrations of atRA (0 μM, 150 μM, or 300 μM) for 0, 3, or 5 h and then, qPCR was performed to analyze the expression levels of Pparγ.

To further investigate whether a new protein translation is required for the induction of Pparγ expression by atRA, 10 mg/ml of CHX, an inhibitor of protein synthesis, was pre-incubated for 1 h and then, after washing with PBS, further incubated with a medium supplemented with different concentrations of atRA (0 μM, 150 μM, or 300 μM) for 5 h. After 5 h, the expression levels of Pparγ were analyzed from each of the cells supplemented with atRA. In addition, to examine if the induction of Pparγ by atRA can be mediated by retinoic acid receptors (RAR), different concentrations (0 μM, 10 μM, or 100 μM) of AGN as an RAR antagonist were supplemented with or without 150 μM of atRA for 5 h in QM7 cells.

BADGE or Rosi, an antagonist or agonist of Pparγ, respectively, was used to investigate the effects of Pparγ activities on atRA-induced transdifferentiation. One or 2 mM of BADGE was co-incubated with 100 μM of atRA, and Rosi (10 nM) was co-incubated with 50 μM of atRA during the induction of adipogenic differentiation for 2 days. At D2 of differentiation, the cells were stained with ORO.

2.5 Statistical Analysis

All data in this study were replicated at least three times ($n \geq 3$) and were expressed as means ± SEM. All statistical analyses were performed by the GraphPad Prism software (ver. 6.02) and detailed numbers of samples were described in each of the figure legends. For *t*-test and one-way ANOVA followed by Tukey's multiple comparison test, *p*-value, $p < 0.05$, was considered as a statistically significant difference.

3 RESULTS

3.1 Effect of atRA on Lipid Accumulation in QM7 Cells

In general, insulin, isobutylmethylxanthine (IBMX), and dexamethasone have been widely used for adipogenic differentiation in a mammal system including 3T3-L1 cells. However, we developed a minimal adipogenic media containing chicken serum alone that can differentiate avian embryonic fibroblasts into adipocytes (Kim et al., 2021b). This minimal adipogenic media for avian species can be used to directly test hormonal and nutritional factors without complex interactions of several factors included in so-called adipogenic cocktails. Using the basal media containing 10% CS, adipogenic potential of atRA has been demonstrated in primary embryonic fibroblasts and a fibroblast cell line in avian systems (Kim D.-H. et al., 2020; Lee et al., 2021). In the current study, the capability of atRA inducing transdifferentiation of myoblasts into adipocytes was also tested in the basal avian adipogenic differentiation media containing CS alone. Therefore, QM7 cells were incubated in 10% CS with/without 100 μM of atRA for 48 h to induce adipogenic differentiation. Morphological and quantitative assessments of lipid droplet formation and lipid accumulation, respectively, were performed by analyses of ORO staining. The degrees of lipid droplet formation were higher in the order of 10% CS with 100 μM atRA, 10% CS with 0 μM atRA, and 10% FBS with 0 μM atRA (**Figures 1A,B**). Also, the quantification of ORO by spectrometrical analysis revealed a significantly increased lipid accumulation by supplementation of atRA in 10% CS (**Figure 1B**). These results suggest that atRA induces lipid accumulation in quail myogenic cell lines.

3.2 Regulation of Adipogenic/Myogenic Fators by atRA

In addition to lipid droplet formation in the quail myoblast cell lines by atRA, it was necessary to verify molecular evidence for transdifferentiation of the QM7 cells into adipogenic cells by measuring the expression of critical genes involved in adipogenesis and myogenesis. Expression levels of the zinc finger protein 423 (Znf423) gene, as a marker of an early stage of adipogenic differentiation (Gupta et al., 2010), were significantly increased by the supplementation of 100 μM atRA in 10% CS (**Figure 2A**). As major adipogenic markers, the expression of Pparγ and fatty acid binding protein 4 (Fabp4) genes were dramatically induced by more than 30-fold with 100 μM atRA compared to other groups ($p < 0.01$) (**Figure 2A**). In addition, fatty acid transporter 4 (Fatp4), acyl-CoA synthetase long-chain family 1 (Acsl1), and acylglycerolphosphate acyltransferase 1 (Agpat1), which are involved in fatty acid uptake and triacylglycerol (TAG) synthesis, were also significantly up-regulated by the 10% CS with 100 μM atRA compared to the other groups (**Figure 2B**). On the other hand, the expression levels of myogenic markers, paired box 7 (Pax7), myogenic factor 5 (Myf5), and myogenin (MyoG) were significantly down-regulated by supplementation of 10% CS with 100 μM atRA compared to the other groups (**Figure 2C**).

3.3 Pro-Adipognegic Effect of atRA in Primary Muscle Cells of Quail and Chickens

In order to investigate whether the muscle-originated primary cells can be differentiated into adipogenic cells by atRA, isolated primary muscle cells were cultured for 48 h in four different media: 1% HS as a standard myogenic medium, 10% FBS as a standard growth medium, 10% CS as a control medium, and 10% CS with 100 μM of atRA as an adipogneic medium. As expected, primary myocytes isolated from quail and chicken have undergone myogenic differentiation by 1% HS, showing the lining up of myocytes to form nascent myotubes as previously shown in our reports (Shin et al., 2015). Although 10% FBS also resulted in mild degrees of myotube formation, there was no accumulation of lipid droplets in cultures of quail and chicken primary myoblasts (**Figures 3A,C**). Although fine lipid droplets appeared after 48 h of incubation with 10% CS (**Figure 3A**), supplementation with 100 μM of atRA seemed to increase sizes and numbers of lipid droplets in cultures of quail and chicken primary myoblasts (**Figures 3A,C**). These were further confirmed by the finding that amounts of ORO were significantly increased

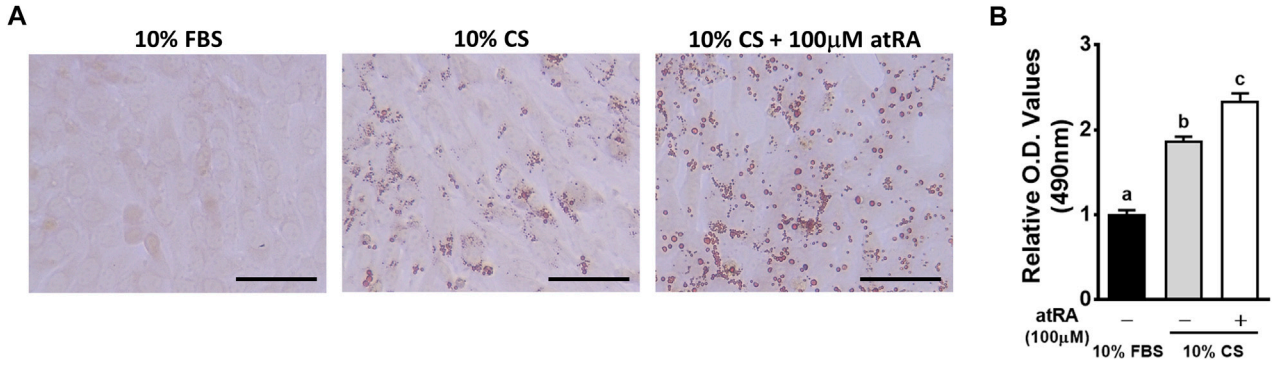

FIGURE 1 | Effects of various media on the lipid accumulation in QM7 cells. Oil-Red-O (ORO) staining **(A)** and O.D. values **(B)**. QM7 cells were incubated with different media, 10% fetal bovine serum (FBS), 10% chicken serum (CS), or a combination of 10% CS and 100 μM all-*trans*-retinoic acid (atRA) for 48 h. Lipid droplets in the cells were visualized under a microscope after ORO staining and quantified by a relative amount of ORO per cell which is normalized by a group of 10% FBS. Scale bar: 100 μm. All data were shown as mean ± SEM (n = 8 from 4 independent experiments). One-way ANOVA followed by Tukey's multiple comparison test was used for statistical analysis by the GraphPad PRISM program and statements of significance noted by **(A-C)** are based on testing at $p < 0.05$.

by the supplementation of 100 μM atRA in both quail and chicken primary muscle cells (**Figures 3B,D**).

3.4 Acute Induction of Pparγ Expression in Myogenic Cells by atRA

Pparγ, a well-known master regulator for adipogenesis both *in vivo* and *in vitro* (Rosen et al., 1999), is expressed in a few hours after inducing adipogenic differentiation of 3T3-L1 cells (Kim et al., 2014; Ambele et al., 2020). To investigate whether the pro-adipogenic effect of atRA in myogenic cells is accompanied with acute regulation of Pparγ for adipogenic differentiation, expression levels of Pparγ were analyzed at 3 and 5 h after atRA treatment in QM7 cells and primary myoblasts (**Figure 4**). Pparγ was significantly up-regulated by both 150 and 300 μM of atRA in QM7 cells (5.4-fold and 7-fold, respectively) and by the 300 mM of atRA in quail and chicken myoblasts (8.7-fold and 7.5-fold, respectively) at 3 h compared to the 0 M controls (**Figure 4**). At 5 h, the expression levels of Pparγ were significantly increased by both 150 and 300 μM of atRA in all three types of cells (5.8-fold and 8.4-fold for the QM7, 18.6-fold and 28.2-fold for the quail myoblasts, and 3.9-fold and 7.3-fold for the chicken myoblasts, respectively, **Figure 4**). Here, the current study showed acute and dramatic induction of Pparγ mRNA expression in the myoblasts by atRA.

3.5 Direct Induction of Pparγ Expression by atRA and Suppression of atRA-Induced Pparγ Expression by an RAR Antagonist in Myoblasts

To investigate whether the acute effects of atRA on Pparγ mRNA were due to a direct action on gene transcription or mediated through an increased expression of atRA-dependent auxiliary proteins or transcription factors, we analyzed the effect of atRA in a shorter time, in the presence of the protein synthesis inhibitor CHX (**Figure 5A**). The expression levels of Pparγ were expectedly increased by atRA at 5 h and those levels were not significantly affected by CHX treatment, showing similar expression patterns at different concentrations of atRA regardless of treatment of CHX (**Figure 5A**). These results support that atRA-induced Pparγ expression was independent of protein synthesis and thus, a direct downstream event of atRA.

To determine if atRA affects the up-regulation of Pparγ through RAR, QM7 cells were treated with 150 μM of atRA in various concentrations (0, 10 or 100 μM) of AGN, an RAR antagonist, for 5 h. The data showed that AGN dose-dependently decreased atRA-mediated induction of Pparγ expression (**Figure 5B**), suggesting that RAR is a mediator of atRA-induced Pparγ expression.

3.6 Effect of Pparγ Antagonist and Agonist on atRA-Induced Transdifferentiation

Due to the acute expression of Pparγ under the direct effect of atRA, it was investigated whether Pparγ is mediated for atRA-induced transdifferentiation. Utilizing an antagonist (BADGE) of Pparγ, we first examined the effect of BADGE on atRA-induced transdifferentiation. QM7 cells were induced to transdifferentiate for 2 days with 100 μM of atRA in the absence or presence of BADGE (0, 1, or 2 mM). As shown in **Figure 6**, treatment with BADGE resulted in a significantly reduced lipid accumulation in cells treated with atRA as observed by ORO measurement.

As QM7 cells are a myogenic cell line, Pparγ mRNA expression remained low at all time points of cell culture in the absense of atRA (black bar in **Figure 7A**). At the low levels of Pparγ expression in the absense of atRA, Rosi, as an agonist of Pparγ, did not significantly affect lipid droplet formation and lipid accumulation compared to a control without Rosi as assessed by ORO staining (**Figures 7B,C**). Treatment of atRA significantly increased the expression levels of Pparγ by 4-fold or 24-fold at D1 or D2, respectively, compared to the absence of atRA (**Figure 7A**). As expected, atRA alone induced lipid accumulation by 2-fold in QM7 cells compared to the control

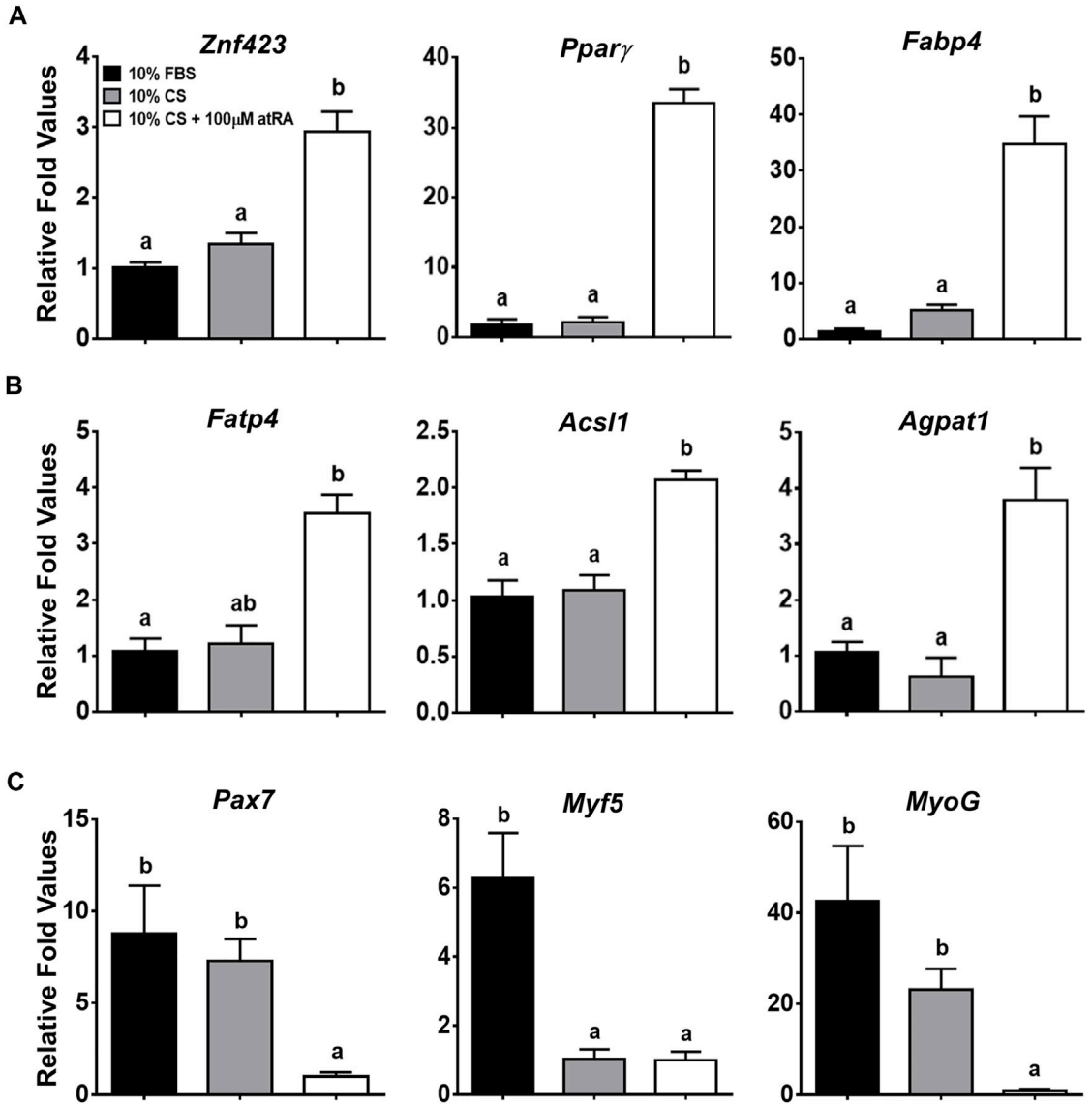

FIGURE 2 | Relative gene expression levels in QM7 cells by quantitative real-time PCR (qPCR). Expression levels of genes involved in adipogenesis **(A)**, fatty acid uptake and triglyceride (TAG) synthesis **(B)**, and myogenesis **(C)** were analyzed at 48 h after incubating with three different media, 10% FBS, 10% CS, or 10% CS with 100 μM atRA. Gapdh was used as a housekeeping gene and all expression levels of each gene were normalized by the levels of a group of 10% FBS. All data were shown as mean ± SEM (n = 4 from 4 independent experiments). One-way ANOVA followed by Tukey's multiple comparison test was used for statistical analysis by the GraphPad PRISM program and statements of significance noted by **(A-B)** are based on testing at $p < 0.05$.

cells (**Figures 7B,C**). Rosi further increased atRA-induced lipid accumulation up to 1.5-fold compared to the cells treated with atRA alone (**Figures 7B,C**).

4 DISCUSSION

Several genetic and nutritional factors have been known to be involved in transdifferentiation of myogenic cells to adipogenic cells *in vitro*. Pparγ and/or C/EBPα, as master regulators of adipogenesis, can induce transdifferentiation of G8 or C2C12 myoblasts onto adipocytes (Hu et al., 1995; Yu et al., 2006). Treatment of $1,25(OH)_2D_3$, an active form of vitamin D, induced lipid droplet formation on C2C12 myoblasts (Ryan et al., 2013). The current study demonstrated for the first time that a derivative of lipid soluble vitamin A (atRA) can convert both primary myogenic cells and the myoblast cell line to adipogenic cells in avian species.

Although high concentrations (over 1 μM) of atRA inhibit lipid accumulation in adipocytes, adipogenic differentiation of murine preadipocyte cell lines including Ob1771 and 3T3-L1 cells is promoted by atRA (Safonova et al., 1994). In chickens, our recent studies showed that atRA promoted lipid accumulation in primary preadipocytes (Kim D.-H. et al., 2020). In addition, *in*

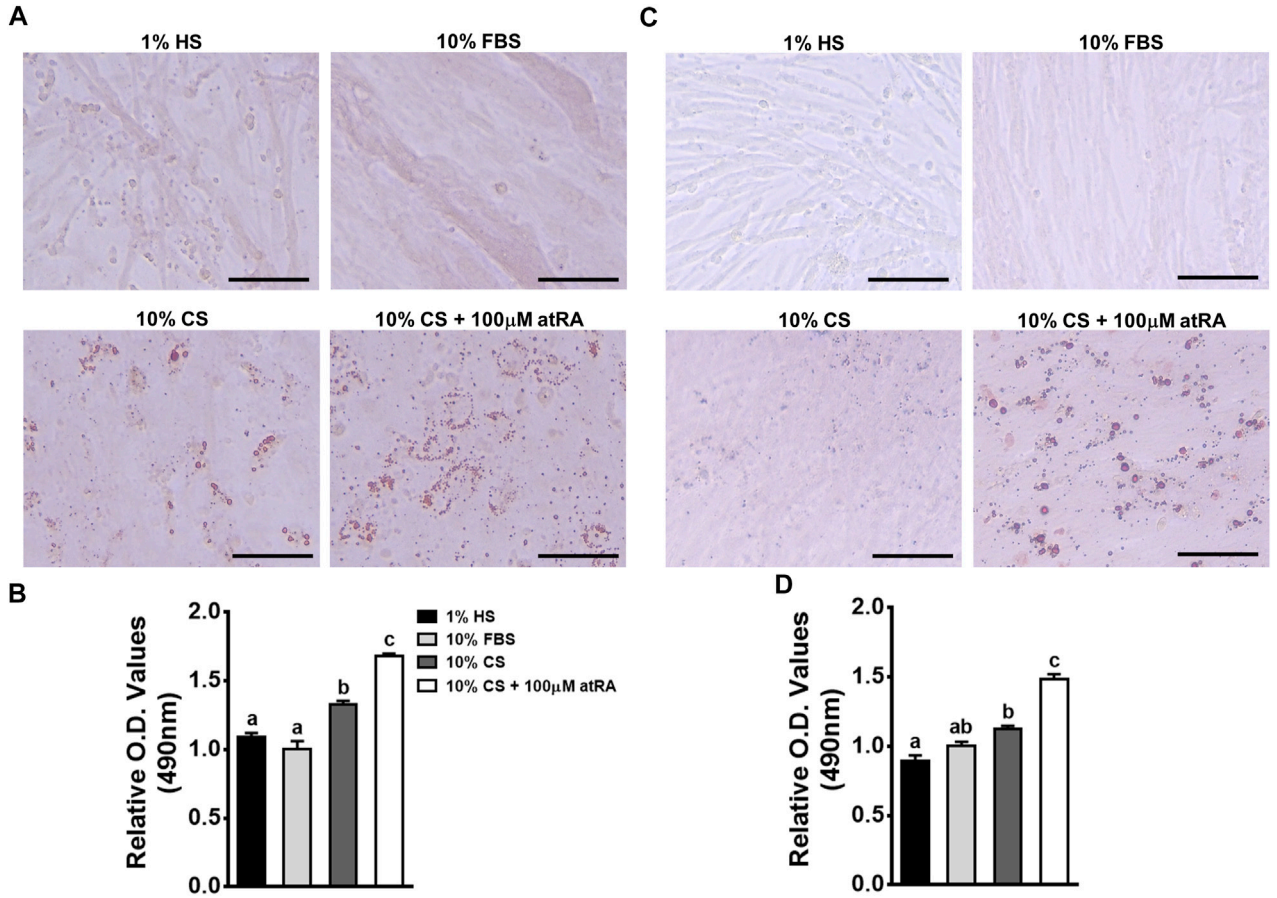

FIGURE 3 | Adipogenic differentiation of avian primary myoblasts by atRA. Primary myoblasts were isolated from breast muscle tissues of quail **(A** and **B)** and chicken **(C** and **D)** embryos at embryonic day 12 and 13, respectively. The cells were grown in four different media for 48 h: 1% HS as a standard myogenic medium, 10% FBS as a standard growth medium, 10% CS as a control medium, and 10% CS with 100 μM of atRA as an adipogenic medium, and then assessed for lipid accumulation. The ORO-stained cells were visualized under a microscope **(A** and **C)** and quantified by a relative amount of ORO per cell which was normalized by a group of 10% FBS **(B** and **D)**. Scale bar: 100 μm. All data were shown as mean ± SEM (n = 8 from 4 independent experiments). One-way ANOVA followed by Tukey's multiple comparison test was used for statistical analysis by the GraphPad PRISM program and statements of significance noted by **(A-C)** are based on testing at $p < 0.05$.

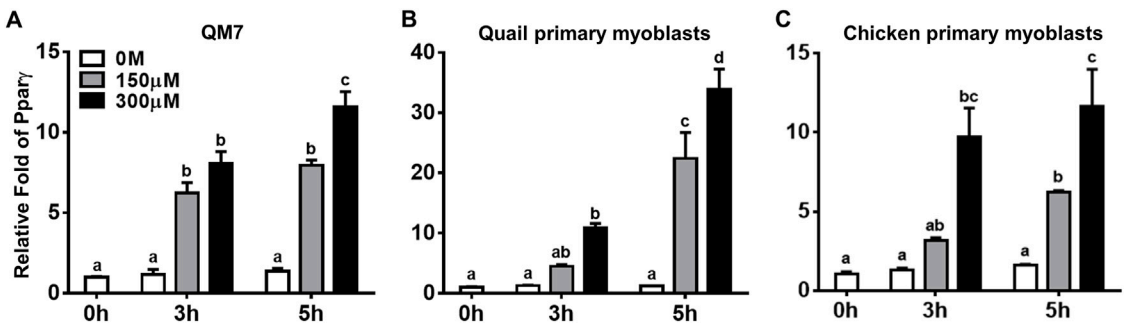

FIGURE 4 | Regulation of Pparγ expression by atRA in myoblasts. Expression levels of Pparγ in QM7 cells **(A)**, and primary myoblasts from quail **(B)** and chickens **(C)** were measured at 0, 3, 5 h after supplementing different concentrations of atRA (0 M, 150 μM, or 300 μM) in 10% CS. Gapdh was used as a housekeeping gene and all expression levels of Pparγ were normalized by the levels of each group at 0 h. All data were shown as mean ± SEM (n = 3 from 3 independent experiments). One-way ANOVA followed by Tukey's multiple comparison test was used for statistical analysis by the GraphPad PRISM program. **(A-D)** indicates statements of significance, $p < 0.05$.

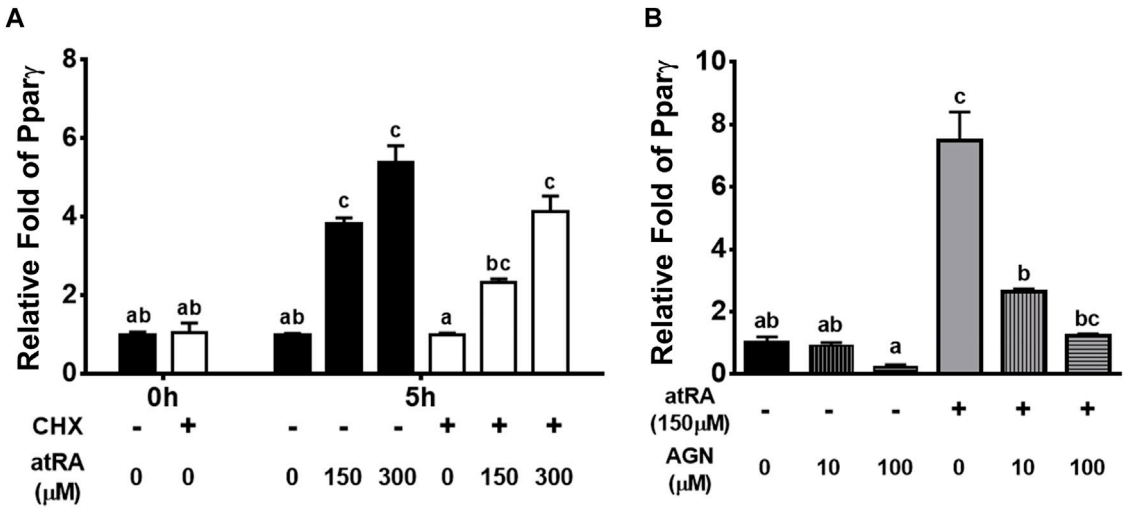

FIGURE 5 | Induction or suppression of Pparγ expression by atRA on the condition of treating cycloheximide or RAR antagonist, respectively, in QM7 cells **(A)** Direct regulation of Pparγ by atRA. Cycloheximide (CHX) was pre-treated for 1 h and then, after washing with PBS, atRA was treated in 10% CS with three different concentrations, 0 M, 150 μM, or 300 μM, for 5 h. The mRNA levels of Pparγ at 1 h after non-treatment of CHX were set as a standard for normalization of relative fold changes **(B)** Suppression of atRA-inducted Pparγ expression by an RAR antagonist. Various concentrations (0 M, 10 μM, and 100 μM) of RAR antagonist (AGN) were treated in 10% CS with 150 μM of atRA. After 5 h, mRNA levels of Pparγ were measured by qPCR, and the group which is 0 M of AGN without 150 μM of atRA was set as a standard for normalization of relative fold changes. All data were shown as mean ± SEM (n = 3 from 3 independent experiments). One-way ANOVA followed by Tukey's multiple comparison test was used for statistical analysis by the GraphPad PRISM program. **(A-C)** indicates statements of significance, $p < 0.05$.

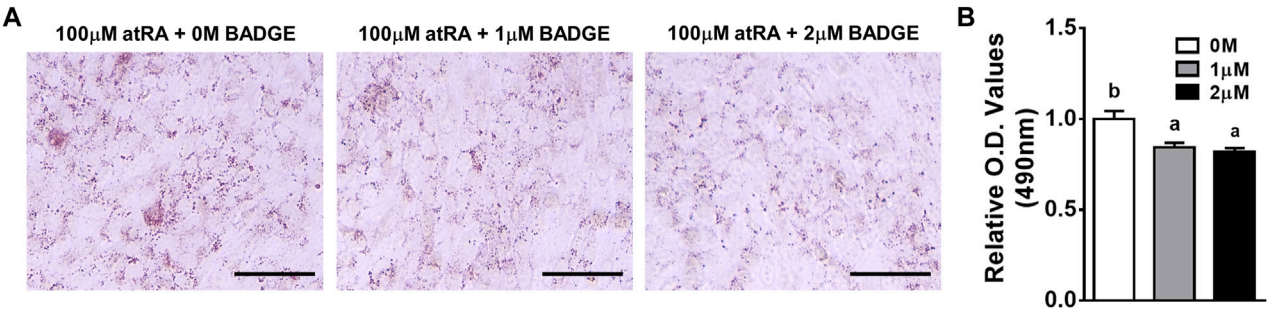

FIGURE 6 | Effects of BADGE as an inhibitor of atRA-induced lipid accumulation in QM7 cells. Oil-Red-O (ORO) staining **(A)** and O.D. values **(B)**. QM7 cells were grown in different concentrations of BADGE (0 M, 1 μM, or 2 μM) in 10% CS with 100 μM of atRA for 2 days, and then assessed for lipid accumulation. Lipid droplets in cells were visualized under a microscope after ORO staining and quantified by a relative amount of ORO per cell which is normalized by a group of the 0 M BADGE. Scale bar: 100 μm. All data were shown as mean ± SEM (n = 3 from 3 independent experiments). One-way ANOVA followed by Tukey's multiple comparison test was used for statistical analysis by the GraphPad PRISM program and statements of significance noted by a-b are based on testing at $p < 0.05$.

ovo injection of atRA in quails resulted in increased fat pad weight with adipocyte hypotrophy (Kim et al., 2021a). These data suggest pro-adipogenic activity of atRA in preadipocyte and adipose tissues *in vitro* and *in vivo*. Interestingly, it has been recently demonstrated that atRA could induce adipogenesis of non-preadipocytes such as chicken embryonic fibroblasts and fibroblast cell line (DF-1) (Lee et al., 2021). Furthermore, the current study revealed that atRA increased lipid accumulation in cultured avian myoblasts, providing morphological evidence of potential adipogenic transdifferentiation (**Figures 1**, **3**).

In diabetic and/or obese conditions, fine lipid droplets can be formed in muscle fibers, called intramyocellular lipid (IMCL) droplets. One might doubt whether lipid droplets formed by atRA are IMCL droplets found in avian myoblasts rather than transdifferentiated adipocytes. Therefore, it was necessary to investigate whether myoblasts treated with atRA are converted into adipocytes by measuring adipogenic and myogenic marker genes. The current study proved that the expression levels of all selected genes involved in adipocyte determination and differentiation (Znf423, Pparγ, and Fabp4), and fatty acid uptake (Fatp4, Acsl1, and Agpat1) were significantly increased, however, the genes in myogenesis (Pax7, Myf5, and MyoG) were significantly decreased by the supplementation of atRA on QM7 myoblasts. Similar with our study, overexpression of adipogenic

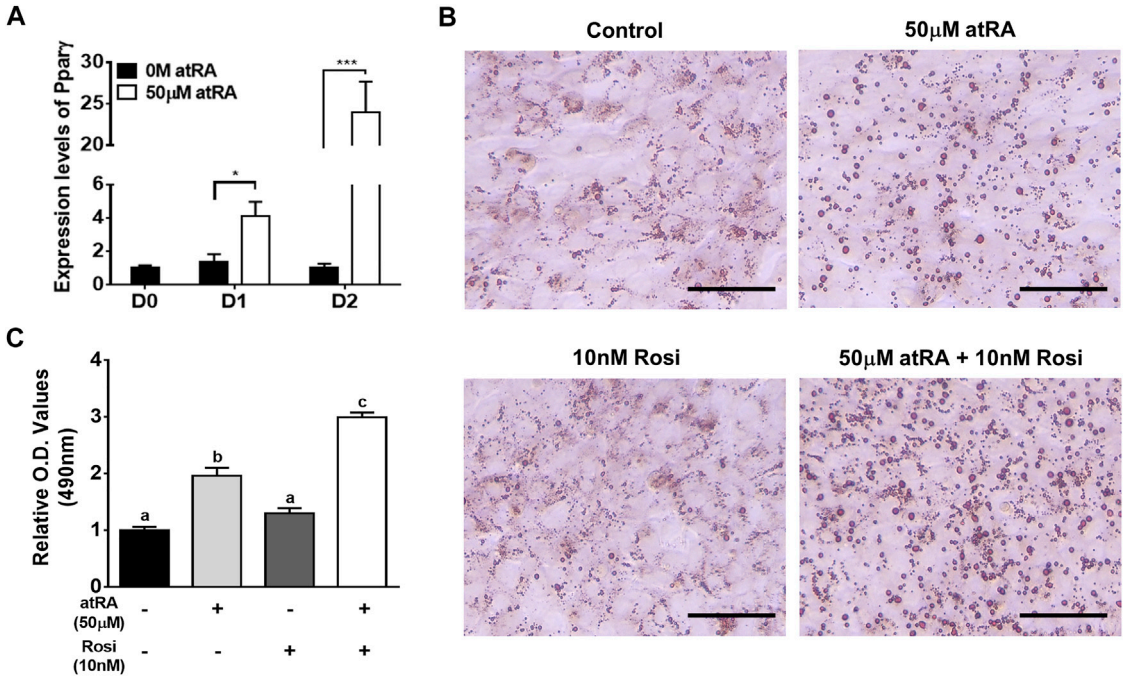

FIGURE 7 | Effect of Rosi as a co-activator on lipid accumulation. Expression levels of Pparγ in QM7 cells **(A)**. Expression levels of Pparγ were measured for 2 days after supplementation of 50 μM of atRA in 10% CS. Gapdh was used as a housekeeping gene and the expression levels are normalized by the levels at day **(D)** 0. *t*-tests were used for statistical analysis between the two groups, the 0 M and 50 μM of atRA, at D1 or D2, respectively, by the GraphPad PRISM 6.02 program. *: $p < 0.05$; ***: $p < 0.001$. Visualization **(B)** and quantification **(C)** of lipid accumulation. QM7 cells were grown in four different media for 2 days: 10% CS as a control media, 10% CS with 50 μM of atRA (50 μM), 10% CS with 10 nM of Rosi, and atRA 10% CS with both 50 μM of atRA and 10 nM of Rosi, both, and then assessed for lipid accumulation. The cells were stained by ORO to visualize lipid droplet accumulation and quantify relative amounts of ORO which is normalized by a group of the 10% CS. Scale bar: 100 μm. One-way ANOVA followed by Tukey's multiple comparison test was used for statistical analysis by the GraphPad PRISM program. **(A-C)** indicates statements of significance, $p < 0.05$. All data in **(A)** and **(C)** were shown as mean ± SEM ($n = 4$ from 4 independent experiments).

factors could convert myogenic cells to adipogenic cells (Hu et al., 1995; Yu et al., 2006), and myogenic factors were suppressed during transdifferentiation of C2C12 cells into mature adipocytes (Teboul et al., 1995; Ryan et al., 2013). Taken together, the morphological and gene expression data, showing inhibition of myofiber formation and promotion of lipid accumulation which are accompanied by the reducing expression of myogenic markers and inducing adipogenic markers, respectively, suggest that atRA could be an inducer of transdifferentiation of avian myoblasts into adipocytes.

As a master regulator of adipogenesis, Pparγ regulates many adipocyte genes involved in lipid metabolism and energy balance (Desvergne and Wahli 1999). Severe lipoatrophy and metabolic disturbance resulted from Pparγ knockout in mice (Jones et al., 2005; Wang et al., 2013) and overexpression of Pparγ in the mouse and pig resulted in increased intramuscular fat with an increased expression of adipogenic markers (Ma et al., 2015; Gu et al., 2021). These genetic models suggest that the ectopic expression of Pparγ in skeletal muscles enhanced lipid accumulation and adipogenic potential. In this study, the expression levels of Pparγ were acutely increased by the supplementation of atRA in avian myogenic cells, suggesting that the initiation of adipogenesis might be achieved by atRA (**Figure 4**). The acute induction of Pparγ expression by atRA leads to a possibility for direct regulation of Pparγ mRNA expression by atRA. Up-regulation of Pparγ by atRA, regardless of protein synthesis inhibitor (**Figure 5A**) indicates that atRA can directly increase Pparγ expression. Moreover, it is known that retinol metabolites and analogs function as ligands for RARs (RARα, β, and γ), and/or retinoid X receptors (RXRs α, β, and γ), and heterodimerized RARs/RXRs act as gene transcriptional factors (Gudas and Wagner 2011). Among retinoid metabolites, atRA are mediated by RARs, but not by RXRs (Lehmann et al., 1992). In the current study, up-regulation of Pparγ expression by atRA was significantly and dose-dependently reduced by the treatment of an RAR antagonist, AGN. Taken together, atRA could directly regulate Pparγ expression by binding to RAR to induce lipid accumulation in myoblasts.

The aforementioned findings favor the hypothesis that induced Pparγ expression in myoblasts by atRA can serve as an intermediate regulator of atRA in inducing transdifferentiation of myoblasts. To test the hypothesis, BADGE or Rosi, as antagonist and agonist of Pparγ, respectively, were treated in the absence or presence of atRA. Supplementation of BADGE in the presence of atRA significantly inhibited lipid droplet formations (**Figure 6**). On the other hand, supplementation of Rosi in the presence of atRA dramatically increased lipid accumulation in QM7 myoblasts compared to the supplementation of atRA alone (**Figure 7**). However, supplementation of Rosi, when the Pparγ expression was not

induced in the absence of atRA treatment, could not increase lipid accumulation in the myoblasts. These data support that the induction of Pparγ expression by atRA is an essential molecular event in myoblasts for atRA-induced transdifferentiation into adipocytes.

So far, it was reported that transdifferentiation of myoblasts to adipocytes could be induced by ectopic expressions of adipogenic transcription factors and treatment with nutritional factors. However, the current study, in avian species, demonstrated first that atRA has effects on inducing transdifferentiation of myoblasts into adipocytes with a direct regulation of Pparγ. Based on the current finding *in vitro*, the challenges for the future are to consolidate the atRA-RAR-Pparγ axis in inducing transdifferentiation of myoblasts into adipocytes and to confirm enhanced marbling fat by atRA *in vivo*.

DATA AVAILABILITY STATEMENT

The raw data supporting the conclusions of this article will be made available by the authors, without undue reservation.

ETHICS STATEMENT

The animal study was reviewed and approved by Experiments using avian embryos are exempt from requiring the University Institutional Animal Care and Use Committee approval because avian embryos are not considered live animals by the Public Health Service Policy.

AUTHOR CONTRIBUTIONS

Conceptualization, D-HK and KL; methodology, D-HK, JL, J-KK and KL; validation, D-HK and KL; investigation, D-HK, JL and YS; resources, J-KK and KL; data curation, D-HK; writing—original draft preparation, D-HK; writing—review and editing, D-HK, JL and KL; visualization, D-HK; supervision, KL; project administration, KL; funding acquisition, KL All authors have read and agreed to the published version of the manuscript.

FUNDING

This work was supported by the United States Department of Agriculture National Institute of Food and Agriculture Grant (Project No. 2021–07162).

SUPPLEMENTARY MATERIAL

The Supplementary Material for this article can be found online at: https://www.frontiersin.org/articles/10.3389/fcell.2022.856881/full#supplementary-material

REFERENCES

Albrecht, E., Teuscher, F., Ender, K., and Wegner, J. (2006). Growth- and Breed-Related Changes of Marbling Characteristics in Cattle1. *J. Anim. Sci.* 84, 1067–1075. doi:10.2527/2006.8451067x

Ambele, M. A., Dhanraj, P., Giles, R., and Pepper, M. S. (2020). Adipogenesis: A Complex Interplay of Multiple Molecular Determinants and Pathways. *Int. J. Mol. Sci.* 21, 4283–4327. doi:10.3390/ijms21124283

Desvergne, B., and Wahli, W. (1999). Peroxisome Proliferator-Activated Receptors: Nuclear Control of Metabolism*. *Endocr. Rev.* 20, 649–688. doi:10.1210/edrv.20.5.0380

Farmer, S. R. (2006). Transcriptional Control of Adipocyte Formation. *Cel Metab.* 4, 263–273. doi:10.1016/j.cmet.2006.07.001

Gu, H., Zhou, Y., Yang, J., Li, J., Peng, Y., Zhang, X., et al. (2021). Targeted Overexpression of PPARγ in Skeletal Muscle by Random Insertion and CRISPR/Cas9 Transgenic Pig Cloning Enhances Oxidative Fiber Formation and Intramuscular Fat Deposition. *FASEB j.* 35, e21308. doi:10.1096/fj.202001812RR

Gudas, L. J., and Wagner, J. A. (2011). Retinoids Regulate Stem Cell Differentiation. *J. Cel. Physiol.* 226, 322–330. doi:10.1002/jcp.22417

Gupta, R. K., Arany, Z., Seale, P., Mepani, R. J., Ye, L., Conroe, H. M., et al. (2010). Transcriptional Control of Preadipocyte Determination by Zfp423. *Nature* 464, 619–623. doi:10.1038/nature08816

Hassan, A., Ahn, J., Suh, Y., Choi, Y. M., Chen, P., and Lee, K. (2014). Selenium Promotes Adipogenic Determination and Differentiation of Chicken Embryonic Fibroblasts with Regulation of Genes Involved in Fatty Acid Uptake, Triacylglycerol Synthesis and Lipolysis. *J. Nutr. Biochem.* 25, 858–867. doi:10.1016/j.jnutbio.2014.03.018

Hu, E., Tontonoz, P., and Spiegelman, B. M. (1995). Transdifferentiation of Myoblasts by the Adipogenic Transcription Factors PPAR Gamma and C/EBP Alpha. *Proc. Natl. Acad. Sci.* 92, 9856–9860. doi:10.1073/pnas.92.21.9856

ILAR News (1991). Office of Laboratory Animal Welfare, the Public Health Service Responds to Commonly Asked Questions, Question #1. Available at: https://olaw.nih.gov/guidance/articles/ilar91.htm (Accessed Nov2021.

Jones, J. R., Barrick, C., Kim, K.-A., Lindner, J., Blondeau, B., Fujimoto, Y., et al. (2005). Deletion of PPAR in Adipose Tissues of Mice Protects against High Fat Diet-Induced Obesity and Insulin Resistance. *Proc. Natl. Acad. Sci.* 102, 6207–6212. doi:10.1073/pnas.0306743102

Kim, D.-H., Lee, J., Kim, S., Lillehoj, H. S., and Lee, K. (2021a). Hypertrophy of Adipose Tissues in Quail Embryos by in Ovo Injection of All-Trans Retinoic Acid. *Front. Physiol.* 12, 1–8. doi:10.3389/fphys.2021.681562

Kim, D.-H., Lee, J., Suh, Y., Cressman, M., and Lee, K. (2021b). Research Note: Adipogenic Differentiation of Embryonic Fibroblasts of Chicken, turkey, Duck, and Quail *In Vitro* by Medium Containing Chicken Serum Alone. *Poult. Sci.* 100, 101277. doi:10.1016/j.psj.2021.101277

Kim, D.-H., Lee, J., Suh, Y., Cressman, M., and Lee, K. (2020a). Research Note: All-Trans Retinoic Acids Induce Adipogenic Differentiation of Chicken Embryonic Fibroblasts and Preadipocytes. *Poult. Sci.* 99, 7142–7146. doi:10.1016/j.psj.2020.09.006

Kim, D. H., Lee, J., Suh, Y., Cressman, M., Lee, S. S., and Lee, K. (2020b). Adipogenic and Myogenic Potentials of Chicken Embryonic Fibroblasts *In Vitro* : Combination of Fatty Acids and Insulin Induces Adipogenesis. *Lipids* 55, 163–171. doi:10.1002/lipd.12220

Kim, D. H., Lee, J. W., and Lee, K. (2019). Supplementation of All- Trans -Retinoic Acid below Cytotoxic Levels Promotes Adipogenesis in 3T3-L1 Cells. *Lipids* 54, 99–107. doi:10.1002/lipd.12123

Kim, T.-H., Jo, S.-H., Choi, H., Park, J.-M., Kim, M.-Y., Nojima, H., et al. (2014). Identification of Creb3l4 as an Essential Negative Regulator of Adipogenesis. *Cell Death Dis* 5, e1527. doi:10.1038/cddis.2014.490

Lee, J., Kim, D.-H., Suh, Y., and Lee, K. (2021). Research Note: Potential Usage of DF-1 Cell Line as a New Cell Model for Avian Adipogenesis. *Poult. Sci.* 100, 101057. doi:10.1016/j.psj.2021.101057

Lehmann, J. M., Jong, L., Fanjul, A., Cameron, J. F., Lu, X. P., Haefner, P., et al. (1992). Retinoids Selective for Retinoid X Receptor Response Pathways. *Science* 258, 1944–1946. doi:10.1126/science.1335166

Liang, X., Yang, Q., Fu, X., Rogers, C. J., Wang, B., Pan, H., et al. (2016). Maternal Obesity Epigenetically Alters Visceral Fat Progenitor Cell Properties in Male Offspring Mice. *J. Physiol.* 594, 4453–4466. doi:10.1113/JP272123

Livak, K. J., and Schmittgen, T. D. (2001). Analysis of Relative Gene Expression Data Using Real-Time Quantitative PCR and the 2−ΔΔCT Method. *Methods* 25, 402–408. doi:10.1006/meth.2001.1262

Lonergan, S., Deeb, N., Fedler, C., and Lamont, S. (2003). Breast Meat Quality and Composition in Unique Chicken Populations. *Poult. Sci.* 82, 1990–1994. doi:10.1093/ps/82.12.1990

Ma, J., Chai, J., Shang, Y., Li, Y., Chen, R., Jia, J., et al. (2015). Swine PPAR-Γ2 Expression Upregulated in Skeletal Muscle of Transgenic Mice via the Swine Myozenin-1 Gene Promoter. *Transgenic Res.* 24, 409–420. doi:10.1007/s11248-014-9849-1

Rodeheffer, M. S., Birsoy, K., and Friedman, J. M. (2008). Identification of White Adipocyte Progenitor Cells *In Vivo*. *Cell* 135, 240–249. doi:10.1016/j.cell.2008.09.036

Rosen, E. D., and MacDougald, O. A. (2006). Adipocyte Differentiation from the inside Out. *Nat. Rev. Mol. Cel Biol.* 7, 885–896. doi:10.1038/nrm2066

Rosen, E. D., Sarraf, P., Troy, A. E., Bradwin, G., Moore, K., Milstone, D. S., et al. (1999). PPARγ Is Required for the Differentiation of Adipose Tissue *In Vivo* and *In Vitro*. *Mol. Cel* 4, 611–617. doi:10.1016/S1097-2765(00)80211-7

Ryan, K. J. P., Daniel, Z. C. T. R., Craggs, L. J. L., Parr, T., and Brameld, J. M. (2013). Dose-dependent Effects of Vitamin D on Transdifferentiation of Skeletal Muscle Cells to Adipose Cells. *J. Endocrinol.* 217, 45–58. doi:10.1530/JOE-12-0234

Safonova, I., Darimont, C., Amri, E.-Z., Grimaldi, P., Ailhaud, G., Reichert, U., et al. (1994). Retinoids Are Positive Effectors of Adipose Cell Differentiation. *Mol. Cell Endocrinol.* 104, 201–211. doi:10.1016/0303-7207(94)90123-6

Shin, S., Song, Y., Ahn, J., Kim, E., Chen, P., Yang, S., et al. (2015). A Novel Mechanism of Myostatin Regulation by its Alternative Splicing Variant during Myogenesis in Avian Species. *Am. J. Physiology-Cell Physiol.* 309, C650–C659. doi:10.1152/ajpcell.00187.2015

Tamori, Y., Masugi, J., Nishino, N., and Kasuga, M. (2002). Role of Peroxisome Proliferator-Activated Receptor-γ in Maintenance of the Characteristics of Mature 3T3-L1 Adipocytes. *Diabetes* 51, 2045–2055. doi:10.2337/diabetes.51.7.2045

Teboul, L., Gaillard, D., Staccini, L., Inadera, H., Amri, E.-Z., and Grimaldi, P. A. (1995). Thiazolidinediones and Fatty Acids Convert Myogenic Cells into Adipose-like Cells. *J. Biol. Chem.* 270, 28183–28187. doi:10.1074/jbc.270.47.28183

Wang, F., Mullican, S. E., DiSpirito, J. R., Peed, L. C., and Lazar, M. A. (2013). Lipoatrophy and Severe Metabolic Disturbance in Mice with Fat-specific Deletion of PPARγ. *Proc. Natl. Acad. Sci. U.S.A.* 110, 18656–18661 LP. doi:10.1073/pnas.1314863110

Yu, Y. H., Liu, B. H., Mersmann, H. J., and Ding, S. T. (2006). Porcine Peroxisome Proliferator-Activated Receptor γ Induces Transdifferentiation of Myocytes into Adipocytes1. *J. Anim. Sci.* 84, 2655–2665. doi:10.2527/jas.2005-645

Conflict of Interest: The authors declare that the research was conducted in the absence of any commercial or financial relationships that could be construed as a potential conflict of interest.

Publisher's Note: All claims expressed in this article are solely those of the authors and do not necessarily represent those of their affiliated organizations, or those of the publisher, the editors, and the reviewers. Any product that may be evaluated in this article, or claim that may be made by its manufacturer, is not guaranteed or endorsed by the publisher.

frontiers | Frontiers in Genetics

ORIGINAL RESEARCH
published: 11 April 2022
doi: 10.3389/fgene.2022.877646

Integrative Analysis of Nanopore and Illumina Sequencing Reveals Alternative Splicing Complexity in Pig Longissimus Dorsi Muscle

*Ze Shu, Ligang Wang *, Jinbu Wang, Longchao Zhang, Xinhua Hou, Hua Yan and Lixian Wang*

Key Laboratory of Farm Animal Genetic Resources and Germplasm Innovation of Ministry of Agriculture of China, Institute of Animal Sciences, Chinese Academy of Agricultural Sciences, Beijing, China

Alternative splicing (AS) is a key step in the post-transcriptional regulation of gene expression that can affect intramuscular fat (IMF). In this study, longissimus dorsi muscles from 30 pigs in high- and low- IMF groups were used to perform Oxford Nanopore Technologies (ONT) full-length sequencing and Illumina strand-specific RNA-seq. A total of 43,688 full-length transcripts were identified, with 4,322 novel genes and 30,795 novel transcripts. Using AStalavista, a total of 14,728 AS events were detected in the longissimus dorsi muscle. About 17.79% of the genes produced splicing isoforms, in which exon skipping was the most frequent AS event. By analyzing the expression differences of mRNAs and splicing isoforms, we found that differentially expressed mRNAs with splicing isoforms could participate in skeletal muscle development and fatty acid metabolism, which might determine muscle-related traits. *SERBP1*, *MYL1*, *TNNT3*, and *TNNT1* were identified with multiple splicing isoforms, with significant differences in expression. AS events occurring in *IFI6* and *GADD45G* may cause significant differences in gene expression. Other AS events, such as ONT.15153.3, may regulate the function of *ART1* by regulating the expression of different transcripts. Moreover, co-expression and protein-protein interaction (PPI) analysis indicated that several genes (*MRPL27*, *AAR2*, *PYGM*, *PSMD4*, *SCNM1*, and *HNRNPDL*) may be related to intramuscular fat. The splicing isoforms investigated in our research provide a reference for the study of alternative splicing regulation of intramuscular fat deposition.

Keywords: alternative splicing, pig, intramuscular fat, nanopore sequencing, RNA-seq

OPEN ACCESS

Edited by:
Xiao Li,
Northwest A&F University, China

Reviewed by:
Haiming Ma,
Hunan Agricultural University, China
Paolo Zambonelli,
University of Bologna, Italy

****Correspondence:***
Ligang Wang
ligwang@126.com

Specialty section:
This article was submitted to Livestock Genomics, a section of the journal Frontiers in Genetics

Received: *17 February 2022*
Accepted: *22 March 2022*
Published: *11 April 2022*

Citation:
Shu Z, Wang L, Wang J, Zhang L, Hou X, Yan H and Wang L (2022) Integrative Analysis of Nanopore and Illumina Sequencing Reveals Alternative Splicing Complexity in Pig Longissimus Dorsi Muscle. Front. Genet. 13:877646. doi: 10.3389/fgene.2022.877646

INTRODUCTION

As pork is the main meat resources for humans, its palatability has always been an important concern. The content of intramuscular fat (IMF) in meat is strongly correlated with the overall meat quality. Increased IMF content not only promotes the sensory attributes (Alfaia et al., 2019), but also affects the flavor and shear force of pork (Zhang et al., 2021). Furthermore, consumers are more likely to accept meat with higher IMF (Malgwi et al., 2022). However, the molecular mechanism and transcriptional regulation process of IMF deposition are still unclear.

Alternative splicing (AS), a key step in the post-transcriptional regulation of gene expression (Lee and Rio, 2015), can directly participate in the pre-transcriptional and post-transcriptional processes and even the processing of RNA and affect the binding between downstream proteins and nucleic acids, proteins, or

TABLE 1 | Sample IMF content details.

Group	Mean IMF content (%)	SD of IMF content (%)
H	5.48	2.06
L	1.27	0.21
F2	2.85	1.83

membranes, and change the localization and enzymatic properties of proteins (Kelemen et al., 2013). AS occurs in different stages of pig development and in different tissues and organs, and affects various economic traits of pig. AS is also involved in the regulation of biological processes and pathways, such as fatty acid degradation (Hao et al., 2022), glyceride metabolism (Li et al., 2012), glucose response (Liu et al., 2010), and fat deposition (Fang et al., 2021).

With the development of the third-generation sequencing (TGS) platform, the nanopore sequencing technology initiated by single-molecule real time (SMRT) technology and Oxford Nanopore Technologies (ONT) (Deamer et al., 2016) have shown great advantages in the identification of AS isoforms (Weirather et al., 2017; Beiki et al., 2019). However, an analysis of ONT-based AS for IMF development in pigs has not yet been conducted.

In this study, we used combined ONT and RNA sequencing analysis to identify potential differential AS factors affecting IMF deposition in pig longissimus dorsi muscle with high and low IMF content. In addition, key candidate genes and AS events affecting IMF deposition were screened by co-expression and PPI analysis. The results can facilitate the study of transcriptional regulatory processes and provide new insights into AS studies in livestock. At the same time, they can be used to provide a new method for improving IMF content in pig breeding.

MATERIALS AND METHODS

Sample Collection and Determination of Intramuscular Fat Content

The animal materials used in this study were all from the F2 generation resource population of large white pig × Min pig at the Changping Experimental Base of the Institute of Animal Sciences, Chinese Academy of Agricultural Sciences. The pig raising and slaughtering environment, tissue collection, and IMF measuring methods were as described in our previous study (Wang et al., 2021). Thirty samples were screened for full-length transcript sequencing based on IMF content: fifteen samples with high IMF content and fifteen samples with low IMF content. The content in the high-IMF group ranged from 4.07% to 12.18%, and that in the low-IMF group ranged from 0.78% to 1.60%. The sample IMF content details are shown in **Table 1** and **Supplementary Table S13**.

Oxford Nanopore Technologies and Strand-Specific RNA-Seq Library Construction and Sequencing

The ONT library construction was performed according to the standard protocol provided by the ONT platform. Before full-length transcript sequencing, 1 μg of total RNA was prepared for the cDNA library using a cDNA-PCR sequencing kit (SQK-PCS109). The libraries were then created using a sequencing library prep kit. We added the defined PCR adapters directly to both ends of the first-strand cDNA. The cDNA library was established by 20 cycles of PCR amplification with LongAmp Tag. The PCR products were then subjected to ONT adapter ligation using T4 DNA ligase. Agencourt XP beads were used for DNA purification according to the ONT protocol. The final cDNA library was added to the FLO-MIN109 flow cell, and the library was sequenced using the MinION Mk1B sequencer. Strand-specific RNA sequencing data were obtained to validate and quantify the sequencing data of the ONT full-length transcripts. Approximately 2 μg of RNA per sample was used to prepare Illumina sequencing libraries, and 30 prepared libraries were sequenced using the Illumina HiSeq 4,000 platform with a 150 bp pair-end sequencing strategy according to the manufacturer's instructions.

Data Analysis of Nanopore Raw Data

For raw data from the Nanopore sequencing fast5 format, Guppy software in the MinKNOW2.2 software package was used to perform base calling and conversion to fastq format. Nanoplot (De Coster et al., 2018) was used to filter the converted data. The clean data were compared with the Silva rRNA database using sortmerna (Kopylova et al., 2012) to delete ribosomal RNA and for subsequent analysis. The sequence containing primers at both ends were determined to be a full-length sequence using pychopper (https://github.com/nanoporetech/pychopper/) software. The obtained full-length sequences were aligned with the pig reference genome (*Sus scrofa* 11.1.96) using minimap2 software (Li, 2018), and the data were cleaned and clustered using pinfish (https://github.com/nanoporetech/pinfish/) to obtain consistency sequences. cDNA_Cupcake (https://github.com/Magdoll/cDNA_Cupcake/) was used to filter the sequences with identity ≤0.9 and coverage ≤0.85. Alignments with differences in only the 5′ end exons were merged, and 43,668 strips of gff file redundancies were obtained for the sequence information of the remaining transcripts. In addition, gffcompare (https://github.com/gpertea/gffcompare) was used to compare the transcripts obtained from full-length sequencing with the known transcripts of the genome, to discover new genes and transcripts and to supplement the genome annotation.

Identification of Alternative Splicing Events

To detect all AS events, we generated gff files after de-redundancy and used AStalavista software (Foissac and Sammeth, 2007) to perform AS analysis. Five types of AS events were obtained: exon skipping (ES), intron retention (IR), alternative 5′ splice site (A5SS), alternative 3′ splice site (A3SS), and mutually exclusive exons (MEE). The results of the AStalavista analysis were then transformed to obtain AS event information for all transcripts.

Validation of the Existence of Alternative Splicing Events by RNA Sanger Sequencing

To verify the accuracy of the identified alternative splicing events, we randomly selected several splicing isoforms for PCR

validation. Specific primers upstream and downstream of the alternative splicing were designed using Primer 5. The PCR amplification reaction mixture was 25 μl, including 12.5 μl of Premix Taq (Takara RR902A), 1 μl of template cDNA, 1 μl of each primer, and 9.5 μl of sterile water. PCR products were examined by 1.0% agarose gel electrophoresis and sequenced using the Sanger sequencing method. The primers used in this study are listed in **Supplementary Table S12**.

Functional Annotation and Enrichment Analysis of Full-Length Transcripts

To obtain comprehensive functional information annotations for all transcripts, seven databases were searched using BLASTX v.2.2.26 (E-value < 1×10^{-5}): Gene Ontology (GO, http://www.geneontology.org), Kyoto Encyclopedia of Genes and Genomes (KEGG, http://www.genome.jp/kegg/), Cluster of Orthologous Groups of proteins (COG, http://www.ncbi.nlm.nih.gov/COG/), Clusters of Orthologous Groups for eukaryotic complete genomes (KOG, ftp://ftp.ncbi.nih.gov/pub/COG/KOG/kyva), Non-Redundant Protein Sequences Database (NR, http://www.ncbi.nlm.nih.gov/), Swiss-Prot (http://www.expasy.org/sprot/), and Pfam database (Pfam, http://pfam.xfam.org/) (Finn et al., 2011) to annotate all de-redundant full-length transcripts. The R package clusterProfiler (Yu et al., 2012) was used to perform GO and KEGG pathway enrichment analysis on alternatively spliced genes, and the significant enrichment criterion was a q-value of <0.05.

Quantitative Gene Expression Analysis, Differentially Expressed Splicing Isoforms, and Differentially Expressed Genes Analysis

The full-length transcripts generated by ONT sequencing were annotated as reference genomes, and the expression levels of all transcripts were further calculated based on the data generated by Illumina sequencing. Hisat2 was used to estimate gene expression levels and to map clean data onto reference sequences. Stringtie with parameter -e was used to limit read alignment processing to estimate and output only assembled transcripts that matched a given reference transcript. We used python script prepDE.py to obtain read count files from the mapping results.

Only the expression data of alternatively spliced transcripts were extracted, and DESeq2 (Love et al., 2014) was used to analyze DESIs and DEGs between the high- and low-IMF groups. The DEseq2 package was used for analysis, the parameter design was set to types and conditions, the type parameter was the sequencing batch, and the conditions parameter was the test grouping. DESIs and DEGs were filtered according to the following criteria: padjust <0.05 and $|\log_2 \text{FoldChange}| \geq 1$.

Expression Proportion Analysis and Protein Structure Prediction of Differentially Expressed Splicing Isoforms

In order to explore the regulatory effect of the identified DESIs on gene expression, we analyzed the proportion of all splicing isoforms in their gene expression:

$$\text{Expression proportion of splicing isoforms (count\%)} = \frac{\text{splicing isoform reads}}{\text{gene reads}}$$

Protein hydrophobicity (ProtScale, https://web.expasy.org/protscale/) and protein tertiary structure prediction (SWISS-MODEL, https://www.swissmodel.expasy.org/) of amino acid sequences of splicing isoforms were analyzed to explore the potential effect mechanism of AS on gene function.

Co-Expression and Protein-Protein Interaction Analysis

In this study, to explore the key factors of AS affecting IMF content, we also performed co-expression analysis using weighted gene co-expression network analysis (WGCNA) on all transcripts that were alternatively spliced. Splicing isoforms with a weighted threshold of 0.08 in the screening module were used as hub splicing isoforms. STRING v11.0 (https://string-db.org/) was used to analyze the protein interaction of splicing isoform genes in the module. Cytoscape (version 3.7.2) was used to display the protein interaction map, and the plugin cytoHubba based on degree values was used to identify hub genes in the PPI network.

RESULTS

Overview of Oxford Nanopore Technologies and Strand-Specific RNA Sequencing Data

Full-length transcript sequencing was performed on 30 samples, and the clean data generated by each sample sequencing amounted to 5.52 GB on average. The average number of sequences per sample generated by nanopore sequencing was 7,290,257, and the quality values of the samples were all above Q8 (**Table 2**). A total of 148 GB of raw data was obtained by strand-specific RNA sequencing, and the annotation files obtained by ONT sequencing were aligned and assembled, with an average overall alignment rate of 95.78%. An overview of the next-generation sequencing data is shown in **Supplementary Table S1**.

Overview of Full-Length Transcripts

For the 30 individuals, the average number of full-length sequences was 5,081,792 and the average matching proportion of full-length sequences was 79.67%, as shown in **Supplementary Table S2**. All consensus transcript sequences were aligned to the reference genome by minimap2 software and then subjected to de-redundancy analysis. Finally, 43,688 full-length transcripts were obtained. Mapping of the Sus scrofa genome by gffcompare identified gene loci and transcript isoforms. A total of 15,130 genes were detected; 10,808 (71.43%) known genes were matched and 4,322 (28.57%) genes were newly discovered (**Figure 1A**). A total of 43,688 transcripts were detected, among which only 6,086 (13.93%) transcripts were known. A total of 30,795 (70.49%) novel transcripts of known genes were identified, and 6,807 novel transcripts of novel genes were identified (15.58%) (**Figure 1B**). A total of 6,548 (43.27%) genes were identified with two or more transcripts

TABLE 2 | Clean reads generated by Nanopore sequencing.

SampleID	ReadNum	BaseNum	N50	MeanLength	MaxLength	MeanQscore
H02	6,752,439	6,175,485,611	962	914	66,795	Q9
H10	5,532,529	5,609,156,050	1,205	1,013	74,639	Q9
H12	6,119,569	6,807,516,576	1,326	1,112	11,721	Q9
H14	6,456,458	6,621,242,447	1,213	1,025	9,744	Q9
H16	5,959,362	5,718,222,829	1,047	959	8,348	Q10
H17	6,603,190	5,758,174,836	925	872	8,386	Q10
H18	7,894,304	8,235,168,413	1,182	1,043	12,564	Q9
H21	7,896,545	7,225,249,807	931	914	15,533	Q10
H22	6,985,943	7,505,345,391	1,252	1,074	15,392	Q9
H24	7,600,605	7,845,590,054	1,129	1,032	12,159	Q9
H25	8,496,048	7,837,286,862	954	922	84,628	Q9
H26	7,469,849	6,585,331,944	904	881	11,670	Q10
H27	5,894,109	5,703,324,956	1,033	967	23,311	Q10
H28	6,376,313	5,618,395,573	908	881	25,245	Q10
H29	5,932,342	5,519,352,014	949	930	13,970	Q10
L04	5,562,596	5,800,700,649	1,215	1,042	13,845	Q9
L06	11,541,467	8,660,383,334	758	750	11,037	Q10
L09	6,491,467	6,103,125,627	1,002	940	10,014	Q9
L14	9,213,725	11,281,078,708	1,426	1,224	15,650	Q8
L16	7,081,487	7,384,134,414	1,227	1,042	13,875	Q9
L19	5,469,901	6,385,532,830	1,378	1,167	11,430	Q9
L21	10,590,964	7,946,674,581	754	750	10,489	Q9
L22	5,890,517	6,526,928,880	1,337	1,108	11,814	Q9
L23	13,079,729	9,621,611,190	744	735	10,721	Q9
L24	5,891,637	5,881,567,295	1,168	998	10,849	Q9
L25	9,107,417	7,198,198,707	781	790	208,750	Q9
L26	6,708,535	5,924,625,514	933	883	9,126	Q9
L27	6,594,848	6,138,091,481	984	930	10,142	Q10
L28	7,043,122	7,191,261,618	1,125	1,021	21,550	Q9
L31	6,470,694	5,937,781,634	936	917	35,868	Q10

ReadNum, number of sequences; BaseNum, the total number of bases; N50, N50 length; MeanLength, average length of reads; MaxLength, longest reads length; MeanQscore, mean quality score.

(**Figure 1C**). Troponin t3, fast skeletal type (TNNT3) had the highest number of transcripts (143 novel and 11 known).

To elucidate their functions, all newly discovered transcripts were annotated to the GO, KEGG, COG, KOG, Pfam, NR, and SwissProt databases. A total of 29,539 transcripts could be annotated in at least one database (**Figure 1D**).

Alternative Splicing Identification

AStalavista was used to identify AS of de-redundant transcripts; a total of 10,949 splicing isoforms (25.06%, 43,688 transcripts detected) were generated, and 14,728 AS events were detected (**Supplementary Table S4**). The largest proportion of AS events was ES (5,040 events, 34.22%), and the smallest proportion was MEE (1,206 events, 8.19%; **Figure 2A**; **Table 3**). A total of 2,691 genes (17.79%, 15,130 genes detected by ONT) were alternatively spliced during transcription, and the top five genes with the most splicing isoforms were *TNNT3* (139 splicing isoforms), troponin t1, slow skeletal type (*TNNT1*, 131 splicing isoforms), Y-box binding protein 3 (*YBX3*, 91 splicing isoforms), myosin binding protein C2 (*MYBPC2*, 72 splicing isoforms), and nebulin (*NEB*, 71 splicing isoforms) (**Figure 2B**).

Validation of Selected Alternative Splicing Isoforms

To confirm the accuracy of the identified AS events, we randomly selected several and verified ONT.6273.5, ONT.15020.2, ONT.1066.3, ONT.8241.1, ONT.9799.3, and ONT.9654.4 for validation (**Figure 2C**). The results support the accuracy of the identified AS events.

Gene Ontology and Kyoto Encyclopedia of Genes and Genomes Analysis of Genes With Specific Splicing Isoforms

After de-redundancy, we counted the number of de-redundant transcripts for each sample. De-redundant transcripts that were not present in the high- and low-IMF groups but were present in the other group were defined as low- or high-IMF group specific splicing isoforms. In total, 1,605 splicing isoforms were found only in the high-IMF group and 2,235 in the low-IMF group. GO and KEGG analysis was performed on genes of these differentially splicing isoforms using clusterProfiler (**Supplementary Table S5**). The results indicate that the significant biological process (BP) terms of high-IMF group genes were mainly ribonucleoprotein complex biogenesis, ribonucleoprotein complex assembly, and ribonucleoprotein complex subunit organization; the significant cellular component (CC) terms were ribonucleoprotein complex, proteasome complex, and endopeptidase complex; and the significant molecular function (MF) terms were RNA binding, structural constituent of ribosome, and structural molecule activity (**Figure 3A**). The

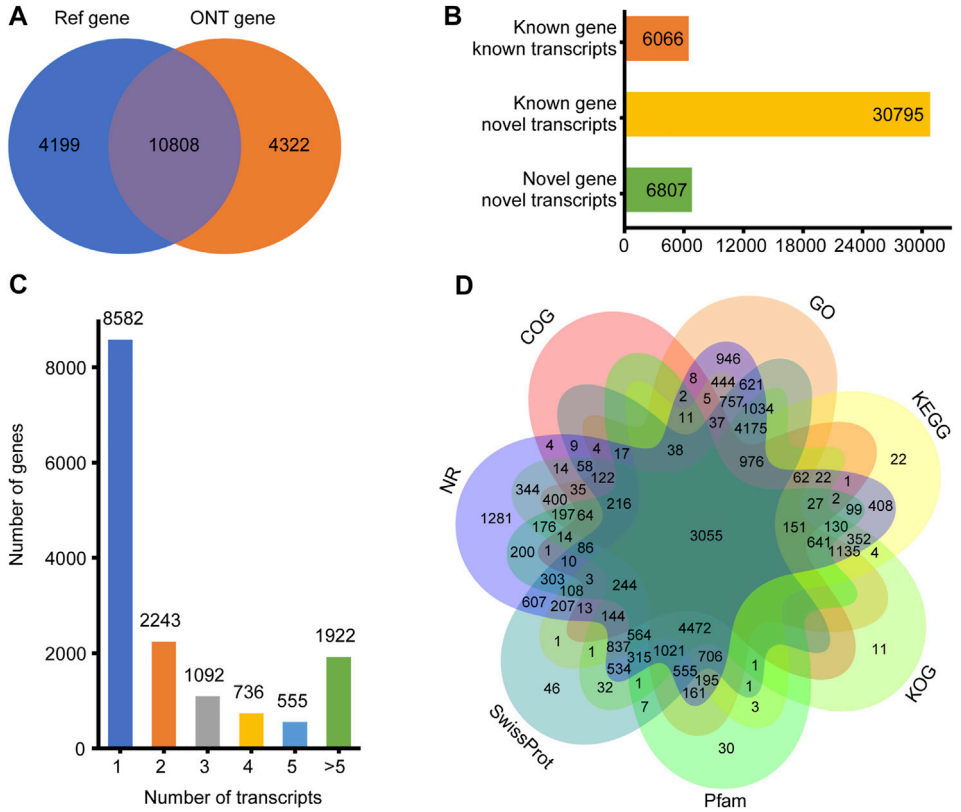

FIGURE 1 | Overview of ONT transcripts. **(A)** Venn diagram of genes identified in ONT data and annotated genomes; **(B)** Distribution diagram of three types of transcripts in ONT data; **(C)** Distribution diagram of gene multi-transcripts; **(D)** Venn diagram of all new transcripts annotation result.

enriched KEGG pathways were ribosome, spliceosome, and proteasome (**Figure 3B**). GO analysis of differentially splicing isoforms in the low-IMF group showed that significant the BP terms were mainly translation, peptide biosynthetic process, and cellular protein-containing complex assembly; significant CC terms were ribonucleoprotein complex, proteasome complex, and endopeptidase complex; and significant MF terms were RNA binding, structural constituent of ribosome, and structural molecule activity (**Figure 3C**). The enriched KEGG pathways were mainly ribosome, Parkinson disease, and Huntington disease (**Figure 3D**).

Differentially Expressed Splicing Isoforms, Differentially Expressed Genes, and Expression Proportion Analysis

Because the ONT method has a disadvantage in quantitating expression, we used RNA-seq data to adjust the expression of ONT sequencing data. Combining ONT with RNA-seq data, a total of 10,760 (98.27%) splicing isoform expressions were matched and assembled. Through differential analysis of the expression data of splicing isoforms occurring between high- and low-IMF groups, 98 DESIs (**Figure 4A** and **Supplementary Figure S1**), including 49 upregulated and 49 downregulated splicing isoforms, were investigated (**Supplementary Table S6**). Among all DESIs, SERPINE1 mRNA binding protein 1 (*SERBP1*) had four upregulated splicing isoforms (ONT.13291.2, ONT.13291.18, ONT.13291.21, ONT.13291.24); myosin light chain 1 (*MYL1*) had three upregulated splicing isoforms (ONT.5824.56, ONT.5824.110, ONT.5824.117); and *TNNT3* had three downregulated splicing isoforms (ONT.7235.51, ONT.7235.143, ONT.7235.171). Interestingly, *TNNT1* had two splicing isoforms, with ONT.12529.9 showing an upregulated trend and ONT.12529.241 a downregulated trend.

Through differential analysis of gene expression data between the high- and low-IMF groups, 15 DEGs were identified, including 3 upregulated and 12 downregulated genes (**Figure 4B**; **Supplementary Table S7**). Combining the results of DEGs and DESIs, among the downregulated DEGs, ONT.12957 [interferon alpha inducible protein 6 (*IFI6*)] had one transcript (ONT.12957.1) identified in the DESIs results, and ONT.4294 [growth arrest and DNA damage inducible gamma (*GADD45G*)] had two transcripts (ONT 0.4294.3, ONT.4294.9) identified in the DESIs results.

As the ONT sequencing transcripts were long and could cover one gene, we used a criterion to screen the DESIs most likely to be effective, which was the proportion of isoform expression to the expression of all isoforms in the same gene above 10%. As shown in **Table 4**, we found that ONT.9523.3, ONT.3832.5, ONT.191.5, ONT.15153.3, ONT.11047.3, ONT.16074.8, ONT.10763.6, ONT.7120.12,

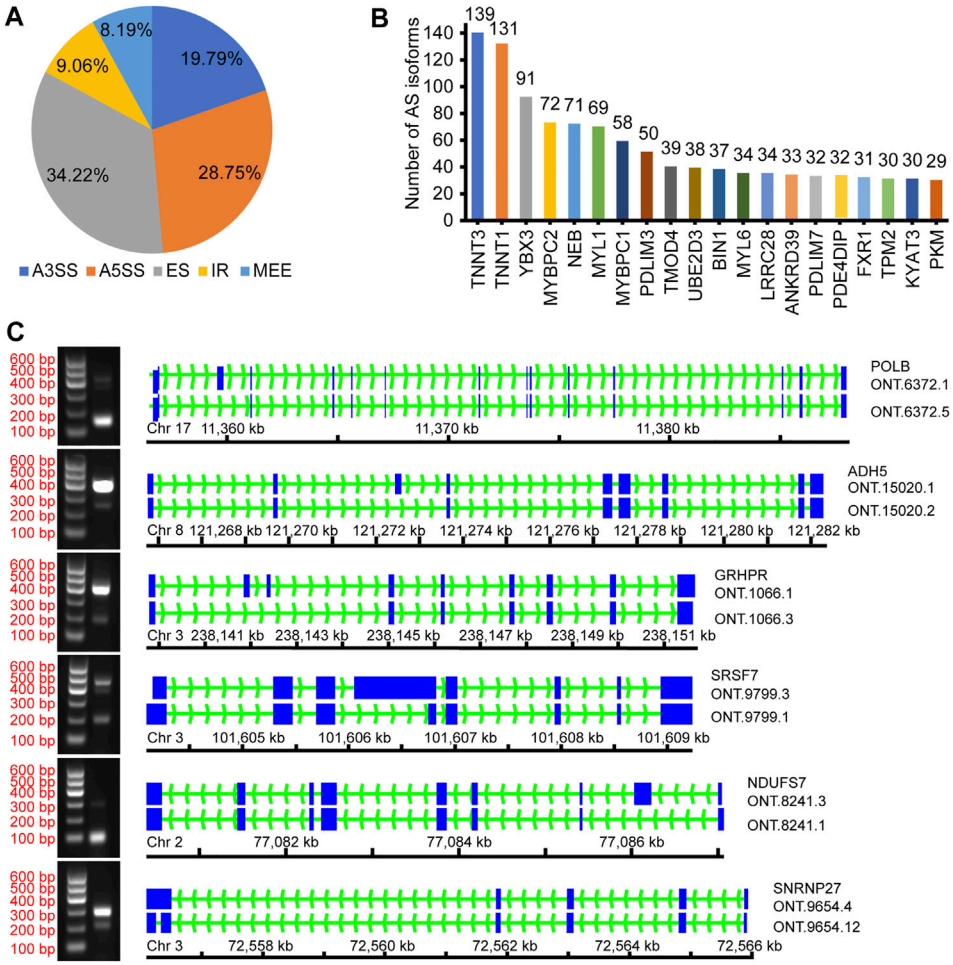

FIGURE 2 | Overview of alternative splicing. **(A)** The proportion of different AS events; **(B)** The number of different gene splicing isoforms; **(C)** Verify different AS events.

TABLE 3 | Number and percentage of AS events.

AS events	Number of AS events	Percentage
Alternative 3′ splice site	2,914	19.79(%)
Alternative 5′ Splice Site	4,234	28.75(%)
Exon skipping	5,040	34.22(%)
Intron retention	1,334	9.06(%)
Mutually exclusive exon	1,206	8.19(%)

ONT.7120.13, ONT.14524.8, and ONT.10349.9 had differences in the proportion of expression between high- and low-IMF pigs ($p < 0.05$).

Protein Structural Analysis of Splicing Isoforms

For most of the above 11 isoforms, their expression change could not result in significant expression difference from other transcription expression except ONT.15153.3 and ONT.10349.2, as shown in **Supplementary Table S8**. From the results, we found that increased expression of ONT.15153.3 will cause reduced expression of ONT.15153.1, and increased expression of ONT.10349.9 will cause reduced expression of ONT.10349.2. We then predicted the protein hydrophobicity and tertiary structure of the genes. We found that the hydrophobicity and tertiary structure of ADP-ribosyltransferase 1 (*ART1*) located in ONT.15153.3 had changed, as shown in **Figures 5A,B**. Thus, we inferred that the occurrence of AS in *ART1* may have an impact on its protein function, thereby regulating the expression of its gene function.

Co-Expression Studies of Splicing Isoforms

A co-expression module of the splicing isoforms and IMF deposition was constructed using the WGCNA package tool. By plotting a cluster plot of sample correlations, it could be seen that there were no obvious outlier samples (**Figure 6A**). We selected the value where the scale-free network graph structure R square reaches 0.95, that is, power = 6 (**Figure 6B**). By constructing a co-expression network, a total of 42 co-expression modules with different splicing isoforms were identified. Each module was displayed in a different color and

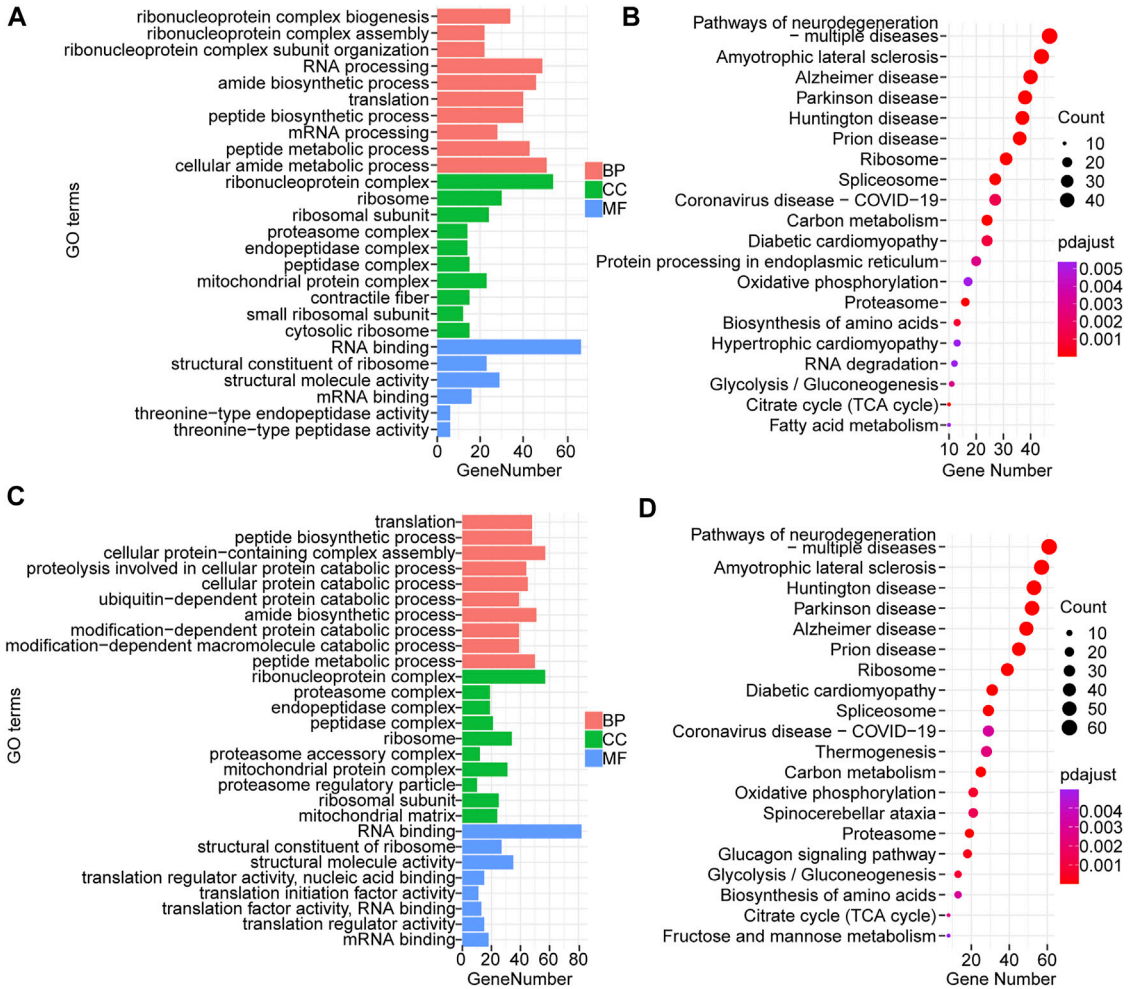

FIGURE 3 | GO and KEGG analysis of splicing isoforms specifically occurring in H and L groups. **(A)** GO results of splicing isoforms that specifically occur in high-IMF group; **(B)** KEGG results of splicing isoforms that occur specifically in high-IMF group; **(C)** GO results of splicing isoforms that specifically occur in low-IMF group; **(D)** KEGG results of splicing isoforms that occur specifically in low-IMF group.

contained different numbers of splicing isoforms. Hierarchical clustering and correlation heatmaps were constructed with the 42 modules and correlation heatmaps (**Figures 6C,D**). Correlation analysis was performed between the co-expression modules and IMF content traits, and correlations and *p*-values between different modules and traits were obtained (**Figure 6E**).

Through co-expression analysis of splicing isoforms, we found a module (MEblack) that was significantly associated with IMF traits. We then plotted the significance of splicing isoform module membership for this module (**Figure 7A**). At the same time, we also performed correlation analysis on the splicing isoforms in the module and traits (**Figure 7B**).

Module MEblack aggregated 191 splicing isoforms (**Supplementary Table S9**), among which 41 hub splicing isoforms were identified by setting a weighted threshold (**Supplementary Table S10**). Corresponding to 162 named genes, they were imported into the String database to construct a PPI network, and Cytoscape was used to display the PPI results (**Figure 8A**). Using the cytoHubba plugin, 30 hub genes were identified by the degree method (**Figure 8B** and **Supplementary Table S11**). The genes and splicing isoforms were mapped and compared with the hub splicing isoforms screened by the co-expression analysis results, and eight hub splicing isoforms were finally identified (ONT.2674.11, ONT.6603.3, ONT.7429.11, ONT.7429.12, ONT.10638.13, ONT.10638.14, ONT.13247.4, ONT.15079.18) (**Figure 8C**). The corresponding genes were found to be mitochondrial ribosomal protein L27 (*MRPL27*), AAR2 splicing factor (*AAR2*), glycogen phosphorylase, muscle associated (*PYGM*), proteasome 26S subunit ubiquitin receptor, non-ATPase 4 (*PSMD4*), sodium channel modifier 1 (*SCNM1*), and heterogeneous nuclear ribonucleoprotein D like (*HNRNPDL*).

DISCUSSION

Full-length transcript sequencing has been shown to be an effective method for studying the post-transcriptional

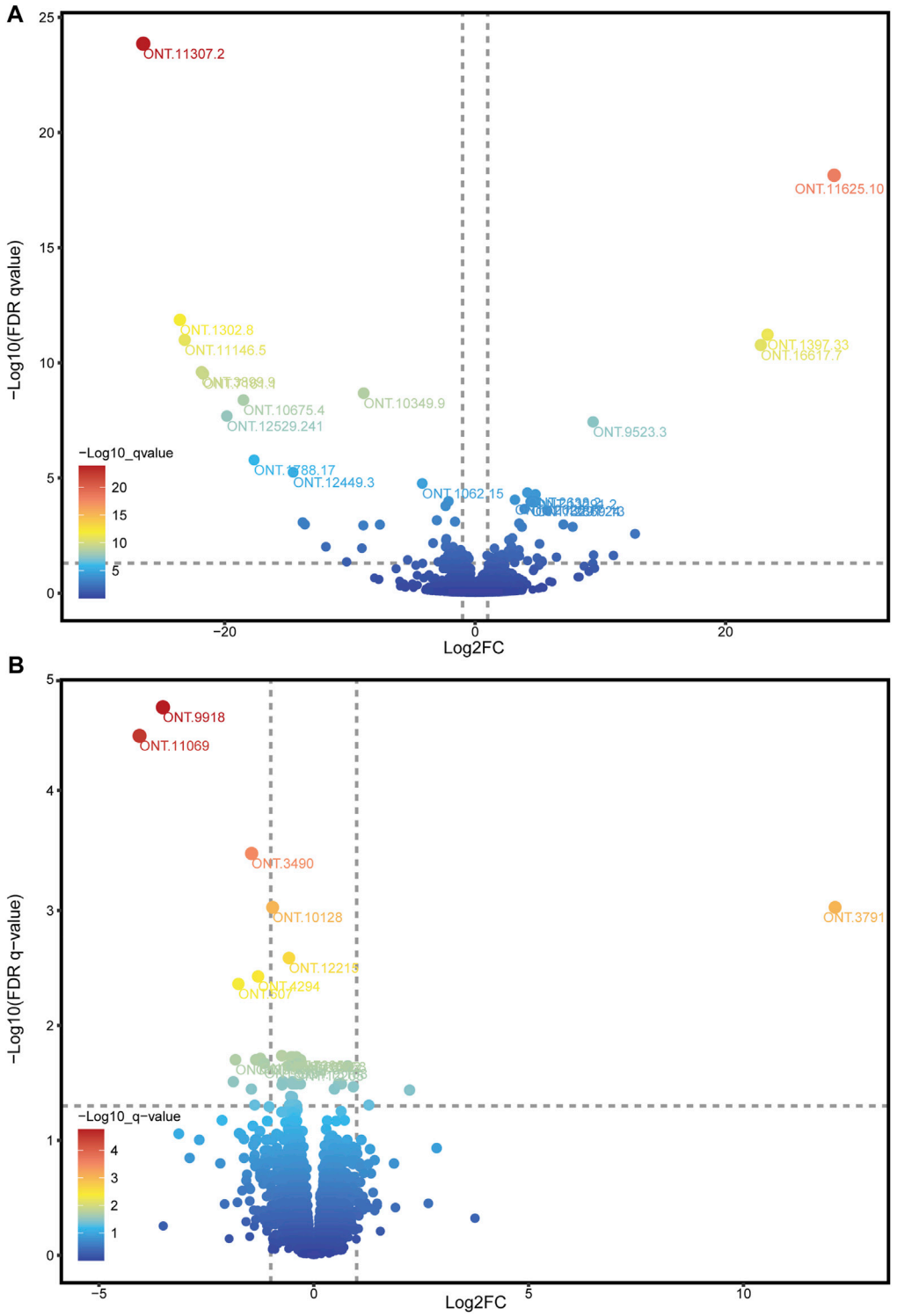

FIGURE 4 | Volcano plot of DESIs and DEGs. **(A)** Volcano plot of DESIs, showing the top 20 splicing isoforms ID with the smallest q-values; **(B)** Volcano plot of DEGs, showing the top 15 genes ID with the smallest q-values.

regulation of genes (Cole et al., 2020), and full-length transcripts can be detected by end-to-end sequencing of most transcript sequences, thereby overcoming the errors caused by the complex transcript assembly steps (Ali et al., 2021) required for short-read sequencing. Using ONT sequencing, a total of 43,688 full-length transcripts were identified in this study, 4,322 novel genes and

TABLE 4 | Proportion of splicing isoforms expression in Group H and L.

DESIs	count%_H	count%_L	*p* value
ONT.9523.3	0.1538	0.0263	0.0025
ONT.3832.5	0.2233	0.0777	0.0069
ONT.191.5	0.1054	0.0409	0.0272
ONT.15153.3	0.0373	0.1700	0.0001
ONT.11047.3	0.0392	0.1768	0.0007
ONT.16074.8	0.2267	0.4325	0.0109
ONT.10763.6	0.1634	0.2448	0.0128
ONT.7120.12	0.1288	0.2803	0.0156
ONT.7120.13	0.0505	0.1090	0.0226
ONT.14524.8	0.1720	0.2395	0.0281
ONT.10349.9	0.0005	0.3011	0.0135

30,795 novel transcripts. In longissimus dorsi samples, exon skipping and alternative 5′ splice site were the most frequent AS events, accounting for 34.22 and 28.75%, respectively. In a previous study, exon skipping and alternative 5′ splice site were the most common AS events in mammalian pre-mRNA (Sammeth et al., 2008), which is consistent with our study.

The analysis of AS events showed that the five genes with the most splicing isoforms were *TNNT3*, *TNNT1*, *YBX3*, *MYBPC2*, and *NEB*. *TNNT3* and *TNNT1* encode troponin T in fast and slow skeletal muscles, respectively, and play important roles in muscle contraction and regulation of calcium concentration (Wei and Jin, 2016). *YBX3* plays an important role in binding to nucleic acids and transcription factors (Lyabin et al., 2020). *MYBPC2* is involved in the regulation of actin binding, protein binding, muscle structural components, cell adhesion, and myofilament sliding (Chen et al., 2021). *NEB* is a structural component of sarcomeres that extend along filaments and regulate key functions of skeletal muscle (Gineste et al., 2020). In pig longissimus dorsi samples, genes related to skeletal muscle function produced numerous splicing isoforms, and skeletal muscle fibers were also found to be a factor affecting IMF deposition (Veloso et al., 2018), suggesting that AS plays an important role in muscle contraction and activity.

In our study, we also investigated 1,605 and 2,235 splicing isoforms generated only in samples from high-IMF and low-IMF groups, respectively. BP entries enriched in the high-IMF group were significantly different from BP entries enriched in the low-IMF group. BP entries enriched in the high-IMF group were ribonucleoprotein complex assembly, ribonucleoprotein complex subunit organization, and ribonucleoprotein complex biogenesis, while those in the low-IMF group were ubiquitin-dependent protein catabolic process, modification-dependent protein catabolic process, and modification-dependent macromolecule catabolic process. In the KEGG analysis, the significantly enriched pathways in the high- and low-IMF groups were all related to ribosomes, spliceosomes and diseases, glycolysis and gluconeogenesis, and fatty acid metabolism partly caused by abnormal muscle function. The functions of splicing isoforms in the high- and low-IMF groups are mostly related to the regulation of transcriptional processes and muscle function and a series of biological processes of fat synthesis and metabolism. The above results indicate that in the longissimus dorsi of pigs, AS is involved in the regulation of transcription and translation processes, and the spliceosome in the regulation of the occurrence of AS events. AS regulates protein synthesis and catabolism and other processes, which affect the differential functional expression of proteins. At the same time, AS also participates in the regulation of complex processes such as muscle function and fat anabolism.

The expression abundance of all full-length transcripts was obtained by comprehensive analysis of ONT and RNA-seq data. A total of 98 DESIs were identified in high- and low-IMF groups. Four upregulated DESIs were identified for *SERBP1*, which is highly expressed in adipose tissue and regarded as a signal of fat deposition (Duarte et al., 2016). *SERBP1* produces plasminogen activator inhibitor 1 RNA-binding protein (PAIRBP1), an inflammatory adipokine mainly present in adipocytes. Studies have shown that fat deposition can lead to steatosis, triggering the development of fibrosis and steatohepatitis, resulting in upregulation of *PAIRBP1* expression (Ota et al., 2007). In addition, the expression of *SERBP1* can inhibit angiostatin to promote angiogenesis (Nishioka et al., 2011), and the processes of adipogenesis and angiogenesis are synchronized. Our study identified four DESIs of *SERBP1* in the high-IMF group, leading us to speculate that AS may play an important role in IMF deposition by regulating *SERBP1* expression. Moreover, three upregulated DESIs were identified for *MYL1*, which encodes myosin light chain 1. Studies have shown that *MYL3*, the paralogous gene of *MYL1*, plays a negative role in adipogenic differentiation (Zhang et al., 2010). *MYL1* is inversely correlated with muscle tenderness (Gagaoua et al., 2020) and is highly expressed in tougher meats and in pigs with leaner carcasses. *MYL1* is present in fast-twitch fibers, which contain less myoglobin, and ATP is produced by glycolytic metabolism, resulting in more fast-twitch fibers and lower IMF content in tougher meat (Rodrigues et al., 2017). In our study, multiple upregulated DESIs of *MYL1* were identified in samples from the high-IMF group, and we speculated that AS may produce functionally opposite splicing isoforms of *MYL1* to make it function abnormally, and these isoforms may compete for *MYL1* translation substrates and reduce *MYL1* expression in high-IMF samples. This result suggests that AS may enhance gene function or generate functionally opposite splicing isoforms to alter gene expression and function.

Three downregulated DESIs were identified for *TNNT3*, which is involved in encoding fast skeletal muscle fibers, and whose dysfunction contributes to the development of muscular dystrophy symptoms. Castrated male bulls produce more IMF, and *TNNT3* showed a trend of upregulation after castration (Silva et al., 2019). The promotion of IMF deposition by *TNNT3* has been verified in chicken (Liu et al., 2016) and cattle (Bong et al., 2009). Interestingly, a study of the DNA-binding motif of *TNNT3* found that its expression levels were inversely correlated with whole-body fat mass ($r_{TNNT3 \sim \text{fat mass}} = -0.49$) (Nunez Lopez et al., 2018). This suggests that different splicing isoforms of *TNNT3* play different roles in the process of IMF deposition, which was also confirmed (Schilder et al., 2011). We found in DESIs analysis that *TNNT1* had one upregulated and one downregulated splicing isoform. *TNNT1* is involved in

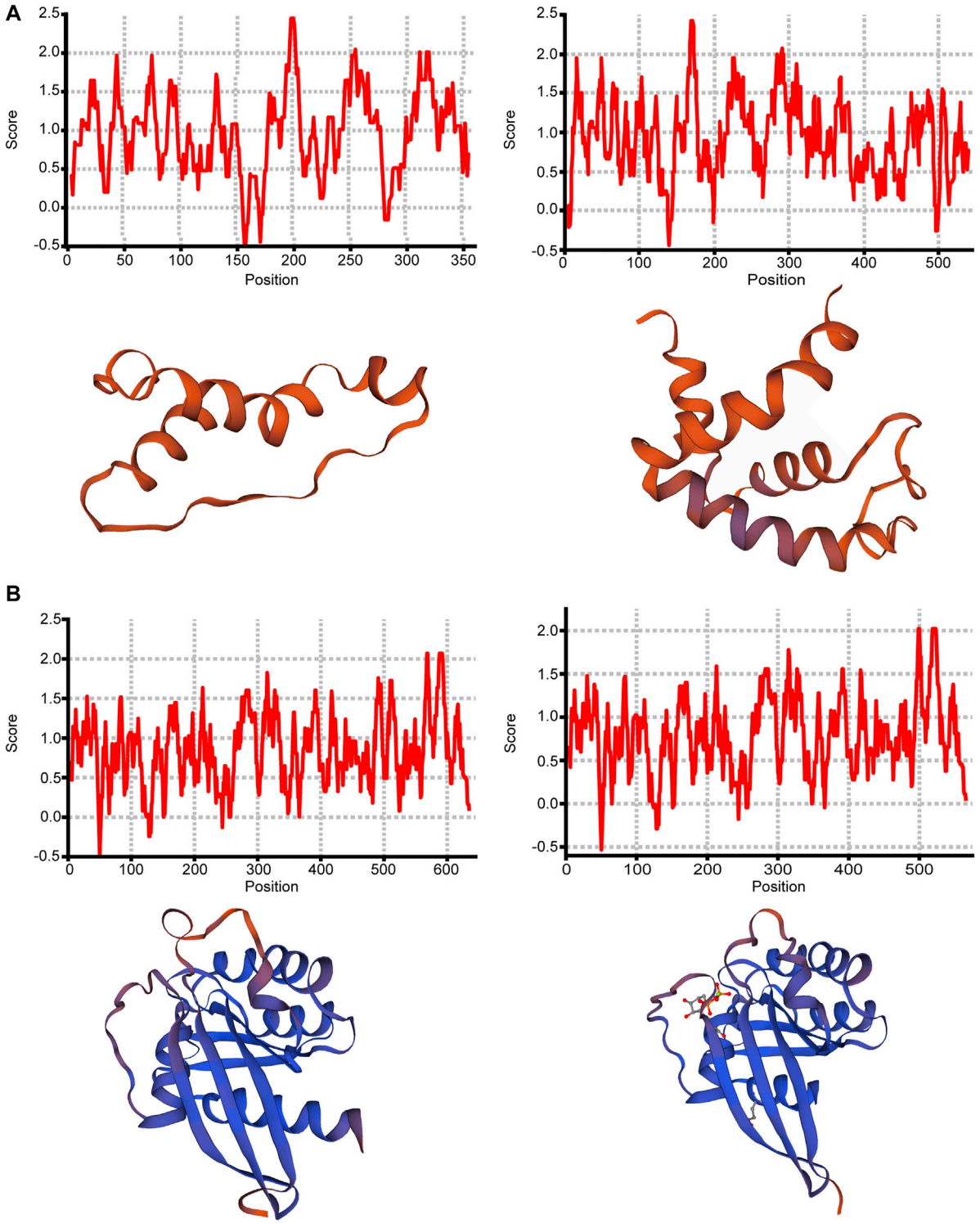

FIGURE 5 | Protein structure analysis of ONT.15153.1, ONT.15153.3, ONT.10349.2 and ONT.10349.9. **(A)** Protein hydrophobicity analysis and protein tertiary structure analysis of ONT.15153.1 and ONT.15153.3; **(B)** Protein hydrophobicity analysis and protein tertiary structure analysis of ONT.10349.2 and ONT.10349.9.

encoding slow skeletal muscle fibers. Studies have found that *TNNT1* is directly associated with obesity traits (Pierzchala et al., 2014), and increased *TNNT1* expression is positively correlated with triglycerides (Nayak et al., 2010). *TNNT1* showed a downward trend in castrated bulls (Silva et al., 2019). The different functions of *TNNT1* may be caused by the opposite

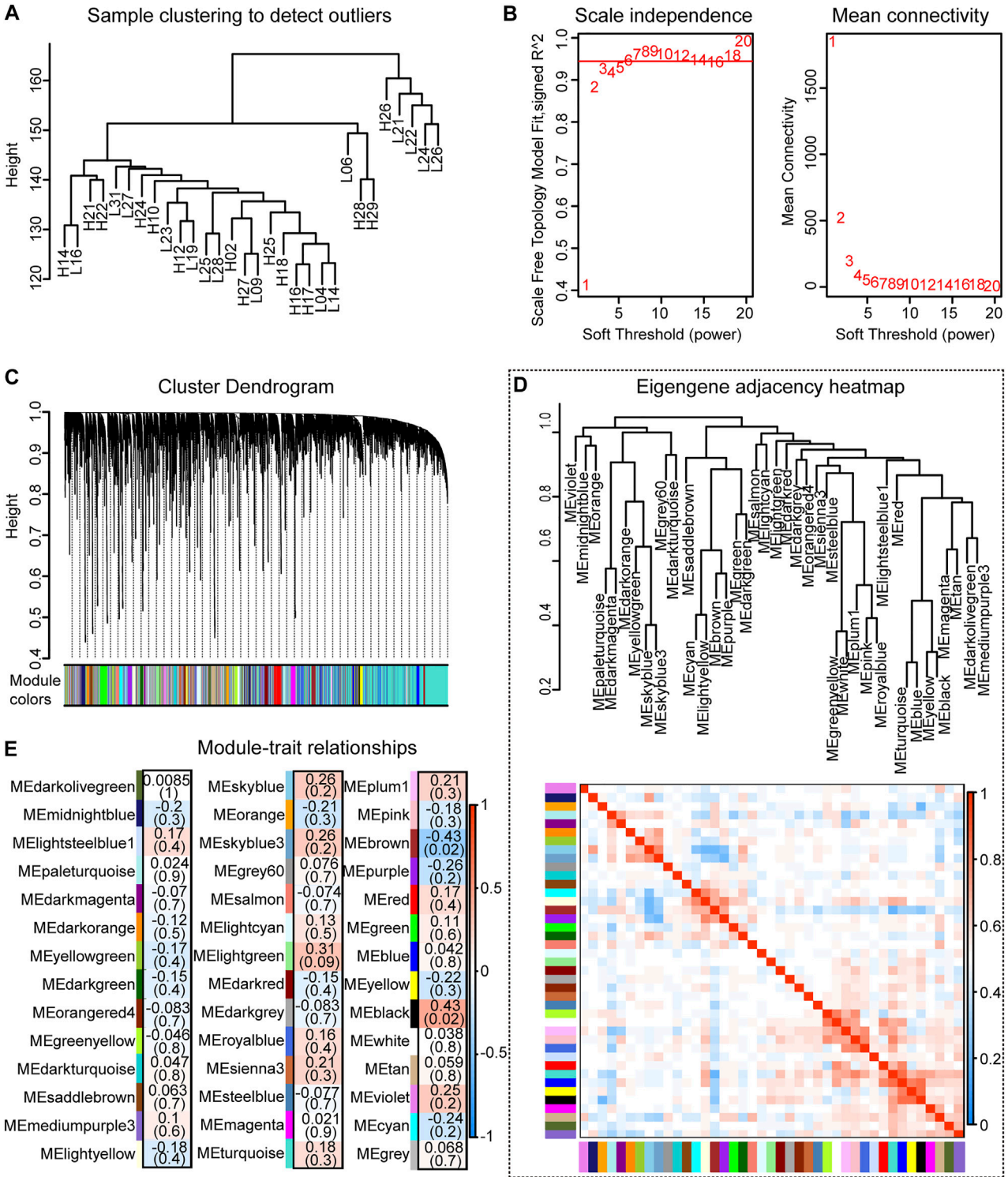

FIGURE 6 | Co-expression analysis results. **(A)** Clustering dendrogram of 30 samples; **(B)** Determination of soft threshold power in co-expression analysis; **(C)** Hierarchical clustering dendrogram of all modules; **(D)** Correlation diagram between modules; **(E)** Relationship between all modules and IMF traits correlation graph.

functions of different splicing isoforms, which is consistent with the results of our analysis. From the multiple regulatory roles of AS of *MYL1*, *TNNT3*, and *TNNT1*, it can be seen that the splicing patterns of skeletal muscle are diverse and complex, and AS has a critical impact on the development and function of muscle fibers and fat deposition. The expression abundance of different

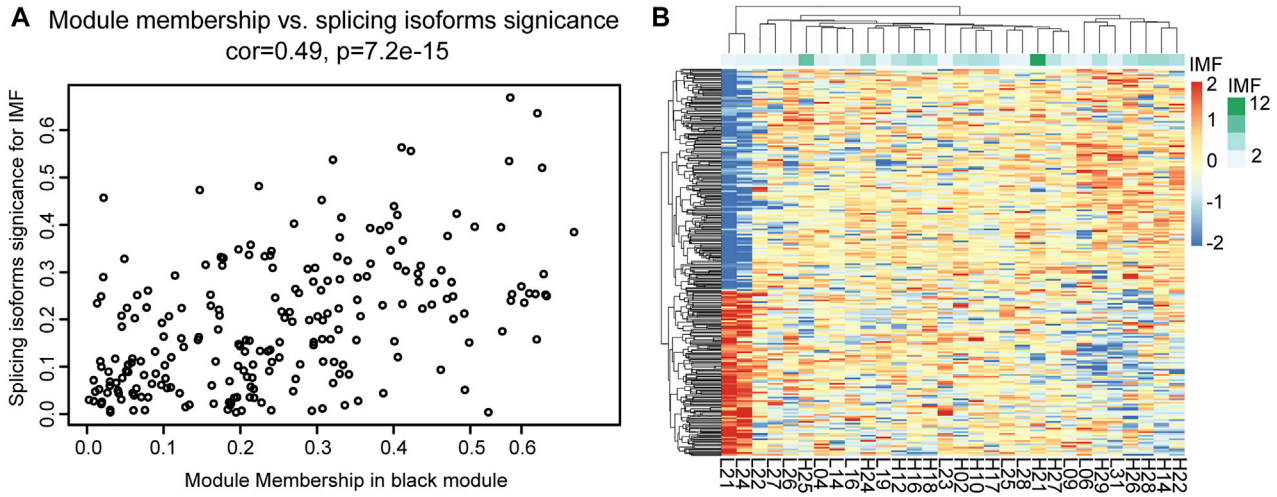

FIGURE 7 | Correlation analysis between MEblack and IMF. **(A)** Dot plot of correlation between splicing isoforms in MEblack and IMF; **(B)** Pheatmap of splicing isoforms in MEblack and 30 samples.

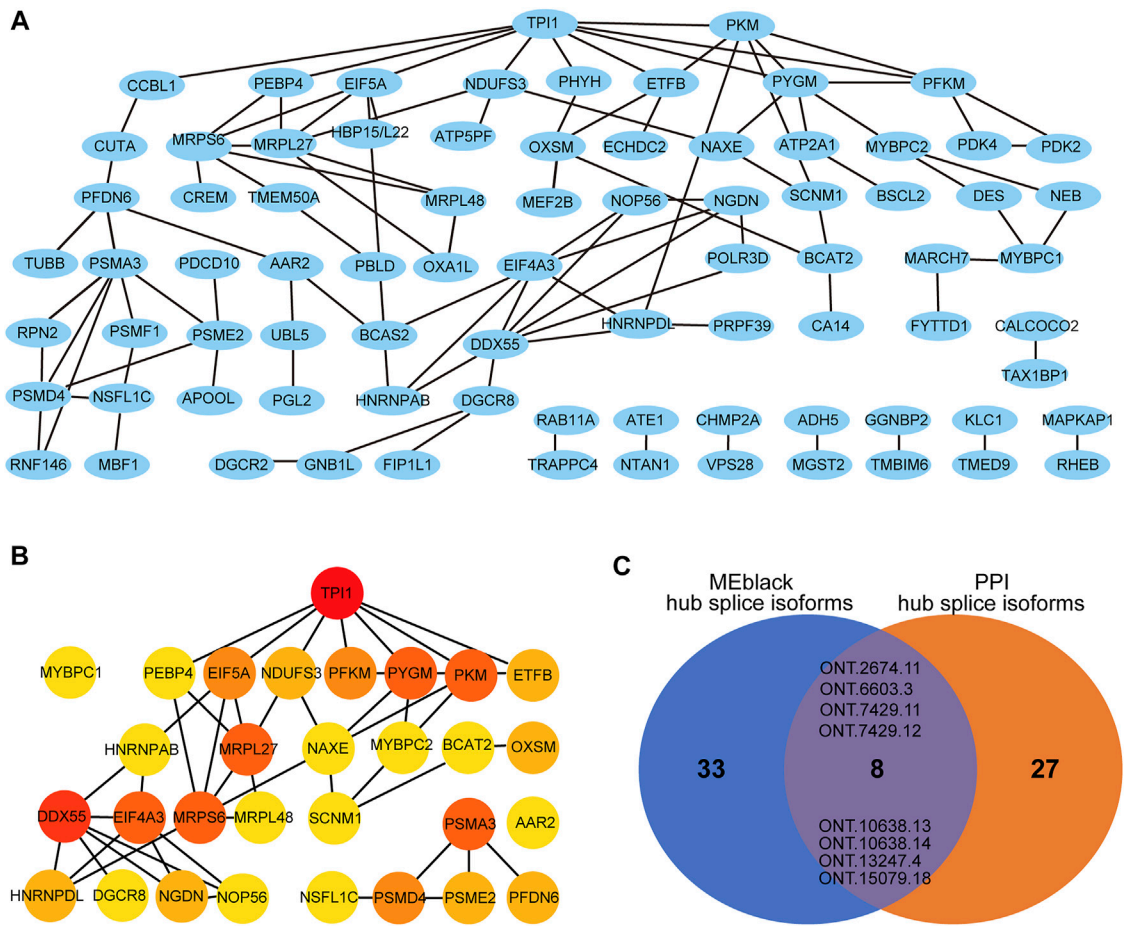

FIGURE 8 | Co-expression and PPI analysis results. **(A)** The gene-PPI network of splicing isoforms in MEblack; **(B)** The PPI network of the Degree top 30 gene; **(C)** The venn diagram of the hub splicing isoforms of MEblack and the hub splicing isoforms of PPI.

splicing isoforms may promote or reverse the realization of gene function, which greatly enriches proteome diversity.

Combining the results of DEGs and DESIs, it was found that the *IFI6* gene and its splicing isoform ONT.12957.1 were both downregulated in the low-IMF group. The *GADD45G* gene and its splicing isoforms ONT.4294.3 and ONT.4294.9 were also downregulated in the low-IMF group. *IFI6* is a gene that may play an important role in meat quality and carcass indicators and is regarded as a candidate gene for improved pork quality (Kayan et al., 2011). *GADD45G* is an inflammation-related gene associated with oxidative stress and cytokine secretion signaling pathways. The expression of *GADD45G* is upregulated in the liver in high-fat-diet-induced non-alcoholic fatty liver disease (NAFLD), and its expression decreases when the high-fat condition is improved (Wang et al., 2022), which may be related to its effect of on hepatic fibrosis and the occurrence of chemical transformation (Hong et al., 2016). The above results suggest that differential expression of spliced isoforms may cause differences in gene expression.

By analyzing the proportion of expression of each DESI in all transcripts, we explored the important role of splicing isoforms in the realization of gene function. Among the DESIs in the high- and low-IMF groups, we found that the average expression proportion of ONT.9523.3, ONT.3832.5, ONT.15153.3, ONT.11047.3, ONT.16074.8, ONT.10763.6, ONT.7120.12, ONT.7120.13, ONT.14524.8, ONT.10349.9, and ONT.191.5 in samples from the two groups was >10%, and the difference between the two was significant ($p < 0.05$). Then, we compared the expression ratio of splicing isoforms and other transcripts of the gene. The proportion of ONT.15153.1 expression in the low-IMF group was significantly lower than that in the high-IMF group. We speculated that increased expression of ONT.15153.3 would cause decreased expression of ONT.15153.1. At the same time, increased expression of ONT.10349.9 also caused decreased expression of ONT.10349.2. The analysis of its protein hydrophobicity and tertiary structure showed that the occurrence of AS events will lead to different coding information of transcripts, which will change the hydrophobic region of the amino acid sequence, and then affect the conformation of the tertiary structure of the protein. The gene encoding ONT.15153.3 is *ART1*, which catalyzes the ADP-ribosylation of arginine residues in the protein. It is highly expressed in skeletal muscle and is associated with the formation of myotubes and muscle fibers (Leutert et al., 2018). The gene encoding ONT.10349.9 is *RAB2A*, a member of the RAS oncogene family (*RAB2A*) and a membrane-bound protein involved in vesicle fusion and trafficking. *RAB2A* knockdown inhibits glucose-stimulated insulin secretion (Sugawara et al., 2014). According to the above results, the occurrence of AS may change the expression of some transcripts of the same gene, thereby affecting gene function.

Through differential analysis of the expression abundance of alternatively spliced transcripts, it was found that AS plays a variety of regulatory roles in the process of fat deposition. In addition, by constructing a co-expression network, the splicing isoforms of eight centers common to the co-expression and PPI networks were screened, which belonged to six genes: *MRPL27*, *AAR2*, *PYGM*, *PSMD4*, *SCNM1*, and *HNRNPDL*. *MRPL27* encodes a mitochondrial ribosomal protein, and its abnormal function may cause small steric dysfunction and muscle atrophy (Bogatikov et al., 2020). *MRPL27* is also regarded as an NAFLD-related hub gene (Zeng et al., 2021). *AAR2* is a splicing factor that is a component of the U5 snRNP complex and is required for spliceosome assembly and pre-mRNA splicing (Weber et al., 2013). *PYGM* encodes glycogen phosphorylase, which provides energy for muscle contraction, and is associated with glycogen storage in skeletal muscle (Tarnopolsky, 2018). *PSMD4* encodes proteasome 26S subunit ubiquitin receptor, which is a proteasome-related gene that is significantly downregulated in hypercholesterolemia (Loke et al., 2017). *SCNM1* encodes a zinc finger protein and putative splicing factor, and its mis-splicing will lead to serious lesions of sodium channels in mice (Buchner et al., 2003). *HNRNPDL* encodes heterogenetic nuclear ribonucleoprotein d like, which is an important transcription regulator that regulates the AS of hundreds of genes (Li et al., 2019).

CONCLUSION

Our study shows that 17.79% of the genes in the longissimus dorsi muscle produced splicing isoforms. Specific splicing isoforms in the high- and low-IMF groups were found to be related to the regulation of the transcription process and muscle fiber function. *MYL1*, *TNNT3*, and *TNNT1* produced different splicing isoforms through AS, which can promote or slow down the process of IMF deposition. The splicing isoforms of *IFI6* and *GADD45G* were differentially expressed, which may cause differences in gene expression, and the expression of the splicing isoforms of *ART1* and *RAB2A* caused changes in the expression of other transcripts. Several genes of hub splicing isoforms, such as *MRPL27*, *AAR2*, *PYGM*, *PSMD4*, *SCNM1*, and *HNRNPDL*, were also investigated with regard to iIMF. These genes may be associated with IMF deposition, but there is currently no direct evidence and further studies are needed to explore their function. Our study preliminarily shows that AS may affect fat deposition in many forms, which also provides further insight into the mechanism of AS regulating IMF content. Our results identified many candidate splice isoforms in IMF that can be used as molecular markers in the breeding and improvement of pig IMF content after validation.

DATA AVAILABILITY STATEMENT

The datasets presented in this study can be found in online repositories. The names of the repository/repositories and accession number(s) can be found in the article/**Supplementary Material**.

ETHICS STATEMENT

The animal study was reviewed and approved by Animal Ethics Committee of the Institute of Animal Science, Chinese Academy of Agricultural Sciences.

AUTHOR CONTRIBUTIONS

LgW and LxW conceived and designed the experimental plan, and ZS participated in the bioinformatics analysis and drafted the

manuscript. LgW, JW, XH, HY and LxW helped revise this manuscript. All authors read and approved the final manuscript.

FUNDING

This work was jointly supported by the National Natural Science Foundation of China (Grant Nos 31872337 and 31501919), China Agriculture Research System of MOF and MARA (CARS-35), and Agricultural Science and Technology Innovation Project (ASTIP-IAS02). The funding bodies had no role in the design of the study, or collection, analysis and interpretation of data and writing the manuscript.

ACKNOWLEDGMENTS

We thank the researchers at our laboratories for their dedication and hard work.

SUPPLEMENTARY MATERIAL

The Supplementary Material for this article can be found online at: https://www.frontiersin.org/articles/10.3389/fgene.2022.877646/full#supplementary-material

Supplementary Figure S1 | Cluster analysis of all samples with differentially splicing isoforms.

REFERENCES

Alfaia, C. M., Lopes, P. A., Madeira, M. S., Pestana, J. M., Coelho, D., Toldrá, F., et al. (2019). Current Feeding Strategies to Improve Pork Intramuscular Fat Content and its Nutritional Quality. *Adv. Food Nutr. Res.* 89, 53–94. doi:10.1016/bs.afnr.2019.03.006

Ali, A., Thorgaard, G. H., and Salem, M. (2021). PacBio Iso-Seq Improves the Rainbow Trout Genome Annotation and Identifies Alternative Splicing Associated with Economically Important Phenotypes. *Front. Genet.* 12, 683408. doi:10.3389/fgene.2021.683408

Beiki, H., Liu, H., Huang, J., Manchanda, N., Nonneman, D., Smith, T. P. L., et al. (2019). Improved Annotation of the Domestic Pig Genome through Integration of Iso-Seq and RNA-Seq Data. *BMC Genomics* 20 (1), 344. doi:10.1186/s12864-019-5709-y

Bogatikov, E., Lindblad, I., Punga, T., and Punga, A. R. (2020). miR-1933-3p Is Upregulated in Skeletal Muscles of MuSK+ EAMG Mice and Affects Impa1 and Mrpl27. *Neurosci. Res.* 151, 46–52. doi:10.1016/j.neures.2019.02.003

Bong, J., Cho, K., and Baik, M. (2009). Comparison of Gene Expression Profiling between Bovine Subcutaneous and Intramusular Adipose Tissues by Serial Analysis of Gene Expression. *Cell Biol. Int.* 34 (1), 125–133. doi:10.1042/CBI20090046

Buchner, D. A., Trudeau, M., and Meisler, M. H. (2003). SCNM1, a Putative RNA Splicing Factor that Modifies Disease Severity in Mice. *Science* 301 (5635), 967–969. doi:10.1126/science.1086187

Chen, Z., Li, X.-y., Guo, P., and Wang, D.-l. (2021). MYBPC2 and MYL1 as Significant Gene Markers for Rhabdomyosarcoma. *Technol. Cancer Res. Treat.* 20, 153303382097966. doi:10.1177/1533033820979669

Cole, C., Byrne, A., Adams, M., Volden, R., and Vollmers, C. (2020). Complete Characterization of the Human Immune Cell Transcriptome Using Accurate Full-Length cDNA Sequencing. *Genome Res.* 30 (4), 589–601. doi:10.1101/gr.257188.119

De Coster, W., D'Hert, S., Schultz, D. T., Cruts, M., and Van Broeckhoven, C. (2018). NanoPack: Visualizing and Processing Long-Read Sequencing Data. *Bioinformatics* 34 (15), 2666–2669. doi:10.1093/bioinformatics/bty149

Deamer, D., Akeson, M., and Branton, D. (2016). Three Decades of Nanopore Sequencing. *Nat. Biotechnol.* 34 (5), 518–524. doi:10.1038/nbt.3423

Duarte, J. L. G., Cantet, R. J. C., Rubio, Y. L. B., Bates, R. O., Ernst, C. W., Raney, N. E., et al. (2016). Refining Genomewide Association for Growth and Fat Deposition Traits in an F2 Pig Population1. *J. Anim. Sci.* 94 (4), 1387–1397. doi:10.2527/jas.2015-0182

Fang, X., Xia, L., Yu, H., He, W., Bai, Z., Qin, L., et al. (2021). Comparative Genome-wide Alternative Splicing Analysis of Longissimus Dorsi Muscles between Japanese Black (Wagyu) and Chinese Red Steppes Cattle. *Front. Vet. Sci.* 8, 634577. doi:10.3389/fvets.2021.634577

Finn, R. D., Clements, J., and Eddy, S. R. (2011). HMMER Web Server: Interactive Sequence Similarity Searching. *Nucleic Acids Res.* 39, W29–W37. Web Server issue. doi:10.1093/nar/gkr367

Foissac, S., and Sammeth, M. (2007). ASTALAVISTA: Dynamic and Flexible Analysis of Alternative Splicing Events in Custom Gene Datasets. *Nucleic Acids Res.* 35, W297–W299. Web Server issue. doi:10.1093/nar/gkm311

Gagaoua, M., Bonnet, M., and Picard, B. (2020). Protein Array-Based Approach to Evaluate Biomarkers of Beef Tenderness and Marbling in Cows: Understanding of the Underlying Mechanisms and Prediction. *Foods* 9 (9), 1180. doi:10.3390/foods9091180

Gineste, C., Ogier, A. C., Varlet, I., Hourani, Z., Bernard, M., Granzier, H., et al. (2020). *In Vivo* characterization of Skeletal Muscle Function in Nebulin-deficient Mice. *Muscle Nerve* 61 (3), 416–424. doi:10.1002/mus.26798

Hao, W., Yang, Z., Sun, Y., Li, J., Zhang, D., Liu, D., et al. (2022). Characterization of Alternative Splicing Events in Porcine Skeletal Muscles with Different Intramuscular Fat Contents. *Biomolecules* 12 (2), 154. doi:10.3390/biom12020154

Hong, L., Sun, Q.-F., Xu, T.-Y., Wu, Y.-H., Zhang, H., Fu, R.-Q., et al. (2016). New Role and Molecular Mechanism of Gadd45a in Hepatic FIbrosis. *Wjg* 22 (9), 2779–2788. doi:10.3748/wjg.v22.i9.2779

Kayan, A., Uddin, M. J., Cinar, M. U., Grosse-Brinkhaus, C., Phatsara, C., Wimmers, K., et al. (2011). Investigation on Interferon Alpha-Inducible Protein 6 (IFI6) Gene as a Candidate for Meat and Carcass Quality in Pig. *Meat Sci.* 88 (4), 755–760. doi:10.1016/j.meatsci.2011.03.009

Kelemen, O., Convertini, P., Zhang, Z., Wen, Y., Shen, M., Falaleeva, M., et al. (2013). Function of Alternative Splicing. *Gene* 514 (1), 1–30. doi:10.1016/j.gene.2012.07.083

Kopylova, E., Noé, L., and Touzet, H. (2012). SortMeRNA: Fast and Accurate Filtering of Ribosomal RNAs in Metatranscriptomic Data. *Bioinformatics* 28 (24), 3211–3217. doi:10.1093/bioinformatics/bts611

Lee, Y., and Rio, D. C. (2015). Mechanisms and Regulation of Alternative Pre-mRNA Splicing. *Annu. Rev. Biochem.* 84, 291–323. doi:10.1146/annurev-biochem-060614-034316

Leutert, M., Menzel, S., Braren, R., Rissiek, B., Hopp, A.-K., Nowak, K., et al. (2018). Proteomic Characterization of the Heart and Skeletal Muscle Reveals Widespread Arginine ADP-Ribosylation by the ARTC1 Ectoenzyme. *Cell Rep.* 24 (7), 1916–1929. doi:10.1016/j.celrep.2018.07.048

Li, H. (2018). Minimap2: Pairwise Alignment for Nucleotide Sequences. *Bioinformatics* 34 (18), 3094–3100. doi:10.1093/bioinformatics/bty191

Li, R. Z., Hou, J., Wei, Y., Luo, X., Ye, Y., and Zhang, Y. (2019). hnRNPDL Extensively Regulates Transcription and Alternative Splicing. *Gene* 687, 125–134. doi:10.1016/j.gene.2018.11.026

Li, X., Suh, Y., Kim, E., Moeller, S. J., and Lee, K. (2012). Alternative Splicing and Developmental and Hormonal Regulation of Porcine Comparative Gene Identification-58 (CGI-58) mRNA1. *J. Anim. Sci.* 90 (12), 4346–4354. doi:10.2527/jas.2012-5151

Liu, J., Fu, R., Liu, R., Zhao, G., Zheng, M., Cui, H., et al. (2016). Protein Profiles for Muscle Development and Intramuscular Fat Accumulation at Different Post-Hatching Ages in Chickens. *PLoS One* 11 (8), e0159722. doi:10.1371/journal.pone.0159722

Liu, K., Wang, G., Zhao, S. H., Liu, B., Huang, J. N., Bai, X., et al. (2010). Molecular Characterization, Chromosomal Location, Alternative Splicing and Polymorphism of Porcine GFAT1 Gene. *Mol. Biol. Rep.* 37 (6), 2711–2717. doi:10.1007/s11033-009-9805-y

Loke, S.-Y., Wong, P. T.-H., and Ong, W.-Y. (2017). Global Gene Expression Changes in the Prefrontal Cortex of Rabbits with Hypercholesterolemia And/or Hypertension. *Neurochem. Int.* 102, 33–56. doi:10.1016/j.neuint.2016.11.010

Love, M. I., Huber, W., and Anders, S. (2014). Moderated Estimation of Fold Change and Dispersion for RNA-Seq Data with DESeq2. *Genome Biol.* 15 (12), 550. doi:10.1186/s13059-014-0550-8

Lyabin, D. N., Eliseeva, I. A., Smolin, E. A., Doronin, A. N., Budkina, K. S., Kulakovskiy, I. V., et al. (2020). YB-3 Substitutes YB-1 in Global mRNA Binding. *RNA Biol.* 17 (4), 487–499. doi:10.1080/15476286.2019.1710050

Malgwi, I. H., Halas, V., Grünvald, P., Schiavon, S., and Jócsák, I. (2022). Genes Related to Fat Metabolism in Pigs and Intramuscular Fat Content of Pork: A Focus on Nutrigenetics and Nutrigenomics. *Animals* 12 (2), 150. doi:10.3390/ani12020150

Nayak, S. B., Pinto Pereira, L. M., Boodoo, S., Kimberlyali, A., Baptiste, C., Maraj, S., et al. (2010). Association of Troponin T and Altered Lipid Profile in Patients Admitted with Acute Myocardial Infarction. *Arch. Physiol. Biochem.* 116 (1), 21–27. doi:10.3109/13813450903397638

Nishioka, N., Matsuoka, T., Yashiro, M., Hirakawa, K., Olden, K., and Roberts, J. D. (2011). Linoleic Acid Enhances Angiogenesis through Suppression of Angiostatin Induced by Plasminogen Activator Inhibitor 1. *Br. J. Cancer* 105 (11), 1750–1758. doi:10.1038/bjc.2011.434

Nunez Lopez, Y. O., Messi, M. L., Pratley, R. E., Zhang, T., and Delbono, O. (2018). Troponin T3 Associates with DNA Consensus Sequence that Overlaps with P53 Binding Motifs. *Exp. Gerontol.* 108, 35–40. doi:10.1016/j.exger.2018.03.012

Ota, T., Takamura, T., Kurita, S., Matsuzawa, N., Kita, Y., Uno, M., et al. (2007). Insulin Resistance Accelerates a Dietary Rat Model of Nonalcoholic Steatohepatitis. *Gastroenterology* 132 (1), 282–293. doi:10.1053/j.gastro.2006.10.014

Pierzchala, M., Hoekman, A. J. W., Urbanski, P., Kruijt, L., Kristensen, L., Young, J. F., et al. (2014). Validation of Biomarkers for Loin Meat Quality (M. Longissimus) of Pigs. *J. Anim. Breed. Genet.* 131 (4), 258–270. doi:10.1111/jbg.12081

Rodrigues, R. T. d. S., Chizzotti, M. L., Vital, C. E., Baracat-Pereira, M. C., Barros, E., Busato, K. C., et al. (2017). Differences in Beef Quality between Angus (*Bos taurus* Taurus) and Nellore (*Bos taurus* Indicus) Cattle through a Proteomic and Phosphoproteomic Approach. *PLoS One* 12 (1), e0170294. doi:10.1371/journal.pone.0170294

Sammeth, M., Foissac, S., and Guigó, R. (2008). A General Definition and Nomenclature for Alternative Splicing Events. *Plos Comput. Biol.* 4 (8), e1000147. doi:10.1371/journal.pcbi.1000147

Schilder, R. J., Kimball, S. R., Marden, J. H., and Jefferson, L. S. (2011). Body Weight-dependent Troponin T Alternative Splicing Is Evolutionarily Conserved from Insects to Mammals and Is Partially Impaired in Skeletal Muscle of Obese Rats. *J. Exp. Biol.* 214 (9), 1523–1532. doi:10.1242/jeb.051763

Silva, L. H. P., Rodrigues, R. T. S., Assis, D. E. F., Benedeti, P. D. B., Duarte, M. S., and Chizzotti, M. L. (2019). Explaining Meat Quality of Bulls and Steers by Differential Proteome and Phosphoproteome Analysis of Skeletal Muscle. *J. Proteomics* 199, 51–66. doi:10.1016/j.jprot.2019.03.004

Sugawara, T., Kano, F., and Murata, M. (2014). Rab2A Is a Pivotal Switch Protein that Promotes Either Secretion or ER-Associated Degradation of (Pro)insulin in Insulin-Secreting Cells. *Sci. Rep.* 4, 6952. doi:10.1038/srep06952

Tarnopolsky, M. A. (2018). Myopathies Related to Glycogen Metabolism Disorders. *Neurotherapeutics* 15 (4), 915–927. doi:10.1007/s13311-018-00684-2

Veloso, R., Lopes, P., Duarte, M., Silva, F., Saraiva, A., Chizzotti, M., et al. (2018). Research Article Expression of Lipid Metabolism and Myosin Heavy Chain Genes in Pigs Is Affected by Genotype and Dietary Lysine. *Genet. Mol. Res.* 17 (2). doi:10.4238/gmr16039904

Wang, L., Zhou, Z.-Y., Zhang, T., Zhang, L., Hou, X., Yan, H., et al. (2021). IRLnc: a Novel Functional Noncoding RNA Contributes to Intramuscular Fat Deposition. *BMC Genomics* 22 (1), 95. doi:10.1186/s12864-020-07349-5

Wang, R., Yao, L., Lin, X., Hu, X., and Wang, L. (2022). Exploring the Potential Mechanism of Rhodomyrtus Tomentosa (Ait.) Hassk Fruit Phenolic Rich Extract on Ameliorating Nonalcoholic Fatty Liver Disease by Integration of Transcriptomics and Metabolomics Profiling. *Food Res. Int.* 151, 110824. doi:10.1016/j.foodres.2021.110824

Weber, G., Cristão, V. F., Santos, K. F., Jovin, S. M., Heroven, A. C., Holton, N., et al. (2013). Structural Basis for Dual Roles of Aar2p in U5 snRNP Assembly. *Genes Dev.* 27 (5), 525–540. doi:10.1101/gad.213207.113

Wei, B., and Jin, J.-P. (2016). TNNT1, TNNT2, and TNNT3: Isoform Genes, Regulation, and Structure-Function Relationships. *Gene* 582 (1), 1–13. doi:10.1016/j.gene.2016.01.006

Weirather, J. L., de Cesare, M., Wang, Y., Piazza, P., Sebastiano, V., Wang, X.-J., et al. (2017). Comprehensive Comparison of Pacific Biosciences and Oxford Nanopore Technologies and Their Applications to Transcriptome Analysis. *F1000Res* 6, 100. doi:10.12688/f1000research.10571.210.12688/f1000research.10571.1

Yu, G., Wang, L.-G., Han, Y., and He, Q.-Y. (2012). clusterProfiler: an R Package for Comparing Biological Themes Among Gene Clusters. *OMICS: A J. Integr. Biol.* 16 (5), 284–287. doi:10.1089/omi.2011.0118

Zeng, F., Shi, M., Xiao, H., and Chi, X. (2021). WGCNA-based Identification of Hub Genes and Key Pathways Involved in Nonalcoholic Fatty Liver Disease. *Biomed. Res. Int.* 2021, 1–16. doi:10.1155/2021/5633211

Zhang, L., Li, F., Guo, Q., Duan, Y., Wang, W., Yang, Y., et al. (2021). Balanced Branched-chain Amino Acids Modulate Meat Quality by Adjusting Muscle Fiber Type Conversion and Intramuscular Fat Deposition in Finishing Pigs. *J. Sci. Food Agric.* doi:10.1002/jsfa.11728

Zhang, Q., Lee, H.-G., Han, J.-A., Kim, E. B., Kang, S. K., Yin, J., et al. (2010). Differentially Expressed Proteins during Fat Accumulation in Bovine Skeletal Muscle. *Meat Sci.* 86 (3), 814–820. doi:10.1016/j.meatsci.2010.07.002

Conflict of Interest: The authors declare that the research was conducted in the absence of any commercial or financial relationships that could be construed as a potential conflict of interest.

Publisher's Note: All claims expressed in this article are solely those of the authors and do not necessarily represent those of their affiliated organizations, or those of the publisher, the editors and the reviewers. Any product that may be evaluated in this article, or claim that may be made by its manufacturer, is not guaranteed or endorsed by the publisher.

GLOSSARY

AS alternative splicing
IMF intramuscular fat
PPI protein-protein interaction
ONT Oxford Nanopore Technologies
PacBio Pacific Biosciences
TGS third-generation sequencing
SMRT single-molecule real time
WGCNA weighted gene co-expression network analysis
PCR polymerase chain reaction
ES exon skipping
IR intron retention
A5SS alternative 5′ splice site
A3SS alternative 3′ splice site
MEE mutually exclusive exons
GO Gene Ontology
KEGG Kyoto Encyclopedia of Genes and Genomes
COG Cluster of Orthologous Groups of proteins
KOG Clusters of orthologous groups for eukaryotic complete genomes
NR NCBI Non-redundant Protein Sequences Database
Pfam Pfamdatabase
BP biological process
CC cellular component
MF molecular function
DEGs differentially expressed genes
DESIs differentially expressed splicing isoforms
TNNT3 troponin t3, fast skeletal type
TNNT1 troponin t1, slow skeletal type
YBX3 Y-box binding protein 3
MYBPC2 myosin binding protein C2
NEB nebulin
SERBP1 SERPINE1 mRNA binding protein 1
MYL1 myosin light chain 1
IFI6 interferon alpha inducible protein 6
GADD45G growth arrest and DNA damage inducible gamma
ART1 ADP-ribosyltransferase 1
MRPL27 mitochondrial ribosomal protein L27
AAR2 AAR2 splicing factor
PYGM glycogen phosphorylase, muscle associated
PSMD4 proteasome 26S subunit ubiquitin receptor, non-ATPase 4
SCNM1 sodium channel modifier 1
HNRNPDL heterogeneous nuclear ribonucleoprotein D like
PAIRBP1 plasminogen activator inhibitor 1 RNA-binding protein
NAFLD nonalcoholic fatty liver disease

frontiers | Frontiers in Veterinary Science

ORIGINAL RESEARCH
published: 31 May 2022
doi: 10.3389/fvets.2022.847363

Expression of *DGAT2* Gene and Its Associations With Intramuscular Fat Content and Breast Muscle Fiber Characteristics in Domestic Pigeons (*Columba livia*)

Haiguang Mao[1], *Zhaozheng Yin*[2], *Mengting Wang*[1], *Wenwen Zhang*[1], *Sayed Haidar Abbas Raza*[3], *Fayez Althobaiti*[4], *Lili Qi*[1]* *and Jinbo Wang*[1]*

[1] School of Biological and Chemical Engineering, NingboTech University, Ningbo, China, [2] College of Animal Science, Zhejiang University, Hangzhou, China, [3] College of Animal Science and Technology, Northwest A&F University, Xianyang, China, [4] Department of Biotechnology, College of Science, Taif University, Taif, Saudi Arabia

OPEN ACCESS

Edited by:
Min Du,
Washington State University,
United States

Reviewed by:
Chunqi Gao,
South China Agricultural University, China
Yuwares Malila,
National Center for Genetic Engineering and Biotechnology (BIOTEC), Thailand

***Correspondence:**
Lili Qi
qll@nbt.edu.cn
Jinbo Wang
wjb@nbt.edu.cn

Specialty section:
This article was submitted to Livestock Genomics, a section of the journal Frontiers in Veterinary Science

Received: 02 January 2022
Accepted: 26 April 2022
Published: 31 May 2022

Citation:
Mao H, Yin Z, Wang M, Zhang W, Raza SHA, Althobaiti F, Qi L and Wang J (2022) Expression of DGAT2 Gene and Its Associations With Intramuscular Fat Content and Breast Muscle Fiber Characteristics in Domestic Pigeons (Columba livia). Front. Vet. Sci. 9:847363. doi: 10.3389/fvets.2022.847363

Diacylglycerol acyltransferase 2 (DGAT2) catalyzes the final step in triglyceride synthesis and plays an important role in the synthesis of fat, but the effects of its expression on intramuscular fat (IMF) content and muscle development are still unknown. In this study, we investigated the expression of the *DGAT2* gene and its associations with IMF content and breast muscle fiber characteristics in pigeons. The spatiotemporal expression profile of the pigeon *DGAT2* gene in breast muscle showed that the mRNA expression level of *DGAT2* gene in subcutaneous fat was the highest ($p < 0.01$) among eight tissues from 0 to 4 weeks of age, and showed an upward trend week by week, followed by liver ($p < 0.05$). Moreover, both mRNA and protein levels of the *DGAT2* gene in breast muscle showed an upward trend from 0 to 4 weeks ($p < 0.05$), accompanied by the upregulation of *MYOD1* and *MSTN*. In addition, the paraffin section analysis results revealed that the diameter and cross-sectional area of pectoralis muscle fiber significantly increased with age ($p < 0.05$), and a significant positive correlation was shown between the *DGAT2* gene expression level and muscle fiber diameter ($p < 0.05$). Furthermore, correlation analysis suggested that the mRNA expression level of the pigeon *DGAT2* gene was significantly ($p < 0.01$) correlated with IMF content in breast muscle. These results imply that the *DGAT2* gene has a close relationship with IMF content and breast muscle fiber characteristics in pigeons, indicating that the DGAT2 gene might be used as a candidate gene marker-assisted breeding in pigeons.

Keywords: *DGAT2*, gene expression, intramuscular fat, muscle fiber, pigeon

INTRODUCTION

Intramuscular fat (IMF) content is a crucial factor in meat quality traits and is economically important in poultry breeding programs (1). With improving living standards, the demands for poultry meat are not only concentrated on carcass composition but also meat quality (2), especially in China, where people prefer to cook poultry meat by steaming and souping. Domestic pigeons are wildly raised in southern China as a kind of meat-type poultry for the abundant nutrients and

delicious taste (3). Numerous studies have been carried out on other poultry, such as chickens and ducks, to identify genes regulating IMF content and muscle fiber characteristics (4, 5), but studies on domestic pigeons are still limited.

Intramuscular fat content is influenced by multiple factors, such as genetic factors, nutritional conditions, feeding method and environment, gender factors, and muscle fiber characteristics (6). It is well-known that IMF is one of the most important factors in meat quality (7). Not only does it greatly improve the meat texture and make it tenderer, but it also enhances the meat flavor and juiciness because the IMF contains a variety of flavor compounds (8). Muscle fiber characteristics can also significantly affect meat quality, mainly such as muscle fiber type, muscle fiber diameter, muscle fiber area, muscle fiber density, muscle fiber length, connective tissue, and IMF content (9, 10). IMF is the fat deposited on the perimysium, endomysium, and epimysium, so to a certain extent, the thickness of the perimysium, endomysium, and epimysium can also reflect the content of IMF (11, 12).

Many studies have demonstrated that there are many genes regulating IMF deposition and muscle fiber characteristics in meat-type animals (1, 3, 13). Diacylglycerol acyltransferase 2 (DGAT2), one of the DGAT family members, is involved in the final and rate-limiting step in the reaction of triacylglycerol synthesis pathways, consequently playing a key role in the fat deposition (1, 14). Previous studies have shown that the expression level of the *DGAT2* gene is positively correlated with IMF content in *longissimus dorsi* muscles of pigs (15) and Korean steers (16). Moreover, the *DGAT2* gene polymorphisms have been reported to affect the milk quality traits and carcass muscle in numerous animals, such as milk yield and butterfat content in goats (17), and lean percentage and backfat thickness in pigs (18, 19). More importantly, our previous research found that the variation in the *DGAT2* gene was closely associated with carcass weight, shear force, and IMF in domestic pigeons (14). Therefore, we speculated that the *DGAT2* gene was a candidate gene affecting meat quality traits in domestic pigeons. However, there have been no reports on the association of *DGAT2* gene expression with meat quality and muscle fiber characteristics traits in domestic pigeons.

Based on the above considerations, the objectives of the present study were to detect the effect of *DGAT2* gene expression on IMF content and breast muscle fiber characteristics in domestic pigeons, thereby providing a theoretical basis for the application of *DGAT2* in molecular-assisted breeding of superior pigeons.

MATERIALS AND METHODS

This research was performed according to the Chinese guidelines for animal welfare and approved by the animal welfare committee of the College of Animal Sciences, Zhejiang University (No.14814).

Animals and Sample Collection

All pigeons used in the present study were obtained from Weitekai Pigeon Industry Co. Ltd (Wuxi, Jiangsu, China). Ten squabs of Taishen King Pigeons were randomly selected each week from the hatching day (0 weeks) to 4 weeks of age (4 weeks) to collect the breast muscle samples. In addition, 8 types of tissues were collected, such as heart, subcutaneous fat, lung, kidney, breast muscle, gizzard, proventriculus, and liver, from each pigeon. Their parents were housed in one pair (male-female paired) per cage under the same managerial conditions in a windowed poultry house and were fed a mixed-grain diet of cereals and pulses (169 g crude protein/kg and energy content of 11.47 MJ/kg), and one poultry house contained 4,000 pairs of pigeons. The left breast muscle parallel to fiber direction was sampled (1 cm × 0.5 cm × 0.5 cm), and fixed in 4% paraformaldehyde to make a microscopical section. The right breast muscle was cut into small pieces and flash-frozen in liquid nitrogen and stored at −80°C to extract RAN and protein. In addition, another set of 50 pigeons was sampled to collect the breast muscle and measure the IMF (IMF) content at 28 days of age. The IMF content was determined by the ether extraction method as has been established by the Association of Official Analytical Chemists regulations (20), and the IMF content was expressed as g of lipid in 100 g of muscle tissue.

Total RNA Extraction, cDNA Synthesis, and Quantitative Real-Time PCR

The total RNA was extracted following the instruction book of TRlzol (Invitrogen, USA). The RNA concentration and purity were measured by the NanoDropND2000 spectrophotometer (Thermo Fisher Scientific, USA). The reverse transcription kit (Takara, China) was used to synthesize the cDNA at 42°C for 60 min with the oligo dT-adaptor primer.

The sequences of designed primer pairs are shown in **Table 1**. The primer pairs of *DGAT2* were designed by Primer-BLAST (https://www.ncbi.nlm.nih.gov/tools/primer-blast/) according to the pigeon *DGAT2* mRNA sequences, and then the specificity of the primers was also performed in Primer-BLAST by Primer Pair Specificity Checking. The other primers were from the previous study as shown in **Table 1**.

The quantitative real-time PCR (qRT-PCR) was performed by the StepOnePlus Real-Time PCR System (Applied Biosystems, USA), with a 20-μl volume, containing 2 μl cDNA (concentration 50 ng /μL), 0.8 μl forward primer (10 μmol/L), 0.8 μl reverse primer (10 μmol/L), 0.4 μl ROX Reference Dye (50×), 10 μl 2 × SYBR Premix Ex Taq II, and 6 μl nuclease-free water. The program for qRT-PCR was one cycle at 95°C for 30 s; 40 cycles at 95°C for 5 s and 60°C for 30 s. For relative quantitative, the results were normalized with the *β-actin* gene by the $2^{-\Delta\Delta Ct}$ method.

***Western blot*:** The protein of the breast muscle (50 mg) was extracted by the Radio Immunoprecipitation Assay (RIPA) lysis buffer with protease inhibitor. The fresh muscle tissue was washed 3 times with precooling phosphate-buffered saline (PBS) of 4°C. Then, a filter paper was used to absorb the rest of the liquid on the muscle tissue surface and then cut the tissue into several smaller pieces. Add all of the muscle tissue pieces into RIPA buffer (Beyotime, Shanghai, China) in a ratio of tissue weight (g): lysate (ml) = 1:10, and homogenized

TABLE 1 | Primer sequences for quantitative real-time PCR (qRT-PCR).

Gene name	Primer sequences (5′→3′)	Accession number	Source
DGAT2	F: AACGGTCCCGCAGAGATTTT	NW_004973235.1	Self-designed
	R: GTCAGTGGGTAGCGACAACA		
MYOD1	F: AACTGCTCTGACGGCATGAT	NW_004973198.1	(21)
	R: GTGCTTTGGATCGTTCGGTG		
MSTN	F: AACGGTCCCGCAGAGATTTT	NW_004973256.1	(22)
	R: GTCAGTGGGTAGCGACAACA		
β-actin	F: GTGGATCAGCAAGCAGGAGT	XM_005504502.2	(22)
	R: TCATCACAAGGGTGTGGGTG		

DGAT2, diacylgycerol acyltransferase 2; MYOD1, myogenic differentiation 1; MSTN, myostatin.

using a homogenizer until no obvious tissue mass can be seen, and then incubated on ice for 30 min (23). The tissue lysates were centrifuged at 14,000 × g at 4°C for 10 min, and the protein concentration was measured by the BCA method (BCA Protein Assay Kit, abcam, ab102536) (24). The equivalent amount (30 μg) of protein samples was mixed with a 4 × protein SDS-PAGE loading buffer (Takara, code No.9173), and the volume ratio of the loading buffer and the protein sample was 1:3. The composition of 4× protein SDS-PAGE loading buffer (1 ml) was 40 mM Tris-HCl pH8.0, 200 mM DTT, 4% SDS, 40% glycerol, and 0.032% bromophenol blue. The mixed samples were then separated by 10% SDS–PAGE gel, which is a precast polyacrylamide gel (Genscript Biotechnology Co., LTD, China, Item No. M01010C). The running buffer is the Tris-MOPS-SDS Running Buffer (Genscript Biotechnology Co., LTD, China, Item No. M00138), and the concentration is 50 mM Tris Base, 50 mM MOPS, 0.1% SDS, and 1 mM EDTA. In addition, electrophoretic at 140 V for 50 min until blue bands of bromophenol arrive at the bottom of the gel. The proteins in the gel were transferred to the polyvinylidene difluoride (PVDF) membranes (Millipore), which were blocked with 5% BSA in Tris-buffered saline containing 0.1% Tween-20 (TBST) at room temperature for 2 h. The transferring was performed by the Bio-Rad standard wet membrane transfer unit under ice bath conditions with 300 mA transferring electric current and 60–70 V transferring voltage, and the transferring time is 50 min. The membrane was then incubated overnight at 4°C with the primary antibodies (Anti-DGAT2, abcam, ab237613) (1:1000 dilution). After that, the membranes were incubated with the secondary antibody (Goat anti-rabbit IgG-HRP, absin, abs2002) for 2 h at room temperature with a secondary antibody concentration of 0.2 μg/ml. The immunoreactive bands were visualized by the Developer and Fixer Kit (BEYOTIME, Shanghai, China), and images were captured by the chemiluminescent imaging system (Sagecreation, China). The densities of the bands were quantified by the NIH Image J software. The ratios of the proteins to the reference proteins (GAPDH, abcam, ab8245) were used as the relative quantitative analysis results.

Histological Analysis of the Breast Muscle

The fixed breast muscle samples were embedded into the paraffin, 5 μm thick of serial cross-sections perpendicular to the direction of muscle fibers were made in the cryostat at −20°C and then stained with the hematoxylin and eosin (H&E). The Pannoramic Viewer software was applied to conduct the histological analysis, including the muscle fiber diameter (D), cross-sectional area (A), and density (d).

Measurement for the muscle fiber cross-sectional area (A): at least 240 breast muscle fibers were measured in six fields randomly under the 40-fold objective microscope. The mean values were represented as the muscle fiber cross-sectional area.

Measurement for muscle fiber diameter (D): on the assumption that the muscle fibers were round, the muscle fiber diameter was calculated by the following formula, $D = 2\sqrt{(A/\pi)}$. The mean values were represented as the muscle fiber diameter.

Measurement for the muscle fiber density: the total area (S) and the number of muscle fibers (N) were calculated by the image analysis software in six different fields of vision, and the density (d) of muscle fibers was calculated by the following, $d = N/S$. The mean values were represented as the muscle fiber diameter.

At the age of 4 weeks, oil red O staining was used on frozen sections of pigeon breast muscle. The slide was incubated in propylene glycol for 2 min and then incubated in oil red O solution for about 6 min. Then the sections were differentiated in the 85% propylene glycol for 1 min and rinsed two times in clear water. After that, the sections were incubated in hematoxylin for 2 min and then rinsed 3 times in clear water, and finally coverslips with an aqueous mounting medium were placed on top of the sections. The sections were examined under a microscope for imaging to observe the amount and size distribution of intramuscular adipocytes.

Statistical Analysis

Statistical analysis was performed by the SPSS20.0 (SPSS, Chicago, IL). Differences between groups were analyzed by one-way ANOVA followed by Bonferroni contrast adjusted for multiple comparisons. The date were presented as mean ± SE. The value of $p < 0.05$ represents statistically significant and $p < 0.01$ represents highly significant. The correlation analysis was performed by bivariate correlation with Pearson's correlation.

RESULTS

The absolute quantitative mRNA expression levels of the *DGAT2* gene in 8 tissues (heart, subcutaneous fat, lung, kidney, breast

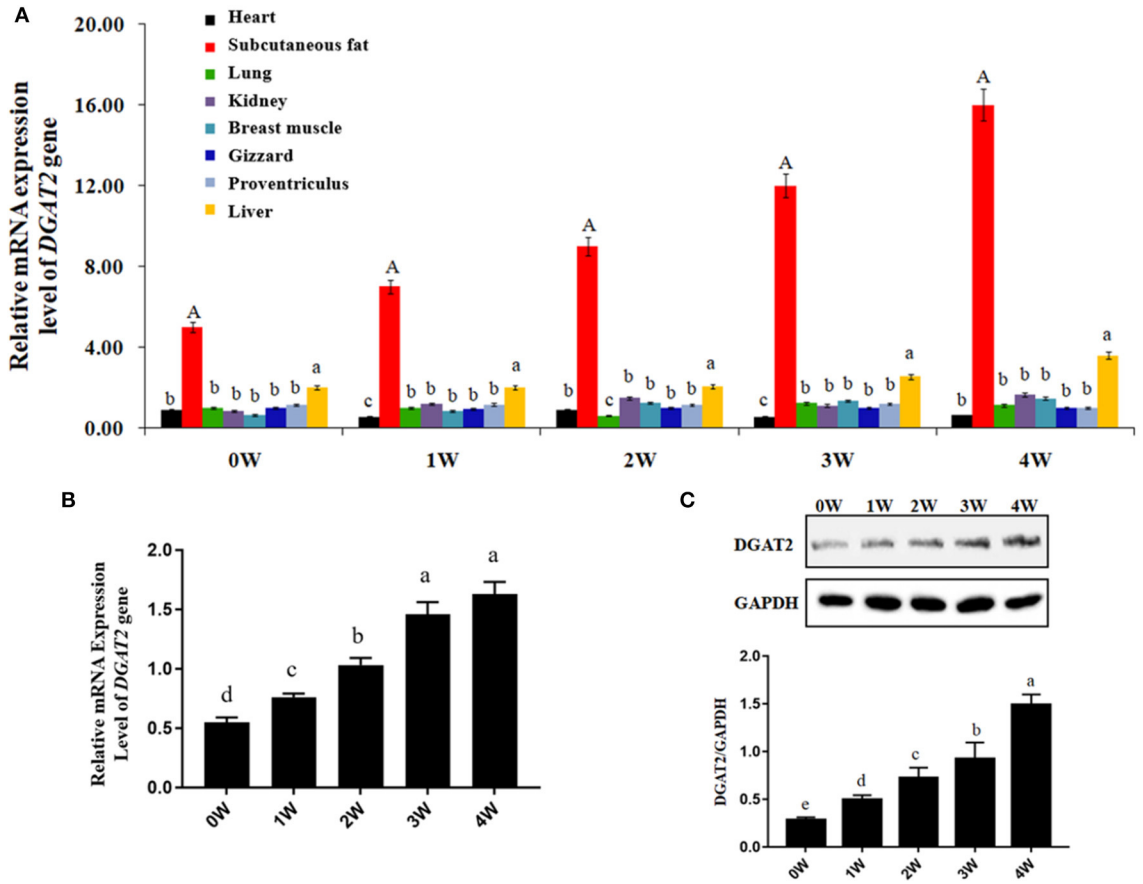

FIGURE 1 | Gene and protein expression levels. **(A)** Absolute quantification of mRNA expression levels of *diacylgycerol acyltransferase 2 (DGAT2)* gene in different tissues at 0, 1, 2, 3, and 4 weeks post-hatching in domestic pigeons. Bars with capital letter and lowercase letter mean highly significant differences ($p < 0.01$) and significant differences ($p < 0.05$), respectively. Data were represented as mean ± SE for 10 pigeons ($n = 10$). **(B)** Relative mRNA expression levels *of DGAT2* gene in the breast muscle of domestic pigeons at 0, 1, 2, 3, and 4 weeks post-hatching. Bars with lowercase letters meant significant differences ($p < 0.05$). Data were represented as mean ± SE for 10 pigeons ($n = 10$). Group 0 week was used as reference. **(C)** Western blot analysis of DGAT2 protein in the breast muscle of domestic pigeons at 0, 1, 2, 3, and 4 weeks post-hatching, normalized with GAPDH. Bars with different lowercase letters were significant differences ($p < 0.05$).

muscle, gizzard, proventriculus, and liver) at 0, 1, 2, 3, and 4 weeks post-hatching in domestic pigeons were shown in **Figure 1A**. The results showed that the mRNA expression level of the *DGAT2* gene in subcutaneous fat showed the highest ($p < 0.01$) among eight tissues of all the ages and showed an upward trend week by week, followed by the liver ($p < 0.05$). The mRNA expression levels in the heart, lung, kidney, breast muscle, gizzard, and proventriculus were relatively low in all the detected weeks.

The results of relative mRNA expression levels of the *DGAT2* gene in the breast muscle of domestic pigeons from 0 to 4 weeks of age post-hatching are shown in **Figure 1B**. It was obvious that the mRNA expression levels of the *DGAT2* gene in breast muscle revealed a significant upward trend ($p < 0.05$) from 0 to 3 weeks of age, and then reached the highest level at the age of 4 weeks.

The results of western blot analysis of DGAT2 protein in the breast muscle of domestic pigeons from 0 to 4 weeks of age post-hatching are shown in **Figure 1C**. After hatching, the DGAT2 protein expression levels significantly increased ($p < 0.05$) by the weeks of age, and finally reached the peak level at the age of 4 weeks.

The representative microphotographs of breast muscle fibers from 0 to 4 weeks of age are shown in **Figure 2A**. At 0 weeks of age (the hatching day), it was difficult to distinguish the muscle fibers for the myoblast cells clustered together and forming multinucleated muscular tubes. At 1 week of age, individually distinguishable muscle fibers started to occur with the development of the muscular tubes, and the endomysium also began to appear clearly among the muscle fibers. Afterward, the breast muscle fibers continuously developed from 2 to 4 weeks of age, and finally became full and plump at the age of 4 weeks. In addition, a perimysium could be observed in the breast muscle during all the weeks of age. Oil red O staining was used on frozen sections of pigeon breast muscle at the age of 4 weeks (**Figure 2B**). The distribution of intramuscular adipocytes was displayed.

The corresponding muscle fiber diameter, cross-section area, and density are shown in **Figures 3A–C**. The diameter and

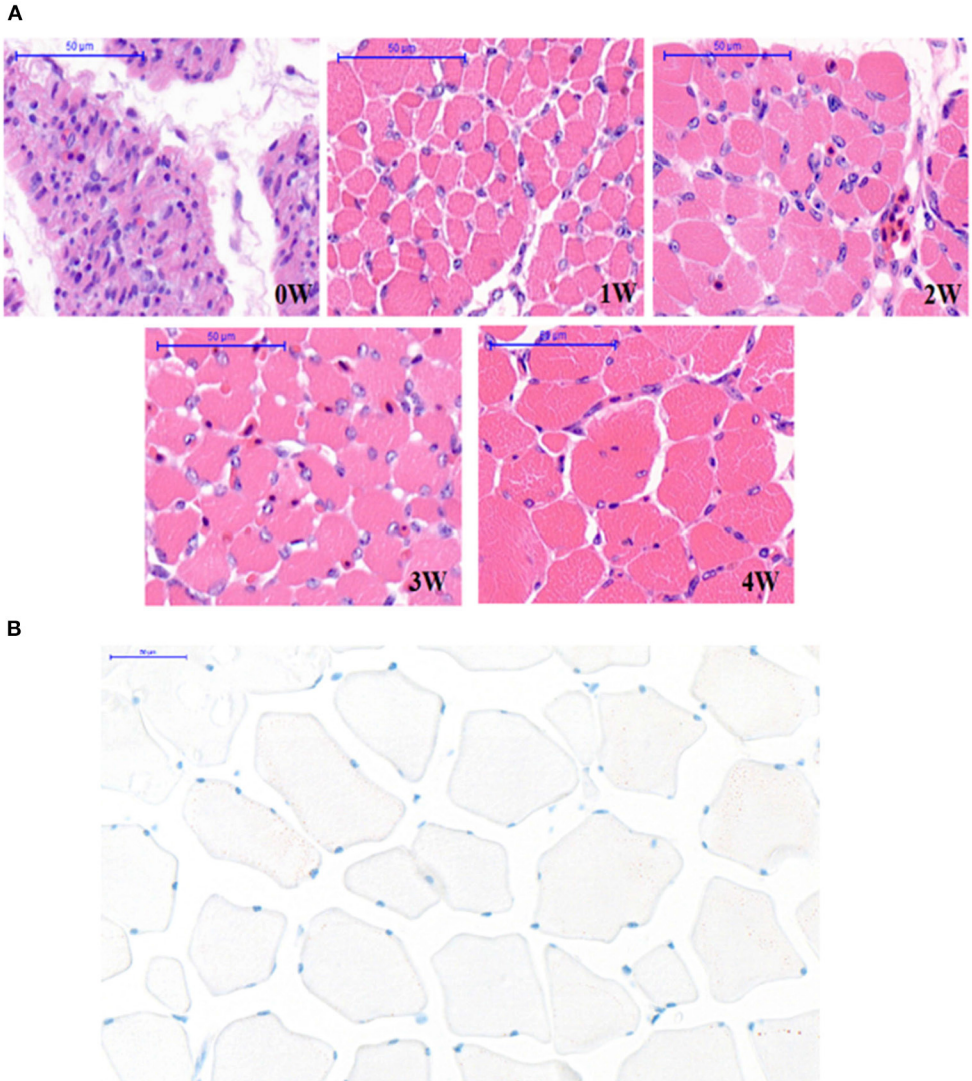

FIGURE 2 | Section of pectoral muscle tissue. **(A)** The breast muscle fiber morphology of pigeons ($n = 10$) with hematoxylin-eosin (H&E) staining at 0, 1, 2, 3, and 4 weeks after hatching (40×). Scale bar: 50 μm. **(B)** Oil red O staining of frozen sections of pigeon breast muscle of 4 weeks ($n = 50$). Scale bar: 50 μm.

cross-section area of breast muscle fibers significantly increased ($p < 0.05$) by the weeks of age from 0 to 4 weeks. Moreover, an enormous increase in muscle fiber diameter and cross-section area was observed from 0 to 1 week of age. On the contrary, the density of the muscle fibers significantly dropped ($p < 0.05$) from 0 to 1 week, and since then the decline continued slowly in the following weeks ($p > 0.05$).

The results of the relative mRNA expression levels *of MYOD1* and *MSTN* genes in the breast muscle of domestic pigeons from 0 to 4 weeks of age post-hatching are shown in **Figure 4**. It was obvious that the mRNA expression levels of the *MYOD1* gene in breast muscle showed a significant upward trend ($p < 0.05$) from 0 to 3 weeks of age, and then reached their peak level at the age of 4 weeks, which is similar to the mRNA expression levels of *DGAT2* gene in **Figure 1B**. The mRNA expression levels of the *MSTN* gene showed a significant decrease ($p < 0.05$) in the first-week post-hatching, and then continued to increase in the next few weeks, and finally reaching the highest level at the age of 4 weeks.

The correlation coefficients (r) of the mRNA and protein expression levels of the *DGAT2* gene with breast muscle fiber diameter, cross-section area, and density at 4 weeks of age are shown in **Table 2**. The results revealed significant positive correlations between the mRNA expression levels of the *DGAT2* gene and fiber diameter ($r = 0.8851$, $p < 0.05$) as well as cross-section area ($r = 0.9420$, $p < 0.01$), and the DGAT2 protein expression level also showed a significant positive correlation with the muscle fiber diameter ($r = 0.8041$, $p < 0.05$) and cross-section area ($r = 0.9062$, $p < 0.01$) of the myofiber. In addition, a significant negative correlation was revealed between the mRNA

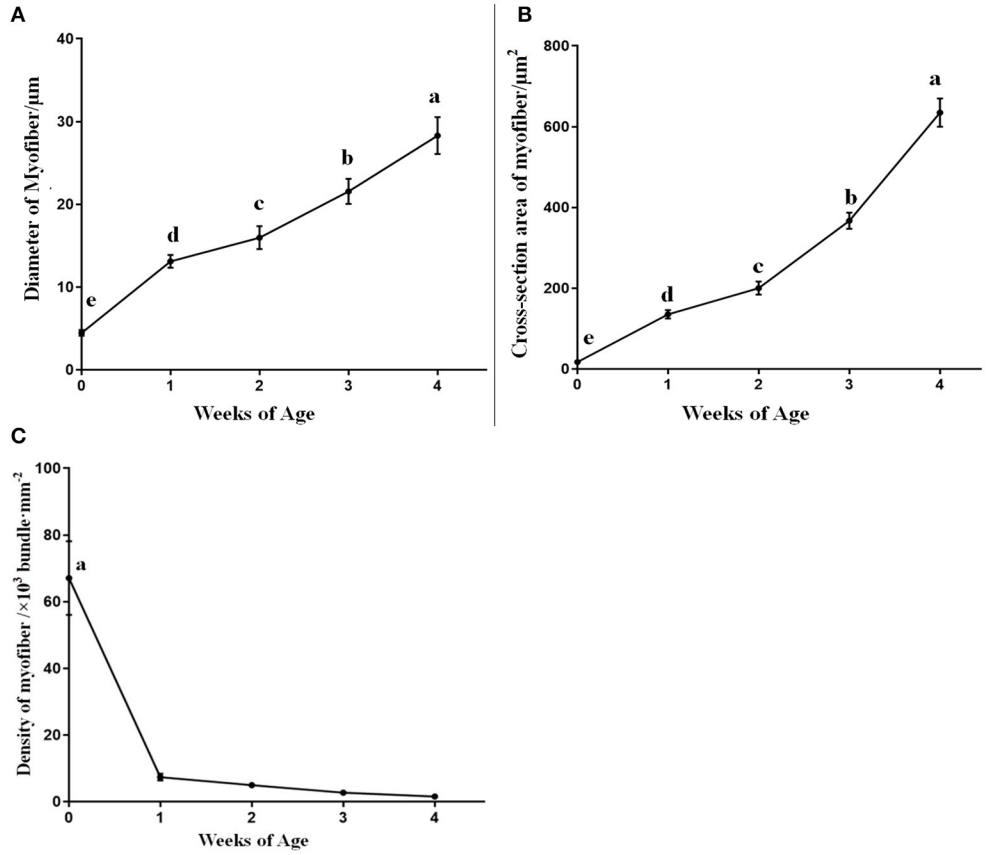

FIGURE 3 | The diameter, cross-section area, and density of breast muscle fibers in domestic pigeons at 0, 1, 2, 3, and 4 weeks post-hatching. Lowercase letters mean significant differences ($p < 0.05$). Data were represented as mean ± SE for 10 pigeons ($n = 10$).

expression level of the *DGAT2* gene and the density of breast muscle fibers ($r = -0.7190$, $p < 0.05$), and the same significant negative correlation was noticed on the DGAT2 protein level ($r = -0.5474$, $p < 0.05$). Correlation coefficients (r) between the relative mRNA expression level of the pigeon *DGAT2* gene and IMF content in breast muscle at 4 weeks of age in pigeons are also shown in **Table 2**. The result indicated that the mRNA expression level of the pigeon *DGAT2* gene was significantly ($r = 0.7720$, $p < 0.01$) correlated with IMF content in breast muscle, and the DGAT2 protein expression also showed a significant difference with the IMF content in breast muscle ($r = 0.6235$, $p < 0.05$). In addition, correlation coefficients (r) analysis between both relative mRNA ($r = 0.5246$, $p < 0.05$) and protein expression level ($r = 0.4852$, $p < 0.05$) of pigeon *DGAT2* and the number of intramuscular adipocytes showed a significant difference, while there was no difference with the size of intramuscular adipocytes ($p > 0.05$).

DISCUSSION

Diacylglycerol acyltransferase 2 is a key member of the DGAT family and plays an important role in the synthesis of fat (1, 14). It is well-known that DGAT2 is essential for the fundamental synthesis of triglycerides, for it is involved in the final and rate-limiting step in the reaction of triacylglycerol synthesis pathways (17–19). Therefore, many previous studies have considered it as an important candidate gene for meat quality and carcass traits in meat-type animals (14, 19). Meanwhile, it is also regarded as a candidate gene for milk fat percentage in milk-type animals mainly focused on ruminants (25–27). Many studies have reported that the expression of *DGAT2* is significantly associated with meat quality traits and carcass traits, especially on IMF content in pigs, steers, yaks, and chickens (1, 2, 15, 16). It is worth noting that in our previous study, we found that *DGAT2* gene polymorphisms were significantly associated with IMF content and muscle tenderness in domestic pigeons, indicating that *DGAT2* might be a promising candidate gene for marker-assisted breeding in pigeons (14). However, there is no study that has reported on the effect of *DGAT2* gene expression on meat quality and muscle fiber characteristics traits in domestic pigeons. Therefore, in the present study, we investigated the associations between the expression of the *DGAT2* gene and IMF content, as well as breast muscle fiber characteristics in domestic pigeons.

We first established a spatiotemporal expression profile of the *DGAT2* gene in eight tissues, namely, the heart, subcutaneous fat, lung, kidney, breast muscle, gizzard, proventriculus, and the

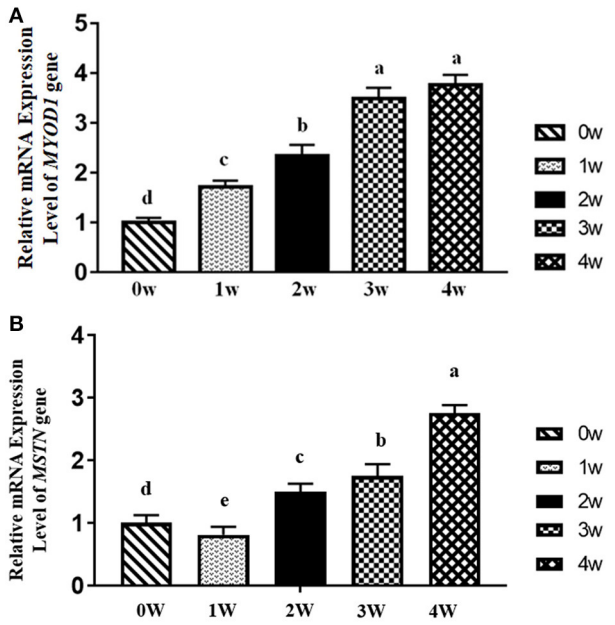

FIGURE 4 | Relative mRNA expression levels *of myogenic differentiation 1 (MYOD1)* and *myostatin (MSTN)* gene in breast muscle of domestic pigeons at 0, 1, 2, 3, and 4 weeks post-hatching. *β-actin* was used as the reference gene. Bars with lowercase letters meant significant differences ($p < 0.05$). Data were represented as mean ± SE for 10 pigeons ($n = 10$). **(A)** Relative mRNA expression levels *of MYOD1*. Group 0 week was used as reference. **(B)** Relative mRNA expression levels *of MSTN.* Group 0 week was used as reference.

TABLE 2 | Correlation coefficients (*r*) between the mRNA/protein expression level of *DGAT2* gene in breast muscle and muscle fiber diameter, cross-section area and density, intramuscular fat (IMF) content, and amount and size of intramuscular adipocytes of 4 weeks of age in pigeons.

Measurements	The mRNA expression of *DGAT2* gene	The protein expression of DGAT2
Diameter of myofiber	0.8851*	0.8041*
Cross-section area of myofiber	0.9420**	0.9062**
Density of myofiber	−0.7190*	−0.5474*
IMF content	0.7720**	0.6235*
Amount of intramuscular adipocytes	0.5426*	0.4852*
Size of intramuscular adipocytes	0.2135	0.2083

*Values with ** and * meant highly significant differences ($p < 0.01$) and significant differences ($p < 0.05$), respectively.*

liver, from birth (0 weeks) to 4 weeks of age (4 weeks). As we expected, *DGAT2* is widely expressed in all the tested tissues, and subcutaneous fat showed the highest ($p < 0.01$) expression level among all the eight tissues at all weeks of age, showing an upward trend week by week, followed by liver ($p < 0.05$). This result is consistent with previous studies reported on yaks, sheep, and chickens (1, 2, 28). DGAT2 is expressed widely in a variety of tissues in animals (1, 29, 30). The high expression level of *DGAT2* in fat tissue indicates an important function in the synthesis and storage of triglycerides (31, 32). In addition, the mRNA expression levels and protein expression levels of DGAT2 in breast muscle revealed a significant upward trend from 0 to 3 weeks of age and then reached the highest level at the age of 4 weeks. As the individual grows and develops, the IMF content continues to deposit and increase within a certain week of age (33), which is consistent with the expression trend of the *DGAT2* gene in the breast muscle. Moreover, the mRNA expression level of the pigeon *DGAT2* gene was significantly ($p < 0.01$) correlated with IMF content in breast muscle ($R = 0.7720$). This also explains well that the *DGAT2* gene plays an important role in IMF deposition. It is interesting to note that the liver also showed a high expression level of the DGAT2 gene because the liver plays an important role in lipid digestion, absorption, synthesis, decomposition, and transportation (34). It also proved the importance of DGAT2 in fat synthesis from another aspect.

Intramuscular fat content is one of the most important acknowledged factors in meat quality (35). Not only does it greatly improve the meat tenderness and texture (10, 11), but it also enhances the meat flavor and juiciness for the IMF as it contains a variety of flavor compounds (8, 36). IMF content is influenced by multiple factors, such as genetic background, gender, nutritional condition, feeding method, and environment and muscle fiber characteristics (6). Muscle fiber characteristics, mainly including muscle fiber type, muscle fiber diameter, muscle fiber area, muscle fiber density, muscle fiber length, connective tissue, and IMF content, can significantly affect meat quality (9, 10). IMF is the fat deposited on the perimysium, endomysium, and epimysium, so to a certain extent, the thickness of the perimysium, endomysium, and epimysium can also reflect the content of IMF (11, 12). Therefore, muscle fiber characteristics could significantly influence meat quality. In this study, we found significant positive correlations between the mRNA expression levels of the *DGAT2* gene and fiber diameter ($p < 0.05$) as well as cross-section area ($p < 0.01$), and the DGAT2 protein expression level also showed a significant positive correlation with the cross-section area ($p < 0.01$) of the myofiber. MYOD1 and MSTN are the two acknowledged gene-affected muscle fiber characteristics (21, 22). The *MYOD1* plays an important role in muscle development and growth from commitment and proliferation through the formation of muscle fibers (37, 38). The MSTN is a negative regulator of skeletal muscle growth and plays an important role in muscle development (22). The present study showed that *the DGAT2* gene in breast muscle revealed a significant upward trend with the ages of pigeons, coupling with the changes in both genes (*MSTN* and *MYOD1*). Furthermore, a significant negative correlation was revealed between the mRNA expression level of the *DGAT2* gene and the density of breast muscle fibers, and the same significant negative correlation was noticed on the DGAT2 protein level. Interestingly, *DGAT2* was positively correlated with muscle fiber diameter, but it was also correlated with IMF content in the breast muscle of pigeons. A previous study had shown that the DGAT2 gene was not only involved in fat synthesis and deposition but also influenced muscle growth and carcass composition (14–16). Above all, DGAT2 might influence IMF content by affecting the muscle fiber development in pigeons.

In conclusion, our results in this study showed that the *DGAT2* gene might play an important role in the meat quality of pigeons by affecting the IMF deposition and breast muscle fiber development, indicating that the *DGAT2* gene might be used as a candidate gene marker-assisted breeding in pigeons. Further functional research should be carried out in the following study to confirm our conclusions.

DATA AVAILABILITY STATEMENT

The original contributions presented in the study are included in the article/supplementary material, further inquiries can be directed to the corresponding author/s.

ETHICS STATEMENT

The animal study was reviewed and approved by the animal welfare committee of the College of Animal Sciences, Zhejiang University.

AUTHOR CONTRIBUTIONS

HM analyzed the data and drafted the manuscript. ZY provided experiment suggestions for this study. MW and WZ performed the RNA extraction and qRT-PCR. SR and FA provided constructive suggestions for the discussion and validation revised manuscript critically for writing—review and editing. LQ and JW conceived the project and designed the experiments. All authors have read and agreed to the published version of the manuscript.

FUNDING

The research was supported by the Key Agriculture Science and Technology Project (No. 2016C02054-16) in Zhejiang province of China, the Ningbo Science and Technology Bureau Project (No. 202003N4305), the Talent Introduction Fund of NingboTech University (20211018Z0216), and the Taif University Research Supporting Project number (TURSP-2020/222), Taif University, Taif, Saudi Arabia.

REFERENCES

1. Hu J, Shi B, Xie J, Zhou H, Wang J, Liu X, et al. Tissue expression and variation of the DGAT2 gene and its effect on carcass and meat quality traits in yak. *Animals.* (2019) 9:61. doi: 10.3390/ani9020061
2. Chen JL, Zhao GP, Zheng MQ, Wen J, Yang N. Estimation of genetic parameters for contents of intramuscular fat and inosine-5′-monophosphate and carcass traits in Chinese Beijing-You Chickens. *Poultry Sci.* (2008) 87:1098–104. doi: 10.3382/ps.2007-00504
3. Mao HG, Cao HY, Liu HH, Dong XY, Xu NY, Yin ZZ. Association of ADSL gene polymorphisms with meat quality and carcass traits in domestic pigeons (Columba livia). *Brit Poultry Sci.* (2018) 59:604–7. doi: 10.1080/00071668.2018.1493188
4. Saez G, Davail S, Gentès G, Hocquette JF, Jourdan T, Degrace P, et al. Gene expression and protein content in relation to intramuscular fat content in Muscovy and Pekin ducks. *Poultry Sci.* (2009) 88:2382–91. doi: 10.3382/ps.2009-00208
5. Cui HX, Wang SL, Guo LP, Liu L, Liu RR, Li QH, et al. Expression and effect of Calpain9 gene genetic polymorphism on slaughter indicators and intramuscular fat content in chickens. *Poultry Sci.* (2018) 97:3414–20. doi: 10.3382/ps/pey232
6. Fowler SM,Wheeler D,Morris S,Mortimer SI, Hopkins DL. Partial least squares and machine learning for the prediction of intramuscular fat content of lamb loin. *Meat Sci.* (2021) 177:108505. doi: 10.1016/j.meatsci.2021.108505
7. Gispert M, Angels Oliver M, Velarde A, Suarez P, Perez J, Furnols MFI. Carcass and meat quality characteristics of immunocastrated male, surgically castrated male, entire male and female pigs. *Meat Sci.* (2010) 85:664–70. doi: 10.1016/j.meatsci.2010.03.021
8. Caroline MK, Paul LS, Ronald GB. Peter JB, Tim P. Tenderness-An enzymatic view. *Meat Sci.* (2010) 84:248–56. doi: 10.1016/j.meatsci.2009.06.008
9. Vestergaard M, Oksbjerg N, Henckel P. Influence of feeding intensity, grazing and finishing feeding on muscle fiber characteristics and meat colour of semitendinosus, longissimus dorsi and supraspinatus muscles of young bulls. *Meat Sci.* (2000) 54:177–85. doi: 10.1016/S0309-1740(99)00097-2
10. Ebarb SM, Drouillard JS, Maddock-Carlin KR, Phelps KJ, Vaughn MA, Burnett DD, et al. Effect of growth-promoting technologies on Longissimus lumborum muscle fiber morphometrics, collagen solubility, and cooked meat tenderness. *J Anim Sci.* (2016) 94:869–81. doi: 10.2527/jas.2015-9888
11. An JY, Zheng JX, Li JY, Zeng D, Qu LJ, Xu GY, et al. Effect of myofiber characteristics and thickness of perimysium and endomysium on meat tenderness of chickens. *Poultry Sci.* (2010) 89:1750–4. doi: 10.3382/ps.2009-00583
12. Light N, Champion AE. Characterization of muscle epimysium, perimysium and endomysium collagens. *Biochem J.* (1984) 219:1017–26. doi: 10.1042/bj2191017
13. Wellmann KB, Kim J, Urso PM, Smith ZK, Johnson BJ. Evaluation of vitamin A status on myogenic gene expression and muscle fiber characteristics. *J Anim Sci.* (2021) 99:skab075. doi: 10.1093/jas/skab075
14. Mao HG, Dong XY, Cao HY, Xu NY, Yin ZZ. Association of DGAT2 gene polymorphisms with carcass and meat quality traits in domestic pigeons (Columba livia). *Brit Poultry Sci.* (2018) 59:149–53. doi: 10.1080/00071668.2017.1413232
15. Cui J, Zeng Y, Wang H, Chen W, Du J, Chen Q, et al. The effects of DGAT1 and DGAT2 mRNA expression on fat deposition in fatty and lean breeds of pig. *Livest Sci.* (2011) 140:292–6. doi: 10.1016/j.livsci.2011.04.007
16. Jeong J, Kwon EG, Im SK, Seo KS, Baik M. Expression of fat deposition and fat removal genes is associated with intramuscular fat content in longissimus dorsi muscle of Korean cattle steers. *J Anim Sci.* (2012) 90:2044–53. doi: 10.2527/jas.2011-4753
17. An X, Song S, Hou J, Zhua C, Penga J, Liua X, et al. Polymorphism identification in goat DGAT2, gene and association analysis with milk yield and fat percentage. *Small Rumin Res.* (2011) 100:107–12. doi: 10.1016/j.smallrumres.2011.05.017
18. Yin Q, Yang H, Han X, Fan B, Liu B. Isolation, mapping, SNP detection and association with backfat traits of the porcine CTNNBL1 and DGAT2 genes. *Mol Biol Rep.* (2012) 39:4485–90. doi: 10.1007/s11033-011-1238-8
19. Li Z, Wang Y, Sun B, Zhang X, Yang C, Kang L, et al. Identification of a 13 bp indel polymorphism in the 30-UTR of DGAT2 gene associated with backfat thickness and lean percentage in pigs. *Gene.* (2016) 576:729–33. doi: 10.1016/j.gene.2015.09.047
20. AOAC. *Official Methods of Analysis of AOAC. International* 17th ed. Gaithersburg, MD: Association of Analytical Communities (2000).
21. Dong XY, Cao HY, Mao HG, Hong QH, Yin ZZ. Association of MyoD1 gene polymorphisms with meat quality traits in domestic pigeons (Columba livia). *J. Poult Sci.* (2019) 56:20–6. doi: 10.2141/jpsa.0170182
22. Liu HH, Mao HG, Dong XY, Cao HY, Liu K, Yin ZZ. Expression of MSTN gene and its correlation with pectoralis muscle fiber traits in the domestic pigeons (Columba livia). *Poult Sci.* (2019) 98:5265–71. doi: 10.3382/ps/pez399
23. Qi LL, Mao HG, Lu XH, Shi TT, Wang JB. Cinnamaldehyde promotes theintestinal barrier functions and reshapes gut microbiome in early weaned rats. *Front Nutr.* (2021) 8:748503. doi: 10.3389/fnut.2021.748503
24. Liang YB, Song PP, Chen W, Xie XM, Luo RX, Su JH, et al. Inhibition of caspase-1 ameliorates ischemia-associated blood-brain barrier dysfunction

and integrity by suppressing pyroptosis activation. *Front Cell Neurosci.* (2020) 14:540669. doi: 10.3389/fncel.2020.540669
25. Pabst B, Futatsugi K, Li Q, Ahn K. Mechanistic characterization of long residence time inhibitors of diacylglycerol acyltransferase 2 (DGAT2). *Biochemistry*. (2018) 57:6997–7010. doi: 10.1021/acs.biochem.8b01096
26. Marchitelli C, Contarini G, Matteis G, De Crisà A, Pariset L, et al. Milk fatty acid variability: effect of some candidate genes involved in lipid synthesis. *J Dairy Res.* (2013) 80:165–73. doi: 10.1017/S002202991300006X
27. Sorensen BM, Kazala EC, Murdoch GK, Keating AF, Cruz-Hernandez Wegner J, et al. Effect of CLA and other C18 unsaturated fatty acids on DGAT in bovine milk fat biosynthetic systems. *Lipids*. (2008) 43:903–12. doi: 10.1007/s11745-008-3216-z
28. Guo B, Kongsuwan K, Greenwood PL, Zhou GH, Zhang WG, Dalrymple BP. A gene expression estimator of intramuscular fat percentage for use in both cattle and sheep. *J Anim Sci Biotechno.* (2014) 5:35. doi: 10.1186/2049-1891-5-35
29. Zhou FT, Zhang YY, Teng XH, Miao YW. Identification, molecular characteristics, and tissue differential expression of DGAT2 full-CDS cDNA sequence in Binglangjiang buffalo (Bubalus bubalis). *Arch Anim Breed.* (2020) 63:81–90. doi: 10.5194/aab-63-81-2020
30. Graber M, Barta H, Wood R, Pappula A, Vo M, Petreaca RC, et al. Comprehensive genetic analysis of DGAT2 mutations and gene expression patterns in human cancers. *Biol Basel.* (2021) 10:714. doi: 10.3390/biology10080714
31. Shen X, Liang XY, Ji XG, You JS, Zhuang XY, Song YD, et al. CD36 and DGAT2 facilitate the lipid-lowering effect of of chitooligosaccharides via fatty acid intake and triglyceride synthesis signaling. *Food Funct*. (2021) 12:8681–93. doi: 10.1039/D1FO01472B
32. Tan SY, Little HC, Sarver DC, Watkins PA, Wong GW. CTRP12 inhibits triglyceride synthesis and export in hepatocytes by suppressing HNF-4 alpha and DGAT2 expression. *Febs Lett*. (2020) 594:3227–39. doi: 10.1002/1873-3468.13895
33. Pinel S, Kelp NY, Bugeja JM, Bolsterlee B, Hug F, Dick TJM. Quantity versus quality: age-related differences in muscle volume, intramuscular fat, and mechanical properties in the triceps surae. *Exp Gerontol.* (2021) 156:111594. doi: 10.1016/j.exger.2021.111594
34. Mataki C, Magnier BC, Houten SM, Annicotte JS, Argmann C, Thomas C. Compromised intestinal lipid absorption in mice with a liver-specific deficiency of liver receptor homolog 1. *Mol Cell Biol.* (2007) 27:8330–9. doi: 10.1128/MCB.00852-07
35. Rosenvold K, Andersen HJ. Factors of significance for pork quality-a review. *Meat Sci.* (2003) 64:219–37. doi: 10.1016/S0309-1740(02)00186-9
36. O'Quinn TG, Woerner DR, Engle TE, Chapman PL, Legako JF, Brooks JC, et al. Identifying consumer preferences for specific beef flavor characteristics in relation to cattle production and postmortem processing parameters. *Meat Sci.* (2016) 112:90–102. doi: 10.1016/j.meatsci.2015.11.001
37. Daou N, Lecolle S, Lefebvre S, della Gaspera B, Charbonnier F, Chanoine C, et al. A new role for the calcineurin/NFAT pathway in neonatal myosin heavy chain expression via the NFATc2/MyoD complex during mouse myogenesis. *Development*. (2013) 140:4914–25.
38. Te Pas MFW, Harders FL, Soumillion A, Born L, Buist W, Meuwissen T.H.E. Genetic variation at the porcine MYF-5 gene locus. Lack of association with meat production traits. *Mammal. Gen.* (1999) 10:123–7.

Conflict of Interest: The authors declare that the research was conducted in the absence of any commercial or financial relationships that could be construed as a potential conflict of interest.

Publisher's Note: All claims expressed in this article are solely those of the authors and do not necessarily represent those of their affiliated organizations, or those of the publisher, the editors and the reviewers. Any product that may be evaluated in this article, or claim that may be made by its manufacturer, is not guaranteed or endorsed by the publisher.

Advantages of publishing in Frontiers

OPEN ACCESS
Articles are free to read for greatest visibility and readership

FAST PUBLICATION
Around 90 days from submission to decision

HIGH QUALITY PEER-REVIEW
Rigorous, collaborative, and constructive peer-review

TRANSPARENT PEER-REVIEW
Editors and reviewers acknowledged by name on published articles

Frontiers
Avenue du Tribunal-Fédéral 34
1005 Lausanne | Switzerland

Visit us: www.frontiersin.org
Contact us: frontiersin.org/about/contact

REPRODUCIBILITY OF RESEARCH
Support open data and methods to enhance research reproducibility

DIGITAL PUBLISHING
Articles designed for optimal readership across devices

FOLLOW US
@frontiersin

IMPACT METRICS
Advanced article metrics track visibility across digital media

EXTENSIVE PROMOTION
Marketing and promotion of impactful research

LOOP RESEARCH NETWORK
Our network increases your article's readership